

Synthesis and Reactivity of Lanthanide(II) Hydrides

A Thesis submitted to Victoria University of Wellington in partial
fulfilment of the requirements for the degree of Doctor of Philosophy

by

Georgia M. Richardson



VICTORIA UNIVERSITY OF
WELLINGTON
TE HERENGA WAKA

Te Herenga Waka – Victoria University of Wellington 2024

Table of Contents

| | |
|---|-----|
| I. Publications as a Result of this Thesis | VI |
| I.I Publications as a Result of the Work Contained Herein | VI |
| I.II Publications as a Result of Other Work Throughout this Thesis..... | VI |
| II. Acknowledgements | VII |
| III. Abstract..... | IX |
| IV. Abbreviations..... | XI |

Introduction

| | |
|---|----|
| 1.1 The Lanthanides..... | 1 |
| 1.2 Lanthanide(III) Hydrides | 3 |
| 1.3 Reactivity of Lanthanide(II) Complexes | 5 |
| 1.3.1 Reduction Chemistry of the Ln(II) Ions..... | 6 |
| 1.3.2 σ -Bond Metathesis | 8 |
| 1.3.3 Insertion Chemistry..... | 9 |
| 1.4 Lanthanide(II) Hydrides | 11 |
| 1.4.1 Synthesis and Reactivity of the First Molecular Ytterbium(II) Hydride | 11 |
| 1.4.2 Synthesis and Reactivity of $[(\text{BDI}^{\text{Dipp}})\text{YbH}(\text{THF})]_2$ | 15 |
| 1.4.3 Synthesis and Reactivity of the Solvent-Free $[(\text{BDI}^{\text{Dipp}})\text{YbH}]_2$ | 17 |
| 1.5 Overview on Lanthanide(II) Hydrides..... | 21 |
| 1.6 Comparisons Between the Lanthanide(II) Ions and Group 2 Hydrides..... | 23 |
| 1.7 Group 2 Hydrides..... | 24 |
| 1.7.1 Synthesis and Reactivity of $[(\text{BDI}^{\text{Dipp}})\text{CaH}(\text{THF})]_2$ | 24 |

| | |
|---|----|
| 1.7.2 Synthesis and Reactivity of the Solvent-free $[(\text{BDI}^{\text{Dipp}})\text{CaH}]_2$ | 25 |
| 1.7.3 White Phosphorus Activation | 27 |
| 1.7.4 Reduction of Aromatic and Polyaromatic Hydrocarbons | 28 |
| 1.7.5 Synthesis and Reactivity of Molecular Strontium and Barium Hydrides..... | 30 |
| 1.8 Benzene Reduction by Organolanthanide Complexes..... | 35 |
| 1.9 Conclusion and Proposal Aims..... | 39 |
| 2.0 References..... | 41 |

Synthesis and Reactivity of Ytterbium(II) Hydrides

| | |
|--|----|
| 2.1 Introduction..... | 44 |
| 2.2 Synthesis of $[(\text{BDI}^{\text{Dipep}})\text{YbH}]_2$ | 45 |
| 2.2.1 Synthesis <i>via</i> $[(\text{BDI}^{\text{Dipep}})\text{YbI}]_2$ | 45 |
| 2.2.2 Preliminary Reactivity of $[(\text{BDI}^{\text{Dipep}})\text{YbH}(\text{THF})]_2$ | 52 |
| 2.3 Synthesis of $[(\text{BDI}^{\text{Dicyp}})\text{YbH}]_2$ | 55 |
| 2.3.1 Synthesis of $(\text{BDI}^{\text{Dicyp}})\text{H}$ | 55 |
| 2.3.2 Synthesis <i>via</i> $[(\text{BDI}^{\text{Dicyp}})\text{YbI}]_2$ | 60 |
| 2.4 Preliminary Reactivity Studies of $[(\text{BDI}^{\text{Dipp}})\text{YbH}]_2$, $[(\text{BDI}^{\text{Dipep}})\text{YbH}(\text{THF})]_2$, and $[(\text{BDI}^{\text{Dicyp}})\text{YbH}]_2$ | 66 |
| 2.4.1 Activation of White Phosphorus | 66 |
| 2.4.2 Reduction of Aromatic and Polyaromatic Hydrocarbons | 73 |
| 2.5 Summary | 85 |
| 2.6 References..... | 86 |

Synthesis and Reactivity of Europium(II) Hydrides

| | |
|---|-----|
| 3.1 Introduction..... | 88 |
| 3.2 Attempted Synthesis of $[(\text{BDI}^{\text{Dipep}})\text{EuH}]_2$ | 89 |
| 3.2.1 Synthesis <i>via</i> $[\text{Eu}(\text{HMDS})_2]$ | 89 |
| 3.2.2 Synthesis <i>via</i> $[(\text{BDI}^{\text{Dipep}})\text{EuI}]_2$ | 92 |
| 3.3 Synthesis of $[(\text{BDI}^{\text{Dicyp}})\text{EuH}]_2$ | 99 |
| 3.3.1 Synthesis <i>via</i> $[(\text{BDI}^{\text{Dicyp}})\text{EuI}]_2$ | 99 |
| 3.3.2 Preliminary Studies for Structural Confirmation of $[(\text{BDI}^{\text{Dicyp}})\text{EuH}]_2$ | 105 |
| 3.4 Synthesis of $[(\text{BDI}^{\text{Dipp,Dicyp}})\text{EuH}]_2$ | 107 |
| 3.4.1 Synthesis of $(\text{BDI}^{\text{Dipp,Dicyp}})\text{H}$ | 107 |
| 3.4.2 Synthesis <i>via</i> $[(\text{BDI}^{\text{Dipp,Dicyp}})\text{EuI}]_2$ | 111 |
| 3.5 Synthesis of $[(\text{BDI}^{\text{Dipp,TCHP}})\text{EuH}]_2$ | 116 |
| 3.5.1 Synthesis <i>via</i> $[(\text{BDI}^{\text{Dipp,TCHP}})\text{EuI}]_2$ | 116 |
| 3.6 Structural Characterisation of $[(\text{BDI}^{\text{Dicyp}})\text{EuH}]_2$ | 120 |
| 3.7 Preliminary Reactivity Studies of $[(\text{BDI}^{\text{Dicyp}})\text{EuH}]_2$, $[(\text{BDI}^{\text{Dipp,Dicyp}})\text{EuH}]_2$, and $[(\text{BDI}^{\text{Dipp,TCHP}})\text{EuH}]_2$ | 121 |
| 3.7.1 Two-Electron Aromatisation of COT | 121 |
| 3.7.2 Preliminary Reactivity of $[(\text{BDI}^{\text{Dicyp}})\text{EuH}]_2$ | 126 |
| 3.7 Summary | 134 |
| 3.8 References..... | 135 |

Four-Electron Reduction of Benzene by a Samarium(II) Alkyl

| | |
|---|-----|
| 4.1 Introduction..... | 137 |
| 4.1.1 Reduction of Benzene and its Derivatives by F–element Complexes | 138 |

| | |
|--|-----|
| 4.2 Synthesis of $[(\text{BDI}^{\text{DicyP}})\text{SmCH}(\text{SiMe}_3)_2]$ | 139 |
| 4.3 Synthesis and Characterisation of a Benzene Tetraanion | 144 |
| 4.4 Synthesis of Tetraanionic Derivatives of Benzene | 150 |
| 4.5 Two-Electron Aromatisation of COT | 155 |
| 4.6 Computational Studies | 159 |
| 4.7 Preliminary Reactivity Studies | 161 |
| 4.7.1 Exploring the Reduction Chemistry of a Benzene Tetraanion | 162 |
| 4.7.2 Exploring the Reduction Chemistry of $[(\text{BDI}^{\text{DicyP}})\text{SmCH}(\text{SiMe}_3)_2]$ | 168 |
| 4.8 Summary | 172 |
| 4.9 Conclusions..... | 173 |
| 4.10 References..... | 175 |

I. Publications as a Result of this Thesis

I.I Publications as a Result of the Work Contained Herein

1. G. M. Richardson, I. Douair, S. A. Cameron, L. Maron and M. D. Anker, *Chem. Eur. J.*, **2021**, 27 (52), 13144-13148.
2. G. M. Richardson, T. Rajeshkumar, F. M. Burke, S. A. Cameron, B. Nicholls, J. Harvey, R. A. Keyzers, T. Butler, S. Granville, L. Liu, L. Maron and M. D. Anker, preprint out at *Nature portfolio*, under revision (*Nat. Chem.*), **2023**.
3. G. M. Richardson, M. J. Evans, T. Rajeshkumar, J. A. McCone, S. A. Cameron, L. Maron, C. Jones and M. D. Anker, *Chem. Eur. J.*, **2024**, 30 (27), e202400681.

I.II Publications as a Result of Other Work Throughout this Thesis

1. G. M. Richardson, I. Douair, S. A. Cameron, J. Bracegirdle, R. A. Keyzers, M. S. Hill, L. Maron and M. D. Anker, *Nat. Comm.*, **2021**, 12 (1), 3147-3147.
2. G. M. Richardson, J. Howarth, M. J. Evans, A. J. Edwards, S. A. Cameron and M. D. Anker, *J. Coord. Chem.*, **2022**, 75 (11-14), 1954-1966.

II. Acknowledgements

First and foremost, I must extend my thanks to Dr. Mathew Anker. You took me on as your first Honours student, where you not only passed on your extensive knowledge of glovebox and Schlenk line techniques but also your passion for inorganic chemistry. Your ability to never switch it off and constantly come up with new ideas to try in the lab is inspiring. You are, dare I say, a genius. It has been a pleasure learning from you over these past four years, and I am proud of the work we have accomplished together. I can only apologise for how much broken glassware it took to get here.

I must also thank Dr. Scott Cameron for the countless crystal structures I have thrown your way. Nothing gave me more joy than seeing a worked-up structure uploaded to the OneDrive folder, but good data set or not, every crystal was a learning experience.

To the various members of the Anker, Coles, and Fulton research groups, present and past, and of course Thursday Club. Thank you for your friendships over the years, it has been enjoyable going through this journey with you all. Tylah, I would like to acknowledge you personally for putting up with me over these past years. The daily coffees and the gossip sessions on things that just aren't our business have been cherished. And Matt, who helped teach me lab techniques, put up with my need to keep the glovebox solvent-free, and taught me how to shoot neutrons at crystals, I thank you.

This Thesis comprises work that would not have been possible without the expertise of our collaborators, Prof. Laurent Maron for all the computational calculations, Assoc. Prof. Robert Keyzers for all the GC-MS work, and Prof. Cameron Jones for the suggestion of unsymmetrical ligands. I also want to thank Dr. Alison Edwards. The trips to ANSTO have been invaluable for my growth as a young researcher, and I thank you for all the crystallography knowledge you have provided me. Maybe one day we will grow a hydride crystal large enough.

I need to acknowledge all the funding that has made this PhD possible. Thank you to the Victoria University of Wellington for awarding me the Wellington Doctoral Scholarship and the MacDiarmid Institute for the top-up funding. I would also like to thank the Curtis-Gordon Scholarship Committee.

Last but not least, to my family and friends. Thank you for standing by and supporting me while I pursued this journey, and for showing an interest despite not fully understanding my research. I can only hope the pages of this Thesis will shed some light on the subject and help you understand why I love what I do.

III. Abstract

The overarching aim of this Thesis is to investigate the synthesis of new molecular lanthanide(II) hydrides in which the lanthanide centres are in the 2+ oxidation state. The synthesis of new ytterbium(II) hydrides will allow for direct comparisons with the current literature with respect to known lanthanide(II) hydrides, systems that are all based on Yb(II). In contrast, there are no reports of the synthesis of molecular europium(II) or samarium(II) hydrides thus isolating these compounds presents a unique opportunity to explore their reactivity for the first time.

Chapter Two first discusses the synthesis of a new molecular ytterbium(II) hydride supported by the previously reported BDI^{Dipep} ancillary ligand. This Chapter then details the synthetic method for a new derivative of the β -diketiminato ligand framework, BDI^{Dicyp}, and the subsequent isolation of a new bulkier ytterbium(II) hydride. The chemistry of these two systems, as well as the previously reported [(BDI^{Dipp})YbH]₂, was explored with respect to the functionalisation of white phosphorus and the two-electron aromatisation of aromatic and polyaromatic hydrocarbons.

Chapter Three demonstrates that synthesising a molecular Eu(II) hydride is not a simple extension of Group 2 chemistry, where utilisation of the BDI^{Dipep} ligand system afforded a plethora of Schlenk-type redistribution or ligand rearrangement products. However, utilisation of bulkier, symmetrical, and unsymmetrical derivatives of the β -diketiminato ligand, BDI^{Dicyp}, BDI^{Dipp,dicyp} and BDI^{Dipp,TCHP}, respectively, produced three of the first examples of divalent europium hydrides. All three systems were proven to affect the two-electron aromatisation of COT to give the respective inverted sandwich complexes, in which the 2+ oxidation state of the europium centre was retained.

Chapter Four diverges from the chemistry presented in the previous two Chapters, focusing on the reduction of benzene and its derivatives by a monomeric samarium(II) alkyl complex. It was found that the respective inverted sandwich complexes contained two Sm(III) ions bridged by a tetraanionic arene, confirmed by magnetic susceptibility calculations in the solution- and solid-state and DFT calculations. This was further confirmed by the ability of the samarium(II) monoalkyl to effect the two-electron reduction of COT by a single samarium centre. Finally, this Chapter continues to explore the reduction chemistry of the Sm(II) alkyl as well as the benzene tetraanion complex.

IV. Abbreviations

| | |
|----------------------------------|--|
| 1,4-CHD | 1,4-Cyclohexadiene |
| AcNac | $[\text{H}_3\text{CC}(\text{O})\text{C}(\text{H})\text{C}(\text{NDipp})\text{CH}_3]^-$ |
| Ad | 1-Adamantyl |
| ANSTO | Australian Nuclear Science and Technology Organisation |
| atm | Atmosphere |
| BDI^{Dipp} | $[\text{CH}(\text{C}(\text{CH}_3)\text{NDipp})_2]^-$ |
| $\text{BDI}^{\text{Dipep}}$ | $[\text{CH}(\text{C}(\text{CH}_3)\text{NDipep})_2]^-$ |
| $\text{BDI}^{\text{Dicyp}}$ | $[\text{CH}(\text{C}(\text{CH}_3)\text{NDicyp})_2]^-$ |
| $\text{BDI}^{\text{Dipp,dicyp}}$ | $[(\text{DippN}(\text{CH}_3)\text{C})\text{CH}(\text{C}(\text{CH}_3)\text{NDicyp})]^-$ |
| $\text{BDI}^{\text{Dipp,TCHP}}$ | $[(\text{DippN}(\text{CH}_3)\text{C})\text{CH}(\text{C}(\text{CH}_3)\text{NTCHP})]^-$ |
| BIAN | bis(mesitylimino)acenaphthene diamine |
| Bu | Butyl |
| c | Concentration |
| °C | Degrees |
| Cent | Centroid |
| COSY | Homonuclear Correlation Spectroscopy |
| COT | 1,3,5,7-cyclooctatetraene |
| Cp | Cyclopentadiene |
| Cp* | 1,3,5,7-pentamethylcyclopentadiene |
| Cy | Cyclohexyl |
| DABCO | Triethylenediamine |
| DFT | Density Functional Theory |
| Dipp | 2,6-Diisopropylphenyl |

| | |
|-------------------|--------------------------------------|
| Dipep | 2,6-Di-(3-pentyl)phenyl |
| Dicyp | 2,6-Dicyclohexylphenyl |
| DMAP | 4-Dimethylaminopyridine |
| EA | Elemental Analysis |
| EPR | Electron Paramagnetic Resonance |
| Et | Ethyl |
| GC-MS | Gas Chromatography-Mass Spectrometry |
| HMDS | Hexamethyldisilazide |
| ⁱ Pent | <i>Iso</i> -pentyl |
| ⁱ Pr | <i>Iso</i> -propyl |
| IR | Infrared |
| Ln | Lanthanide |
| LUMO | Lowest Unoccupied Molecular Orbital |
| Me | Methyl |
| Mes | Mesityl |
| NHE | Normal Hydrogen Electrode |
| NMR | Nuclear Magnetic Resonance |
| <i>n</i> | <i>Normal</i> |
| <i>p</i> | <i>Para</i> |
| Ph | Phenyl |
| ppm | Parts Per Million |
| RT | Room Temperature |
| SCE | Saturated Calomel Electrode |
| SOMO | Singly Occupied Molecular Orbital |

| | |
|--------------------|--|
| SQUID | Superconducting Quantum Interference Device |
| T | Temperature |
| <i>t</i> Bu | <i>tert</i> -Butyl |
| TCHP | 2,4,6-Tricyclohexylphenyl |
| THF | Tetrahydrofuran |
| Tp | Hydrotris(3- <i>t</i> Bu-5-Me-pyrazolyl)borate |
| UV-Vis | Ultraviolet-Visible Spectroscopy |
| χ_m | Molar Magnetic Susceptibility |
| Δf | Change in frequency |
| f | Frequency |
| μ_{eff} | Effective magnetic moment |

Chapter One

Introduction

1.1 The Lanthanides

Despite being named the “Rare Earths”, the lanthanide elements are not as “rare” as was once believed.¹ The natural abundance of these elements in the Earth’s crust can be greater than commonly utilised metallic elements, for example, the second least common lanthanide, thulium, has a higher abundance than precious metals such as gold or silver.²

In contrast to the transition metals, the chemistry of the lanthanide elements has, to date, received markedly less attention.^{1, 3} This was initially attributed to the electronic structure of the lanthanide ions and the belief that these elements lacked the proper valence orbitals to provide effective metal-based chemistry. The lanthanides, known as the f–elements, have the general ground-state electronic configuration of $[\text{Xe}]6s^24f^n$, with minor exceptions. Upon ionisation, the lanthanide metals tend to lose three valence electrons because the first three ionisation energies are relatively low in energy compared to the fourth ionisation energy, resulting in the 3+ oxidation state being the most stable for the lanthanide ions.⁴

The valence electrons in the outermost shell are what differentiate the chemistry of the lanthanides from that of the transition metals, as they have limited radial extension.¹ This means the 4f–electrons penetrate the [Xe] core and are strongly affected by the increasing nuclear charge across the series, thus resulting in a concurrent decrease in ionic radii from lanthanum(III) (1.216 Å) through to lutetium(III) (1.032 Å). This phenomenon is commonly referred to as the lanthanide contraction (Figure 1.1).

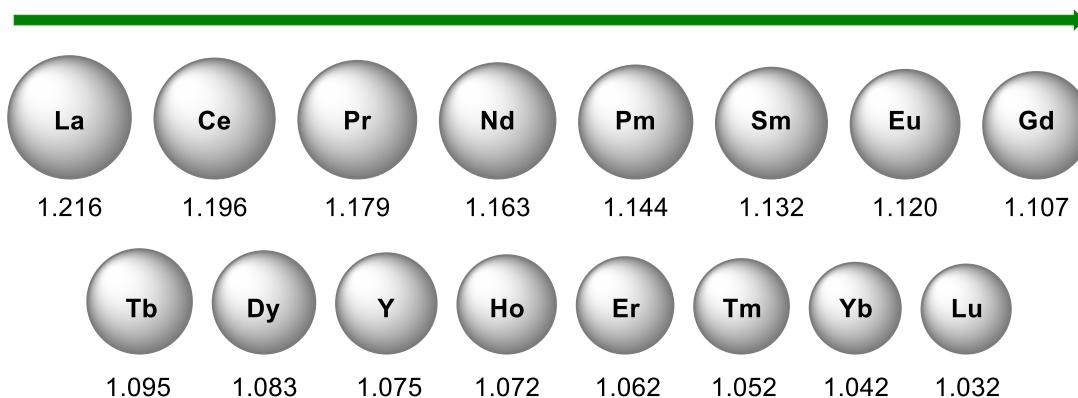
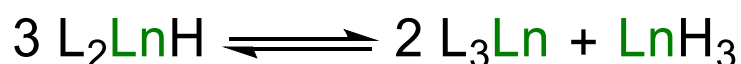


Figure 1.1. Ionic radii (Å) of the lanthanide(III) ions.

The contracted nature of the 4f-orbitals means that these electrons tend not to play a role in metal-ligand bonding, thus the bonding and reactivity is dominated by non-directional, ionic interactions. This is posed as the first “rule” for understanding the organometallic reactivity of the lanthanide ions.^{1, 5}

The second influential factor in the reactivity of lanthanide complexes is sterics. Because the lanthanide ions are electropositive, the electrostatic requirement of balancing the charge on the metal centre using stable organic anions is always met. As such, the steric bulk of said organic ligands determines how these organometallic compounds will react.

In summary, the organometallic chemistry of the lanthanides can be directly correlated to the size of the lanthanide ions and the steric demands of the organic ligand.^{1, 5} These bonding characteristics mean that the formation of well-defined, heteroleptic lanthanide complexes are frustrated by a phenomenon known as Schlenk-type equilibria (Scheme 1.1).⁶



Scheme 1.1. Schlenk-type redistribution of a heteroleptic lanthanide(III) hydride (left) into the respective homoleptic species (right).

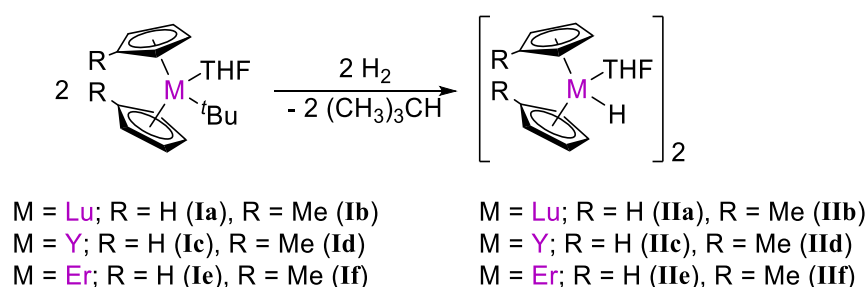
Heteroleptic lanthanide(III) complexes are only stable if this equilibrium is steered exclusively to the left, as, the formation of poorly soluble LnH_3 is entropically favoured and will drive this equilibrium towards the right. This redistribution concurrently generates a metal centre ligated by three large stabilising ligands; while these complexes are still regarded as highly regarded species, they may be considered less reactive in comparison to the heteroleptic lanthanide(III) hydrides.

Therefore, strongly bonding ligands with sufficient steric bulk are an absolute prerequisite to aid in the kinetic stability of heteroleptic lanthanide complexes. Design of suitable ancillary ligands focus on polydentate anionic frameworks containing hard donor sites to increase electrostatic attraction to the metal centre and reduce ligand lability. One of the most prevalent ligand systems utilised with Ln(III) ions is the polyhaptic cyclopentadienyl anion, which can be modified for greater steric control of the respective trivalent lanthanide complexes.^{1,3} As the focus of this Thesis is lanthanide hydride species, the following Section introduces heteroleptic lanthanide(III) complexes, species initially thought to be inaccessible if not for this cyclopentadienyl ligand and its derivatives.⁷

1.2 Lanthanide(III) Hydrides

The first crystallographically characterised molecular lanthanide hydrides were reported in 1982 by Evans and Atwood.⁷ Here, they described the synthesis of lutetium(III), erbium(III) and yttrium(III) hydrides containing derivatives of the cyclopentadienyl ancillary ligand (Scheme 1.2). They began with selecting the metals, basing their choices on the fact that these three metals were not readily reduced to the 2+ oxidation state.¹ At the time, hydrogenolysis of a metal alkyl species was the most common synthetic method for synthesising metal hydrides, so this work was an extension of previous research on hydrogenolysis.⁸ For each lanthanide ion, they explored the reactivity of both unsubstituted cyclopentadiene and

methylcyclopentadiene *tert*-butyl complexes (**Ia** – **If**) towards exposure to hydrogen gas, thus resulting in the synthesis of six new hydride complexes (**IIa** – **IIf**).



Scheme 1.2. Synthesis of the first lanthanide(III) hydrides.

The success continued with the isolation of the first crystallographically characterised organosamarium(III) hydride in 1983,⁹ and in the following years, the research into lanthanide(III) hydride complexes only continued to unfold. To date, the use of cyclopentadienyl and its derivatives continues to be the ligand of choice, with the exploitation of alternate amidinate and guanidinate systems developing from 2006.^{10, 11}

The development of trivalent lanthanide hydride species has experienced impressive growth, so much so that this chemistry has now been extended to most f-elements. Their reactivities have become well established in the literature, being found to favour small molecule activation as well as demonstrating high catalytic activity towards a range of chemical transformations; such examples include hydrosilylation, hydrogenation, hydroboration and alkene polymerisation.^{10, 12, 13}

In contrast, the synthesis and reactivity of lanthanide(II) hydrides is largely underdeveloped, with the only reported examples of divalent lanthanide hydrides being based on ytterbium(II).¹⁴⁻¹⁹ As the focal point of this Thesis will be the synthesis and reactivity of new Ln(II) hydrides, only literature relating to these compounds will be discussed herein.

1.3 Reactivity of Lanthanide(II) Complexes

From the outset of research into lanthanide chemistry, it was established that the predominant and most stable oxidation state in the series was the 3+, with minor exceptions.^{1, 5} Ytterbium, europium, and samarium are known to be the “classically” stable lanthanide elements to commonly adopt the 2+ oxidation state under normal conditions. Importantly, this change to the lower valent state is concurrent with an increase in ionic radii (Figure 1.2).

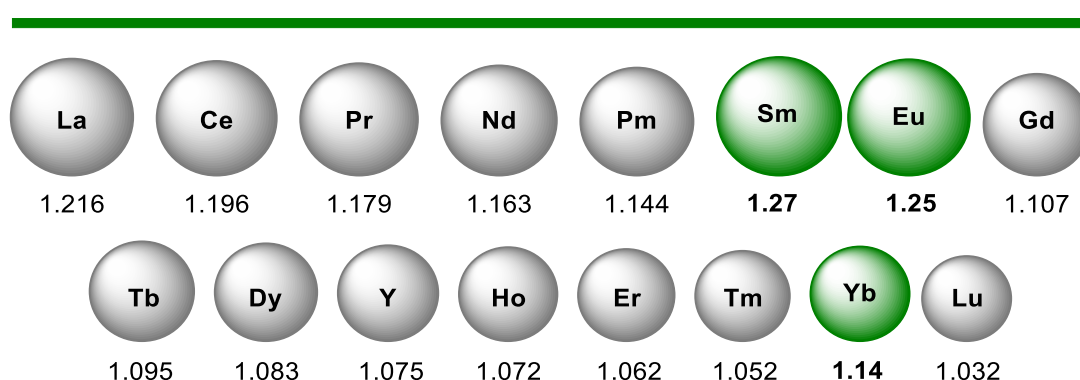


Figure 1.2. Lanthanide contraction, highlighting the increased ionic radii of Ln(II) ions (Å).

As the lanthanides ions go from the trivalent to the divalent state, the increase in ionic radii of the f-elements means that steric saturation of the coordination sphere of the metal centres becomes more challenging.¹ Ytterbium is the smallest Ln(II) ion and increases from 1.04 to 1.14 Å, europium increases from 1.12 to 1.25 Å, samarium is the largest and increases from 1.13 to 1.27 Å.¹ This means that of the three “classically” stable Ln(II) ions, ytterbium should be the easiest metal centre to stabilise, and the larger samarium ion should be the most difficult.

Despite this, the large ionic radii of both samarium(II) and europium(II) can be comparable to that of the larger Group 2 ions, strontium, and barium.²⁰ The successful stabilisation of heteroleptic organometallic compounds containing both Group 2 elements has now been reported, leading to the ideology that this can also be possible for the larger two lanthanides in the 2+ oxidation state.^{21, 22} While this Thesis will focus on the “classically” stable

Yb(II), Eu(II) and Sm(II) ions, it is noteworthy that divalent complexes of all non-radioactive lanthanides have since been reported.²³⁻²⁸

The reactivity of the Ln(II) ions can be split into three broad categories: Redox chemistry, σ -bond metathesis, and insertion chemistry. These will each be discussed separately in the following Section.

1.3.1 Reduction Chemistry of the Ln(II) Ions

In addition to samarium, europium and ytterbium being “classically” stable in the 2+ oxidation state, only one other lanthanide element, cerium, has been reported to be “classically” stable in a non-trivalent state (Ce^{4+}).¹ Despite the possible range, no lanthanides are “classically” stable in both the 2+ and 4+ oxidation state, thus meaning that two-electron redox processes could not occur for a single lanthanide metal centre. This starkly contrasts to the redox-active transition metals, which are known to undergo common redox processes, such as oxidative addition or reductive elimination.¹

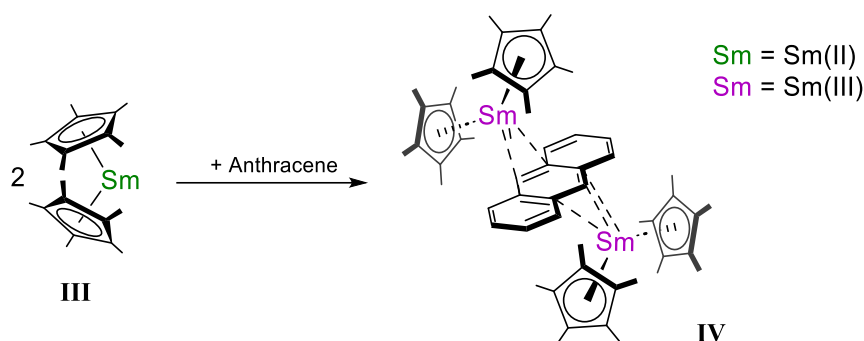
Table 1.1. Properties of the three most common lanthanides in the 2+ oxidation state.

| | $E_{1/2}$ (V) vs NHE | | Electronic configuration of |
|------------------|--|-------------------------------|-----------------------------|
| | $\text{Ln}^{3+} + \text{e}^- \rightarrow \text{Ln}^{2+}$ | Ionic radius (\AA) | Ln^{2+} |
| Eu ²⁺ | −0.35 | 1.25 | [Xe]4f ⁷ |
| Yb ²⁺ | −1.15 | 1.14 | [Xe]4f ¹⁴ |
| Sm ²⁺ | −1.55 | 1.27 | [Xe]4f ⁶ |

The reactivity and stability of Sm(II), Eu(II) and Yb(II) can be paralleled to their respective reduction potentials and ionic radii listed in Table 1.1.¹ Samarium has the more negative reduction potential of the three, consequently demonstrating the strongest reducing ability. However, having the largest ionic radii and an electronic configuration only

approaching the half-filled 4f-shell, samarium also becomes the least stable “classical” ion in the 2+ oxidation state. Inversely, the half-filled electronic configuration of europium(II) makes it the most stable, and the less negative reduction potential also gives it the lowest reactivity. Ytterbium falls in the middle of these two lanthanides, with a stable full f-configuration, the smallest ionic radii, and a middle-range reduction potential.

Being regarded as the more reactive ion of the three, samarium(II) has been involved in reduction chemistry since the 1980s.²⁹ One example involves a homoleptic samarium(II) metallocene complex (**III**), which was reported to reduce a variety of unsaturated polycyclic hydrocarbons with known reduction potentials.³⁰ This includes the hydrocarbon anthracene, demonstrating the ability of two equivalents of **III** to perform one-electron reductions, thus carrying out an overall two-electron reduction process to give **IV** (Scheme 1.3).



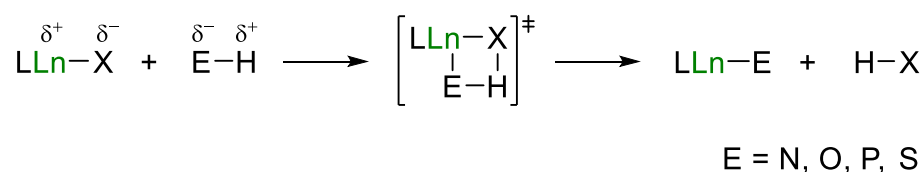
Scheme 1.3. Anthracene reduction by a decamethylsamarocene complex (**III**).

In comparison, the reduction chemistry of ytterbium and europium is far less developed because of their less negative reduction potentials (−1.15 vs NHE and −0.35 vs NHE, respectively).¹ Therefore, after the successful isolation of new divalent ytterbium and europium hydrides, one focal point of this Thesis will be to explore the reductive chemistry of the Yb–H and Eu–H bonds within these hydride complexes, whilst maintaining the 2+ oxidation state.

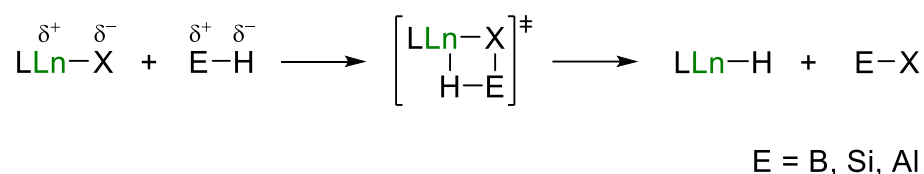
1.3.2 σ -Bond Metathesis

The second of the three principal reactions that dominates the chemistry of the lanthanide(II) ions is σ -bond metathesis.^{5, 31} This mechanism can follow two forms, occurring in either a protic or hydridic manner (Scheme 1.4).

(i) Protic



(ii) Hydridic



Scheme 1.4. Overview of the σ -bond metathesis reaction mechanism.

The protic mechanism (Scheme 1.4, (i)), which the hydrogen carries a partial positive charge, results in polarisation of the E–H bond (E = N, O, P, S). Here, LLn–X (L = ancillary ligand) and the substrate E–H will align in a 4-membered transition state based on opposing electronegativities, breaking these two σ -bonds and generating a new LLn–E bond and a new H–X bond. Most importantly, this mechanism occurs with the retention of the 2+ oxidation state of the Ln metal centre. An example of this protic mechanism is the σ -bond metathesis reaction of a heteroleptic lanthanide hydride, LLn–H, with a protonated amine substrate, N–H, for the formation of a new heteroleptic lanthanide amide complex, LLn–N, concomitant with the extrusion of H₂ gas.

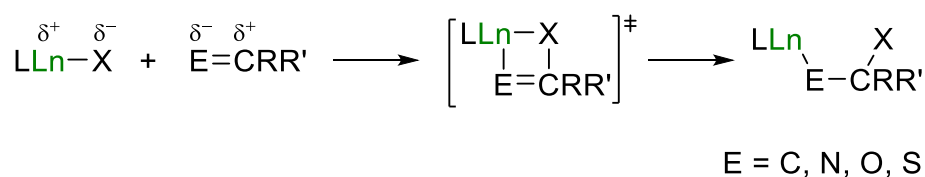
In the hydridic mechanism (Scheme 1.4, (ii)), the E–H bond (E = B, Si, Al) is polarised with a greater electron density upon the hydrogen. Here, LLn–X (L = ancillary ligand) and the substrate E–H will once again align in a 4-membered transition state based on opposing

electronegativities, breaking these two σ -bonds and generating a new $LLn-H$ bond and a new $E-X$ bond. In this hydridic mechanism, a heteroleptic lanthanide amide complex, $LLn-N$, can react with a hydridic source of hydrogen, such as $H-Si$, to generate the respective lanthanide hydride, $LLn-H$, and a new $N-Si$ bond. This particular example will be utilised throughout this Thesis when discussing the synthesis of all lanthanide(II) hydride complexes. This mechanism also occurs without a change in the oxidation state of the lanthanide ion; hence, this type of reactivity proves effective for the redox-inactive lanthanide ions.^{1, 5}

1.3.3 Insertion Chemistry

Insertion reactivity is deemed the third principal reaction mechanism to dominate lanthanide chemistry (Scheme 1.5, (i)).

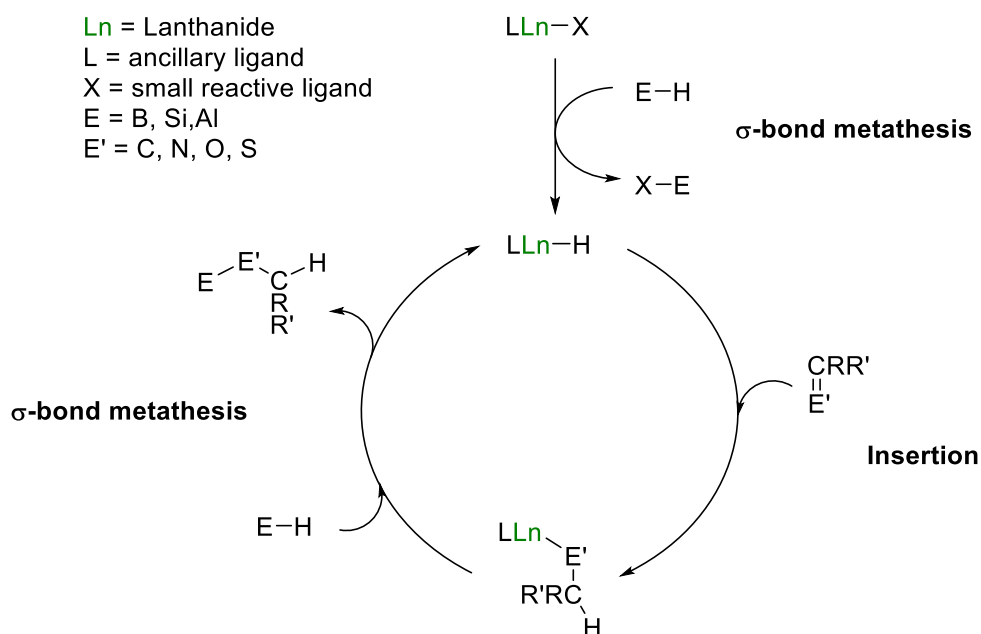
(i) Insertion of unsaturated bond into $Ln-X$ σ -bond



Scheme 1.5. Overview of the insertion reaction mechanism.

Here, an unsaturated chemical entity, $E=CRR'$ ($E = C, N, O, S$), is inserted into the σ -bond of the $LLn-X$ species (L = ancillary ligand). The two substrates will align based on respective electronegativities in the same 4-membered transition state to generate a singular, σ -bonded reaction product, $LLn-E-C(X)RR'$. Like the σ -bond metathesis reaction, insertion occurs without changing the metal oxidation state. An example is the addition of the $C=C$ double bond of ethene into the $LLn-H$ σ -bond of a heteroleptic lanthanide hydride to afford the respective heteroleptic lanthanide alkyl complex.

Through the combination of both σ -bond metathesis and insertion chemistries, catalytic cycles can be constructed based on either a protic or hydridic pathway, both of which can be mediated by a lanthanide(II) centre (Scheme 1.6).



Scheme 1.6. Example of a hydridic catalytic cycle, mediated by a lanthanide(II) centre.

Like the trivalent lanthanides, the chemistry of the electropositive Ln(II) ions is dominated by non-directional, electrostatic interactions.¹ As a result, heteroleptic lanthanide(II) complexes are highly prone to undergoing Schlenk-type redistribution (Scheme 1.7).¹⁵



Scheme 1.7. Schlenk-type redistribution of a heteroleptic lanthanide(II) hydride (left) to the respective homoleptic products (right).

These heteroleptic lanthanide(II) complexes will only remain stable if this equilibrium is steered exclusively to the left, as the formation of poorly soluble LnH_2 will drive this equilibrium towards the right. This redistribution concurrently generates the unreactive homoleptic species, two large stabilising ligands ligate a lanthanide metal centre. Therefore,

the same principles as the Ln(III) ions apply, where large, sterically demanding, monoanionic ligand systems containing hard donor atoms are required to block the Schlenk-type redistribution pathway.³²

Examples pertinent to this Thesis include bidentate and tetradentate β -diketiminato-based (**V** and **VI**),^{17, 19} bidentate amidinates (**VII**),^{12, 16} as well as tetradentate tris(pyrazolyl)borylates (**VIII**) ligand environments (Figure 1.3).^{14, 18}

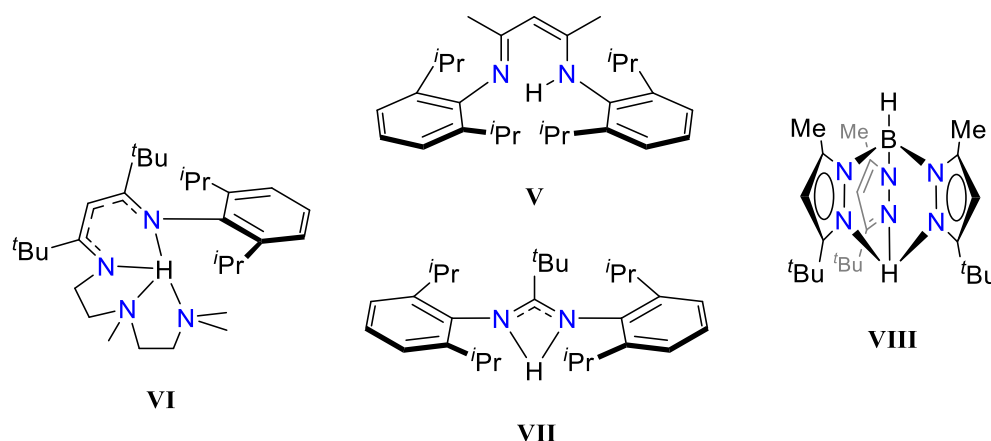


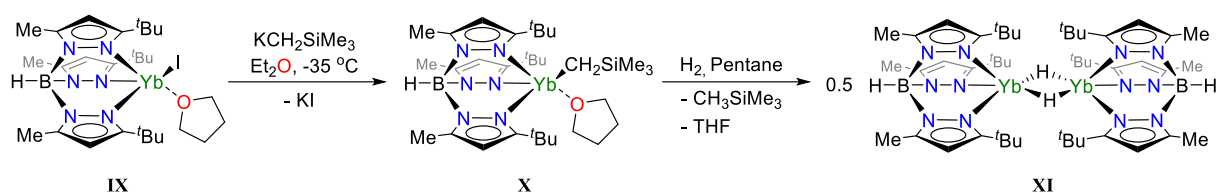
Figure 1.3. Examples of pro-ligands for stabilising heteroleptic lanthanide(II) complexes.

1.4 Lanthanide(II) Hydrides

1.4.1 Synthesis and Reactivity of the First Molecular Ytterbium(II) Hydride

Prior to the isolation of the first example of a lanthanide(II) hydride, divalent lanthanides were predominantly limited to borohydride complexes.³³ This was attributed to the assumption that the larger ionic radii and the strong reducibility of the metal ions posed a challenge in the synthesis and stabilisation of well-defined, discrete lanthanide(II) hydrides.¹⁹

However, in 1999, this assumption was defied, and a milestone in the development of lanthanide(II) hydrides was made.¹⁴ A report by Takats details the successful synthesis and isolation of the first molecular, heteroleptic ytterbium(II) hydride (**XI**), supported by the bulky $\text{Tp}^{t\text{Bu}, \text{Me}}$ ligand ($\text{Tp}^{t\text{Bu}, \text{Me}}$ = hydrotris(3-*t*Bu-5-Me-pyrazolyl)borate) (**VIII**) (Scheme 1.8).



Scheme 1.8. Synthesis overview to form $[(\text{Tp}^{\text{tBu,Me}})\text{YbH}]_2$ (**XI**).

This was achieved through the initial synthesis of an ytterbium iodide species **IX** and a subsequent salt metathesis reaction with potassium [(trimethyl)silyl]methyl to generate compound **X**. This silyl-alkyl substrate and its derivatives play a vital role in the synthesis of most lanthanide hydrides.^{19, 34}

Despite the solvated ytterbium centre within the alkyl precursor (**X**), the reaction with hydrogen gas led to the synthesis of the solvent-free ytterbium(II) hydride. Evans has previously reported on hydrogenolysis of alkyl complexes to afford lanthanide(III) hydride species; however, Takats found it essential to perform the synthesis of **XI** in an autoclave with very high H_2 pressures of 1000 psi to obtain gram scale yields.^{7, 14}

Alongside the smaller ionic radii and the resultant ease of saturating the coordination sphere of the Yb(II) ions compared to other Ln(II) ions, one of the advantages of ytterbium is that the divalent ion has a full f-configuration ($[\text{Xe}]4f^{14}$).¹ The absence of any unpaired electrons means Yb(II) ions are diamagnetic, making it possible for complete structural characterisation of Yb(II) containing complexes in the solution-state by multinuclear NMR spectroscopy.

Multinuclear NMR experiments were used to corroborate the dimeric structure of **XI**.¹⁴ The ^1H NMR spectrum of **XI** displays a quintet-like signal centred at δ_{H} 10.50 ppm with integration ratios of 0.5:12.2:74.5:12.2:0.5. The reported peak ratios indicate that this is not a quintet, but rather several overlapping resonances because of the ^{171}Yb nuclei being 14.3% abundant ($I = 1/2$). Consequently, the proton signal displays ^{171}Yb satellites with the appropriate

coupling constant ($^1J_{\text{YbH}} = 368 \text{ Hz}$) (Figure 1.4). This is representative of a singular bridging hydride ligand coupling to two ytterbium(II) centres. A ^{171}Yb NMR experiment, which exhibits a triplet signal at $\delta_{\text{Yb}} 772 \text{ ppm}$ ($^1J_{\text{YbH}} = 368 \text{ Hz}$), further confirms that each ytterbium(II) centre within the dimer is coupling to both hydride ligands.

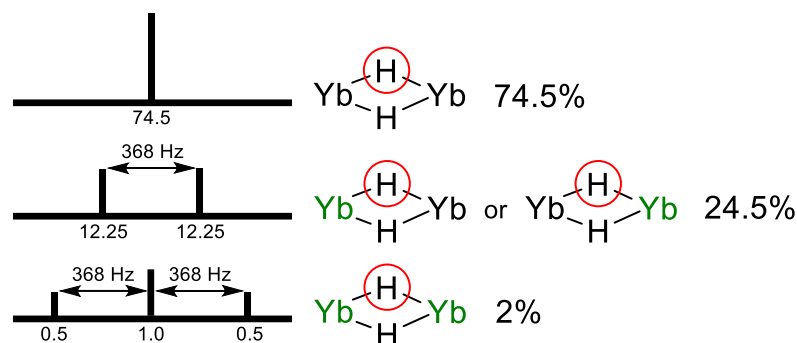


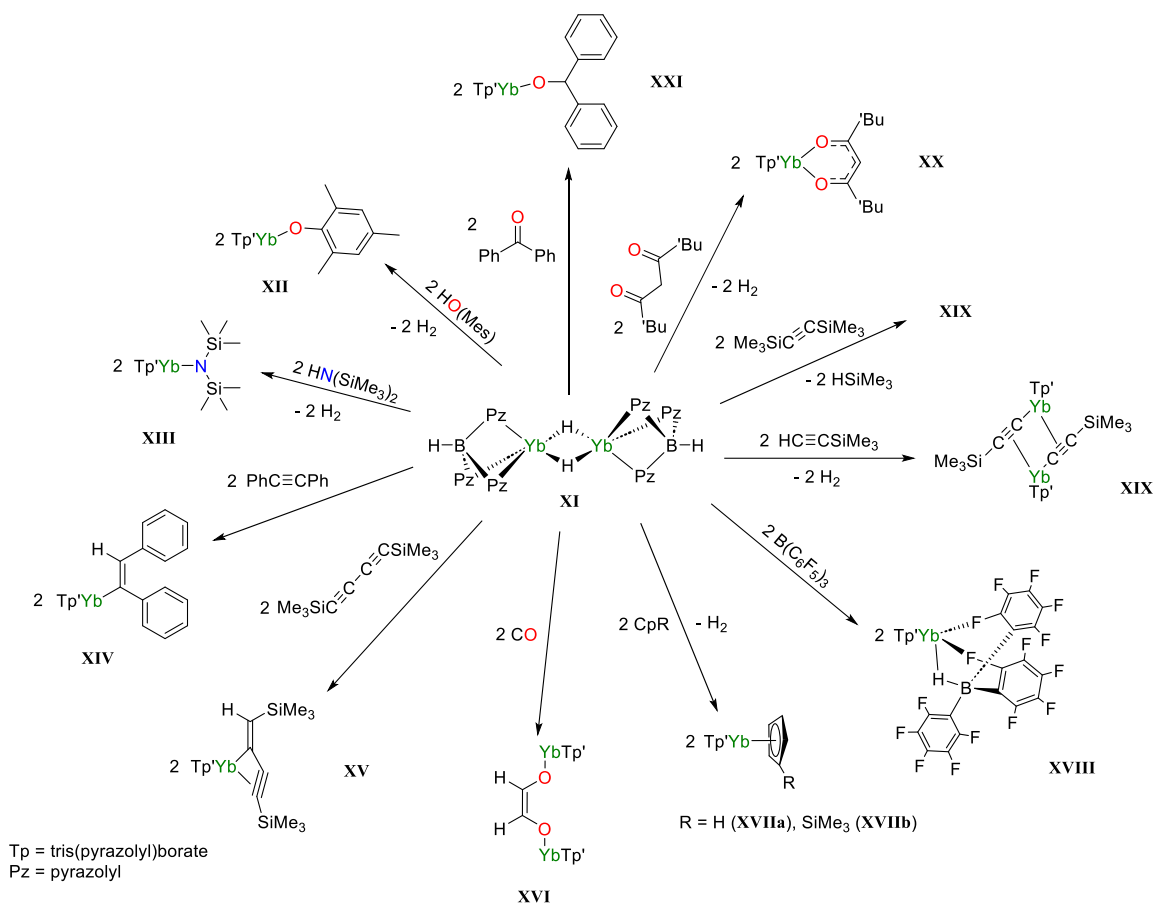
Figure 1.4. Illustration of the three overlapping ^1H NMR resonances for the bridging hydride ligand (circled in red) of **XI**.

The Yb nuclei has been coloured green to demonstrate when the Yb centre is coupling to the circled hydride ligand.

The de-solvation of a THF molecule within **XI** can be attributed to the steric protection of the ytterbium metal centre, provided by the bulky pyrazolyl *tert*-butyl groups of the selected ligand environment. This absence was analysed by adding up to forty equivalents of THF to a C_6D_6 solution of (**XI**), where ^1H NMR analysis showed no definitive change in any proton resonances, further confirming the relative stability of the structure in solution. This is not to say **XI** is exempt from Schlenk-like redistribution, which occurred when dissolved in pure THF solvent.

It is important to note that the isolation of this ytterbium(II) hydride was limited to the solvent, pentane. Different solvents such as toluene or benzene vastly affected the compounds stability, such that uncharacterised side product formation was observed.¹⁴

Despite the steric stability provided by the ancillary ligand, Takats found his ytterbium(II) hydride (**XI**) to be reactive towards a vast range of both saturated and unsaturated substrates (Scheme 1.9).³⁵



Scheme 1.9. Explosion diagram illustrating the reactivity of **XI** with a range of substrates.

Like trivalent lanthanide hydrides, **XI** was demonstrated to undergo a series of stoichiometric σ -bond metathesis reactions with protic substrates, H-E (E = N, O, P, S), with the resultant formation of (Tp^{tBu,Me})Yb-E derivatives concomitant with the elimination of hydrogen gas. Substrate examples include a terminal alcohol to produce the aryloxy (**XII**) as well as H-HMDS (HMDS = N(SiMe₃)₂) to give the heteroleptic amide (**XIII**).³⁵

Compound **XI** displays a great ability to functionalise unsaturated bonds to give a range of insertion products (compounds **XII** – **XXI**). The expected *cis*-alkenyl **XIV** is produced in the example with diphenylacetylene. A similar insertion product (**XV**) is formed when **XI** is

reacted with bis(trimethylsilyl)diacetylene, however, this complex also displays an η^3 -bonding interaction with the second triple bond of the substrate.

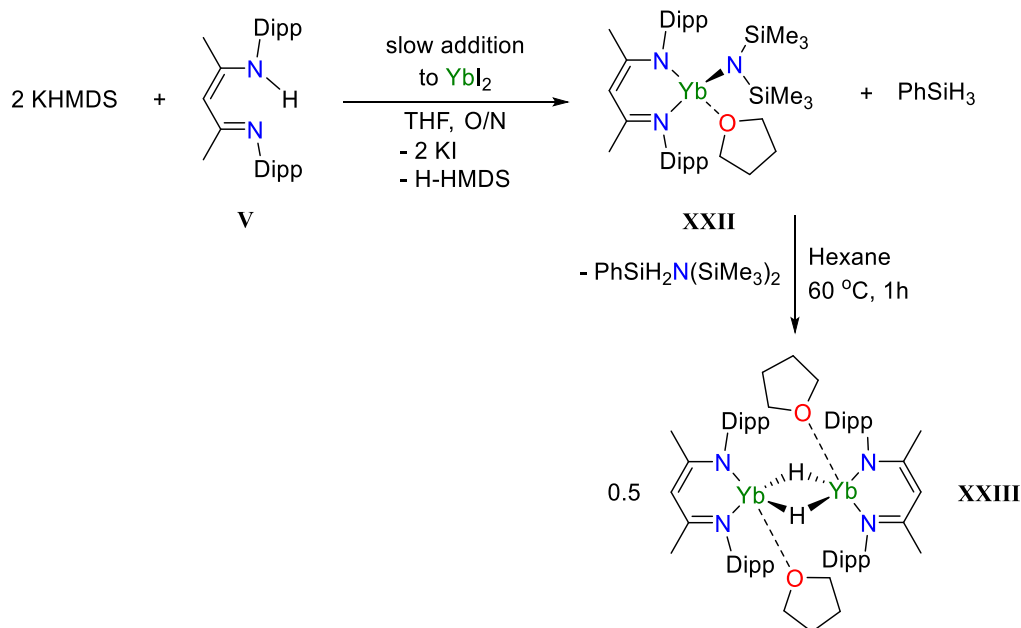
In another example, the *cis*-ene-diolate (**XVI**) could be formed *via* the treatment of **XI** with two equivalents of carbon monoxide through a reductive coupling mechanism.^{35, 36} Finally, **XI** could be reacted with arene substrates, such as cyclopentadienyl derivatives to yield compounds **XVIIa** or **XVIIb**, or with Lewis acids, though in the case of **XVIII** coordination of the $\text{B}(\text{C}_6\text{F}_5)_3$ reagent was observed rather than the expected hydride abstraction.

Despite the isolation of **XI** in 1999, and the subsequent report on the reactivity towards a wide range of substrates in 2001, the second example of a divalent ytterbium hydride was not published until much later.^{14, 35}

1.4.2 Synthesis and Reactivity of $[(\text{BDI}^{\text{Dipp}})\text{YbH}(\text{THF})]_2$

In 2007, Harder detailed an alternative synthetic route synthesising a divalent ytterbium hydride complex. Rather than hydrogenolysis of alkyl precursors, he reported a hydridic σ -bond metathesis reaction between phenylsilane and a ytterbium amido precursor supported by the bidentate β -diketiminate ligand, BDI^{Dipp} ($\text{BDI} = \text{CH}[\text{C}(\text{CH}_3)\text{NDipp}]_2$, $\text{Dipp} = 2,6$ -diisopropylphenyl).¹⁵

Utilising the one pot method, the slow addition of YbI_2 to both the pro-ligand and two equivalents of KHMDS (HMDS = bis(trimethylsilyl)amine)) generated the ytterbium amide **XXII** (Scheme 1.10).



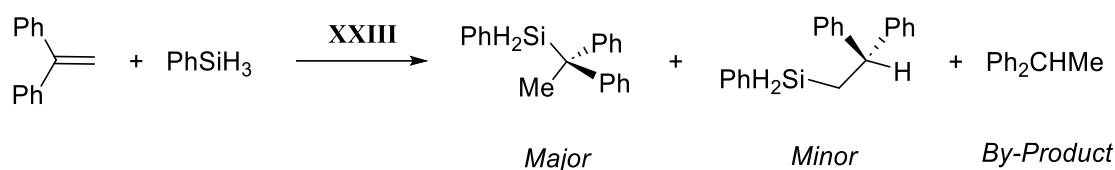
Scheme 1.10. Synthesis overview to form $[(\text{BDI}^{\text{Dipp}})\text{YbH}(\text{THF})]_2$ (**XXIII**).

The subsequent σ -bond metathesis between **XXII** and phenylsilane gave the ytterbium(II) hydride **XXIII**.¹⁵ Unlike the system developed by Takats,¹⁴ the relative steric stability of the bidentate BDI^{Dipp} ligand environment proved to be less than the tridentate scorpionate ligand, such that Yb(II) centres of Harder's system remain solvated by THF. This provided a higher stability when dissolved in ethereal solvents, and temperatures greater than 70 °C which were needed for **XXIII** to decompose to the homoleptic species, $[(\text{BDI}^{\text{Dipp}})_2\text{Yb}]$.³⁷

The structural features of the ytterbium hydride system developed by Takats (**XI**) was also characterised in both the solid- and solution-states. It was found to adopt a dimeric structure, which was confirmed *via* the Yb–H triplet-like signal centred at δ_{H} 9.92 ppm ($^1J_{\text{YbH}} = 398$ Hz) in the ^1H NMR spectrum. No reports on recording a ^{171}Yb NMR experiment were made.¹⁵

The β -diketiminate-based system **XXIII** was shown to catalyse the hydrosilylation of 1,1-diphenylacetylene and phenylsilane (Scheme 1.11).¹⁵ Regardless of the solvent

environment, the major product was formed in yields greater than 95%, with a small percentage of Ph₂CHMe forming as the by-product.



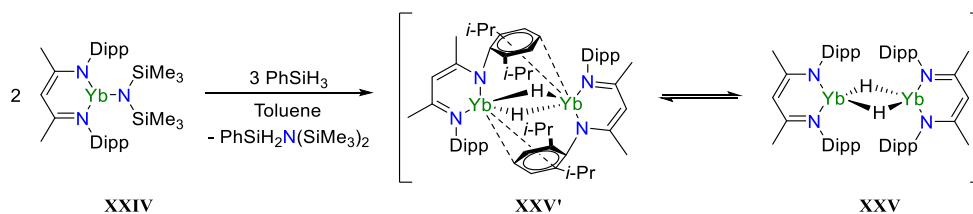
Scheme 1.11. Hydrosilylation with phenylsilane, catalysed by [(BDI^{Dipp})YbH(THF)]₂ (**XXIV**).

Despite the seemingly limited reactivity, **XXIII** provided the first insight into the catalytic potential of lanthanide(II) hydride species.

1.4.3 Synthesis and Reactivity of the Solvent-Free [(BDI^{Dipp})YbH]₂

In 2021, the synthesis of our own divalent ytterbium hydride system was reported in *Nature Communications*.¹⁷ While the methodology and ligand environment were analogous to Harder's, our efforts focused on the complete exclusion of solvent coordination to the ytterbium metal centre, with hopes of providing access to new reactivities.¹⁵

The subsequent addition of the selected hydride source, phenylsilane, to a toluene solution of the amido precursor (**XXIV**) at room temperature results in the synthesis of the low-coordinate ytterbium(II) hydride (**XXV**) within 30 minutes, as an extremely air- and moisture-sensitive black crystalline solid (Scheme 1.12).¹⁷



Scheme 1.12. Synthesis of [(BDI^{Dipp})YbH]₂ (**XXV**) and the two different isomers in solution.

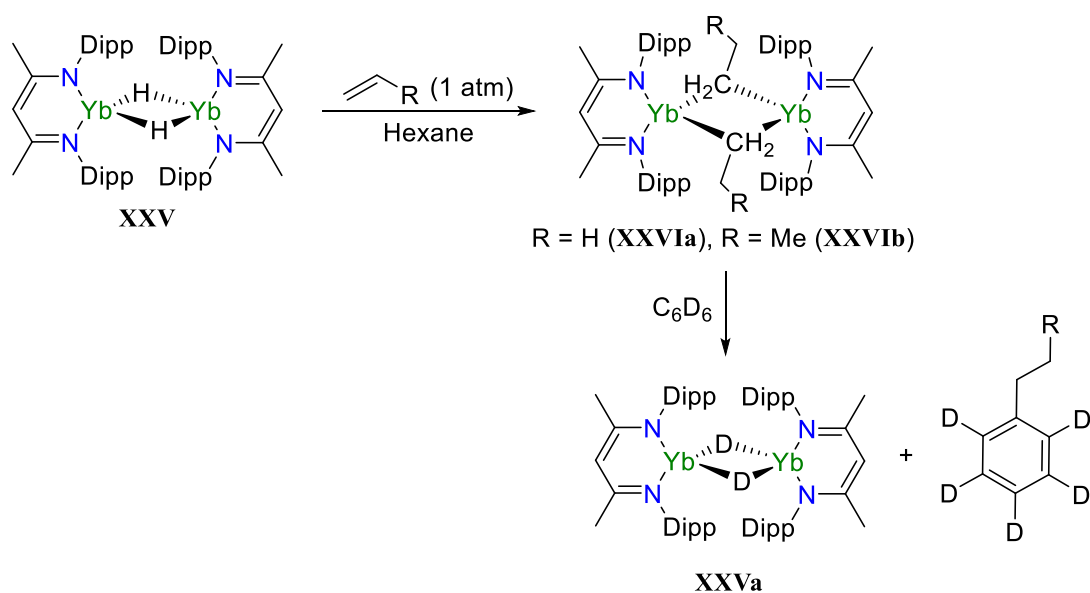
A single crystal X-ray diffraction experiment disclosed disparities in the geometry of **XXV** in comparison to the THF-coordinated analogue, **XXIII**.^{15, 17} Both compounds retain a

dimeric structure with two hydride ligands μ^2 -bridging the two metal centres and each ytterbium centre binding to both nitrogen atoms of the β -diketiminato ligand system. However, the Yb(II) centres of our solvent-free ytterbium hydride also interact with an aryl ring of the Dipp substituent of the second [(BDI^{Dipp})YbH] unit of the dimer in an η^6 -coordination mode.

When pure samples of **XXV** were dissolved into benzene-*d*₆ solvent, ¹H NMR spectroscopy indicated that there were always two distinct species in the solution-state in a 25:1 ratio.¹⁷ This is apparent by the two separate Yb–H resonances centred at δ_{H} 7.82 and 9.64 ppm, respectively. The major species was assigned to the dimeric hydride with a geometry like that found in the solid-state (**XXV'**), as it shows a significant up-field shift (δ_{H} 7.82 ppm, $^1J_{\text{YbH}} = 233$ Hz) in contrast to the THF-coordinated derivative, **XXIII** (δ_{H} 9.92 ppm) which is in an *N,N*-coordination environment.¹⁵ This shift can be explained by the donation of electron density from the aromatic π -system of the 2,6-diisopropylphenyl substituent to the ytterbium centre, which is consistent with other Yb(II) hydride resonances also containing η^6 -arene interactions.¹⁶

The second hydride resonance centred at δ_{H} 9.64 ppm ($^1J_{\text{YbH}} = 151$ Hz) is associated with the minor component in solution (**XXV**). This resonance is consistent with other dimeric ytterbium hydrides only containing two hydride ligands μ^2 -bridging two Yb(II) centres and no arene interactions. Thus, the minor product was ascribed to having a geometry akin to the systems reported by Takats (**XI**) and Harder (**XXIII**).^{14, 15}

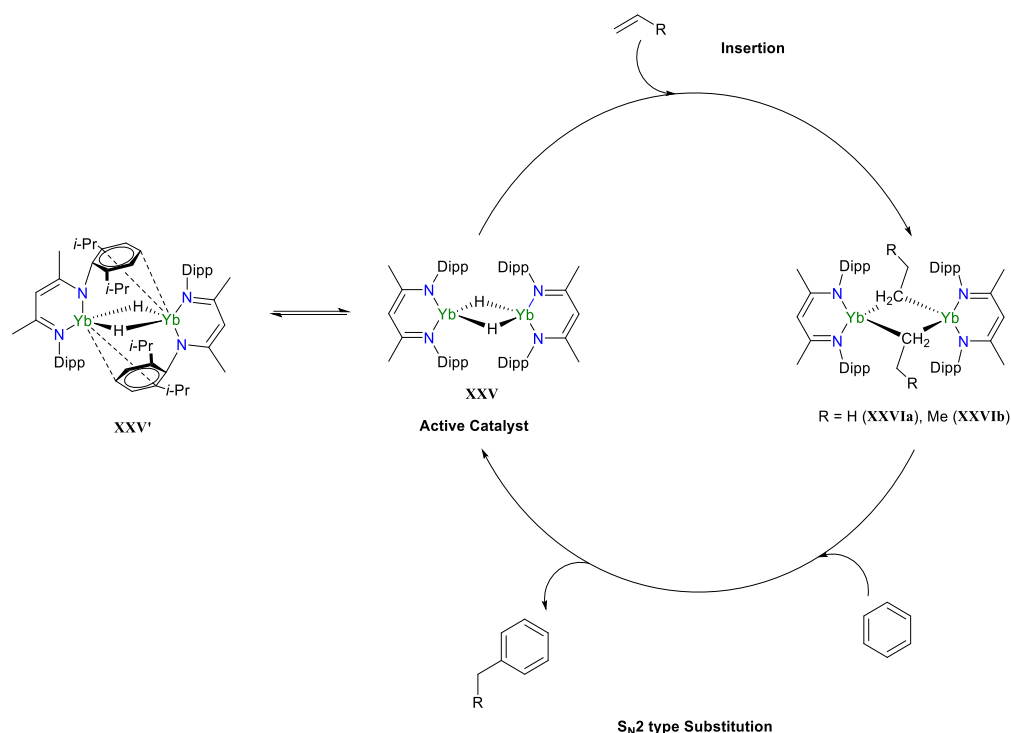
The stoichiometric reaction of **XXV** with the unsaturated substrates, ethylene and propylene, yielded the respective low-coordinate ytterbium(II) ethyl (**XXVIa**) and ytterbium(II) *n*-propyl (**XXVIb**) complexes, respectively (Scheme 1.13).¹⁷



Scheme 1.13. Stoichiometric formation of **XXVIa** and **XXVIb** and the subsequent alkylation of benzene.

The 1H NMR spectrum showed the high-field resonance characteristic of the α -methylene protons for both species (**XXVIa**: quartet, **XXVIb**: triplet) noticeably decreased over a few hours at room temperature, concurrent with the formation of a signal around δ_H 2.45 ppm, representing an alkylated benzene product. In both cases, the 1H NMR spectrum also revealed the formation of the β -diketiminate $Yb(II)$ deuteride (**XXVa**) as the by-product for both stoichiometric reactions. This regeneration of the ytterbium(II) deuteride, therefore, hinted that this observed nucleophilic alkylation of benzene could follow a catalytic regime.

Catalytic amounts of **XXV** were dissolved in C_6H_6 in an NMR tube fitted with a J. Youngs tap, exposed to either ethene or propene and monitored by 1H NMR spectroscopy (Scheme 1.14).



Scheme 1.14. Proposed cycle for the catalytic generation of the alkylated benzene product, mediated by $[(\text{BDI}^{\text{Dipp}})\text{YbH}]_2$ (XXV).

In the case of ethylene, the catalytic production of ethylbenzene was ceased after 5 days at room temperature. ^1H NMR and GC–MS analysis of the resultant sample concluded that multiple ethene insertions were occurring to provide a small portion of *n*–butylbenzene.¹⁷

In the case of propylene, the catalytic reactivity was entirely selective for *n*–propylbenzene. Product turnover ceased after 8 days at room temperature, with a single crystal X–ray diffraction experiment identifying a tetrameric ytterbium(II) allyl complex, $[(\text{BDI}^{\text{Dipp}})\text{Yb}(\text{CH}_2\text{C}(\text{H})\text{CH}_2)]_4$, as a catalyst deactivation product. Such η^3 –allyl complexes have been previously reported as common breakdown products during transition metal–mediated benzene alkylation, forming through competing C–H activation.³⁸

1.5 Overview on Lanthanide(II) Hydrides

The previous section has addressed the synthesis and reactivity of the first example of a heteroleptic ytterbium(II) hydride, **XI**, in a landmark report by Takats in 1999.¹⁴ This was followed by the introduction of two analogous hydride species, both utilising the same BDI^{Dipp} ligand, one of which has additional steric stability provided by solvent molecules (Harder: **XXIII**) and one which is low-coordinate (Anker: **XXV**).^{15, 17}

To date, the literature discloses a total of six reports on the isolation of lanthanide(II) hydride complexes (Figure 1.5).¹⁴⁻¹⁹

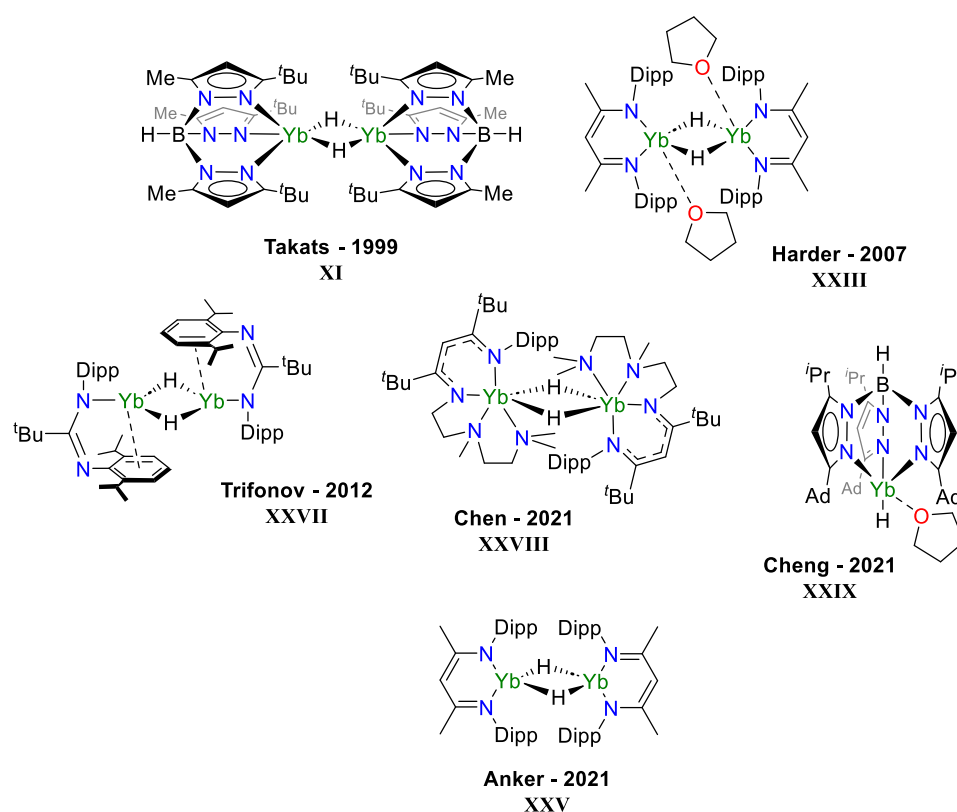


Figure 1.5. Overview of all six examples of all ytterbium(II) hydrides reported to date.

Each system is synthesised through similar methodologies: either the hydrogenolysis of an alkyl-based precursor or *via* the σ -bond metathesis reaction between an amide-based precursor and PhSiH_3 , negating further in-depth discussions. It should be mentioned that the variations in the ligand environment provide different degrees of steric saturation of the

ytterbium(II) centres within each hydride complex. Thus each complex exhibits contrasting stabilities in the solution-state, yet all demonstrate the ability to perform similar redox, σ -bond metathesis or insertion chemistries.^{14-19, 39, 40}

It is important to highlight just how few lanthanide(II) hydrides there are, despite the isolation of the first example over 20 years ago, and that all six systems are based on ytterbium(II). There are no reports on the synthesis of molecular europium(II) and samarium(II) hydrides despite these ions being “classically” stable in the 2+ oxidation state.¹

Europium has the electronic configuration of $[\text{Xe}]6s^24f^7$ and can readily lose two electrons from the 6s energy level to generate the highly stable, half-filled $4f^7$ shell. This means the lack of reported hydride species for this lanthanide element is likely ascribed to the larger ionic radius and the challenge of finding a suitable ligand environment for stability. There have also been no reports of a samarium(II) hydride. Unlike europium, this is less surprising based on the lower stability of samarium in the 2+ oxidation state.¹ Samarium has a ground state electronic structure of $[\text{Xe}]6s^24f^6$, meaning that losing two electrons from the 6s subshell gives an f-configuration only approaching the stable half-filled $4f$ -shell. Despite this, well-known samarium(II) compounds have been reported in the literature.⁴¹ This means that while the synthesis and characterisation of a samarium(II) hydride will be more challenging compared to europium, it should be attainable.

The successful synthesis of molecular europium(II) and samarium(II) hydrides presents a unique opportunity to explore their reactivity for the first time. It allows for comparisons of their reactivity with respect to redox vs σ -bond metathesis/insertion chemistry with the current literature as we attempt known lanthanide(II) hydride chemistry.^{16-19, 31, 35, 39}

1.6 Comparisons Between the Lanthanide(II) Ions and Group 2 Hydrides

The chemistry of the Group 2 ions is defined by their extremely stable 2+ oxidation state.⁴² A marked increase in the ionic radii is observed upon descending the group, concurrent with an increase in polarisability and electropositivity. This means that two principle mechanistic steps dominate the reactivity of these Group 2 complexes; σ -bond metathesis and insertion chemistry, which occur *via* a 4-membered transition state and without a change in oxidation state (redox-inactive). Metal-ligand bonding for the Group 2 cations is also dominated by increasingly non-directional ionic interactions as the group is descended.⁴² These bonding characteristics mean the formation of heteroleptic heavier Group 2 complexes are also frustrated by Schlenk-like equilibrium.^{21, 32}

For these reasons, comparisons have been made between the divalent lanthanide ions and Group 2 ions. Specifically, there is ample evidence for considerable similarities in the chemistry of calcium and ytterbium(II) complexes.³⁷ For example, both ions have a similar ionic radius (Ca^{2+} : 1.12 Å, Yb^{2+} : 1.14 Å)⁴³ and crystal structures of calcium and ytterbium analogues have proved to be isostructural to each other. Despite this, the electronic structures of the two elements are distinctly different as the chemistry of calcium involves the s-orbitals (ground state electronic configuration: $[\text{Ar}]4s^2$), while ytterbium also has access to f-orbitals (ground state electron configuration: $[\text{Xe}]6s^24f^{14}$). It was discussed in Section 1.1 that these valence electrons of the f-elements have limited radial extension and, therefore, do not affect the chemistry of the lanthanides. Yet, these differences allow for a potential divergence in reactivities between the two elements.^{1, 42}

The following Sections delve further into the synthesis and reactivity of Group 2 hydrides. It will first focus on the smaller alkaline-earth metal, calcium, describing key details so that comparisons with ytterbium may be made in later Chapters of this Thesis.³⁷ This will then be extended to the heavier Group 2 elements, strontium (Sr^{2+} : 1.26 Å) and barium (Ba^{2+} :

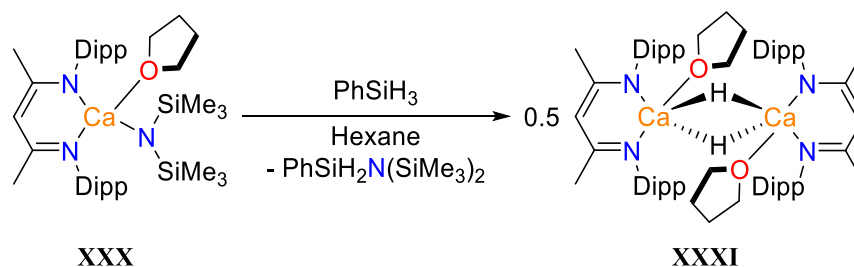
1.42 Å), so that correlations between these and the larger lanthanide ions that have similar ionic radii, europium (Eu^{2+} : 1.25 Å), and samarium (Sm^{2+} : 1.27 Å), respectively, can be made.^{1, 20, 43}

1.7 Group 2 Hydrides

1.7.1 Synthesis and Reactivity of $[(\text{BDI}^{\text{Dipp}})\text{CaH}(\text{THF})]_2$

Initially, Harder focused on synthesising a divalent calcium hydride analogous to that of Takats' ytterbium species **XI**.¹⁴ While he utilised the same bulky tris(pyrozolyl)borate ligand system, his synthetic method diverged towards the treatment of a calcium amide precursor with the hydridic hydrogen source, phenylsilane.³² Despite ^1H NMR analysis of the reaction mixture indicating the clear formation of the expected by-product, $\text{PhH}_2\text{SiN}(\text{SiMe}_3)_2$, and thereby hinting at the successful synthesis of the heteroleptic hydride, a single crystal X-ray diffraction experiment disclosed only the formation of the Schlenk-like redistribution complex, $[(\text{Tp}^{\text{tBu}})_2\text{Ca}]$.

This led to the introduction of the bidentate β -diketiminate system, which has since become a leading ancillary ligand in the synthesis and stability of Group 2 hydride complexes.^{32, 44-46} In 2006, Harder synthesised the first well-defined soluble calcium(II) hydride bearing the BDI^{Dipp} ligand, **XXXI**, through the same σ -bond metathesis reaction between a heteroleptic calcium amido complex and phenylsilane (Scheme 1.15).³²

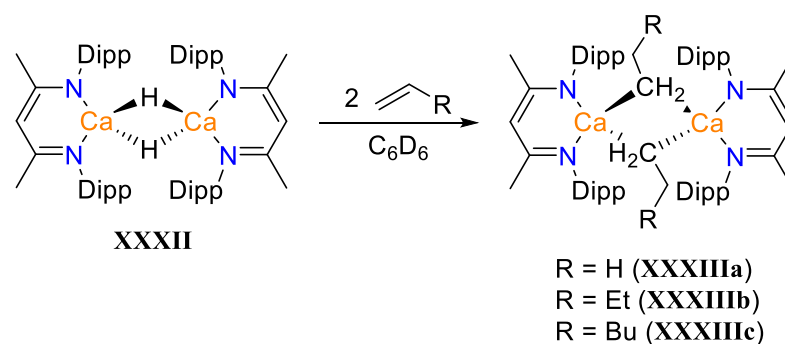


Scheme 1.15. Synthesis overview to form $[(\text{BDI}^{\text{Dipp}})\text{CaH}(\text{THF})]_2$.

This hydrocarbon-soluble calcium hydride (**XXXI**) was later found to be reactive towards a vast range of unsaturated compounds, as well as epoxides and Lewis Acids.⁴⁷ An example includes the reduction of the C≡N triple bond in an isocyanide substrate, to give the 1,1–insertion product, [(BDI^{Dipp})Ca(C(H)=NR)] (R = cyclohexyl) in which the two calcium centres are bridged by two [RN=(H)C][−] anions. In contrast, the reaction of **XXXI** towards unsaturated C=C substrates was limited: **XXXI** could facilitate the catalytic hydrogenation of conjugated alkenes, such as styrene. However, its stoichiometric reactivity was limited to 1,1–diphenylethylene under mild conditions, though the resultant product was not crystallographically characterised.^{47, 48}

1.7.2 Synthesis and Reactivity of the Solvent-free [(BDI^{Dipp})CaH]₂

Building on the development of highly reactive calcium reagents as suitable catalysts for the hydrogenation of alkenes, Hill et. al describe the isolation of the solvent-free, heteroleptic calcium hydride, **XXXII**, supported by the BDI^{Dipp} ancillary ligand (Scheme 1.16).⁴⁴ This complex was synthesised *via* similar methods used to generate the solvated analogue, **XXXI**, however, the coordinated THF molecules were first removed from the calcium centre of the amide (**XXX**) by heating the product under vacuum for 40 minutes at 150 °C. The de-solvated amido precursor could then be treated with three equivalents of phenylsilane in hexane to give **XXXII**.⁴⁴



Scheme 1.16. Insertion of alkenes into the Ca–H bond of **XXXII** to give the respective *n*–alkyl complexes.

It was found that **XXXII** facilitated reactions with non-activated terminal alkenes, ethene, 1-butene and 1-hexene to form the calcium *n*-alkyl complexes, **XXXIIIa**, **XXXIIIb**, and **XXXIIIc**, respectively.⁴⁴ These products were stable at room temperature and allowed for full structural characterisation in both the solution- and solid-state, contradicting reports in the literature.

The reaction of **XXXII** with ethene was conducted in C₆D₆ solvent, and through these studies, the formation of the organic product, *d*₅-ethylbenzene, was realised by the appearance of a quartet at δ_{H} 2.45 ppm in the ¹H NMR spectrum, demonstrating the ability of **XXXII** to affect the direct nucleophilic alkylation of benzene. This reactivity was extended to 1-butene and 1-hexene to afford the formation of *d*₅-*n*-butylbenzene and *d*₅-*n*-hexylbenzene, respectively, at moderately elevated temperatures.

Further analysis of the ²H NMR spectrum showed the regeneration of the heteroleptic calcium deuteride, [(BDI^{Dipp})CaD]₂, inferring this nucleophilic reactivity could follow a catalytic regime. Yet, the formation of the *n*-ethyl-, *n*-butyl- and *n*-hexyl-benzene organic products was strictly stoichiometric due to Schlenk-type equilibrium acting as a competing pathway.

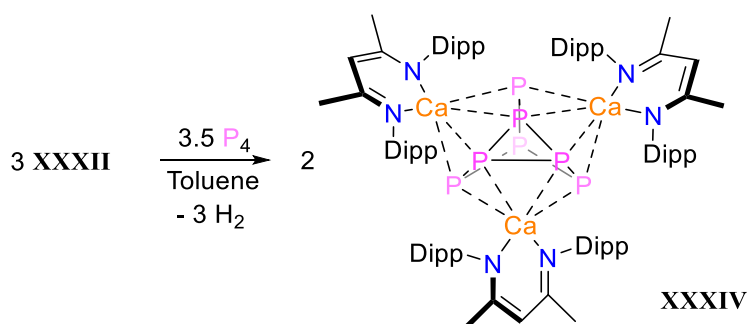
A second study, however, demonstrates the ability of **XXXII** to mediate the catalytic hydrogenation of a selection of alkene substrates. This first step of the catalytic cycle is proposed to occur *via* the insertion of an alkene into one of the Ca-H bonds to give a mixed calcium hydride-alkyl intermediate, which can then split into two separate pathways: the first is the subsequent σ -bond metathesis with H₂ to regenerate **XXXII** and the respective alkyl substrate, or this same mixed calcium hydride-alkyl can undergo a second alkene insertion to give the calcium *n*-alkyl complexes, which undergoes the final cleavage of H₂ to regenerate **XXXII** and the respective alkyl product.⁴⁹

Overall, the work presented by Harder and Hill highlights that the subtle structural differences between **XXXI** and **XXXII** result in vast differences in the reactivity profile of these hydride species.^{44, 47-49}

Since the isolation of the first molecular calcium hydride in 2006, a series of calcium hydrides supported by the same β -diketiminate ancillary ligand have also been reported.^{50, 51} A calcium hydride bearing a derivate of the bulky amidinate ligand system and the cyclopentadienyl ligand has also been reported within the literature.^{52, 53} However, the following Sections focus only on the extended reactivity of the solvent-free complex, **XXXII**, as is pertinent to the work presented in the following Chapters of this Thesis.

1.7.3 White Phosphorus Activation

The synthesis of organophosphanes and phosphorus-containing compounds is typically through activating white phosphorus (P_4), with common methodologies focusing on alkali-metal or transition metal reagents.^{54, 55} In comparison, the use of the earth-abundant Group 2 reagents for the functionalisation of P_4 is less intensively researched. In 2015, Hill et al. reported the first example of P_4 activation with organomagnesium reagents, providing a range of products containing P_n polyphosphide cages ($n = 4$ to 8).⁵⁴ Pertinent to our research is a report by Roesky et al., who later explores the reduction of white phosphorus with the calcium hydride species **XXXII** (Scheme 1.17).⁵⁵



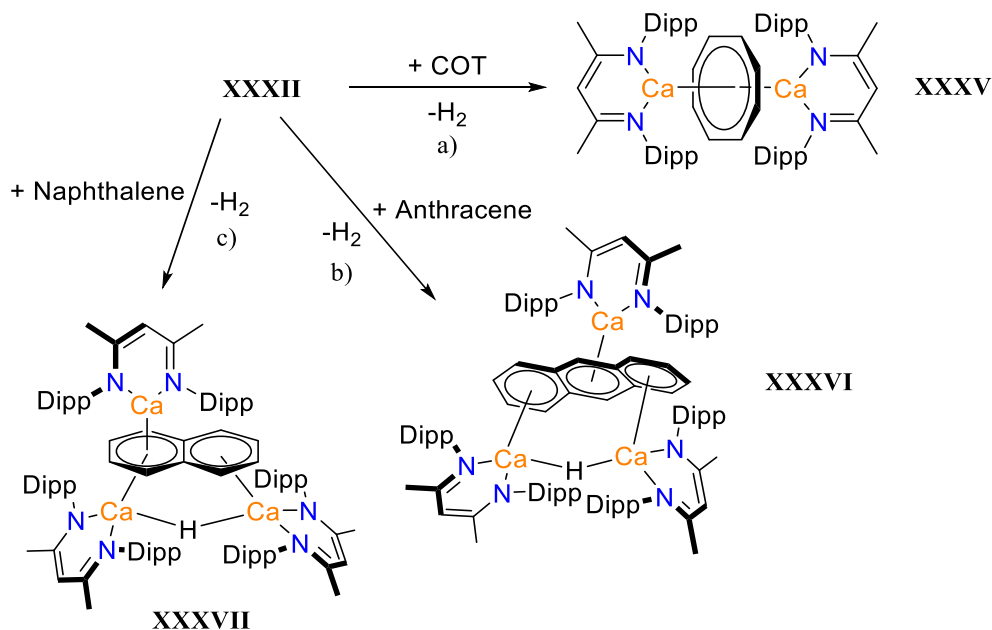
Scheme 1.17. Functionalisation of white phosphorus by **XXXII** to give **XXXIV**.

Monitoring of this reaction by $^{31}\text{P}\{^1\text{H}\}$ NMR spectroscopy alluded to two phosphorus-containing products in solution: the signal at $\delta_{\text{P}} -241.3$ ppm remains unidentified, but the broad signal at $\delta_{\text{P}} -87.7$ ppm was confirmed as a $[\text{P}_7]^{3-}$ Zintl ion cage decorated with three $[(\text{BDI}^{\text{Dipp}})\text{Ca}]^+$ units (**XXXIV**) through crystallographic analysis.⁵⁵ Variable temperature $^{31}\text{P}\{^1\text{H}\}$ NMR experiments showed the transformation of the peak centred at $\delta_{\text{P}} -87.7$ ppm into three new signals at $\delta_{\text{P}} -137.8$, $\delta_{\text{P}} -60.5$ and $\delta_{\text{P}} -40.9$ ppm, upon cooling a solution of **XXXIV** to -90 °C. Each new signal was tentatively assigned as one of the three phosphorus environments and was correlated to previous reports of $[\text{P}_7]^{3-}$ complexes, which also displayed three sets of resonances in the $^{31}\text{P}\{^1\text{H}\}$ NMR spectrum at low temperatures. No J -coupling values were obtained for the phosphorus signals of **XXXIV** due to the rapid rearrangement of the polyphosphorus cluster in solution.⁵⁵

1.7.4 Reduction of Aromatic and Polyaromatic Hydrocarbons

A later report describes several structurally characterised Group 2 complexes in the literature containing the $[\text{COT}]^{2-}$ (COT = 1,3,5,7-cyclooctatetraene) dianion.⁵⁶ These species were generated either through salt metathesis reactions, where the reduction of COT (-1.83 and -1.99 V vs SCE)³¹ was facilitated by a Group 1 metal or through the oxidation of the Group 2 metal centre.^{57, 58} In contrast, there were no reports on the direct reduction of COT to the $[\text{COT}]^{2-}$ dianion by a Group 2 hydride complex. Therefore, this study aimed to explore the reductive chemistry of Group 2 hydrides.⁵⁶

The reaction of **XXXII** with one equivalent of COT was observed to bubble, indicative of the release of H_2 gas and the formation of the inverse sandwich complex, **XXXV** (Scheme 1.18, a)).



Scheme 1.18. Two electron aromatisation of COT (a) and reduction of anthracene (b) and naphthalene (c) by **XXXII**.

The product was confirmed in the solution-state, where an ^1H NMR spectrum obtained of **XXXV** displayed a new β -diketiminate methine resonance in a 2:8 ratio with a singlet at δ_{H} 5.60 ppm, corresponding to the $[\text{COT}]^{2-}$ dianion. The structure was also crystallographically characterised and confirms the two-electron aromatisation of COT, computed to proceed *via* a series of polarised Ca–H/C=C insertion and σ –bond metathesis reactions.⁵⁶

This facile reduction of COT by **XXXII** was extended to the more challenging polyaromatic substrates, anthracene and naphthalene (–1.98 and –2.60 V vs SCE, respectively).^{59, 60} The reaction of **XXXII** with anthracene, (Scheme 1.18, b)), proceeds readily at room temperature, to afford the trinuclear complex, **XXXVI**. A single crystal X-ray diffraction experiment on crystals of **XXXVI** discloses one $[(\text{BDI}^{\text{Dipp}})\text{Ca}]^+$ unit coordinates to the central C_6 -ring of the reduced anthracene dianion, while the calcium centres of the other two $[(\text{BDI}^{\text{Dipp}})\text{Ca}]$ units are μ^1 -bridged by a hydride ligand and coordinate to the terminal rings from the opposing face of the $[\text{C}_{14}\text{H}_{10}]^{2-}$ ligand. The anthracene dianion is no longer planar,

exhibiting a dihedral angle of 26.5° and is consistent with the two-electron reduction of anthracene.⁶⁰

The reduction of naphthalene by **XXXII** (Scheme 1.18, c)) occurs over 60 days at room temperature to give **XXXVII** in poor yields, reflecting the more negative reduction potential of naphthalene in comparison to both COT and anthracene. The efficiency of the reaction could be improved, however, by adding an excess of naphthalene or directly heating **XXXII** and naphthalene in the solid-state at 80°C , followed by purification by sublimation. Like **XXXVI**, the solid-state structure of **XXXVII** revealed two different calcium environments, with the two calcium centres of $[(\text{BDI}^{\text{Dipp}})\text{Ca}-(\mu\text{-H})-\text{Ca}(\text{BDI}^{\text{Dipp}})]$ coordinate in an η^4 -fashion to the two rings of the naphthalene dianion, while the $[(\text{BDI}^{\text{Dipp}})\text{Ca}]^+$ unit coordinates to one of C_6 -rings on the opposing face of the $[\text{C}_{10}\text{H}_8]^{2-}$ ligand.⁶⁰

Though slow, the two-electron reduction of the challenging polyaromatic substrate, naphthalene, demonstrates the potential of these calcium hydrides to act as suitable reducing agents.

1.7.5 Synthesis and Reactivity of Molecular Strontium and Barium Hydrides

Prior to 2017, the only report of a strontium hydride was a strontium hydride cluster, described as contact ion pairs between a cationic amido strontium hydride cage and hydride anions, respectively.⁶¹ This starkly contrasts the smaller Group 2 elements, magnesium and calcium, for which there were already reported examples of discrete, molecular hydride complexes.⁶² The lack of reports on the isolation of analogous compounds for the larger strontium and barium ions is due to the bonding characteristics of Group 2 complexes: as the group is descended there is an increase in the ionic character and increase in bond lengths, therefore, heteroleptic complexes of the heavier Group 2 are more prone to the Schlenk-like redistribution pathways.²² As a result, larger anionic ancillary ligands with hard donor sites are generally

required to saturate the larger coordination sphere of the strontium and barium ions in comparison to magnesium and calcium.

Now, there are a total of two crystallographically characterised heteroleptic barium hydrides (**XXXVIII** and **XLb**) and three strontium hydrides (**XXXIX**, **XLa** and **XLI**) disclosed within the literature (Figure 1.6).^{45, 52, 62, 63} These species herein have been discussed in order of dates published within the literature.

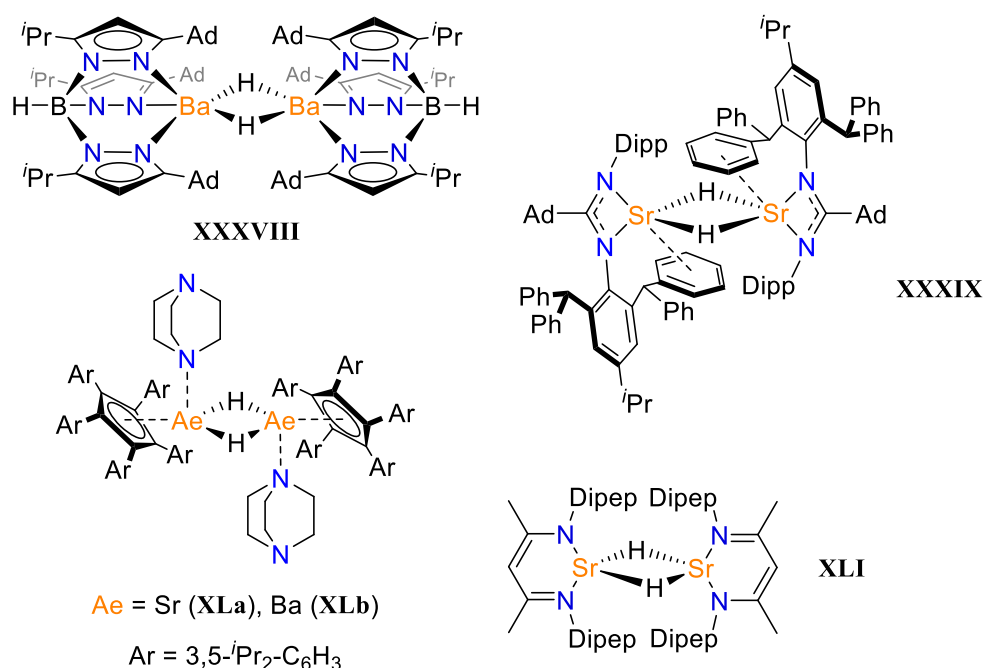
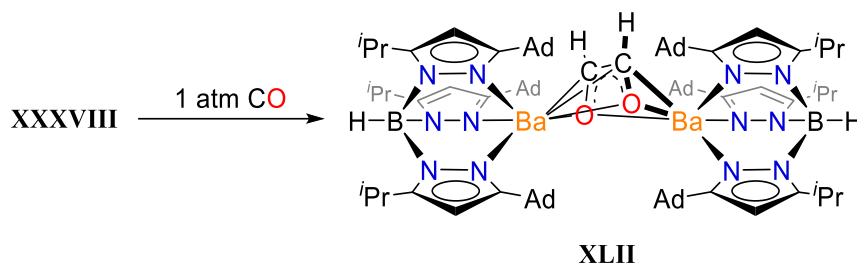


Figure 1.6. Overview of all characterised examples of strontium and barium hydrides (**XXXVIII** – **XLI**).

In 2017, Cheng reported the first discrete hydride complex of a larger Group 2 ion: a heteroleptic barium hydride (**XXXVIII**) supported by the widely utilised scorpionate ligand system, synthesised through hydrogenolysis of a heteroleptic barium alkyl precursor with H₂ gas.⁶² The barium centre within the alkyl complex was solvated by a THF molecule, attributed to the large ionic radii of the Ba²⁺ ion, however, solvent coordination is not observed within **XXXVIII** and demonstrates the sufficient steric protection of the tris(pyrazolyl)borate ligand to the barium metal centre.

Compound **XXXVIII** was found to react with both unsaturated $\text{C}\equiv\text{C}$ bonds and $\text{C}\equiv\text{O}$ bonds.⁶² For example, when exposed to one atmosphere of carbon monoxide, compound **XXXVIII** was rapidly generated a dimeric species where the two barium centres are bridged by the *cis*-ethene-diolate moiety (**XLII**) (Scheme 1.19).



Scheme 1.19. Reductive coupling of CO by **XXXVIII**.

This reactivity is reminiscent of previously published work, where β -diketiminato magnesium hydrides afford analogous reaction products *via* the reductive coupling of CO.³⁶

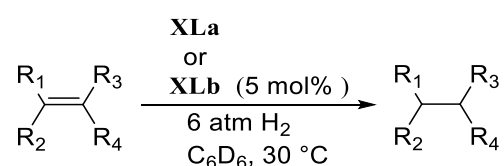
The same ancillary ligand was used to isolate a heteroleptic strontium alkyl complex. However, the subsequent hydrogenolysis reaction afforded a mixture of products, thus no molecular strontium hydride complex was structurally elucidated.⁶²

The following year, Jones reported the isolation of a molecular strontium hydride by utilising the bulky amidinate ancillary ligand (**XXXIX**) (Figure 1.6).⁶³ This complex was afforded through the σ -bond metathesis reaction between a heteroleptic strontium amide with PhSiH_3 after 1 hour at room temperature. The structure was confirmed in the solution-state as well through a single crystal X-ray diffraction experiment, where the solid-state structure was revealed as a dimer with two strontium centres *N,N*-chelated to the nitrogen atoms of the amidinate ligand and μ^2 -bridged by two hydride ligands. Unlike the solid-state structures of all Group 2 hydrides described thus far,^{32, 44, 62} each strontium centre within **XXXIX** displays metal-aryl interactions with a phenyl ring within the amidinate ancillary ligand, providing additional stability in place of coordinative saturation by donor solvent molecules. Despite this,

compound **XXXIX** was highly unstable, decomposing after 24 hours at room temperature in the solid-state, and within hours in the solution-state.⁶³

The work by Cheng and Jones was succeeded by the isolation of new strontium and barium hydrides supported by a bulky derivate of the polyhaptic, cyclopentadienyl ligand (**XLa** and **XLb**, respectively) (Figure 1.6).⁵² Both complexes were synthesised through the hydrogenolysis of an alkyl precursor complex, giving hydride complexes where DABCO (triethylenediamine) molecules solvated the large strontium and barium metal centres. Analogues of these hydrides were also reported in this work, for example a strontium hydride solvated by THF molecules, however, this species was not crystallographically characterised. A second derivative of the bulky cyclopentadienyl ligand was also synthesised and used for stabilisation of both strontium and barium hydride complexes, but due to poor quality of crystal data, these compounds have not been fully characterised in the solid-state.⁵²

Preliminary reactivity studies were conducted, where both **XLa** and **XLb** were found to catalytically hydrogenate alkenes, much like the calcium hydrides (**XXXI** and **XXXII**) discussed earlier in this Chapter (Scheme 1.20).⁵²



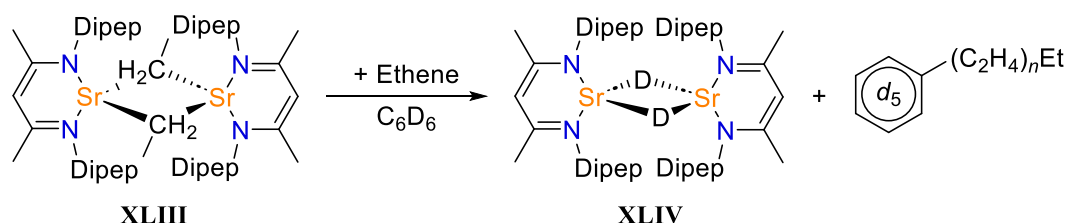
Scheme 1.20. General overview for the hydrogenation of alkenes by **XLa** or **XLb**.

Their capabilities to facilitate this catalytic reactivity were relatively high, and both **XLa** and **XLb** demonstrated an affinity for a broad scope of alkene-based substrates.

Pertinent to the work presented in this Thesis is the example of a molecular strontium hydride reported by Harder, which was supported by the BDI^{Dipep} (Dipep = 2,6-di-(3-pentyl) phenyl) ancillary ligand (**XLI**) (Figure 1.6).⁴⁵ This β -diketiminato ligand is a bulkier derivative

of the commonly utilised BDI^{Dipp} ligand framework, where the isopropyl groups have been exchanged for 3-pentyl chains. The heteroleptic strontium amide was first isolated and subsequently reacted with PhSiH_3 in hexane, where warming of the reaction mixture from -80°C to room temperature afforded **XLI** in average yields. Like the smaller calcium analogue, **XXXII**,⁴⁴ an X-ray diffraction experiment disclosed a dimeric structure where the strontium centres are μ^2 -bridged by hydride ligands and the absence of any metal-arene interaction of a phenyl group of the ligand or solvent coordination. The solid-state structure of **XLI** did display agostic interactions of a carbon of the 3-pentyl group to the strontium centre, completing the larger coordination sphere of strontium and demonstrating the relative flexibility of this new ligand *N*-substituent.⁴⁵

In line with the reactivity profile of the solvent-free calcium hydride, **XXXII** could react with the unsaturated substrate, ethene, to provide the respective strontium *n*-ethyl complex (**XLIII**) within minutes at room temperature, which could then facilitate the nucleophilic alkylation of benzene (Scheme 1.21).⁴⁵



Scheme 1.21. Stoichiometric alkylation of benzene by **XLIII**.

In contrast to **XXXII**, Schlenk-like redistribution of the alkyl intermediate to the homoleptic $[(\text{BDI}^{\text{Dipep}})_2\text{Sr}]$ was not observed, and therefore, it was postulated that this chemistry could follow a catalytic regime. Unfortunately, this reactivity was not selective, with ethene polymerisation and oligomerisation revealed as competing pathways. Oligomerisation afforded strontium *n*-butyl, *n*-hexyl, and higher oligomers, which could all facilitate the

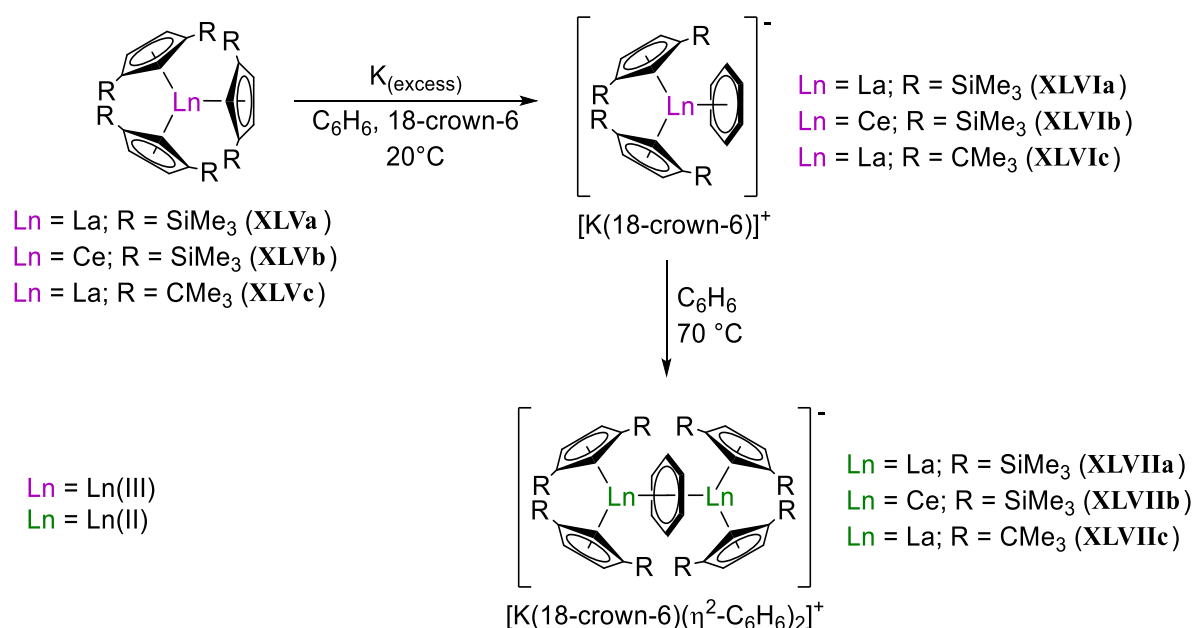
stoichiometric alkylation of benzene to give a mixture of *n*-alkylbenzene products and the deuteride [(BDI^{Dipep})SrD]₂ (**XLIV**).⁴⁵

Lastly, **XLI** was considerably more stable in the solution-state compared to Jones' species, **XXXIX**,⁶³ highlighting the suitability of derivatives of the β-diketiminato ancillary ligand for stabilisation of heteroleptic hydride complexes of larger Group 2 ions.^{22, 45}

1.8 Benzene Reduction by Organolanthanide Complexes

Throughout research covered within this Thesis, we found that our Ln(II) complexes could activate benzene. Therefore, a brief overview of f-element reduction of benzene will be covered herein.

In 1996, Lappert reported on the reduction of benzene by trivalent lanthanide cyclopentadienyl complexes and potassium metal to afford separated ion pairs in which they structurally characterised as being two Ln(III) centres (Ln = La or Ce) bridged by a 1,4-cyclohexa-2,5-diene dianion (Scheme 1.22).⁶⁴ This was corroborated in the solid-state by X-ray diffraction studies on single crystals of **XLVIa** and **XLVIb**, where the C=C bond lengths at the C2 and C5 positions of the bridging C₆H₆ ring are considerably shorter (1.358(10) and 1.337(11) Å) than the remaining C–C bond lengths (1.447(10) – 1.480(9) Å).⁶⁴

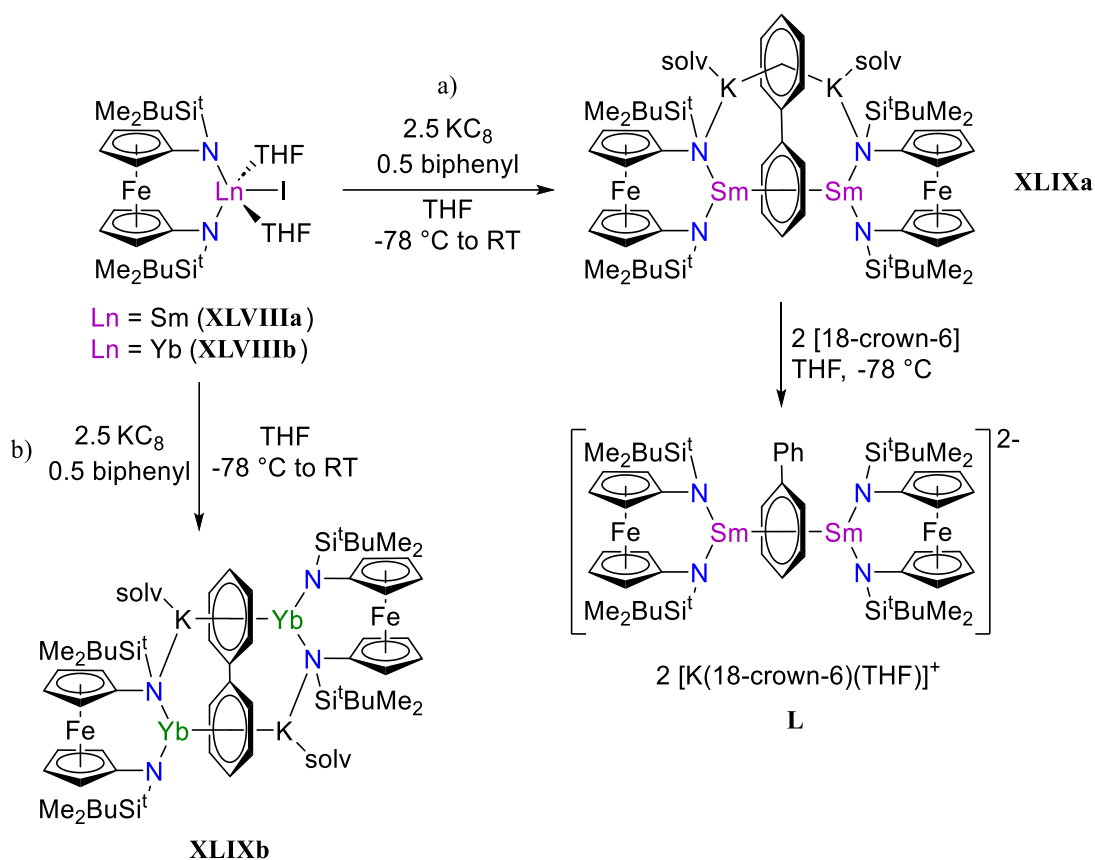


Scheme 1.22. Reduction of benzene by compounds **XLVa**, **XLVb** and **XLVc** in the presence of a potassium reducing agent.

This work was succeeded by a second report, where after the reduction to give **XLVla**, **XLVlb** and **XLVlc**, these compounds could be heated in C_6H_6 solvent to afford new lanthanide-containing products, where two lanthanide centres were bridged by a nearly planar C_6H_6 moiety (**XLVIIa**, **XLVIIb** and **XLVIIc**, respectively).⁶⁵ Using characterisation techniques such as UV–Vis spectroscopy, electron paramagnetic resonance (EPR) spectroscopy, mass spectrometry, and multinuclear NMR spectroscopy, Lappert structurally elucidated the isolation of the first example of a subvalent lanthanum complex: two La(II) ions are bridged by a monoanionic benzenide ligand. This structure was confirmed in the solid-state by crystallographic analysis, where the reported C–C bond lengths within the benzenide ligand of **XLVIIc** ranged from 1.42(1) to 1.45(1) Å.⁶⁵

Almost 20 years later, Diaconescu reported a series of Ln(III) complexes (Ln = La, Lu, Gd, Dy, Er), where reduction by KC_8 in the presence of biphenyl afforded a dimeric species with two Ln(III) ions $\mu\text{-}\eta^6\text{:}\eta^6\text{-}$ interacted with the tetra-reduced $\text{C}_6\text{-ring}$ of a biphenyl moiety.⁶⁶

This work was later extended to the “classically” stable Ln(II) ions, samarium and ytterbium, which will be the focus of this discussion herein (Scheme 1.23).⁶⁷



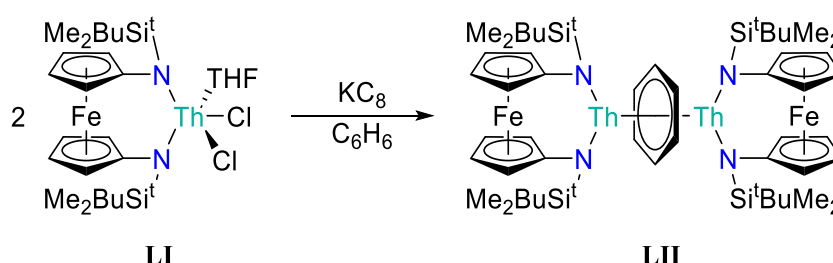
Scheme 1.23. Reduction of biphenyl by a) compound **XLVIIIa** and b) compound **XLVIIIb** in the presence of a potassium reducing agent.

The reaction products from the reduction of ytterbium and samarium precursors were structurally characterised by a range of characterisation techniques: in the case of samarium (Scheme 1.23, a)), it was concluded that the product (**XLIXa**) comprised of two Sm(III) ions bridged by a biphenyl tetraanion, whereby the C–C bond lengths of the Sm–bound phenyl ring ranged from 1.421(5) to 1.476(1) Å (unbound ring C–C average: 1.41 Å).⁶⁷

The reduction of the ytterbium precursor, **XLVIIIb** (Scheme 1.23, b)) resulted in a structurally different ytterbium-containing product (**XLIXb**). The product was still a dimer but was characterised as two Yb(II) ions bridged by a reduced biphenyl moiety, with each Yb(II)

centre η^6 -binding to one terminal C₆-ring from opposing sides of the biphenyl ligand. The solid-state data disclosed the phenyl rings consist of four C–C bond lengths ranging between 1.412(1) and 1.471(9) Å with two more localised double bonds (1.376(6) and 1.378(8) Å) and a short C_{ipso}–C_{ipso} bond distance of 1.396(4) Å (**XLIXa**, C_{ipso}–C_{ipso}: 1.413(4) Å), confirming a reduced biphenyl dianion, where the charge is delocalised over both C₆-rings.⁶⁷

A final species pertinent to this Thesis is the isolation of the dimeric thorium(IV) complex containing the parent tetraanionic benzene (**LII**), synthesised from the reduction of **LI** by KC₈ in C₆H₆ solvent (Scheme 1.24).⁶⁸



Scheme 1.24. Reduction of benzene to give the [C₆H₆]⁴⁺ tetraanion.

The product (**LII**) was structurally characterised in the solid-state, where the C–C bond lengths of the tetra-reduced benzene ring were reported as ranging from 1.441(7) to 1.459(7) Å, and further spectroscopic analysis in collaboration with computation techniques confirmed the 4+ oxidation state of the Th metal centres.⁶⁸

All these examples demonstrate the reduction of benzene and its derivatives to a range of anions. The first example gave Ln(III) products containing the 1,4-cyclohexa-2,5-diene dianion followed by Ln(II) species bridged by the monoanionic benzenide ligand. In contrast, the following example gave either the Sm(III) biphenyl tetraanion or the Yb(II) biphenyl dianion, respectively.^{64, 65, 67} Finally, **LII** is the only example of a metal complex containing the benzene tetraanion.⁶⁸ This is attributed to the highly negative reduction potential of benzene (–3.42 V vs SCE)⁶⁹ and the lack of sufficiently potent reducing agents. That said, it is important

to highlight that each reduction occurred in the presence of a strong Group 1 reducing agent, and there are currently no reports on the reduction of benzene or its derivatives where no external reducing agent is present in the reaction mixture.

1.9 Conclusion and Proposal Aims

Since the isolation of the first divalent lanthanide hydride complex in a landmark report by Takats in 1999, only a total of six molecular lanthanide(II) hydrides have been structurally characterised within the literature, and all six systems are based on ytterbium(II). Therefore, the aim of this Thesis is to investigate the synthesis of new molecular lanthanide hydrides in which the lanthanide centres are in the 2+ oxidation state.

Chapter Two focuses on synthesising new ytterbium(II) hydrides, utilising a previously reported BDI^{Dipep} ligand and a new derivative of the β -diketiminato ligand system, BDI^{Dicyp}. This allows for comparisons with the current literature with respect to known lanthanide(II) redox, σ -bond metathesis and insertion chemistry, as described in Chapter One. As there is ample evidence for considerable similarities in the chemistry of ytterbium(II) complexes and complexes containing the Group 2 ion, calcium, comparative studies between β -diketiminato ytterbium(II) hydrides and analogous β -diketiminato calcium hydrides will be made where deemed appropriate.

Chapter Three explores synthesising the first examples of a molecular europium(II) hydride. This work begins as an extension of Group 2 chemistry, following similar methodologies that allowed for the isolation of a β -diketiminato-based strontium hydride. However, it was established that the isolation of an analogous BDI^{Dipep} Eu(II) hydride might not be that simple. This Chapter then focuses on the synthesis of a Eu(II) hydride species using three different derivatives of the β -diketiminato ancillary ligand, followed by a comparative

introduction to the reactivity of these complexes with respect to known ytterbium(II) redox, σ -bond metathesis and insertion chemistry.

Chapter Four diverges from the chemistry presented in the previous two Chapters. The initial aim was synthesising the first example of a samarium(II) hydride supported by a β -diketiminate ancillary ligand, thought to be possible because two structurally characterised barium hydrides are reported within the literature. Instead, this Chapter focuses on the reduction chemistry of a monomeric samarium(II) alkyl, investigating the ability of this complex to reduce benzene and its derivatives, affording inverse sandwich complexes containing the respective tetra-reduced arene. Finally, this Chapter continues to explore the reduction chemistry of the Sm(II) alkyl as well as the benzene tetraanion complex.

2.0 References

1. W. J. Evans, *Inorg. Chem.*, **2007**, 46 (9), 3435-3449.
2. K. W. Hans, *Geochim. Cosmochim. Acta.*, **1995**, 59 (7), 1217-1232.
3. W. J. Evans, *Adv. Organomet. Chem.*, **1985**, 24, 131-177.
4. P. F. Lang and C. B. Smith, *J. Chem. Ed.*, **2010**, 87 (8), 875-881.
5. W. J. Evans, *Polyhedron*, **1987**, 6 (5), 803-835.
6. J. C. Wedal and W. J. Evans, *J. Am. Chem. Soc.*, **2021**, 143 (44), 18354-18367.
7. W. J. Evans, J. H. Meadows, A. L. Wayda, W. E. Hunter and J. L. Atwood, *J. Am. Chem. Soc.*, **1982**, 104 (7), 2008-2014.
8. M. Ephritikhine, *Chem. Rev.*, **1997**, 97 (6), 2193-2242.
9. W. J. Evans, I. Bloom, W. E. Hunter and J. L. Atwood, *J. Am. Chem. Soc.*, **1983**, 105 (5), 1401-1403.
10. F. T. Edelmann, *Chem. Soc. Rev.*, **2012**, 41 (23), 7657-7672.
11. A. A. Trifonov, G. G. Skvortsov, D. M. Lyubov, N. A. Skorodumova, G. K. Fukin, E. V. Baranov and V. N. Glushakova, *Chem. Eur. J.*, **2006**, 12 (20), 5320-5327.
12. A. A. Trifonov, *Coord. Chem. Rev.*, **2010**, 254 (11-12), 1327-1347.
13. G. A. Molander and J. A. C. Romero, *Chem. Rev.*, **2002**, 102 (6), 2161-2186.
14. G. M. Ferrence, R. McDonald and J. Takats, *Angew. Chem. Int. Ed.*, **1999**, 38 (15), 2233-2237.
15. C. Ruspici, J. Spielmann, and S. Harder, *Inorg. Chem.*, **2007**, 46 (13), 5320-5326.
16. I. V. Basalov, D. M. Lyubov, G. K. Fukin, A. S. Shavyrin, and A. A. Trifonov, *Angew. Chem. Int. Ed.*, **2012**, 51 (14), 3444-3447.
17. G. M. Richardson, I. Douair, S. A. Cameron, J. Bracegirdle, R. A. Keyzers, M. S. Hill, L. Maron and M. D. Anker, *Nat. Comm.*, **2021**, 12 (1), 1-7.
18. X. Shi, P. Deng, T. Rajeshkumar, L. Zhao, L. Maron and J. Cheng, *Chem. Comm.*, **2021**, 57 (78), 10047-10050.
19. Q. Wen, B. Feng, L. Xiang, X. Leng and Y. Chen, *Inorg. Chem.*, **2021**, 60 (18), 13913-13919.
20. T. K. Panda, A. Zulys, M. T. Gamer, and P. W. Roesky, *J. Organomet. Chem.*, **2005**, 690 (23), 5078-5089.
21. T. X. Gentner, B. Rösch, K. Thum, J. Langer, G. Ballmann, J. Pahl, W. A. Donaubauer, F. Hampel and S. Harder, *Organomet.*, **2019**, 38 (12), 2485-2493.
22. A. G. Avent, M. R. Crimmin, M. S. Hill and P. B. Hitchcock, *Dalton Trans.*, **2005**, (2), 278-284.
23. M. N. Bochkarev, I. L. Fedushkin, A. A. Fagin, T. V. Petrovskaya, J. W. Ziller, R. N. R. Broomhall-Dillard and W. J. Evans, *Angew. Chem. Int. Ed.*, **1997**, 36 (1-2), 133-135.
24. W. J. Evans, N. T. Allen and J. W. Ziller, *J. Am. Chem. Soc.*, **2000**, 122 (47), 11749-11750.
25. M. R. MacDonald, J. W. Ziller and W. J. Evans, *J. Am. Chem. Soc.*, **2011**, 133 (40), 15914-15917.
26. M. R. MacDonald, J. E. Bates, M. E. Fieser, J. W. Ziller, F. Furche and W. J. Evans, *J. Am. Chem. Soc.*, **2012**, 134 (20), 8420-8423.
27. M. R. MacDonald, J. E. Bates, J. W. Ziller, F. Furche and W. J. Evans, *J. Am. Chem. Soc.*, **2013**, 135 (26), 9857-9868.
28. M. N. Bochkarev and A. A. Fagin, *Chem. Eur. J.*, **1999**, 5 (10), 2990-2992.

29. W. J. Evans, T. A. Ulibarri and J. W. Ziller, *J. Am. Chem. Soc.*, **1988**, 110 (20), 6877-6879.
30. W. J. Evans, S. L. Gonzales and J. W. Ziller, *J. Am. Chem. Soc.*, **1994**, 116 (6), 2600-2608.
31. G. M. Richardson, I. Douair, S. A. Cameron, L. Maron and M. D. Anker, *Chem. Eur. J.*, **2021**, 27 (52), 13144-13148.
32. S. Harder and J. Brettar, *Angew. Chem. Int. Ed.*, **2006**, 45 (21), 3474-3478.
33. J. P. White, H. Deng and S. G. Shore, *Inorg. Chem.*, **1991**, 30 (10), 2337-2342.
34. C. Eaborn, P. B. Hitchcock, K. Izod and J. D. A. Smith, *J. Am. Chem. Soc.*, **1994**, 116 (26), 12071-12072.
35. G. M. Ferrence and J. Takats, *J. Organomet. Chem.*, **2002**, 647 (1-2), 84-93.
36. M. D. Anker, C. E. Kefalidis, Y. Yang, J. Fang, M. S. Hill, M. F. Mahon and L. Maron, *J. Am. Chem. Soc.*, **2017**, 139 (29), 10036-10054.
37. S. Harder, *Angew. Chem. Int. Ed.*, **2004**, 43 (20), 2714-2718.
38. M. Vatamanu, G. Stojcevic and M. C. Baird, *J. Am. Chem. Soc.*, **2008**, 130 (2), 454-456.
39. I. V. Basalov, D. M. Lyubov, G. K. Fukin, A. V. Cherkasov and A. A. Trifonov, *Organomet.*, **2013**, 32 (5), 1507-1516.
40. G. M. Richardson, J. Howarth, M. J. Evans, A. J. Edwards, S. A. Cameron and M. D. Anker, *J. Coord. Chem.*, **2022**, 75 (11-14), 1954-1966.
41. W. J. Evans, I. Bloom, W. E. Hunter and J. L. Atwood, *Organomet.*, **1985**, 4 (1), 112-119.
42. S. Kriek and M. Westerhausen, *Inorganics*, **2017**, 5 (1), 2304-6740.
43. R. Shannon, *Acta Cryst. A.*, **1976**, 32 (5), 751-767.
44. A. S. Wilson, M. S. Hill, M. F. Mahon, C. Dinoi and L. Maron, *Science*, **2017**, 358 (6367), 1168-1171.
45. B. Rösch, T. X. Gentner, H. Elsen, C. A. Fischer, J. Langer, M. Wiesinger and S. Harder, *Angew. Chem. Int. Ed.*, **2019**, 58 (16), 5396-5401.
46. M. M. D. Roy, A. A. Omaña, A. S. S. Wilson, M. S. Hill, S. Aldridge and E. Rivard, *Chem. Rev.*, **2021**, 121 (20), 12784-12965.
47. J. Spielmann and S. Harder, *Chem. Eur. J.*, **2007**, 13 (32), 8928-8938.
48. J. Spielmann, F. Buch and S. Harder, *Angew. Chem.*, **2008**, 120 (49), 9576-9580.
49. A. S. S. Wilson, C. Dinoi, M. S. Hill, M. F. Mahon and L. Maron, *Angew. Chem. Int. Ed.*, **2018**, 57 (47), 15500-15504.
50. A. Causero, G. Ballmann, J. Pahl, C. Färber, J. Intemann and S. Harder, *Dalton Trans.*, **2017**, 46 (6), 1822-1831.
51. B. Rösch, T. X. Gentner, J. Langer, C. Färber, J. Eyselein, L. Zhao, C. Ding, G. Frenking and S. Harder, *Science*, **2021**, 371 (6534), 1125-1128.
52. X. Shi, G. Qin, Y. Wang, L. Zhao, Z. Liu and J. Cheng, *Angew. Chem. Int. Ed.*, **2019**, 58 (13), 4356-4360.
53. A. Causero, G. Ballmann, J. Pahl, H. Zijlstra, C. Färber and S. Harder, *Organomet.*, **2016**, 35 (19), 3350-3360.
54. M. Arrowsmith, M. S. Hill, A. L. Johnson, G. Kociok-Köhn and M. F. Mahon, *Angew. Chem. Int. Ed.*, **2015**, 54 (27), 7882-7885.
55. R. Yadav, M. Weber, A. K. Singh, L. Münzfeld, J. Gramüller, R. M. Gschwind, M. Scheer and P. W. Roesky, *Chem. Eur. J.*, **2021**, 27 (56), 14128-14137.

56. M. S. Hill, M. F. Mahon, A. S. S. Wilson, C. Dinoi, L. Maron and E. Richards, *Chem. Comm.*, **2019**, 55 (40), 5732-5735.
57. S. J. Bonyhady, S. P. Green, C. Jones, S. Nembenna and A. Stasch, *Angew. Chem. Int. Ed.*, **2009**, 48 (16), 2973-2977.
58. M. D. Walter, G. Wolmershäuser and H. Sitzmann, *J. Am. Chem. Soc.*, **2005**, 127 (49), 17494-17503.
59. S. Bank and D. A. Juckett, *J. Am. Chem. Soc.*, **1976**, 98 (24), 7742-7746.
60. A. S. S. Wilson, C. Dinoi, M. S. Hill, M. F. Mahon, L. Maron and E. Richards, *Angew. Chem. Int. Ed. Engl.*, **2020**, 59 (3), 1232-1237.
61. B. Maitland, M. Wiesinger, J. Langer, G. Ballmann, J. Pahl, H. Elsen, C. Färber and S. Harder, *Angew. Chem. Int. Ed.*, **2017**, 56 (39), 11880-11884.
62. X. Shi, C. Hou, C. Zhou, Y. Song and J. Cheng, *Angew. Chem. Int. Ed.*, **2017**, 56 (52), 16650-16653.
63. C. N. De Bruin-Dickason, T. Sutcliffe, C. Alvarez Lamsfus, G. B. Deacon, L. Maron and C. Jones, *Chem. Comm.*, **2018**, 54 (7), 786-789.
64. M. C. Cassani, Y. K. Gun'ko, P. B. Hitchcock and M. F. Lappert, *Chem. Comm.*, **1996**, (16), 1987-1988.
65. M. C. Cassani, D. J. Duncalf and M. F. Lappert, *J. Am. Chem. Soc.*, **1998**, 120 (49), 12958-12959.
66. W. Huang, J. J. Le Roy, S. I. Khan, L. Ungur, M. Murugesu and P. L. Diaconescu, *Inorg. Chem.*, **2015**, 54 (5), 2374-2382.
67. Y. Xiao, X. K. Zhao, T. Wu, J. T. Miller, H. S. Hu, J. Li, W. Huang and P. L. Diaconescu, *Chem. Sci.*, **2021**, 12 (1), 227-238.
68. C. Yu, J. Liang, C. Deng, G. Lefèvre, T. Cantat, P. L. Diaconescu and W. Huang, *J. Am. Chem. Soc.*, **2020**, 142 (51), 21292-21297.
69. J. Mortensen and J. Heinze, *Angew. Chem. Int. Ed.*, **1984**, 23 (1), 84-85.

Chapter Two

Synthesis and Reactivity of Ytterbium(II) Hydrides

2.1 Introduction

We recently reported that the ytterbium(II) hydride **XXV** could react with ethene and propene at room temperature, generating the ytterbium(II) *n*-ethyl (**XXVIa**) and -propyl (**XXVIb**) intermediates, respectively, which could then facilitate the catalytic nucleophilic alkylation of benzene.¹ Despite this, further stoichiometric reactivity studies with a variety of unsaturated substrates were hindered by the Schlenk-type redistribution to the unreactive, homoleptic Yb(II) complex, [(BDI^{Dipp})₂Yb].² To overcome the Schlenk-type redistribution, the ligand system can be altered to provide the metal centre with greater kinetic stability.

Several *N*-substituents other than Dipp have been placed on the β-diketiminate framework, providing varying degrees of steric protection to the metal centre.³ It was important that the selected substituent provided more steric protection than Dipp to block the redistribution pathway, but not so much that it would render our well-defined lanthanide(II) hydride unreactive. It has been demonstrated within the literature that the additional stability provided by donor THF molecules to the Yb(II) centre in **XXIII** results in a less reactive complex in comparison to our analogous, low-coordinate species, **XXV**.^{1, 4-6} Therefore, the selected substituent should also provide enough kinetic stability for our desired heteroleptic hydride complexes without the need for coordination of donor molecules. It was also necessary to select a chemically inert substituent, as well as synthetically simple.

As outlined within Chapter One, there are reports on the similarities between both the divalent lanthanide ions and Group 2 ions, including the successful utilisation of the β-

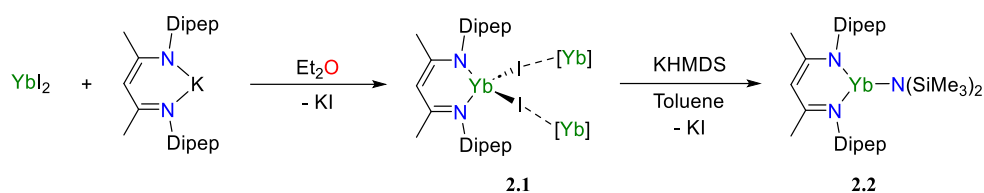
diketiminat ligand for molecular hydride chemistry.^{1, 2, 5, 7, 8} In 2019, Harder introduced the synthesis of a new ligand, BDI^{Dipep} (Dipep = 2,6-di-(3-pentyl)phenyl), in which the carbon chain length of the phenyl ring has been increased, for the stabilisation of a low-valent magnesium centre.³ In the following years, he reported the same ligand for stabilising a variety of calcium compounds, including a heteroleptic calcium hydride.⁹⁻¹¹

As the divalent ytterbium ion is similar in size to calcium (Yb²⁺: 1.14 Å, Ca²⁺: 1.12 Å),^{2, 12} the β-diketiminat ligand containing this Dipep substituent becomes a viable starting point for the synthesis of a new, low-coordinate ytterbium(II) hydride.

2.2 Synthesis of [(BDI^{Dipep})YbH]₂

2.2.1 Synthesis *via* [(BDI^{Dipep})YbI]₂

The synthesis of this new hydride complex deviated from the methodology used to generate **XXV** but was analogous to the synthetic route employed by Takats (**XI**) and Chen (**XXVIII**).^{1, 13-15} Here, a heteroleptic ytterbium iodide (**2.1**) was first synthesised from the reaction of YbI₂ and the potassium salt of the BDI^{Dipep} ligand (Scheme 2.1). This reaction was conducted in diethyl ether to afford a red solution with a pale precipitate after 48 hours at room temperature, which was dried under vacuum, extracted with toluene, filtered and re-dried *in vacuo* to provide the crude product as a red powder. Multinuclear NMR analysis concluded that the BDI^{Dipep} framework provided enough steric stability, such that no coordination of a solvent molecule to the ytterbium metal centre was observed, by the absence of the quartet at ca. δ_H 3.26 ppm or a signal at ca. δ_H 3.57 ppm, characteristic of Et₂O or THF solvent, respectively.



Scheme 2.1. Synthesis overview to form a heteroleptic iodide complex (**2.1**), which is a coordinated polymer in the solid-state. Each iodide ligand is shown to coordinate to a second $[(\text{BDI}^{\text{Dipep}})\text{YbI}]$ unit, denoted $[\text{Yb}]$. This is followed by synthesis of a heteroleptic ytterbium(II) amide (**2.2**).

A single crystal X-ray diffraction experiment on single crystals of **2.1** obtained from a saturated hexane solution disclosed the heteroleptic ytterbium iodide to have a mononuclear constitution within the asymmetric unit and is four-coordinate, with two contacts made up by the β -diketiminato ligand and two provided by iodide ligands (Figure 2.1, a)).

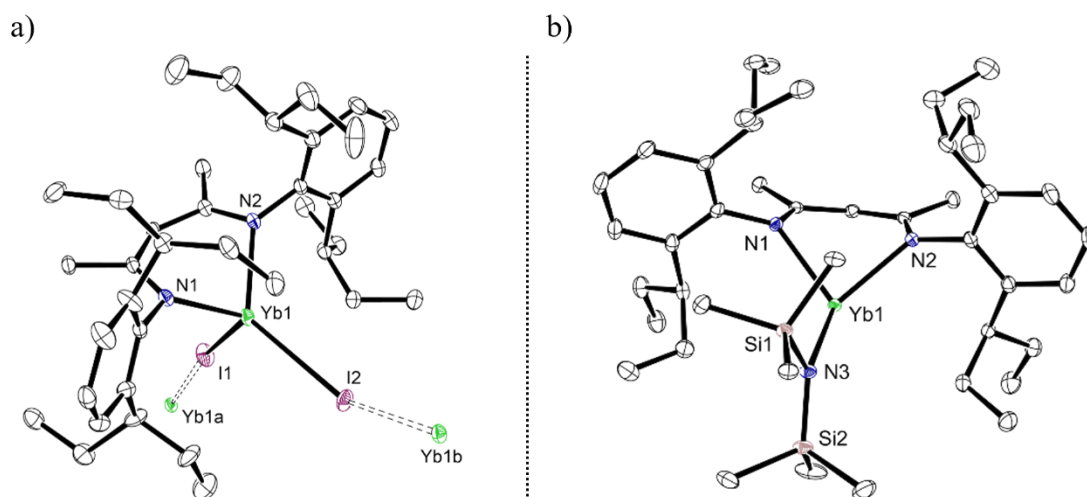


Figure 2.1. Ortep representations (30% probability ellipsoids) of compound **2.1** (left) and compound **2.2** (right). Hydrogen atoms have been omitted for clarity. Selected bond lengths (Å) and angles (°): **2.1**: Yb1–I1 3.1089(2), Yb1–I2 3.063(1), Yb1–N1 2.329(3), Yb1–N2 2.325(3), I1–Yb1–I2 144.89(1), I1–Yb1–N1 102.99(7), I1–Yb1–N2 105.68(7), N1–Yb1–N2 85.9(1), Yb1a–I1–Yb1 171.32(2), Yb1b–I2–Yb1 147.92(3). **2.2**: Yb1–N1 2.366(2), Yb1–N2 2.366(2), Yb1–N3 2.354(2), N1–Yb1–N2 85.53(6), N1–Yb1–N3 117.43(6), N2–Yb1–N3 127.85(6).

The Yb1–N bonds lengths are 2.329(3) and 2.325(3) Å, and the Yb1–I bond lengths are 3.1089(2) and 3.063(1) Å, respectively, and are all within the range for other divalent ytterbium iodide complexes bearing β -diketiminato- and amidinate-based ligands (Yb–N: 2.369(1) –

2.449(7) Å, Yb–I: 3.0946(14) – 3.298(1) Å).^{13, 16–19} Each iodide interacts further with a second ytterbium(II) centre of a second [(BDI^{Dipep})YbI] unit, resulting in a polymeric structure, which contrasts the geometry of other reported examples of dimeric Yb(II) iodides, which display μ^2 –bridging of the two iodide ligands to two ytterbium(II) centres, with minor exceptions.¹⁶

The subsequent metathesis between **2.1** and KHMDS was carried out in toluene, where stirring the reaction mixture for 48 hours at room temperature gave the respective monomeric amido complex **2.2**, after workup (Scheme 2.1). The structure was confirmed in the solution-state by the appearance of the methine peak of the β –diketiminato ligand in a 1:18 ratio with a signal situated at δ_{H} 0.22 ppm, corresponding to the methyl of the N(SiMe₃)₂ ligand. Crystallisation from a saturated toluene solution provided **2.2** as brown plates, allowing for structural characterisation in the solid-state through an X–ray diffraction experiment (Figure 2.1, b)).

The coordination sphere of the Yb(II) centre in **2.2** is made up by three *N*–substituents, two being the κ^2 –*N,N*–amidinato contacts (Yb–N: 2.366(2) Å) of the BDI^{Dipep} and the third by the terminal bis(trimethylsilyl)amide (2.354(2) Å), with Yb–N bond lengths consistent with the solvent-free, BDI^{Dipp} analogue, **XXV** (2.347(2), 2.344(3) and 2.321(3) Å, respectively).¹ In the asymmetric unit, the Yb(II) centre of **2.2** displays a distorted trigonal planar geometry, however, a fourth intermolecular contact is present between the Yb(II) centre and the methyl of the N(SiMe₃)₂ functionality of a second [(BDI^{Dipep})YbN(SiMe₃)₂] monomer. This results in a pseudo polymeric structure and contrasts with what is observed with **XXIV**, which is tetrameric in the solid-state.¹

Solvent coordination was not observed for **2.2**, as demonstrated in both ¹H NMR spectroscopy and crystallographic analysis; however, it should be noted that the stability in ethereal solvents themselves was not investigated. In the case of **XXV**, solvent coordination

could occur simply from THF or diethyl ether vapours residing in the nitrogen atmosphere of the glovebox, which was not observed for **2.2**, suggesting this *N*-Dipep substituent in collaboration with the silyl-amido functionality provides increased steric protection of the ytterbium(II) centre towards ethereal solvents, eliminating the need for a possible fourth contact for stability.

It was still possible to afford the undesired homoleptic species during syntheses, albeit to a much lower extent compared to the synthesis of **XXV**, and the impurity could be easily washed away with hexane but at the cost of lower yields of **2.2**. The original homoleptic species contains a four-coordinate Yb(II) centre, with *N,N*-chelation from two BDI^{Dipp} ligands.² This new homoleptic species (**2.3**) only contains three contacts to make up the primary coordination sphere of the ytterbium centre; two contacts are provided by the nitrogen atoms of one BDI^{Dipep} framework bonded in a bidentate *N,N*-binding mode, the third contact is provided by the second BDI^{Dipep} unit κ^1 -bonding through one *N*-substituent of the β -diketimate ligand (Figure 2.2).

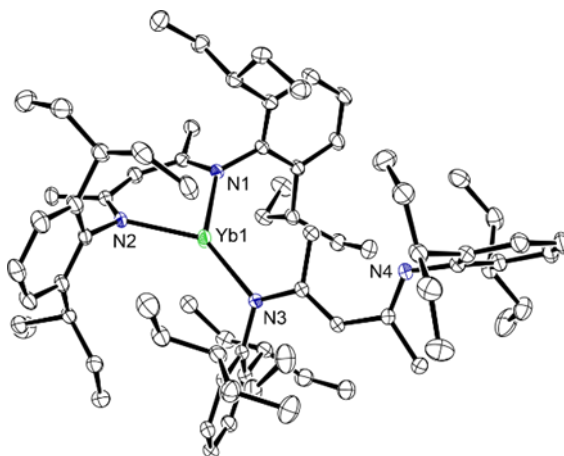
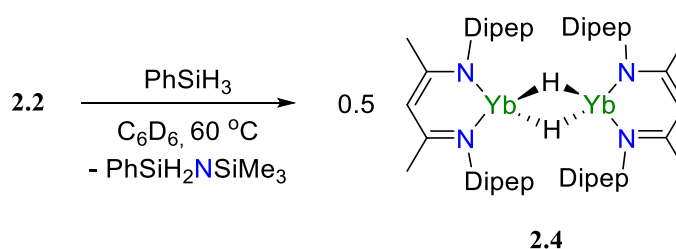


Figure 2.2. Ortep representations (30% probability ellipsoids) of compound **2.3**. Hydrogen atoms have been omitted for clarity. Selected bond lengths (Å) and angles (°): Yb1–N1 2.345(2), Yb1–N2 2.329(2), Yb1–N3 2.316(2), N3–C42 1.364(3), N3–C62 1.430(3), N4–C44 1.294(4), N4–C46 1.409(3), N1–Yb1–N2 86.77(7), N1–Yb1–N3 133.83(8), N2–Yb1–N3 139.00(8).

The N3–C_{Dipep} and N4–C_{Dipep} bond lengths are 1.4303(3) and 1.409(3) Å, respectively, and are in the range for N–C single bonds, while the N4–C44 bond length is significantly shorter at 1.294(4) Å, sitting in the range for N=C double bonds (1.27 – 1.31 Å), resulting in an imine-like structure. It is postulated that the structural differences of the homoleptic species (**2.3**) are due to the increased steric bulk of the BDI^{Dipep} ancillary ligand and the likelihood that the ligand framework is now too large that the small Yb(II) metal centre cannot accommodate four Yb–N contacts provided by two β–diketiminato scaffolds. It should be noted that an analogous homoleptic species was also isolated for calcium with this same BDI^{Dipep} ligand.¹¹

An initial attempt at synthesising the new low-coordinate ytterbium hydride was conducted in a J. Youngs tap NMR tube and monitored *via* ¹H NMR spectroscopy. The addition of ten equivalents of phenylsilane to a red C₆D₆ solution of **2.2** provided complete conversion to a new ytterbium-containing product (**2.4**) after heating the reaction mixture at 60°C for 24 hours (Scheme 2.2).



Scheme 2.2. Synthesis overview to form [(BDI^{Dipep})YbH]₂.

The methine resonance for **2.2** situated at δ_{H} 4.80 ppm was seen to shift to δ_{H} 4.74 ppm, concurrent with the growth of a new hydride signal at δ_{H} 9.08 ppm with Yb–H satellites (¹J_{YbH} = 418 Hz), characteristic of the formation of the dimeric hydride species, **2.4** (Figure 2.3).

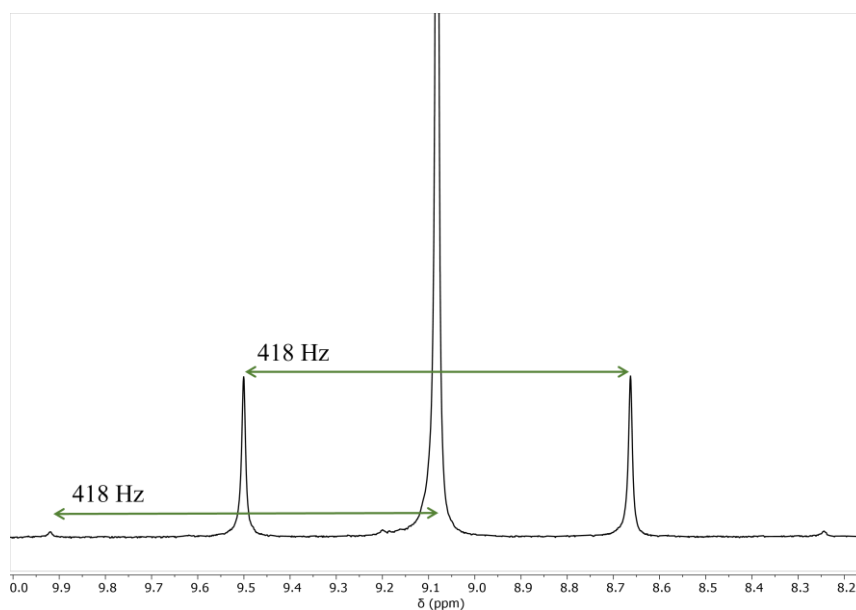


Figure 2.3. Close-up of the ^1H NMR spectrum (500 MHz, C_6D_6) of **2.4**, displaying the Yb–H resonance and $^1J_{\text{YbH}}$ coupling values.

The δ_{H} shift of this Yb–H resonance is consistent with other hydride species containing Yb(II) centres μ^2 -bridged by two hydride ligands, but no arene interactions (**XXIII**: δ_{H} 9.92 ppm, **XXV**: δ_{H} 9.64 ppm), alluding to structural features reminiscent of the solvent-free calcium hydride, $[(\text{BDI}^{\text{Dipep}})\text{CaH}]_2$.^{1, 4, 9, 11, 13, 14, 20}

While the low-coordinate structure was confirmed in the solution-state *via* ^1H NMR spectroscopy, shown by the lack of a signal at ca. δ_{H} 3.26 (Et_2O) or δ_{H} 3.57 (THF), crystals suitable for single crystal X-ray diffraction analysis has not yet been obtained, and therefore, the structure of **2.4** has not been elucidated in the solid-state.

It was found that compounds containing this $\text{BDI}^{\text{Dipep}}$ ligand environment required long crystallisation periods due to the high solubility in both aliphatic and aromatic solvents imparted by these Dipep substituents. Therefore, any attempts at crystallising **2.4** resulted in the formation of a new analogous compound, **2.5**, in which a THF donor molecule now saturates the coordination sphere of the ytterbium metal centre, displaying a much lower stability towards ethereal solvents than its amido precursor (**2.2**) (Figure 2.4).

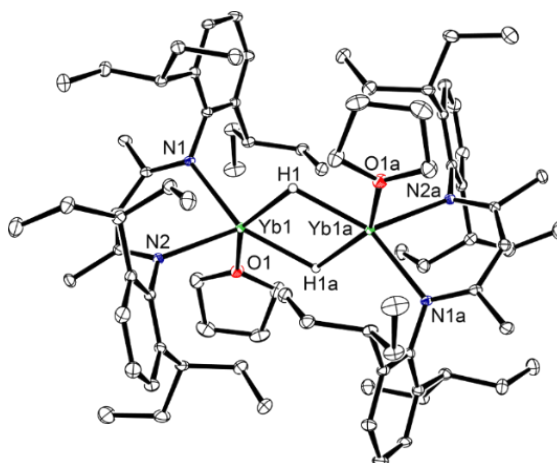


Figure 2.4. Ortep representations (30% probability ellipsoids) of compound **2.5**. Hydrogen atoms (except for the bridging H1 and H1a ligands) have been omitted for clarity. Selected bond lengths (Å) and angles (°): Yb1–N1 2.432(2), Yb1–N2 2.429(2), Yb1–O1 2.469(2), N1–Yb1–N2 81.12(7), N1–Yb1–O1 92.23(6).

Crystallographic analysis of **2.5** shows that both BDI^{Dipep} ligands adopt a bidentate *N,N*-coordination mode to both ytterbium centres within the dimer with the metal centres μ^2 -bridged by two hydride ligands. The Yb–N1 and Yb–N2 bond lengths (2.432(2) and 2.429(2) Å, respectively) are elongated compared to the Yb–N bond lengths of Harder’s solvated system (**XXIII**, average Yb–N: 2.3775 Å) but comparable to the solvated calcium hydride also bearing the BDI^{Dipep} ligand (average: 2.4305 Å).^{4, 9, 11} This lengthening of the Yb–N bond distances is to accommodate the coordination of a donor solvent molecule as the final contact to the respective metal centres in collaboration with the larger ligand system: the Ca–N bond lengths in the solvent-free [(BDI^{Dipep})CaH]₂ analogue are shorter, sitting at an average distance of 2.3652 Å.^{9, 11}

This solid-state structure coincides with the observed ¹H NMR spectrum for pure samples of **2.5**, which displays a hydride signal with Yb–H satellites centred at δ_{H} 9.10 ppm (¹*J*_{YbH} = 418 Hz) and is comparable to other β -diketiminate Yb(II) hydrides that display this similar bonding geometry (**XXIII**: δ_{H} 9.92 ppm (¹*J*_{YbH} = 398 Hz)) but contrasting those that

display additional arene interactions to the ytterbium metal centre (**XXV**: δ_{H} 7.82 ppm ($^1J_{\text{YbH}} = 233$ Hz)).^{1, 4}

2.2.2 Preliminary Reactivity of [(BDI^{Dipep})YbH(THF)]₂

Stoichiometric Alkylation of Benzene

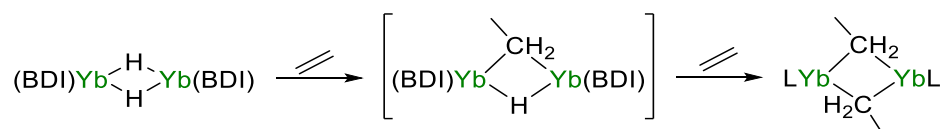
After successfully synthesising and crystallographically characterising the new divalent ytterbium hydride (**2.5**), the next aim was to synthesise an *n*-ethyl complex analogous to **XXVIa**, thus providing a comparison of the reactivities between the BDI^{Dipp} and BDI^{Dipep} ligand systems in relation to the nucleophilic alkylation of benzene.^{1, 7, 21} Such work has been discussed in greater detail in Chapter One.

When conducting both the stoichiometric and catalytic alkylation of benzene with the ytterbium(II) hydride bearing the BDI^{Dipp} ancillary ligand (**XXV**), it was imperative that donor solvents were not coordinated to the metal centre nor present in the reaction solvents as it ceased any desired reactivity through decomposition of the *n*-ethyl intermediate (**XXVIa**).¹ Despite this, this work was extended towards the newly synthesised BDI^{Dipep} ytterbium(II) hydride, **2.5**, containing metal centres coordinated with THF molecules due to the ease of isolating this product over the solvent-free analogue, **2.4**.

A J. Youngs tap NMR tube containing a brown C₆D₆ solution of **2.5** was degassed *via* three freeze-pump-thaw cycles before being exposed to one atmosphere of ethene gas at room temperature. Though no obvious colour change was observed upon addition, an initial ¹H NMR experiment was conducted and confirmed the presence of ethene within the reaction mixture by the singlet resonance situated at δ_{H} 5.26 ppm.

After 1 hour at room temperature, the hydride signal representative of **2.5** had significantly decreased concomitant with the formation of a new downfield hydride resonance centred at δ_{H} 10.50 ppm ($^1J_{\text{YbH}} = 443$ Hz) and the growth of a quartet centred at δ_{H} -0.58 ppm,

postulated to be the Yb–H signal and α -methylene protons of a mixed Yb(II) hydride-ethyl complex, respectively. This product is likely formed through an insertion reaction between the dimeric hydride, **2.5**, and one equivalent of ethene, which can then undergo a second insertion of ethene to generate the desired [(BDI^{Dipep})Yb] *n*-ethyl species (Scheme 2.3).



Scheme 2.3. A generalised scheme for the insertion of ethene into the Yb–H bonds of [(BDI)YbH]₂.

Possible broad signals representing the α -methylene protons of the ytterbium *n*-alkyl was also present in the region between δ_{H} 0.05 and –0.4 ppm of the ¹H NMR spectrum, however, this could not be confirmed solely in the solution-state.

The presence of free ethene and the possible mixed Yb(II) hydride-alkyl species hints that the conversion to the dimeric ytterbium *n*-alkyl was not complete after a few hours at room temperature. However, a discernible peak situated at ca. δ_{H} 2.49 ppm was also growing in, representing the organic by-product, ethylbenzene. This suggested the nucleophilic alkylation of benzene could already be occurring through a σ -bond metathesis reaction between the Yb(II) *n*-ethyl intermediate and the C₆D₆ solvent, therefore, it was decided to work up the reaction mixture early in an attempt to characterise any reaction products or intermediates within the solid-state. Volatiles were removed *in vacuo* and the brown residue was crystallised from a saturated pentane/toluene solution at room temperature, growing brown blocks suitable for a single crystal X-ray diffraction experiment (Figure 2.5).

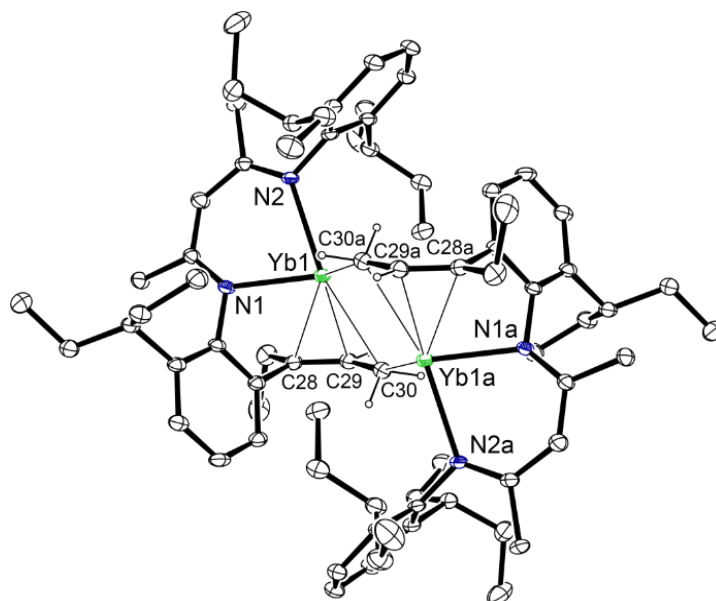


Figure 2.5. Ortep representation (30% probability ellipsoids) of compound **2.6**. Hydrogen atoms have been omitted for clarity (except those on C28, C29 and C30). Poor crystal quality meant sufficient bond length and angle data could not be obtained.

Due to poor crystal quality, only the structural connectivity of compound **2.6** could be determined and was revealed as a new ytterbium-containing species where one 3-pentyl chain of one Dipecp *N*-substituent within each $[(\text{BDI}^{\text{Dipecp}})\text{Yb}]$ unit of the dimer had been deprotonated to generate an allyl functionality.

This preliminary study highlighted that both the BDI^{Dipp} and $\text{BDI}^{\text{Dipecp}}$ ancillary ligands present their own problems with respect to the stoichiometric alkylation of benzene, and it seems evident that this nucleophilic regime cannot be affected by the THF derivatives **XXIII** or **2.5**.⁷ In the case of **2.5**, it cannot be concluded that solvent saturation of the Yb(II) sphere is the primary reason as the increase in the carbon chain to the new 3-pentyl *N*-substituent is accompanied by an increase in flexibility, revealing ligand activation as a competing pathway.

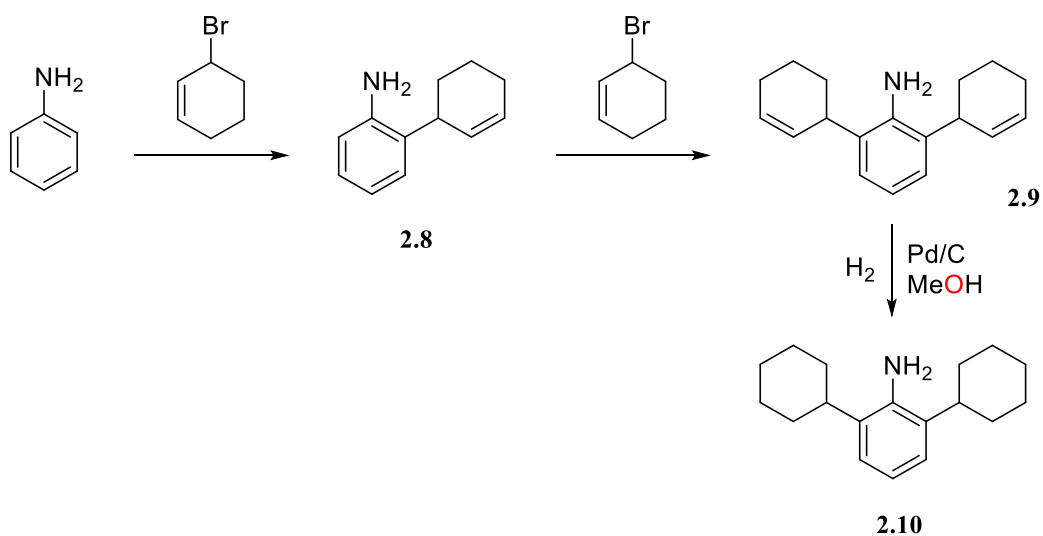
2.3 Synthesis of [(BDI^{Dicyp})YbH]₂

The BDI^{Dipep} ligand system has been proven to successfully stabilise a low-valent ytterbium(II) centre, both with- and without the additive coordinated saturation from a donor solvent molecule. Despite the larger size of the ligand substituents, the problem of Schlenk-type redistribution was still occurring throughout the synthesis, albeit not as frequently as observed with our original ytterbium(II) hydride (**XXV**).¹

Therefore, it was proposed that a new derivative of the β -diketiminato ligand system, BDI^{Dicyp} (**2.7**) (Dicyp = 2,6-dicyclohexylphenyl), will be utilised.²² The exchange to cyclohexyl rings is envisioned to provide greater steric protection of our metal centre than BDI^{Dipep}, with the goal of completely eradicating Schlenk-type redistribution. The increase in rigidity of the new *N*-substituent seems advantageous in the expectation that they will not interfere with any desired reactivity between the new divalent ytterbium hydride and the selected substrates, as demonstrated in Section 2.2.2.

2.3.1 Synthesis of (BDI^{Dicyp})H

Before synthesising the new derivative of the β -diketiminato, we first had to synthesise the Dicyp aniline. This synthesis began with an amino-Claisen rearrangement reaction between aniline and 3-bromocyclohexene to yield the monosubstituted aniline, **2.8** (Scheme 2.4).^{22, 23} This is carried out neat, hence aniline reagent is used in an excess and acts as the solvent system for this reaction. After a basic organic workup, aniline and **2.8** can be separated and purified *via* vacuum distillation, with the first collection regenerating aniline as a colourless liquid and the second isolating **2.8** as a pale yellow oil.



Scheme 2.4. Three-step synthesis to afford the 2,6-dicyclohexyl amine (**2.10**).

This was further reacted with 3-bromocyclohexene to obtain the disubstituted aniline (**2.9**) after workup and purification *via* vacuum distillation, which could be subsequently reduced under hydrogen (2 atm) to give the 2,6-dicyclohexyl amine (**2.10**) as a pale pink solid. The structure of **2.10** was primarily confirmed through ^1H NMR analysis and was consistent with the literature.²³ The pale pink powder could also be recrystallised from a mixed hexane/toluene solution, allowing for secondary confirmation in the solid-state through a single crystal X-ray experiment (Figure 2.6).

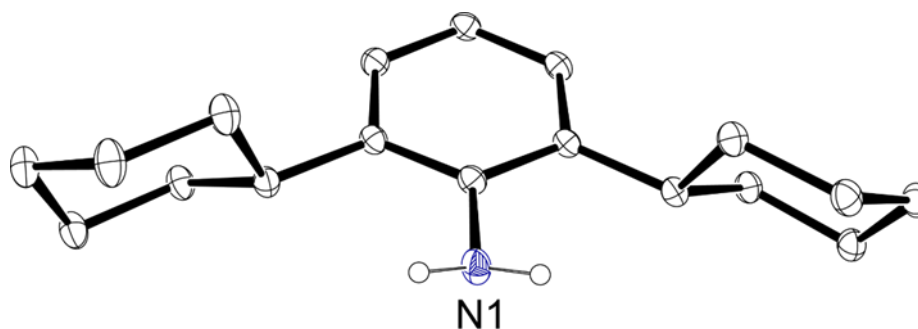
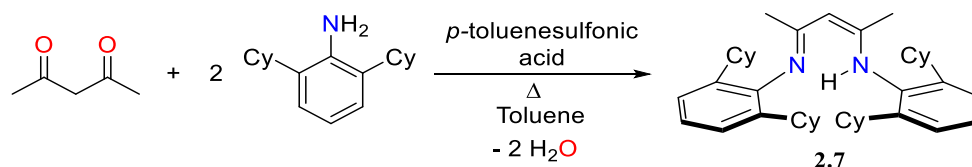


Figure 2.6. Ortep representations (30% probability ellipsoids) of compound **2.10**. Hydrogen atoms (except on N1) have been omitted for clarity. Selected bond lengths (Å) and angles (°): N1–C1 1.402(1), C–C_{Ph}(Average) 1.398, C–C_{Cy}(Average) 1.53.

Synthesis of the pro-ligand follows the general procedures for β -diketiminates analogues, with the addition of an acid catalyst to acetylacetone and the appropriate aniline derivative under refluxing conditions in a Dean-Stark apparatus (Scheme 2.5).



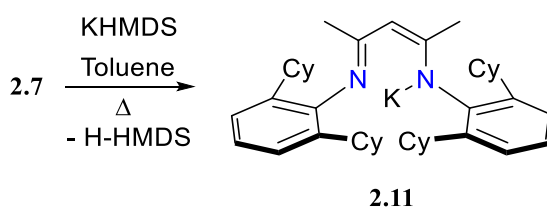
Scheme 2.5. Condensation reaction to give **2.7**.

Following a similar methodology to the synthesis of (BDI^{Dipep})H, the reaction was initially refluxed for 3 days then the resultant red-brown mixture was quenched with one molar equivalent of triethylamine and stirred at room temperature for 1 hour.³ The organic phase was washed with distilled water, then twice with brine, before drying over anhydrous MgSO₄ and removing the solvent under vacuum to yield a brown residue. The crude product could be heated into the minimum volume of methanol solvent, where cooling of the solution resulted in precipitation of pure **2.7** as a beige crystalline solid.

After workup, the ligand system **2.7** was consistently isolated in poor yields (<50%). Therefore, the reaction time was experimented with, ranging from 1 – 10 days, and ¹H NMR analysis disclosed that longer periods typically resulted in a higher percentage of unreacted **2.10**. This suggests the reaction conditions could be too acidic, and therefore, the desired product was hydrolysing back to the starting materials, which is commonly found with imine formation reactions as these are reversible. On the other hand, conversion to **2.7** may not be occurring in the first place due to reaction conditions being too basic, thus hindering the elimination of water.

Though neither the starting materials nor the product are air-sensitive compounds, the next reaction attempt was treated as such. Acetylacetone, **2.10** and the *p*-toluenesulfonic acid were added into a round bottom flask with anhydrous toluene solvent; the flask was fitted with a rubber septum and argon gas was bubbled through the mixture for ca. 30 minutes prior to refluxing the mixture overnight. The Dean-Stark condenser was also fitted with a rubber septum so that an argon-filled balloon could be inserted to keep the mixture under an inert atmosphere. While this experimental procedure may not address the pH level problem of the reaction, repeating this synthetic method proved effective, consistently generating **2.7** in good yields (ca. 80%), the structure of which was characterised in both the solution- and solid-state (Figure 2.7, a)).²²

The pro-ligand can then undergo subsequent deprotonation with a base, such as KHMDS, in toluene to form the respective potassium salt of the ligand (**2.11**) as a beige precipitate, concomitant with the production of H-HMDS (Scheme 2.6).



Scheme 2.6. Deprotonation of **2.7** to give the potassium salt, **2.11**.

Isolation and drying of the crude product, followed by dissolving an aliquot in C_6D_6 , allowed for structural confirmation through an 1H NMR experiment. The spectrum indicated that no free ligand remained within the sample by the disappearance of the low-field N–H signal and a single new β -diketiminato methine resonance at δ_H 4.76 ppm.

The potassium salt of the ligand was largely insoluble in both aliphatic and aromatic solvents, highly soluble in THF but only partially soluble in Et_2O . Therefore, the crude **2.11** was washed with diethyl ether, the pale yellow solution decanted into a new scintillation vial

and left to slowly crystallise at room temperature, affording single crystals suitable for X-ray diffraction analysis (Figure 2.7, b)).

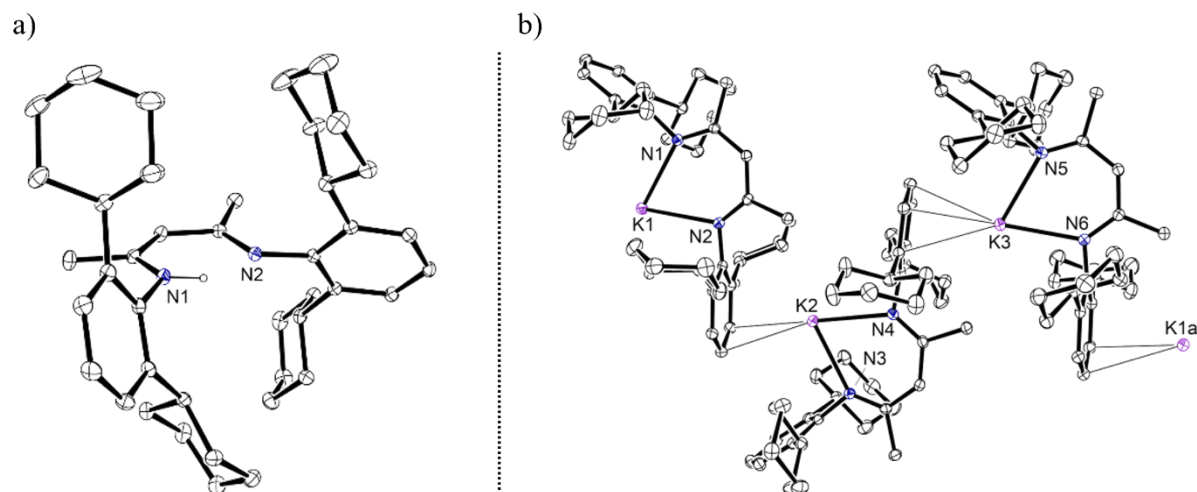


Figure 2.7. Ortep representations (30% probability ellipsoids) compound **2.7** (left) and compound **2.11** (right). Hydrogen atoms (except for N1–H for **2.7**) have been omitted for clarity. Selected bond lengths (Å) and angles (°): **2.7**: N1–C24 1.427(1), N1–C2 1.354(1), C2–C3 1.375(1), C3–C4 1.439(2), N2–C4 1.302(1), N2–C6 1.419(1). **2.11**: K1–N1 2.644(2), K1–N2 2.723(2), K1–C_{para} 3.257(3), K1–C_{meta} 3.397(3), K1–C_{meta} 3.237(3), K1–C_{ortho} 3.351(3), K2–N3 2.643(2), K2–N4 2.717(2), K2–C_{meta} 3.326(3), K2–C_{meta} 3.267(3), K2–C_{para} 3.231(3), K3–N5 2.658(2), K3–N6 2.673(2), K3–C_{ortho} 3.317(3), K3–C_{meta} 3.085(3), K3–C_{para} 3.203(3), N1–K1–N2 69.09(7), N3–K3–C_{Cent} 165.54(6), N5–K3–C_{Cent} 123.91(6).

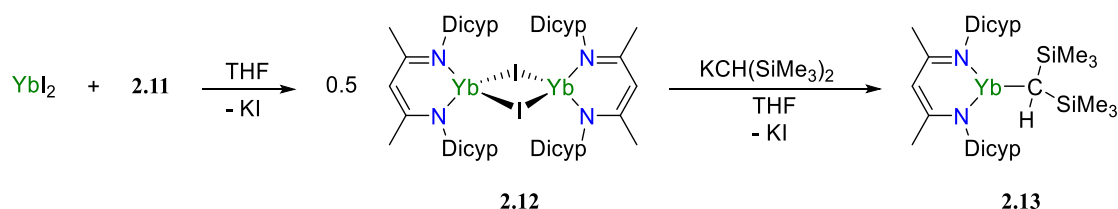
In the solid-state, each monomer of **2.11** contains a potassium ion *N,N*-chelated to the nitrogens of the BDI^{Dicyp} ligand, and contains potassium-aryl interactions with a phenyl ring of a Dicyp substituent of a second (BDI^{Dicyp})K unit. This results in a polymeric structure, with three β-diketimate monomers within the asymmetric unit. The K1–N1 and K1–N2 bond lengths are 2.644(2) and 2.723(3) Å, respectively, and are consistent with other previously reported unsolvated β-diketimate-based salts, such as (BDI^{Dipp})K and (BDI^{TCHP})K (2.619(3) – 2.7398(19) Å).^{24, 25} The K1–C_{para} distance of 3.257(3) Å and K1–C_{meta} distances of 3.237(3) and 3.397(3) Å are greater than the sum of the covalent radii for potassium and carbon (2.71 Å),^{24, 26} but within the sum of their van der Waals radii (4.45 Å),^{24, 27} alluding to weak

intermolecular interactions. The K1–C_{para} and two K1–C_{meta} distances are like what is reported for (BDI^{Dipp})K (3.214(3), 3.351(3) and 3.276(3) Å, respectively).^{24, 25} The other reported distances for K2 and K3 contacts within the polymer are like that of K1, negating further comment.

2.3.2 Synthesis *via* [(BDI^{Dicyp})YbI]₂

To test the steric bulk of our new ligand, the synthesis of the heteroleptic iodide, **2.12**, was carried out in THF solvent (Scheme 2.7). The addition of YbI₂ to the potassium salt of the ligand resulted in a red solution with beige precipitates after 4 hours at room temperature. Removal of the volatiles *in vacuo* and extraction of the crude red solid with toluene still afforded the product as the solvent-free analogue, which was first confirmed in the solution-state through multinuclear NMR analysis.

An ¹H NMR spectrum obtained of **2.12** indicated that two β-diketimate ligand environments were present in solution due to the presence of two methine resonances: The major signal was centred at δ_H 4.78 ppm and was assigned as the methine resonance of the BDI^{Dicyp} ytterbium(II) iodide and the minor peak situated at δ_H 4.83 ppm was assigned as the methine of the free β-diketimate ligand, **2.7**, as the peak was in a 1:1 ratio with a broad N–H signal at δ_H 11.39 ppm.



Scheme 2.7. Synthesis of the heteroleptic iodide (**2.12**) and subsequent σ-bond metathesis reaction to give **2.13**.

The formation of **2.7** alongside **2.12** indicates that the iodide complex is likely decomposing throughout the synthetic method. However, **2.12** can be washed with hexane

solvent to remove any residual **2.7** as the iodide complex is only partially soluble in aliphatic solvents, albeit this is at the cost of isolating **2.12** in high yields (ca. 10 – 50%).

Pure samples of **2.12** could be recrystallised from toluene solvent, allowing for structural confirmation through a single crystal X-ray diffraction experiment (Figure 2.8, a)). In the solid-state, **2.12** adopts a dimeric structure in which the two μ^2 -iodide ligands bridge the two ytterbium(II) centres (Yb–I: 3.0736(6), 3.0384(5) Å). Each Yb(II) centre also binds to the β -diketiminato-*N* atoms (Yb–N: 2.331(3), 2.349(4) Å), completing the coordination sphere. This geometry is analogous to the smaller BDI^{Dipp} ytterbium iodide complex but diverges from the geometry observed with the BDI^{Dipep} system (**2.1**) described earlier in this Chapter.¹⁷ All Yb–N and Yb–I bond lengths within **2.12** are consistent with these two examples of iodide complexes containing ytterbium in the 2+ oxidation state (Yb–N: 2.325(3) – 2.414, Yb–I: 3.063 – 3.142 Å).

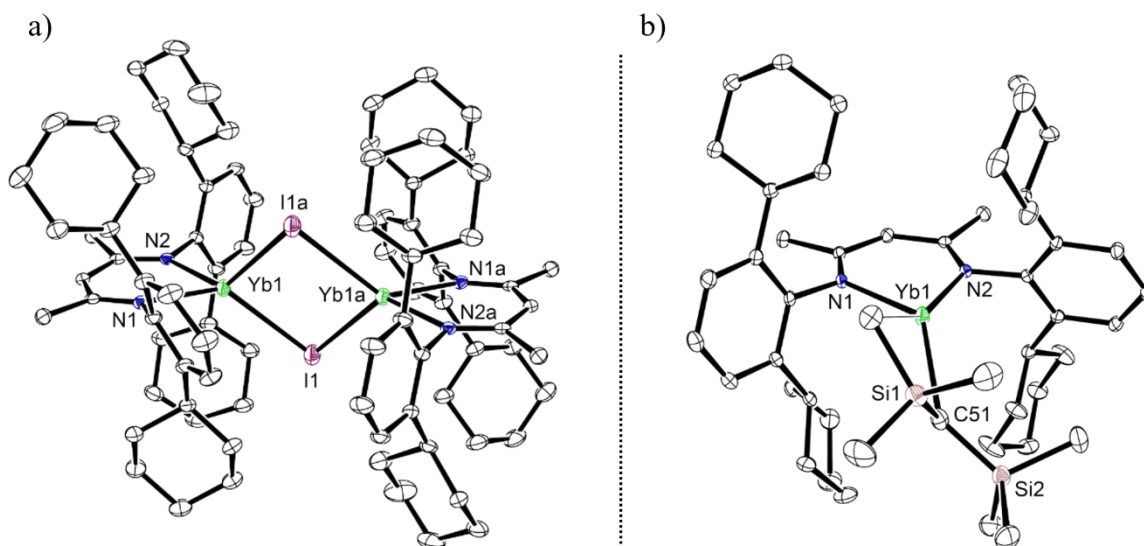


Figure 2.8. Ortep representations (30% probability ellipsoids) of compound **2.12** (left) and compound **2.13** (right).

Hydrogen atoms have been omitted for clarity. Selected bond lengths (Å) and angles (°): **2.12**: Yb1–I1 3.0736(6), Yb1–N1 2.331(3), Yb1–N2 2.349(4), Yb1–I1a 3.0384(5), I1–Yb1–N1 136.23(9), I1–Yb1–N2 116.25(9), I1–Yb1–I1a 77.7(1), Yb1–I1–Yb1a 86.05(2). **2.13**: Yb1–N1 2.383(2), Yb1–N2 2.350(2), Yb1–C51 2.527(3), Yb1···C13 2.874, N1–Yb1–N2 76.63(6), N1–Yb1–C51 130.37(8), N2–Yb1–C51 132.34(8).

Chapter One outlined the synthesis of the current six examples of ytterbium(II) hydrides reported to date.^{1, 4, 13, 14, 20, 28} Of those examples, three systems are synthesised *via* the reaction of a heteroleptic alkyl precursor with a hydride source.^{13, 14, 20} Both Chapter One and Two details the ability of the de-solvated hydride **XXV** to react with ethene to give the respective ytterbium(II) *n*-ethyl intermediate, which in turn facilitates the catalytic alkylation of benzene at room temperature.¹ In Section 2.2.2, this work was extended towards the newly isolated hydride, **2.5**, however preliminary studies showed an analogous ytterbium alkyl complex bearing the BDI^{Dipep} was not isolated. Therefore, it became beneficial to explore the possibility that we could instead synthesise a heteroleptic Yb(II) monoalkyl precursor supported by this new BDI^{Dicyp} ancillary ligand for two reasons: firstly, it provides an opportunity to explore an alternate pathway towards gaining new divalent lanthanide hydrides, as our work has focused on synthesising amido precursor complexes thus far. Secondly, it would provide the opportunity to test the stability of the successful isolation of this BDI^{Dicyp} ytterbium(II) monoalkyl compound towards benzene solvent and allow for further comparative studies to the original complex, **XXV**.

The synthetic method was approached with the assumption that performing a σ -bond metathesis reaction between **2.12** and the potassium salt of Lappert's alkyl, (KCH(SiMe₃)₂), in THF would afford the low-coordinate complex, **2.13**, after workup (Scheme 2.7). Crystallisation of the dark red-brown hexane solution yielded single crystals suitable for X-ray diffraction analysis, which disclosed that the primary coordination sphere of the Yb(II) centre was made up by three contacts (Figure 2.8, b)). Two contacts are made up of the N-atoms of the β -diketiminate ligand, with Yb1–N1 and Yb1–N2 bond lengths of 2.384(2) and 2.350(2) Å being similar to the Yb–N bond lengths (Yb–N: 2.366(2) Å) of the ytterbium amido complex bearing the BDI^{Dipep} ligand (**2.2**), discussed earlier in this Chapter. The third contact is to the bis(trimethylsilyl)methyl ligand, with the Yb–C51 bond length of 2.527(3) Å being

slightly shorter than the only other BDI-based ytterbium(II) alkyl complex bearing the same $\text{CH}(\text{SiMe}_3)_2$ ligand; in this example, the increased bond distances is likely the result of accommodating solvent coordination to the Yb(II) metal centre, whereas a final contact to the Yb(II) centre within **2.13** is from an agostic interaction of a methyl of the $\text{CH}(\text{SiMe}_3)_2$ moiety ($\text{Yb1}\cdots\text{C13}$ 2.874 Å) relieving steric unsaturation.¹⁷

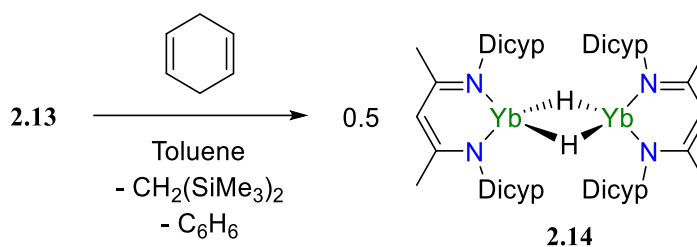
As outlined in Chapter One, two common sources of hydridic hydrogen are reported within the literature for synthesising divalent lanthanide hydrides. For systems that contain an alkyl ligand, the hydride source is typically H_2 gas and for amido precursors, phenylsilane, respectively.^{1, 14}

In our previous research, we performed a σ -bond metathesis reaction between a divalent ytterbium amido complex and phenylsilane, which forms the hydride alongside the reaction by-product, $\text{PhSiH}_2\text{N}(\text{SiMe}_3)_2$. This product is not volatile, therefore, washing or crystallising away from such impurities is required and is typically at the cost of high product yields.

In 2019, Harder reported using 1,4-cyclohexadiene (1,4-CHD) in the alkene transfer hydrogenation with Group 2 catalysts, where benzene is the by-product formed.²⁹ It was plausible that reacting 1,4-CHD as the selected hydride source with a ytterbium(II) monoalkyl precursor would be advantageous over phenylsilane as the side products generated would be benzene and $\text{CH}_2(\text{SiMe}_3)_2$, thus these impurities can be removed from our desired product *in vacuo*. Herein, 1,4-CHD will be the hydride source of choice when utilising the respective lanthanide monoalkyl precursor, but phenylsilane will still be used when utilising the heteroleptic amido precursors. If 1,4-CHD was reacted with a lanthanide amido complex, the formation of the respective Ln(II) hydride would be alongside the formation of H-HMDS,

which the hydride could react with *via* a protic σ -bond metathesis reaction to regenerate the amide precursor concomitant with extrusion of hydrogen gas.

To monitor the synthesis of the new ytterbium(II) hydride through ^1H NMR analysis, the below reaction was initially conducted in a J. Youngs tap NMR tube (Scheme 2.8).



Scheme 2.8. Synthesis of a molecular ytterbium(II) hydride (**2.14**).

The addition of 1,4-CHD to a red-brown C_6D_6 solution of **2.13** resulted in the precipitation of a purple solid almost instantaneously, and therefore, the product could not be characterised in the solution-state. Instead, **2.13** was dissolved into toluene in a scintillation vial inside the glovebox, a saturated toluene solution containing the hydride source was gently layered on top and left to slowly diffuse together at room temperature. After 48 hours, small purple crystals of **2.14** had deposited on the vial's walls and were suitable for X-ray diffraction analysis (Figure 2.9).

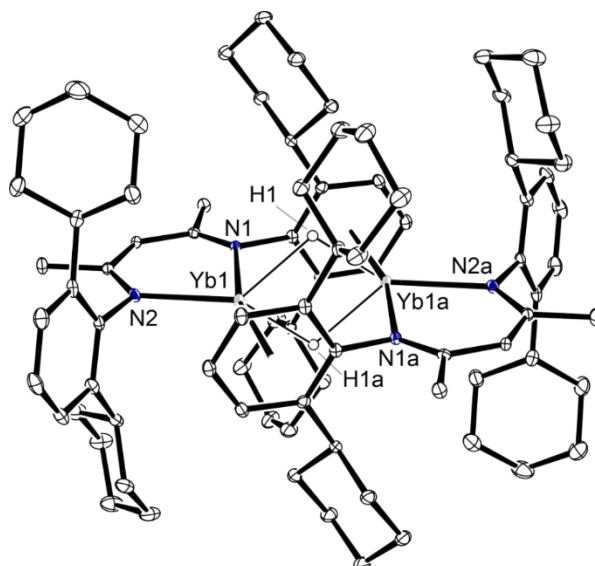


Figure 2.9. Ortep representations (30% probability ellipsoids) of compound **2.14**. Hydrogen atoms (except for the bridging H1 and H1a ligands) have been omitted for clarity. Selected bond lengths (Å) and angles (°): Yb1–N1 2.489(2), Yb1–N2 2.452(2), Yb1–C_{cent} 2.7239(9), N1–Yb1–N2 74.70(6), N1–Yb1–C_{cent} 166.00(5), N2–Yb1–C_{cent} 119.30(5).

In the solid-state, **2.14** is a centrosymmetric dimer with two μ^2 -hydride ligands bridging the two Yb(II) centres. Each Yb centre interacts in an η^6 -coordination mode with the phenyl ring of one Dicyc *N*-substituent of the second [(BDI^{Dicyp})YbH] unit within the dimer. The Yb1–N1 and Yb1–N2 bond lengths of 2.489(2) and 2.452(2) Å are within the range of Yb–N bond lengths for other β -diketiminato based Yb(II) hydrides (2.376 – 2.502 Å).^{1, 4, 13} This geometry contrasts the solvated hydride complex (**2.5**) but is reminiscent of the solid-state structure the solvent-free hydride (**XXV**) which also displays metal-aryl interactions.¹ The Yb–C_{Cent} distance (2.7239(9) Å) within **2.14** is slightly longer than the Yb–C_{cent} distance found in **XXV** (2.7099(9) Å) and is a result of the less sterically bulky Dipp *N*-substituent being able to fit in closer proximity to the second Yb(II) centre within the dimer.

Thus far, **2.14** displays significant differences in stability in comparison to the other β -diketiminato based hydrides, **XXV** and **2.5**. The less bulky system (**XXV**) is completely soluble in aromatic solvents, partially solubility in aliphatic solvents, and while it is completely soluble in ethereal solvents, displays low stability as it is prone to solvation of the ytterbium centre.

This complex is also highly susceptible to Schlenk-type redistribution in the solution-state, forming the homoleptic species, $[(\text{BDI}^{\text{Dipp}})_2\text{Yb}]$, in any solvent system at room temperature after short time periods.^{1, 2} In comparison, the bulkier hydride **2.5** is highly soluble in aliphatic, aromatic, and ethereal solvents imparted by the Dipec substituents and was found to be less prone to Schlenk-type redistribution, albeit not entirely. Lastly, **2.14** has demonstrated negligible solubility in aliphatic, aromatic, and ethereal solvents, with no evidence for solvent coordination or the formation of a Schlenk-type redistribution product, reminiscent of **2.3**.

2.4 Preliminary Reactivity Studies of $[(\text{BDI}^{\text{Dipp}})\text{YbH}]_2$, $[(\text{BDI}^{\text{Dipec}})\text{YbH}(\text{THF})]_2$, and $[(\text{BDI}^{\text{Dicyp}})\text{YbH}]_2$

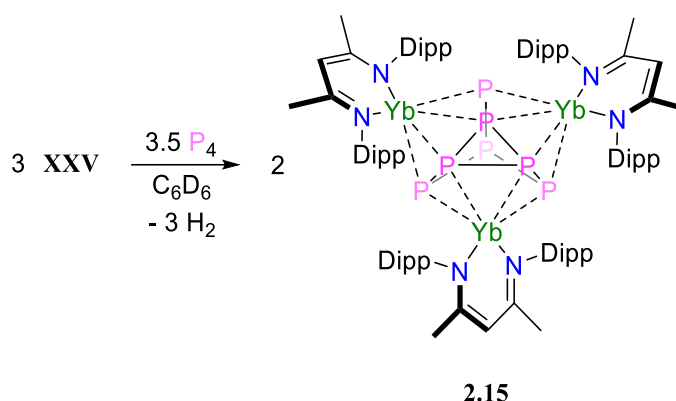
Chapter One outlined that divalent lanthanide complexes undergo three primary reactivities: σ -bond metathesis, insertion chemistry, and redox chemistry.³⁰⁻³² These reaction chemistries are much like Group 2, so much so that direct comparative studies have been made between both calcium and ytterbium(II) within the literature.² This following Section further delves into the reductive chemistry of heteroleptic hydrides and ytterbium(II) hydrides with selected substrates. Thus far, Chapter Two has introduced the synthesis and structure of two new ytterbium(II) hydrides bearing analogues of the β -diketiminato ligand framework. However, any chosen reaction chemistry will also be conducted with **XXV** before being extended towards these two new compounds as a further testament of their respective stabilities, provided by either the steric differences of the ancillary ligand substituents or solvent saturation.

2.4.1 Activation of White Phosphorus

The functionalisation of white phosphorus by Group 2 alkyl or hydride complexes is introduced in Chapter One, focusing on the ability of the unsolvated calcium hydride, **XXXII**, to act as a reductant for the isolation of a new polyphosphorus-containing compound, **XXXIV**.^{33, 34} While this chemistry is in its infancy, the same functionalisation of white phosphorus by a ytterbium(II) based reagent is yet to be realised. This Section details the ability of three

ytterbium hydride complexes to activate P_4 , with structural comparisons of the resulting polyphosphorus complexes.

The reaction of **XXV** with one equivalent of P_4 was conducted in C_6D_6 in a J. Youngs tap NMR tube (Scheme 2.9). Over 24 hours, the black solution became a deep red colour, and a single broad peak centred at $\delta_P -78$ ppm in the $^{31}P\{^1H\}$ NMR spectrum was observed, indicating the formation of a single phosphorus-containing compound (**2.15**) with only one phosphorus environment.



Scheme 2.9. Synthesis of a trinuclear ytterbium(II) Zintl ion complex (**2.15**).

With no discernible peaks representative of the hydride starting material in the 1H NMR spectrum, the solution was dried under vacuum, and the crude product crystallised from a saturated hexane solution, yielding brown needles suitable for X-ray diffraction analysis (Figure 2.10).

The solid-state structure of **2.15** was identified to be a $[P_7]^{3-}$ Zintl ion cage surrounded with three $[(BDI^{Dipp})Yb]^+$ units and is analogous to the calcium complex **XXXIV**.³⁴ Each ytterbium centre is four-coordinate, with two contacts provided by bidentate N,N -chelation of the BDI^{Dipp} ligand ($Yb-N$: 2.342(3) – 2.370(3) Å) and two contacts η^2 -binding to the $[P_7]^{3-}$ ion ($Yb-P$: 2.874(1) – 2.934(1) Å).

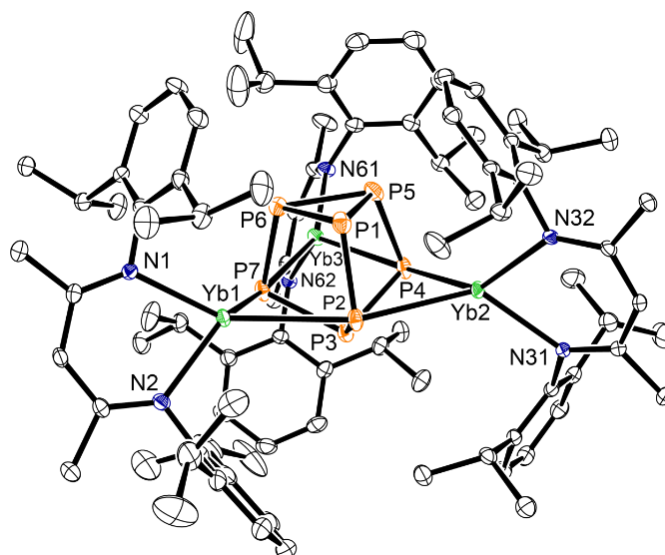
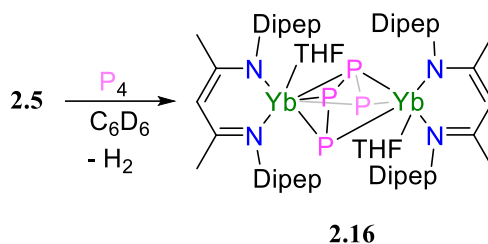


Figure 2.10. Ortep representations (30% probability ellipsoids) of compound **2.15**. Hydrogen atoms have been omitted for clarity. Selected bond lengths (Å) and angles (°): Yb1–N1 2.358(3), Yb1–N2 2.346(3), Yb1–P2 2.934(1), Yb1–P7 2.874(1), Yb2–N31 2.350(3), Yb2–N32 2.342(3), Yb2–P2 2.899(1), Yb2–P4 2.904(1), Yb3–N61 2.353(3), Yb3–N62 2.370(3), Yb3–P4 2.913(1), Yb3–P7 2.913(1), P1–P2 2.174(1), P1–P5 2.257(1), P1–P6 2.264(1), P2–P3 2.213(1), P3–P4 2.201(1), P3–P5 2.204(1), P4–P5 2.169(2), P5–P6 2.255(1), P6–P7 2.177(1), N1–Yb1–N2 76.99(9), N1–Yb1–P7 115.03(7), N1–Yb1–P2 150.40(7), P2–P1–P5 105.95(5), P2–P1–P6 104.88(5), P5–P1–P6 59.84(5), P1–P2–P3 99.22(5), P2–P3–P4 101.13(5), P2–P3–P7 100.75(5), P4–P3–P7 100.64(5).

The Yb–N bond lengths are within the range of other ytterbium(II) complexes supported by the BDI^{Dipp} ligand (2.328 – 2.399 Å)^{1, 2, 4, 17} and the Yb–P bond lengths are comparable to the Ca–P bond distances reported for **XXXIV** (2.8667(9) – 2.9346(9) Å). The reported P–P bond lengths within the Zintl ion of **2.15** range from 2.169(2)– 2.264(1) Å and are within literature values for nortricyclane-like phosphorus cages and comparable to what is observed in **XXXIV** (2.1748(10) – 2.2586(11) Å).^{34–36}

The reaction of **2.5** with an equimolar amount of P₄ under the same reaction conditions resulted in the dimeric species **2.16** through the extrusion of hydrogen gas (Scheme 2.10).



Scheme 2.10. Activation of P₄ to give **2.16**.

An initial $^{31}\text{P}\{^1\text{H}\}$ NMR experiment on the crude reaction mixture showed three signals situated at δ_{P} 324.3, 62.5 and -241.56 ppm, indicating three possible phosphorus environments. Therefore, for better structural characterisation, the C₆D₆ solvent was removed *in vacuo*, and the resulting red solid was dissolved in a saturated hexane solution, affording single crystals of **2.16** from slow evaporation at room temperature (Figure 2.11).

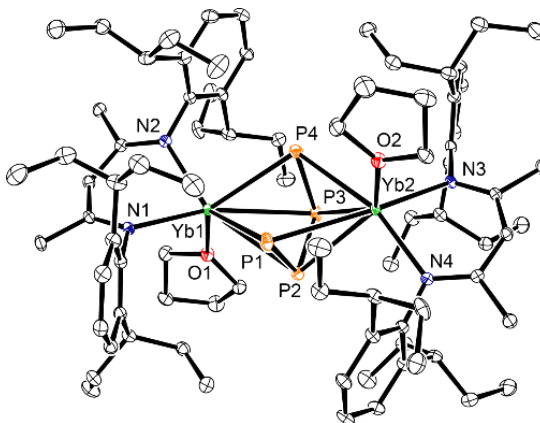


Figure 2.11. Ortep representations (30% probability ellipsoids) of compound **2.16**. Hydrogen atoms have been omitted for clarity. Selected bond lengths (Å) and angles (°): Yb1–N1 2.394(3), Yb1–N2 2.399(2), Yb1–P1 2.9796(8), Yb1–P2 3.0993(9), Yb1–P3 3.084(1), Yb1–P4 2.972(2), Yb1–O1 2.385(2), Yb2–N3 2.398(3), Yb2–N4 2.386(2), Yb2–P1 3.054(1), Yb2–P2 3.039(1), Yb2–P3 3.0049(8), Yb2–P4 2.9891(9), P1–P2 2.136(1), P2–P3 2.108(1), P3–P4 2.142(1), N1–Yb1–N2 80.85(8), P1–Yb1–P2 41.08(2), P1–Yb1–P3 66.83(2), P1–Yb1–P4 63.40(2), N1–Yb1–P1 96.68(6), Yb1–P1–Yb2 11053(3), P1–P2–P3 103.83(5), P2–P3–P4 103.75(5), N1–Yb1–O1 101.39(8).

In the solid-state, **2.16** is a dimer with two ytterbium centres bridged by a [P₄]²⁻ moiety. Each Yb(II) binds to the N-atoms of the β-diketiminato ligand (2.386(2) – 2.399(2) Å) and η^4 -interacts with the P₄ chain (Yb–P distances: 2.9796(8) – 3.0993(9) Å). Though structurally

different, these values are all slightly elongated compared to the Yb–N (2.342(3) – 2.370(3) Å) and Yb–P (2.874(1) – 2.934(1) Å) in compound **2.15**, with the longer Yb–N distances a result of the increase in the steric bulk of the Dipecp *N*-substituent and the need to accommodate the final Yb–O contact provided by the THF solvent. The P–P bond lengths in **2.16** are reported to be 2.136(1), 2.108(1) and 2.142(1) Å, which are shorter than the average reported values for P–P single bonds found within P₄ (2.19 Å) but significantly longer than P=P double bonds (2.0 Å), with the internal P–P bond length being shorter than the two terminal P–P bond distances.^{35, 37, 38} The P1–P4 bond distance is considerably longer at 3.128 Å. To our knowledge, there are no dimeric Group 2 complexes containing a related bridging tetraphosphorus chain. There are two transition metal-lanthanide bimetallic systems, [(Cp^{'''}Co)₂P₄Sm(C₅Me₄R)₂] (Cp^{'''} = 1,2,4-^tBu₃C₅H₂, R = Me or *n*-propyl), however, these were formed through reduction of a cobalt polyphosphide by a divalent samarium complex.³⁹ The terminal P–P bond lengths (2.149(1) – 2.2150(2) Å) within [(Cp^{'''}Co)₂P₄Sm(C₅Me₄R)₂] are comparable to **2.16**, however the internal P2–P3 bond distance of 2.241(2) Å or 2.253(3) Å is over 0.13 Å longer than the P2–P3 distance in **2.16**. The bridging P₄ moiety in **2.16** is nearly planar (2.316(2)°), but not within [(Cp^{'''}Co)₂P₄Sm(C₅Me₄R)₂] and therefore these compounds are not structurally similar and negate further comparisons.

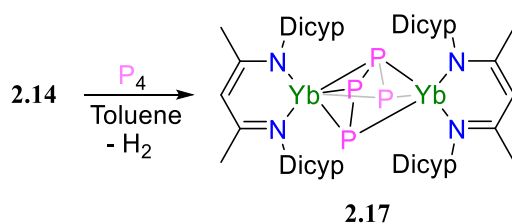
In the solution-state, the ³¹P{¹H} NMR spectrum of **2.16** displays a set of resonances that appear representative of an AA'XX' spin system, where the A and X nuclei are chemically equivalent but not magnetically equivalent.⁴⁰ This spin system is commonly encountered for symmetrical fragments of four spin-active nuclei.

The two sets of resonances centred at δ_P 324.3 and 62.5 ppm are of similar intensity and could be the two phosphorus environments within the product, **2.16**. The gross features of the ³¹P{¹H} NMR appear visually similar to the spectrum reported for the bimetallic complex, [(^{Mes}BIAN)Co(μ-η⁴:η²-P₄)Ga(BDI^{Dipp})][–] (BIAN = bis(mesitylimino)acenaphthene diamine),

which also discusses an AA'XX' spin state for this related phosphorus system.³⁸ In this work, they assign the low-field resonance (δ_P 74.0 ppm) as P_{AA'} and the higher field resonance as P_{XX'} (δ_P -125.4 ppm); therefore, the shift at δ_P 324.3 ppm in the $^{31}\text{P}\{^1\text{H}\}$ NMR of **2.16** is tentatively assigned to P_{AA'} and the shift at δ_P 62.5 ppm as the P_{XX'} environment. However, further analysis by spectral simulation software is typically employed to confidently assign each signal as either the AA' or XX' phosphorus nuclei and to gain insights on the respective *J*-couplings of this more complex system.

When the calcium hydride was reacted with P₄ on an NMR scale, the $^{31}\text{P}\{^1\text{H}\}$ NMR spectrum showed a signal at δ_P -87.7 ppm, corresponding to compound **XXXIV**, and a second peak at δ_P -241.3 ppm, the structure of which could not be isolated nor characterised.³⁴ The last notable feature of the $^{31}\text{P}\{^1\text{H}\}$ NMR spectrum for **2.16** is the singlet resonance situated at δ_P -241.56 ppm, indicating the presence of a second phosphorus-containing compound. Due to the similarities in chemical shifts of this unidentified peak, it could be that the by-products of **XXXIV** and **2.16** are closely related, but like calcium, this second product could not be isolated.

Finally, the bulky ytterbium(II) hydride, **2.14**, was reacted with white phosphorus to obtain compound **2.17** (Scheme 2.11). Due to this insolubility of **2.14** in C₆D₆ solvent, the reaction was carried out in toluene in a scintillation vial inside the glovebox.



Scheme 2.11. Activation of P₄ to give **2.17**.

After stirring the mixture for 2 hours at room temperature, any residual solid starting material had disappeared to give a dark red-brown solution and red-brown precipitate. The solution was filtered, concentrated under vacuum, and left to crystallise at room temperature, giving small red crystals suitable for an X-ray diffraction experiment (Figure 2.12).

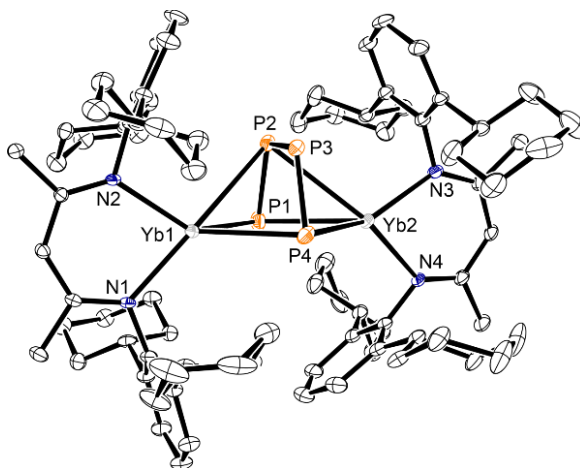


Figure 2.12. Ortep representations (30% probability ellipsoids) of compound **2.17**. Hydrogen atoms have been omitted for clarity. Selected bond lengths (Å) and angles (°): Yb1–N1 2.354(2), Yb1–N2 2.331(1), Yb1–P1 2.885(1), Yb1–P2 3.235(1), Yb1–P4 2.898(1), Yb2–N3 2.339(3), Yb2–N4 2.340(4), Yb2–P1 2.878(1), Yb2–P2 3.192(1), Yb2–P4 2.2930(1), P1–P2 2.169(2), P2–P3 2.062(2), P3–P4 2.154(2), N1–Yb1–N2 79.8(1), P1–Yb1–P2 41.03(3), P1–Yb1–P4 73.37(4), N1–Yb1–P1 123.71(8), Yb1–P1–Yb2 107.66(4), P1–P2–P3 110.07(6), P2–P3–P4 107.51(6).

The overall structure features of **2.17** appear to be the same as the BDI^{Dipep} analogue, **2.16**, though this complex does not contain any solvent coordination to the ytterbium centres within the dimer. The solid-state data of **2.17** discloses two ytterbium centres bridged by a [P₄]²⁻ moiety. Each Yb(II) centre is chelated by the N-atoms of the β-diketiminato ligand (2.331(1) – 2.354(2) Å) and η³-interacts with the P₄ chain (Yb–P distances: 2.878(1) – 3.3235(1) Å), the values of which are comparable to the Yb–N and Yb–P bond distances of **2.16** (Yb–N: 2.386(2) – 2.399(2), Yb–P: 2.9796(8) – 3.0993(9) Å, respectively). The two terminal P–P bond distances are 2.169(2) and 2.1154(2) Å, with a shorter the internal P–P bond distance of 2.062(2) Å, much like the features of the tetraphosphorus chain in **2.16** (terminal

P–P distance: 2.136(1) and 2.142(1), internal P–P distance: 2.108(1) Å). The P1–P4 distance within **2.17** is significantly longer at 3.455 Å (**2.16**, P1–P4: 3.128 Å).

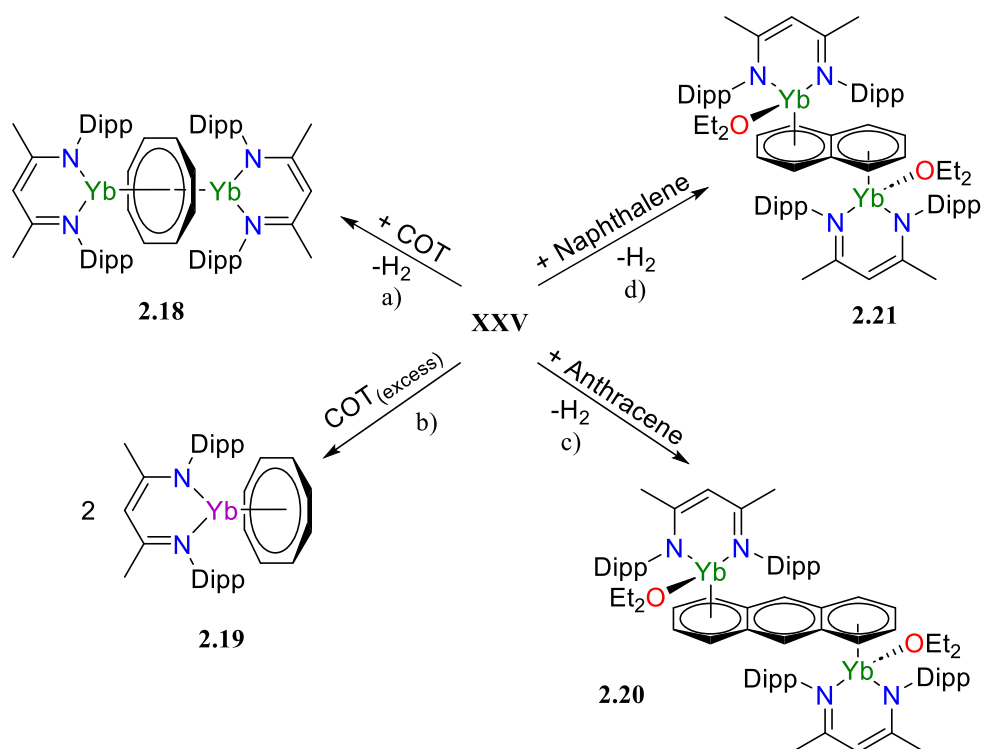
In the solution-state, the ^1H NMR spectrum of **2.17** displays multiple resonances between δ_{H} 5.00 and 4.55 ppm, indicating the possibility of multiple β -diketiminato environments. One peak is likely representative of the methine of the $\text{BDI}^{\text{DicyP}}$ ligand environment within **2.17**, while the singlet at δ_{H} 4.83 ppm was confirmed as free ligand, **2.7**, as this was in a 1:1 ratio with a broad N–H signal centred at δ_{H} 11.55 ppm. To confirm whether more than one phosphorus-containing compound was also present within the reaction mixture, a $^{31}\text{P}\{^1\text{H}\}$ NMR spectrum on **2.17** was obtained, however, no discernible phosphorus signals were observed. Attempts at purifying **2.17** with solvent washes were made, but subsequent multinuclear NMR analysis remained inconclusive.

This Section demonstrates the ability of three different molecular ytterbium(II) hydrides to functionalise white phosphorus. Each system contains a different derivative of the β -diketiminato ancillary ligand, yet the reaction of both **2.5** and **2.14** with P_4 afford analogous reaction products in which a $[\text{P}_4]^{2-}$ dianion bridges the two ytterbium(II) centres of the dimers. In comparison, the reaction of the smallest hydride, **XXV**, gives a trinuclear complex containing the $[\text{P}_7]^{3-}$ Zintl ion cage, resembling the calcium analogue.³⁴

2.4.2 Reduction of Aromatic and Polyaromatic Hydrocarbons

Despite the ideology that lanthanide complexes comprising hydride ligands are usually associated with insertion and σ -bond metathesis reactions, there are reports which discuss the reductive nature of lanthanide hydrides.^{5, 30, 41} Efforts were focused on developing the reductive chemistry of the Yb–H bond within **XXV**, with respect to common cyclic hydrocarbons; 1,3,5,7-cyclooctatetraene (COT) (–1.86 V vs SCE), anthracene (–1.99 V vs SCE) and naphthalene (–2.60 V vs SCE).⁴²

Treatment of **XXV** with COT resulted in an instantaneous colour change from black to dark red and the formation of the inverted sandwich complex (**2.18**) along with the production of hydrogen gas (Scheme 2.12, a)).⁵



Scheme 2.12. Two-electron aromatisation of COT (a)), formation **2.19** (b)), reduction of anthracene (c)) and naphthalene (d)).

The structure of **2.18** was firstly confirmed in the solution-state, where an ^1H NMR spectrum displayed a new β -diketiminato methine resonance at δ_{H} 4.50 ppm, which is in a 2:8 ratio with a singlet at δ_{H} 5.42 ppm, indicative of the reaction between the dimeric hydride **XXV** with a single equivalent of COT. Crystallisation of **2.18** from a saturated hexane solution afforded single crystals at $-30\text{ }^\circ\text{C}$, allowing for corroboration of the solution- and solid-state structures through X-ray diffraction analysis (Figure 2.13).

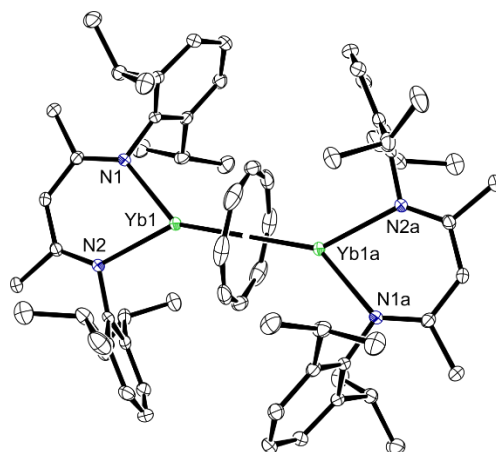


Figure 2.13. ORTEP representation (30 % probability ellipsoids) of compound **2.18**. Hydrogen atoms have been omitted for clarity. Selected bond lengths (Å) and angles (°): Yb1–N1 2.389(2), Yb1–N2 2.403(2), Yb1–C30 2.718(3), Yb1–C31 2.723(3), Yb1–C32 2.716(3), Yb1–C33 2.709(3), N1–Yb1–N2 75.97(6), N1–Yb1–C30 139.29(11), N2–Yb1–C30 116.00(1), N1–Yb1–C31 166.40(1), N2–Yb1–C31 102.31(8), N1–Yb1–C32 163.69(1), N2–Yb1–C32 101.60(8), N1–Yb1–C33 136.46(1), N2–Yb1–C33 114.70(1).

The asymmetric unit of **2.18** comprises only half of the dimer, displaying a Yb(II) centre *N,N*-chelated to the BDI^{Dipp} ligand and interacting with half of the [COT]²⁻ dianion. The Yb1–N1 and Yb1–N2 bond lengths (2.389(2) and 2.403(2) Å) are consistent with the Yb–N bond lengths of other Yb(II) complexes supported by the same BDI^{Dipp} ligand framework (2.328 – 2.495 Å).^{1, 4, 17} The remainder of the complex is generated through an inversion centre coinciding with the centroid of the C₈-ring, giving the inverted sandwich complex in which two [(BDI^{Dicy})Yb] units are bridged by the [COT]²⁻ dianion, in an η⁸-coordination mode. The Yb1–C_{cent} distance (2.008(3) Å) and Yb1–C_{cent}–Yb1a angle of 180.0(6)° are like other Yb(II) inverted sandwich complexes containing the [COT]²⁻ dianion (1.909 – 2.109 Å and 178.9 – 179.5°, respectively).⁴³⁻⁴⁵ To our knowledge, there are only three reports of bimetallic Yb(II) complexes containing the μ-[COT]²⁻ dianion, however, these complexes were synthesised through a salt metathesis reaction between a ytterbium dihalide and the potassium salt of COT,⁴⁴ or through a metathesis reaction between COT and Cp^{*}₂Yb.^{43, 45} Compound **2.18** was

found to be isostructural with the calcium analogue, **XXXV**, which reports a similar Ca1–C_{Cent} distance of 2.0144(4) Å and Ca1–C_{Cent}–Ca1a angle of 180.00(2)°. ⁸

Density Functional Theory (DFT) studies (B3PW91), provided by international collaborators at Université de Toulouse, Prof. Laurent Maron and Iskander Douair, were calculated and confirmed the two-electron aromatisation reaction by which formation of **2.18** was occurring (Figure 2.14).

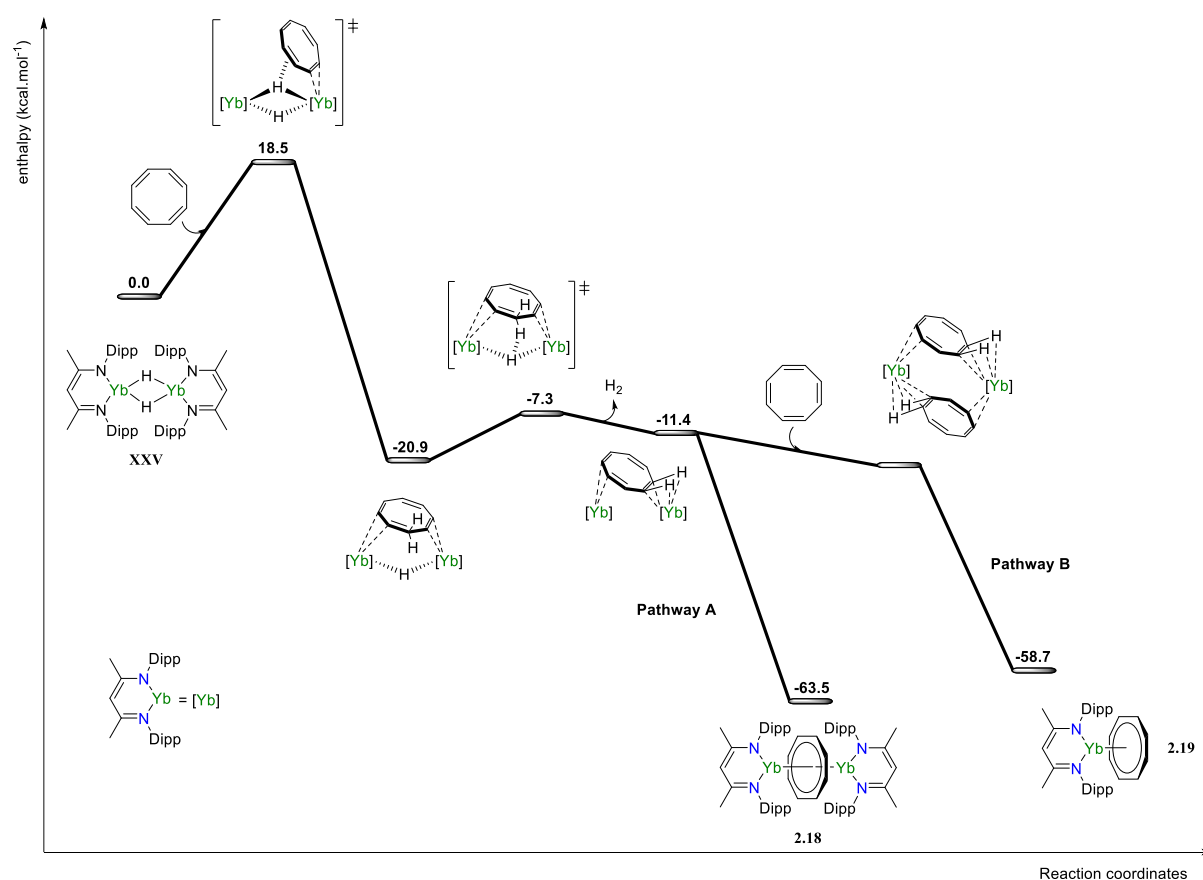


Figure 2.14. Computed enthalpy profile for the two-electron aromatisation of COT by compound **XXV** to give **2.18** (pathway A) or **2.19** (Pathway B).

The reaction began with the initial coordination of an equivalent of COT to **XXV** (+18.5 kcal.mol⁻¹) and the subsequent nucleophilic delivery of a hydride to a C–C double bond. The formation of the bridging intermediate occurs through an exothermic reaction ($\Delta H = -20.9$ kcal.mol⁻¹) and is ensued by the kinetically accessible deprotonation between the second

hydride ligand of **XXV** and the now monoanionic $[\text{C}_8\text{H}_9]^-$ unit ($\Delta H = -13.6 \text{ kcal.mol}^{-1}$). The resultant intermediate formed was then computed to undergo two possible reaction pathways, one resulting in a direct flip-over to give the experimentally observed compound (**2.18**, $\Delta H = -63.5 \text{ kcal.mol}^{-1}$). The second pathway informs that a second insertion of COT and the concurrent oxidation of Yb(II) to Yb(III) can provide the monometallic species **2.19**, also through an exothermic reaction ($\Delta H = -58.7 \text{ kcal.mol}^{-1}$). The synthesis of this Yb(III) compound was also experimentally possible, found to be the minor isolated product from the addition of an excess of COT to **XXV** (Scheme 2.12, b)).

In the solution-state, the oxidation of the Yb(II) centre to Yb(III) within **2.19** is confirmed as the ^1H NMR spectrum displays large chemical shift ranges, broadening of linewidths and loss of J -couplings, indicative of the paramagnetic Yb(III) ion (electronic configuration: $[\text{Xe}]4f^{13}$).^{30,46} A single crystal X-ray diffraction experiment further corroborates the structure of **2.19** in the solid-state (Figure 2.15). The complex displays a slight decrease in Yb1–N1 and Yb1–N2 bond lengths (2.3286(2) and 2.3245(2) and Yb1–C_{Cent} distance (1.7290(7) Å) compared to the dimeric species **2.18** (Yb–N: 2.389(2) and 2.403(2), Yb1–C_{Cent}: 2.008(3) Å, respectively) and aligns with the presence of the smaller Yb(III) ion compared to Yb(II). The $[\text{COT}]^{2-}$ ligand is not planar, displaying a fold angle of $3.54(2)^\circ$.

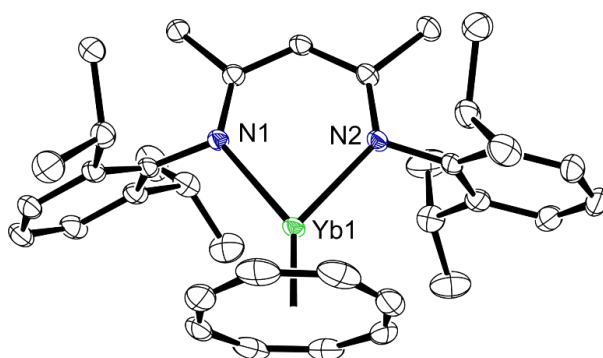


Figure 2.15. ORTEP representation (30 % probability ellipsoids) of compound **2.19**. Hydrogen atoms have been omitted for clarity. Selected bond lengths (Å) and angles ($^\circ$): Yb1–N1 2.3286(2), Yb1–N2 2.3245(2), Yb1–C_{Cent} 1.7290(7), N1–Yb1–N2 80.06(6).

Optimistic in the reductive ability of the Yb–H in **XXV**, this work was extended to the more challenging polycyclic hydrocarbons, anthracene and naphthalene (–1.99 V and –2.60 V vs SCE, respectively).⁴² The reaction of both anthracene and naphthalene with **XXV** was observed to occur overnight at room temperature, with extrusion of hydrogen gas, giving both **2.20** and **2.21**, respectively (Scheme 2.12, c) and d)). Both reactions were conducted in toluene solvent, presumably providing the solvent-free analogues of compounds **2.20** and **2.21**, however, diethyl ether was utilised to aid in the solubility of both complexes during the crystallisation process. Single crystal X-ray diffraction experiments confirmed that both products contained two [(BDI^{Dipp})Yb] units interacting in an η^4 -fashion with the terminal C₆-rings from opposing faces of respective dianions (Figure 2.16).

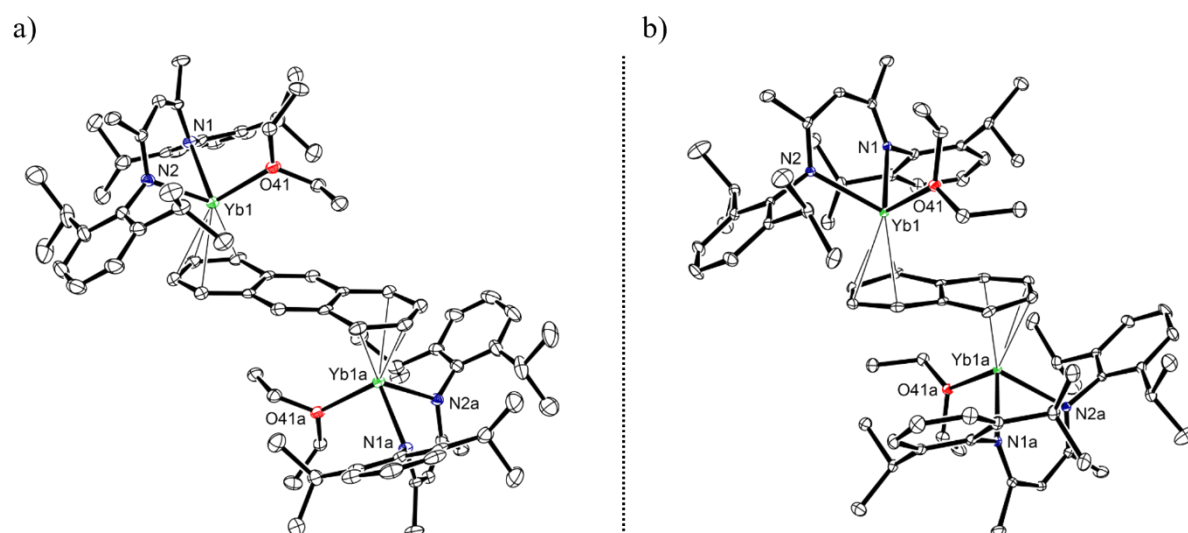


Figure 2.16. ORTEP representation (30 % probability ellipsoids) of compound **2.20** (left) and compound **2.21** (right).

Hydrogen atoms have been removed for clarity. Selected bond lengths (Å) and angles (°): **2.20**: Yb1–N1 2.370(5), Yb1–N2 2.360(6), Yb1–C31 2.960(6), Yb1–C32 2.770(8), Yb1–C33 2.666(9), Yb1–C34 2.701(8), Yb1–C35 2.757(7), Yb1–C36 2.944(6), N1–Yb1–C31 125.38(19), N2–Yb1–C31 147.08(19), N2–Yb1–N1 80.10(19), N1–Yb1–C33 95.8(2), N2–Yb1–C33 152.2(2), N2–Yb1–C36 120.43(19). **2.21**: Yb1–N1 2.420(2), Yb1–N2 2.3803(2), Yb1–C31 3.1119(1), Yb1–C32 2.83(3), Yb1–C33 2.765(2), Yb1–C34 2.657(1), Yb1–C35 2.619(1), Yb1–C36 2.94(3), N2–Yb1–N1 77.35(6), N1–Yb1–C31 140.62(8), N2–Yb1–C31 137.26(7), N1–Yb1–C32 153.7(4), N2–Yb1–C32 109.8(5), N1–Yb1–C33 127.4(4), N2–Yb1–C33 94.5(3), N1–Yb1–C34 102.6(3), N2–Yb1–C34 104.0(3), N1–Yb1–C35 95.1(2), N2–Yb1–C35 132.4(2), N1–Yb1–C36 112.84(14), N2–Yb1–C36 154.3(3).

With respect to **2.20** (Figure 2.16, a)), the solid-state structure is monomeric in the asymmetric unit, with the $[\text{C}_{14}\text{H}_{10}]^{2-}$ ligand is located on an inversion centre. The data discloses that each Yb(II) centre within the dimer are *N,N*-bound to the nitrogen atoms of the BDI^{Dipp} ligand (Yb1–N1: 2.370(5), Yb1–N2: 2.360(6) Å) and η^4 -interact with one of the terminal C_6 -rings from opposing faces of the anthracene dianion. The primary coordination sphere of the Yb(II) centre is made up by the coordination of a diethyl ether molecule. This contrasts the structural features of the reaction product formed by the reduction of anthracene with the analogous calcium hydride (**XXXVI**): one $[(\text{BDI}^{\text{Dipp}})\text{Ca}]$ unit is coordinated to the central ring on the top face of the anthracene dianion and two $[(\text{BDI}^{\text{Dipp}})\text{Ca}]$ units coordinated to the terminal C_6 -rings on the opposing face of the $[\text{C}_{14}\text{H}_{10}]^{2-}$ ligand, linked by a bridging hydride ligand.⁴⁷ To date, there are no reports on other crystallographically characterised ytterbium complexes bearing the anthracene dianion ligand. However, there are two reports of two other lanthanide complexes, $[\text{Cp}^*_2\text{Ln}(\mu\text{-C}_{14}\text{H}_{10})\text{LnCp}^*_2]$ ($\text{Ln} = \text{La}, \text{Sm}$), which contain two $[\text{Cp}^*_2\text{Ln}]$ units that are bonded in an η^3 -fashion from opposing sides to the central C_6 -ring of a nearly planar anthracene moiety.^{48, 49}

For compound **2.21** (Figure 2.16, b)), the asymmetric unit contains two independent molecules, both lying on an inversion centre. Overall, the solid-state structure is dimeric, with two $[(\text{BDI}^{\text{Dipp}})\text{Yb}]$ units interacting in a similar η^4 -fashion to the terminal C_6 -rings from opposing faces of the naphthalene dianion. It is important to note that the reduced naphthalene dianion of **2.21** is no longer planar, acquiring a slight trans-decalin distortion (dihedral angle = $10.4(2)^\circ$ between C32–C33–C34–C35 and C32–C31–C31a–C35 planes) which is consistent with the reduction of naphthalene to the $[\text{C}_{10}\text{H}_8]^{2-}$ dianion and comparable to the only other example of a Yb(II) complex containing the naphthalene dianion.⁵⁰ This complex was not synthesised *via* the reduction of naphthalene by a lanthanide complex, however, and was instead afforded from a salt metathesis reaction with the naphthalene Group 1 salt. Like with

anthracene, the related reduction of naphthalene by the calcium hydride gave the trinuclear species (**XXXVII**) where one $[(\text{BDI}^{\text{Dipp}})\text{Ca}]$ unit is coordinated to a ring on the top face of the $[\text{C}_{10}\text{H}_8]^{2-}$ dianion and two $[(\text{BDI}^{\text{Dipp}})\text{Ca}]$ units coordinated to each ring on the opposing face of the naphthalene ligand, also linked by a bridging hydride ligand.⁴⁷

This study highlights that compounds containing calcium and ytterbium(II) are not always isostructural to each other, and these two heteroleptic hydride complexes display subtle differences in reactivity. For example, the reduction of naphthalene by **XXXII** occurred over 60 days at room temperature, only yielding **XXXVII** in a 50% yield. In contrast, the ytterbium hydride (**XXV**) could react within 24 hours at room temperature to give **2.21**. This facile reduction chemistry highlights **XXV** to be a powerful two-electron reductant and contradicts the reports that lanthanide hydride complexes could only reduce substrates with reduction potentials more positive than -1.99 V vs SCE .^{5, 43}

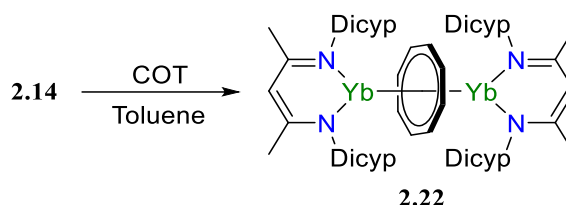
Analogous reaction pathways were computed for the synthesis of **2.20** and **2.21**, with calculated barriers higher than those computed for COT and is consistent with the increased steric bulk of the anthracene and naphthalene substrates. However, in contrast to COT, the increased steric bulk of anthracene and naphthalene impedes a second insertion of the polyaromatics such that the dimeric intermediate will not form. Instead, the only likely pathway is *via* the direct flip-over to form the experimentally isolated final products, in which the 2+ oxidation state of the ytterbium centre is retained.

Chapter One discloses two crystallographically characterised calcium complexes containing a reduced anthracene and naphthalene dianion, respectively, which the larger $\text{BDI}^{\text{Dipep}}$ ligand system supports the calcium centre.¹⁰ However, the reduction of both polyaromatic substrates by the ytterbium hydride **2.5** was not attempted for two reasons: firstly, on account of the solvated Yb(II) centre but also because of the flexibility of the Dipep *N*-

substituents of the ligand and the prediction that we would end up activating the BDI^{Dipep} ligand in a similar manner to compound **2.6**.

Instead, the following Section discusses the reduction of COT and the more challenging substrate anthracene by the BDI^{Dicyp} system, **2.14**, to provide a direct comparison of the reactivity profile of the two ytterbium hydride complexes, affected by the relative steric bulk of the two β -diketiminato ligands.

Despite **2.14** being largely insoluble in aromatic solvents, one equivalent of COT was added to a suspension of **2.14** in toluene and stirred at room temperature (Scheme 2.13).



Scheme 2.13. Two-electron aromatisation of COT to give **2.22**.

After 1 week at room temperature, the scintillation vial still contained a purple-black solid, indicating the presence of unreacted hydride. However, upon settling the mixture, the toluene solution was very faintly pink. This solution was filtered and concentrated under vacuum, forming small crystals within a few hours at room temperature, allowing for analysis by an X-ray diffraction experiment (Figure 2.17, a)).

The asymmetric unit comprises the entire molecule of **2.22**, displaying a Yb(II) centre that is *N,N*-chelated to the BDI^{Dicyp} ligand and interacting with the [COT]²⁻ dianion in an η^8 -coordination mode. The Yb–N bond distances of 2.361(2) – 2.401(2) Å are comparable to those found in the smaller analogue (**2.18**: 2.389(2) and 2.403(2) Å).⁵ The Yb1–C_{cent} distance of 1.9939(1) Å in **2.22** is marginally longer than the Yb2–C_{Cent} distance of 1.9771(1) Å, showing

a slight asymmetric bridging of the [COT]²⁻ dianion between the two Yb(II) centres within **2.22**, which is not seen with **2.18** (Yb1–C_{cent}: 2.008(3) Å).

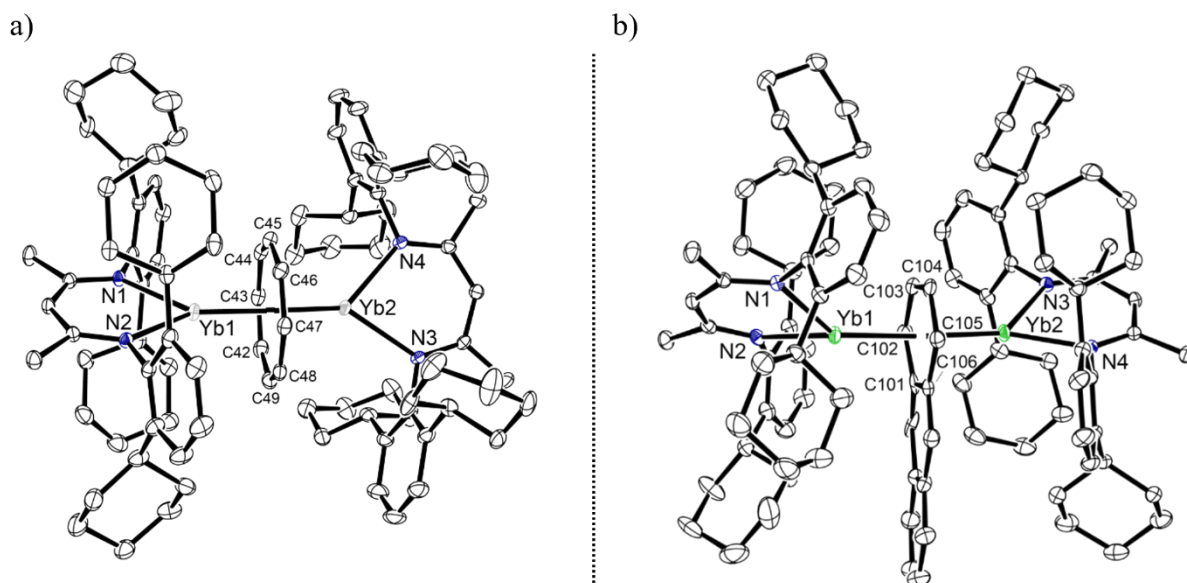


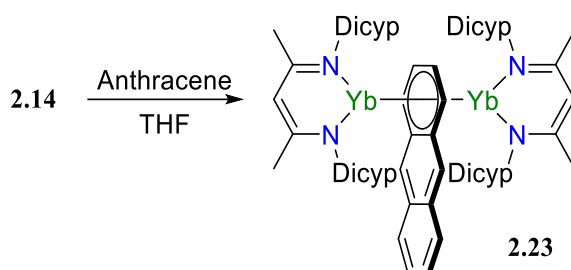
Figure 2.17. Ortep representation (30% probability ellipsoids) of compound **2.22** (left) and compound **2.23** (right).

Hydrogen atoms have been omitted for clarity. Selected bond lengths (Å) and angles (°): **2.22**: Yb1–N1 2.401(2), Yb1–N2 2.361(2), Yb1–C_{cent} 1.9939(1), Yb2–N3 2.369(2), Yb2–N4 2.378(2), Yb2–C_{cent} 1.9771(1), N1–Yb1–N2 79.26(8), N3–Yb2–N4 80.67(8), Yb1–C_{cent}–Yb2 177.97(7). **2.23**: Yb1–N1 2.342(1), Yb1–N2 2.353(2), Yb1–C_{cent} 2.3053(1), Yb2–N3 2.367(2), Yb2–N4 2.336(2), Yb2–C_{cent} 2.288(1), N1–Yb1–N2 77.92(7), N1–Yb1–C_{cent} 136.20(8), Yb1–C_{cent}–Yb2 176.85(5).

So far, the structure has not been confirmed in the solution-state because of the poor solubility and low isolated yields of **2.22**, hindering the ability to purify the clean product away from impurities. However, this preliminary study shows the impact of the larger BDI^{Dicyp} on the reduction of COT by a ytterbium(II) hydride, apparent by the changes in the solubility of the starting compounds and the increased reaction time.

The poor ability of **2.14** to reduce COT meant it seemed unlikely that this same hydride could reduce the more challenging polyaromatic substrates, anthracene (–1.83 and –1.99 V vs SCE) or naphthalene (–2.60 V vs SCE), under similar reaction conditions.⁴² Of the two, anthracene has the less negative reduction potential, hence, only the reduction of anthracene by **2.14** was attempted. This theory was confirmed after adding an excess of anthracene to a

stirring slurry of **2.14** in toluene, where no change was observed after multiple weeks at room temperature. In contrast, removal of the volatiles and adding THF solvent afforded a brown solution of **2.23** after 24 hours at room temperature (Scheme 2.14).



Scheme 2.14. Reduction of anthracene by **2.14**.

The solvent was dried under vacuum, and the crude product dissolved into toluene, giving a green-black colour, and left to crystallise at room temperature. Inspection of an aliquot of the resultant crystalline sample under a microscope inferred that multiple reaction products had formed, apparent by the presence of dark brown, pale yellow and colourless crystals. The identity of these three species was solely confirmed through crystallographic analysis.

An X-ray diffraction experiment identified the brown crystals as the dimeric ytterbium(II) complex containing a reduced $[C_{14}H_{10}]^{2-}$ dianion (**2.23**) (Figure 2.17, b)). The coordination sphere of each Yb(II) metal centre is firstly made up by two contacts from the *N,N*-chelated β -diketiminate ligand with Yb–N bonds lengths between 2.336(2) and 2.367(2) Å, the values which align with Yb–N bond lengths in **2.20** (2.370(5) and 2.360(6) Å).⁵ Each Yb(II) centre then η^6 -interacts from opposing faces of the same terminal C_6 -ring of the anthracene dianion (Yb1– C_{Cent} : 2.3053(1) and 2.288(1) Å) and is in stark contrast to the geometry found with the BDI^{Dipp} analogue, **2.20**, but reminiscent of the geometry of the calcium complex, which also contains two $[(BDI^{Dipp})Ca]$ units coordinating the same terminal ring of the bridging $[C_{14}H_{10}]^{2-}$ ligand.¹⁰ Compound **2.23** displays an average C–C bond length of the uncoordinated C_6 -ring of 1.3997 Å, which is shorter than the average C–C bond length

of the Yb-bound ring (average C–C: 1.4493 Å) and is a result of increased electron density located on this terminal C₆-ring of the anthracene dianion. The bridging [C₁₄H₁₀]²⁻ ligand is no longer planar and exhibits a C101–C102–C103–C104–C105–C106 to plane twist angle of 5.81(7)°.

An X-ray diffraction experiment on the colourless crystals present in the sample identified the free ligand, **2.7**,²² but crystallographic analysis on the yellow crystals identified a new ytterbium-containing compound, **2.24** (Figure 2.18).

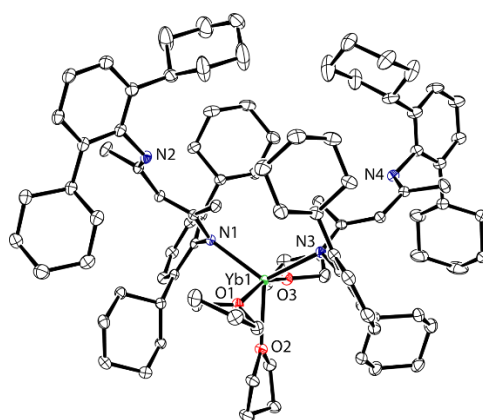


Figure 2.18. Ortep representation (30% probability ellipsoids) of compound **2.24**. Hydrogen atoms have been omitted for clarity. Selected bond lengths (Å) and angles (°): Yb1–N1 2.403(2), Yb1–N3 2.393(2), Yb1–O1 2.488(1), Yb1–O2 2.492(1), Yb1–O3 2.499(1), N2–C_{Dicyclopentadienyl} 1.413(2), N2–C4 1.299(2), N4–C_{Dicyclopentadienyl} 1.409(3), N4–C54 1.296(2), N1–Yb1–N3 118.00(6), O1–Yb1–O2 80.92(5), O2–Yb1–O3 80.67(5).

The solid-state structure of **2.24** was revealed to be a five-coordinate, homoleptic Yb(II) species. Two contacts to the Yb(II) centre were made up by κ^1 -binding of the BDI^{Dicyclopentadienyl} ancillary ligands, reminiscent of one of the ligand binding modes observed within the previously isolated decomposition product, **2.3**. The Yb–N1 and Yb–N3 bond lengths (2.403(2) and 2.393(2) Å) are slightly elongated compared to the Yb1–N3 bond length within **2.3** and could be to accommodate the three THF molecules coordinating to the Yb(II) metal centre (Yb–O: 2.488(1), 2.492(1) and 2.499(1) Å), completing the coordination sphere and giving the compound **2.24** an overall distorted trigonal bipyramidal geometry.

2.5 Summary

In summary, this Chapter introduces the synthesis of a new derivative of the β -diketiminato containing the bulky Dicyc *N*-substituent, as well as the synthesis and structure of two new divalent ytterbium hydrides, **2.5** and **2.14**, bearing the larger BDI^{Dipep} and BDI^{Dicyc} ancillary ligands, respectively. This work aimed to highlight the apparent differences in the structural geometry of these complexes with respect to each other and the original BDI^{Dipp} hydride, **XXV**.¹ Preliminary reactivity studies were conducted with all three species, focusing on the functionalisation of white phosphorus and the two-electron reduction of aromatic hydrocarbons, where alteration of the ligand environment was confirmed to affect reaction outcomes. Overall, this work aimed to optimise the stability and reactivity profile of a new Yb(II) hydride bearing the β -diketiminato ligand, however, each hydride species in this Chapter could be improved upon for different reasons. For example, **2.14** displayed negligible solubility in all solvent systems, thereby affecting this compounds reactivity profile. In the future, this could be addressed through re-evaluating the ligand system and designing new β -diketiminato derivatives that increase the solubility of our complexes without hindering desired reactivity, as seen with **2.5**. This would allow us to isolate a plethora of ytterbium(II) hydrides for developing new novel catalytic and stoichiometric chemical transformations, such as hydrosilylation, hydrogenation, hydroboration, or alkene polymerisation reactions.

2.6 References

1. G. M. Richardson, I. Douair, S. A. Cameron, J. Bracegirdle, R. A. Keyzers, M. S. Hill, L. Maron and M. D. Anker, *Nat. Comm.*, **2021**, 12 (1), 1-7.
2. S. Harder, *Angew. Chem. Int. Ed.*, **2004**, 43 (20), 2714-2718.
3. T. X. Gentner, B. Rösch, G. Ballmann, J. Langer, H. Elsen and S. Harder, *Angew. Chem. Int. Ed.*, **2019**, 58 (2), 607-611.
4. C. Ruspici, J. Spielmann and S. Harder, *Inorg. Chem.*, **2007**, 46 (13), 5320-5326.
5. G. M. Richardson, I. Douair, S. A. Cameron, L. Maron and M. D. Anker, *Chem. Eur. J.*, **2021**, 27 (52), 13144-13148.
6. G. M. Richardson, J. Howarth, M. J. Evans, A. J. Edwards, S. A. Cameron and M. D. Anker, *J. Coord. Chem.*, **2022**, 75 (11-14), 1954-1966.
7. A. S. Wilson, M. S. Hill, M. F. Mahon, C. Dinoi and L. Maron, *Science*, **2017**, 358 (6367), 1168-1171.
8. M. S. Hill, M. F. Mahon, A. S. S. Wilson, C. Dinoi, L. Maron and E. Richards, *Chem. Comm.*, **2019**, 55 (40), 5732-5735.
9. J. Mai, B. Rösch, J. Langer, S. Grams, M. Morasch and S. Harder, *Eur. J. Inorg. Chem.*, **2023**, 26 (31), e202300421.
10. J. Mai, B. Rösch, N. Patel, J. Langer and S. Harder, *Chem. Sci.*, **2023**, 14 (18), 4724-4734.
11. B. Rösch, T. X. Gentner, J. Langer, C. Färber, J. Eyselein, L. Zhao, C. Ding, G. Frenking and S. Harder, *Science*, **2021**, 371 (6534), 1125-1128.
12. R. Shannon, *Acta Cryst. A.*, **1976**, 32 (5), 751-767.
13. Q. Wen, B. Feng, L. Xiang, X. Leng and Y. Chen, *Inorg. Chem.*, **2021**, 60 (18), 13913-13919.
14. G. M. Ferrence, R. McDonald and J. Takats, *Angew. Chem. Int. Ed.*, **1999**, 38 (15), 2233-2237.
15. G. M. Ferrence and J. Takats, *J. Organomet. Chem.*, **2002**, 647 (1-2), 84-93.
16. B. Maitland, A. Stasch and C. Jones, *Aust. J. Chem.*, **2022**, 75 (9), 543-548.
17. P. B. Hitchcock, A. V. Khvostov, M. F. Lappert and A. V. Protchenko, *Dalton Trans.*, **2009**, (13), 2383-2391.
18. D. Heitmann, C. Jones, D. P. Mills and A. Stasch, *Dalton Trans.*, **2010**, 39 (7), 1877-1882.
19. X. Liu, L. Xiang, E. Louyriac, L. Maron, X. Leng and Y. Chen, *J. Am. Chem. Soc.*, **2019**, 141 (1), 138-142.
20. X. Shi, P. Deng, T. Rajeshkumar, L. Zhao, L. Maron and J. Cheng, *Chem. Comm.*, **2021**, 57 (78), 10047-10050.
21. B. Rösch, T. X. Gentner, H. Elsen, C. A. Fischer, J. Langer, M. Wiesinger and S. Harder, *Angew. Chem. Int. Ed.*, **2019**, 58 (16), 5396-5401.
22. G. M. Richardson, T. Rajeshkumar, F. M. Burke, S. A. Cameron, B. Nicholls, J. Harvey, R. A. Keyzers, T. Butler, S. Granville, L. Liu, L. Maron and M. D. Anker, preprint out at *Nature Portfolio*, under revision (*Nat. Chem.*), **2023**.
23. I. I. Oleinik, I. V. Oleinik, I. B. Abdrakhmanov, S. S. Ivanchev and G. A. Tolstikov, *Russ. J. Gen. Chem.*, **2004**, 74 (9), 1423-1427.
24. D. D. L. Jones, S. Watts and C. Jones, *Inorganics*, **2021**, 9 (9).
25. A. G. Avent, M. R. Crimmin, M. S. Hill and P. B. Hitchcock, *J. Organomet. Chem.*, **2006**, 691 (6), 1242-1250.

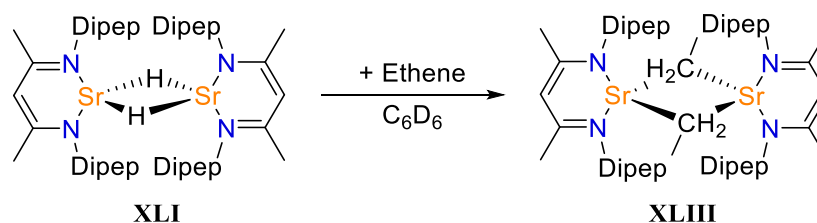
26. P. Pykkö and M. Atsumi, *Chem. Eur. J.*, **2009**, 15 (1), 186-197.
27. M. Mantina, A. C. Chamberlin, R. Valero, C. J. Cramer and D. G. Truhlar, *J. Phys. Chem. A.*, **2009**, 113 (19), 5806-5812.
28. I. V. Basalov, D. M. Lyubov, G. K. Fukin, A. S. Shavyrin and A. A. Trifonov, *Angew. Chem. Int. Ed.*, **2012**, 51 (14), 3444-3447.
29. H. Bauer, K. Thum, M. Alonso, C. Fischer and S. Harder, *Angew. Chem. Int. Ed.*, **2019**, 58 (13), 4248-4253.
30. W. J. Evans, *Inorg. Chem.*, **2007**, 46 (9), 3435-3449.
31. W. J. Evans, *Adv. Organomet. Chem.*, **1985**, 24, 131-177.
32. W. J. Evans, *Polyhedron*, **1987**, 6 (5), 803-835.
33. M. Arrowsmith, M. S. Hill, A. L. Johnson, G. Kociok-Köhn and M. F. Mahon, *Angew. Chem. Int. Ed.*, **2015**, 54 (27), 7882-7885.
34. R. Yadav, M. Weber, A. K. Singh, L. Münzfeld, J. Gramüller, R. M. Gschwind, M. Scheer and P. W. Roesky, *Chem. Eur. J.*, **2021**, 27 (56), 14128-14137.
35. J. D. Protasiewicz, M. P. Washington, V. B. Gudimetla, J. L. Payton and M. C. Simpson, *Inorganica Chim. Acta.*, **2010**, 364 (1), 39-45.
36. R. S. P. Turbervill and J. M. Goicoechea, *Chem. Rev.*, **2014**, 114 (21), 10807-10828.
37. L. Weber, *Chem. Rev.*, **1992**, 92 (8), 1839-1906.
38. C. G. P. Ziegler, T. M. Maier, S. Pelties, C. Taube, F. Hennersdorf, A. W. Ehlers, J. J. Weigand and R. Wolf, *Chem. Sci.*, **2019**, 10 (5), 1302-1308.
39. T. Li, N. Arleth, M. T. Gamer, R. Köppe, T. Augenstein, F. Dielmann, M. Scheer, S. N. Konchenko and P. W. Roesky, *Inorg. Chem.*, **2013**, 52 (24), 14231-14236.
40. H. Günther, *Angew. Chem. Int. Ed.*, **1972**, 11 (10), 861-874.
41. W. J. Evans, B. M. Schmiede, S. E. Lorenz, K. A. Miller, T. M. Champagne, J. W. Ziller, A. G. DiPasquale and A. L. Rheingold, *J. Am. Chem. Soc.*, **2008**, 130 (26), 8555-8563.
42. S. Bank and D. A. Juckett, *J. Am. Chem. Soc.*, **1976**, 98 (24), 7742-7746.
43. W. J. Evans, M. A. Johnston, R. D. Clark and J. W. Ziller, *J. Chem. Soc., Dalton Trans.*, **2000**, (10), 1609-1612.
44. W. J. Evans, M. A. Johnston, M. A. Greci and J. W. Ziller, *Organometallics*, **1999**, 18 (8), 1460-1464.
45. W. J. Evans, T. M. Champagne, B. L. Davis, N. T. Allen, G. W. Nyce, M. A. Johnston, Y. C. Lin, A. Khvostov and J. W. Ziller, *J. Coord. Chem.*, **2006**, 59 (10), 1069-1087.
46. A. J. Pell, G. Pintacuda and C. P. Grey, *Prog. in Nucl. Mag. Reason. Spectrosc.*, **2019**, 111, 1-271.
47. A. S. S. Wilson, C. Dinoi, M. S. Hill, M. F. Mahon, L. Maron and E. Richards, *Angew. Chem. Int. Ed. Engl.*, **2020**, 59 (3), 1232-1237.
48. K. H. Thiele, S. Bambirra, H. Schumann and H. Hemling, *J. Organomet. Chem.*, **1996**, 517 (1), 161-163.
49. W. J. Evans, S. L. Gonzales and J. W. Ziller, *J. Am. Chem. Soc.*, **1994**, 116 (6), 2600-2608.
50. A. N. Selikhov, T. V. Mahrova, A. V. Cherkasov, G. K. Fukin, E. Kirillov, C. Alvarez Lamsfus, L. Maron, L and A. A. Trifonov, *Organometallics*, **2016**, 35 (14), 2401-2409.

Chapter Three

Synthesis and Reactivity of Europium(II) Hydrides

3.1 Introduction

In 2019, Harder reported on the successful isolation of the heteroleptic strontium hydride supported by the $\text{BDI}^{\text{Dipep}}$ ancillary ligand.¹ This strontium species could react with the unsaturated substrate, ethene, to generate the respective strontium *n*-alkyl intermediate capable of facilitating the nucleophilic alkylation of benzene (Scheme 3.1).¹



Scheme 3.1. Reactivity of a heteroleptic strontium hydride (**XLI**) with ethene to give **XLIII**.

It is important to note that this reactivity only followed a stoichiometric regime. However, unlike the calcium hydride (**XXXII**), this nucleophilic reactivity was not hindered by the Schlenk-like redistribution of **XLI** to the unreactive homoleptic species, $[(\text{BDI}^{\text{Dipep}})_2\text{Sr}]$. This report, therefore, demonstrates the ability of the $\text{BDI}^{\text{Dipep}}$ ancillary ligand to provide enough steric protection of the large strontium ion without the need for additional stability provided by donor solvent molecules.

As the ionic radius of europium(II) is comparable to strontium (Eu^{2+} : 1.25 Å, Sr^{2+} : 1.26 Å),² it is plausible that this β -diketiminato ligand system can also accommodate this divalent lanthanide ion. Thus, it was the starting point for our attempts to synthesise the first example of a molecular, europium(II) hydride.

3.2 Attempted Synthesis of [(BDI^{Dipep})EuH]₂

3.2.1 Synthesis *via* [Eu(HMDS)₂]

The first approach towards isolating a molecular europium(II) hydride was modelled off the synthetic method used to generate our original ytterbium(II) hydride complex, **XXV**, where we first synthesise the solvent-free Yb(II) bis amide, followed by the heteroleptic ytterbium amide as the precursor complex to synthesising the desired hydride.³ However, attempts to synthesise the homoleptic europium amide *via* a salt metathesis reaction between EuI₂ and two molar equivalents of KHMDS in benzene instead resulted in the formation of the potassium europium(II) tris[bis(trimethylsilyl)amide] “ate” complex, **3.1**, which was characterised through a single crystal X-ray diffraction experiment and found to be structurally similar to the reported sodium tris[bis(trimethylsilyl)amido] europium(II) “ate” complex (Figure 3.1).⁴

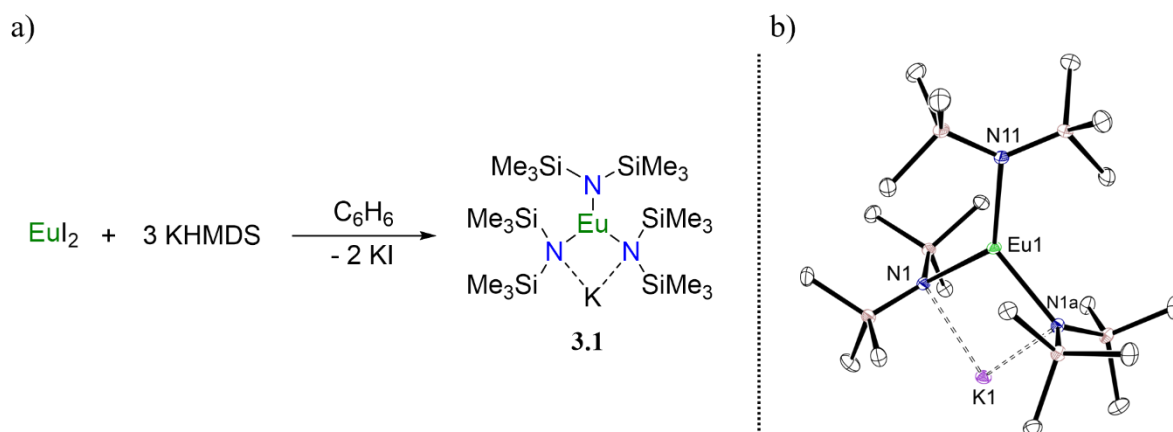


Figure 3.1. Left: Formation of the potassium tris[bis(trimethylsilyl)amido] europium(II) “ate” complex (**3.1**). Right: Ortep representation (30% probability ellipsoids) of compound **3.1**. Hydrogen atoms have been omitted for clarity. Selected bond lengths (Å) and angles (°): Eu1–N11 2.448(4), Eu1–N1 2.518(3), N1–K1 2.898(3), N1–Eu1–N11 129.39(6), N1–Eu1–N1 101.21(1), Eu1–N1–Si1 126.95(1), Eu1–N1–Si2 105.90(1), Eu1–N1–K1 87.21(8).

The divalent europium ion has the stable, half-filled f-configuration ([Xe]4f⁷) and can have up to seven unpaired electrons.⁵ As a result, the Eu(II) nucleus is paramagnetic. Structural characterisation of paramagnetic species in the solution-state *via* multinuclear NMR techniques can be obtained, albeit data acquisition is greatly affected by the fast relaxation times: spectra

display large chemical shift ranges, broadening of linewidths, decrease in resolution correlating to loss of J -couplings, and in some instances, the short relaxation times result in loss of signals entirely.⁶ While spectroscopic data for most europium(II) complexes were attempted, neither full nor partial structural analysis could be determined in solution, thus all complexes herein were structurally elucidated in the solid-state through single crystal X-ray diffraction experiments, with some compounds also supported by Infrared (IR) spectroscopy and elemental analysis (EA).

Prior to conducting the reaction in C_6H_6 solvent, the initial synthesis of the Yb(II) bis amide was carried out in diethyl ether at room temperature to generate the solvated analogue, of which the donor Et_2O molecules could be removed under vacuum. Therefore, it was plausible we could transfer this synthetic method toward europium, where conducting the reaction of EuI_2 and KHMDS in diethyl ether did provide the desired europium bis(amide) (**3.2**) in good yields (85%) (Figure 3.2).

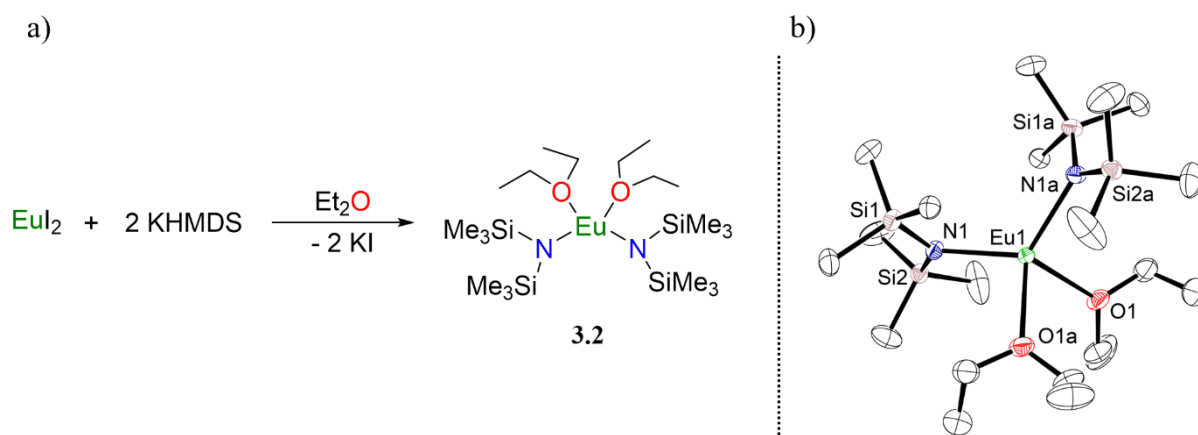


Figure 3.2. Left: Synthesis of the homoleptic Eu(II) bis(amide) (**3.2**). Right: Ortep representation (30% probability ellipsoids) of compound **3.2**. Hydrogen atoms have been omitted for clarity. Selected bond lengths (Å) and angles (°): Eu1–N1 2.437(4), Eu–O1 2.527(5), N1–Eu1–N1 121.4(1), N1–Eu1–O1 124.6(2), Eu1–N1–Si1 111.3(2).

The structure was characterised in the solid-state through an X-ray diffraction experiment on yellow blocks obtained from a saturated hexane solution at $-30\text{ }^{\circ}\text{C}$, confirming

a four-coordinate Eu(II) centre. Two contacts of the coordination sphere are made up of the bis(trimethylsilyl) amide ligands (Eu1–N1 2.437(4) Å) and two from donor Et₂O molecules (Eu1–O1 2.527(5) Å), with bond lengths matching those of the THF analogue, Eu(HMDS)₂(THF)₂ (Eu–N: 2.438 Å, Eu–O: 2.523 Å).⁷

No attempts to remove the diethyl ether molecules *in vacuo* from the Eu(II) centre within **3.2** were made. These first two reactions have already established differences in the stability of these compounds in comparison to the ytterbium analogues, imparted by the increase of ionic radii for the Eu(II) ion; it was likely that striving for the solvent-free analogue might instead result in the decomposition of **3.2**.

The subsequent reaction of **3.2** with the BDI^{Dipep} pro-ligand was expected to generate the heteroleptic europium amide.¹ Instead, crystallisation of the saturated yellow toluene solution yielded single crystals identified as a europium hydroxyl complex, **3.3**, via an X-ray diffraction experiment (Figure 3.3).

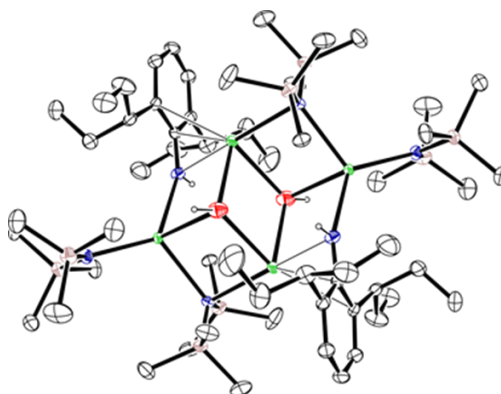


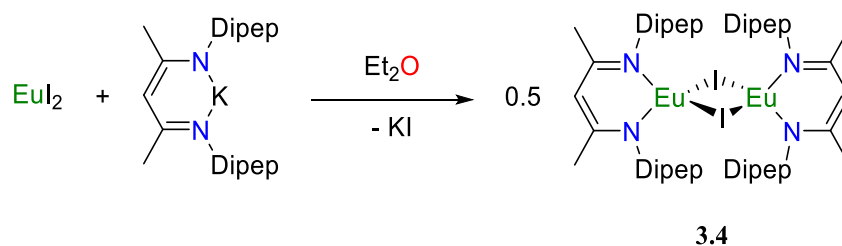
Figure 3.3. Ortep representation (30% probability ellipsoids) of compound **3.3**. Hydrogen atoms (except those on the bridging O atoms and N atoms of the Dipep substituents) and have been omitted for clarity. Poor crystal quality meant sufficient bond length and angle data could not be obtained.

There are reports of a similar magnesium-containing compound; however, this species was isolated after the reaction of impure *n*-BuMgCl in ether solution with sodium diisopropylaniline, with the introduction of the ‘oxo’ ligand tracing back to the Grignard

starting material.⁸ No further insights into the mechanism of how **3.3** formed were made, and insufficient crystallographic data due to poor crystal quality negates further comments past determining this species' structural connectivity.

3.2.2 Synthesis *via* [(BDI^{Dipep})EuI]₂

The following synthetic approach begins to diverge from the reported methods used to synthesise all three examples of strontium hydrides,^{1,9,10} but analogous to the methods outlined in Chapter Two during the synthesis of the two new ytterbium(II) hydrides, **2.5** and **2.14**. The reaction of EuI₂ and the potassium salt of the BDI^{Dipep} ligand was conducted in the coordinating solvent, Et₂O, and provided ready access to the heteroleptic europium iodide, **3.4** (Scheme 3.2).



Scheme 3.2. Salt metathesis reaction to form the heteroleptic Eu(II) iodide (**3.4**).

An X-ray diffraction experiment disclosed **3.4** as a dimer with the europium(II) centres described as being low-coordinate, despite the large coordination sphere of the europium ions: two contacts from the κ^2 -*N,N*-chelated β -diketiminato ligand and two from both of the μ^2 -iodide ligands (Figure 3.4).

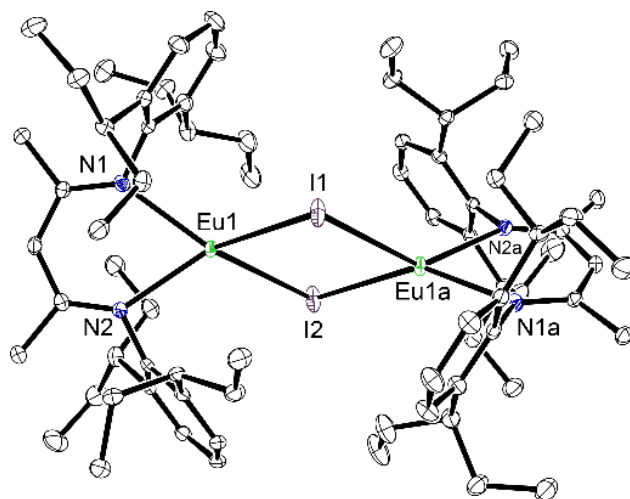
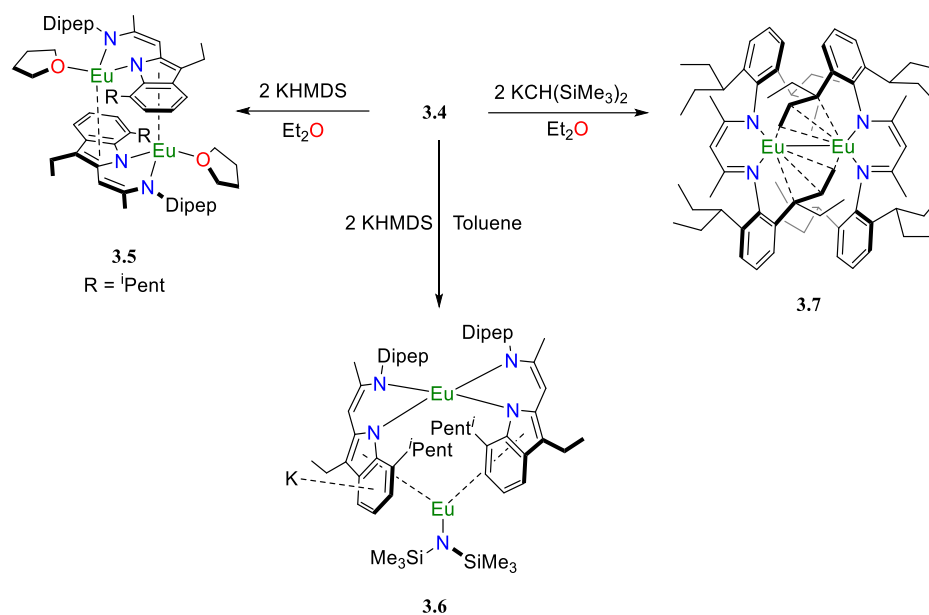


Figure 3.4. Ortep representation (30% probability ellipsoids) of **3.4**. Hydrogen atoms have been omitted for clarity. Selected bond lengths (Å) and angles (°): Eu1–I1 3.2077(5), Eu1–I2 3.2367(5), Eu1–N1 2.479(4), Eu1–N2 2.459(5), I1–Eu1–I2 85.37(1), I1–Eu1–N1 114.78(1), I1–Eu1–N2 136.64(1), N1–Eu1–N2 70.43(1), Eu1–I1–Eu1a 95.19(2).

While there are currently no reports of any other BDI-based Eu(II) iodides, the Eu–N1 and Eu1–N2 bond lengths of 2.479(4) and 2.459(5) Å are within the range of other Eu(II) complexes bearing the β -diketiminate ancillary ligand (2.407 – 2.603 Å).^{11–14} The Eu1–I1 and Eu1–I2 bond lengths are 3.207(5) and 3.2367(5) Å and are closely related to those found in the three reports of dimeric europium iodide complexes (3.246 – 3.352 Å) in which the europium metal centres are also in the 2+ oxidation state.^{15–17}

Solvent has been demonstrated to play a vital role in successfully synthesising the desired europium(II) complexes thus far. Therefore, attempts to synthesise a heteroleptic europium(II) amide were conducted in both diethyl ether and toluene, where a colourless Et₂O or toluene solution containing KHMDS was added to a yellow Et₂O or toluene solution of **3.4**, to yield compounds **3.5** and **3.6**, respectively (Scheme 3.3).



Scheme 3.3. Attempted synthesis of a heteroleptic Eu(II) amido or alkyl complex.

Both reactions resulted in yellow-orange suspensions, with yellow crystalline blocks obtained from saturated hexane solutions after workup, allowing for elucidation of both products in the solid-state by X-ray diffraction experiments (Figure 3.5).

The product formed from the reaction conducted in diethyl ether, **3.5** (Figure 3.5, a)), was disclosed as a dinuclear europium(II) species. Both Eu(II) centres are bound to the amidinate–N–atoms of a $\text{BDI}^{\text{Dipep}}$ ligand, where one Dipep substituent has ring closed to form an indole functionality. Each metal centre then displays an η^5 –interaction with the 5–membered ring of the second indole group within the dimer. The final contact to the Eu(II) centre is a coordinated THF molecule. No THF solvent was present within the reaction mixture, but solvent vapours were likely present in the atmosphere of the glovebox. It could be postulated that an Et_2O molecule was originally coordinated to the Eu(II) centres to stabilise the formation of **3.5** in solution. However, as THF is a stronger Lewis base, the Et_2O molecules could have been exchanged.

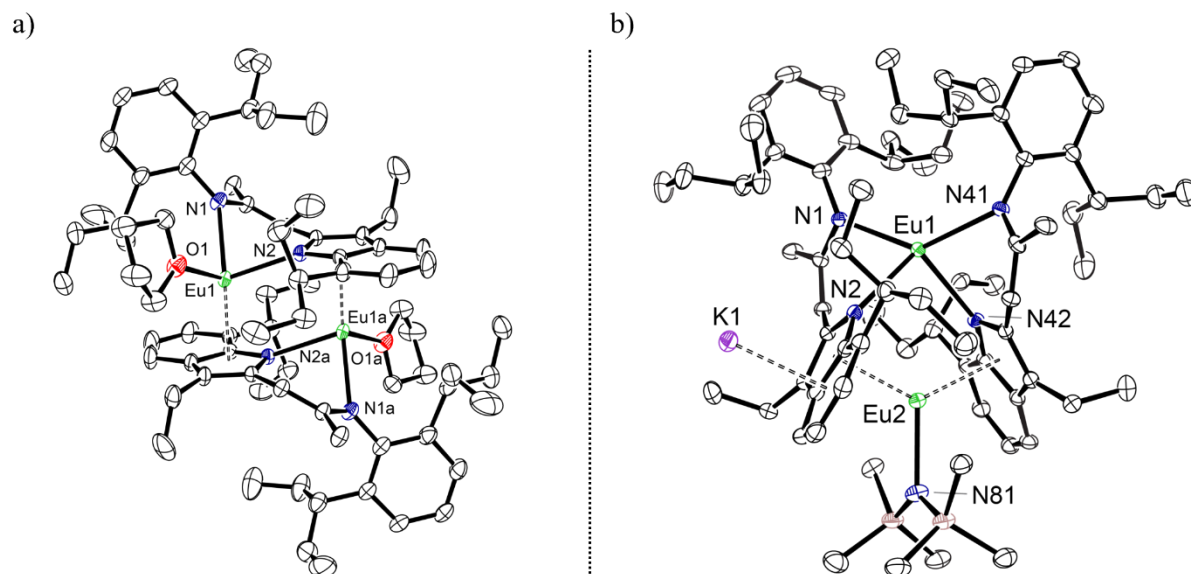


Figure 3.5. Ortep representations (30% probability ellipsoids) of compound **3.5** (left) and compound **3.6** (right). Hydrogen atoms have been omitted for clarity. Selected bond lengths (Å) and angles (°): **3.5**: Eu1–N1 2.412(4), Eu1–N2 2.456(3), Eu1–O1 2.608(7), Eu1–C_{cent} 2.605(3), N1–Eu1–N2 80.9(1), N1–Eu1–O1 92.0(2), N1–Eu1–N2a 139.5(1). **3.6**: Eu1–N1 2.481(4), Eu1–N2 2.537(4), Eu2–N81 2.386(5), Eu2–Cent 2.651(2), K1–C_{cent} 3.327(2), N1–Eu1–N2 82.2(1), N1–Eu1–N41 135.7(1).

The product formed from the reaction conducted in toluene, **3.6** (Figure 3.5, b)), was characterised as a dinuclear europium “ate” complex. One europium centre is bound in an *N,N*-coordination mode to two BDI^{Dipep} ligands, representative of a homoleptic decomposition product. Like **3.5**, one Dipep substituent of each BDI^{Dipep} framework has ring closed to generate an indole functionality. The second europium metal centre within the unit is bound to the nitrogen of a bis(trimethylsilyl)amide group as well as coordinating in an η^5 -fashion to the 5-membered rings of the indole groups. The C₆-ring of the indole group has a potassium contact, which interacts with a C₆-ring of an indole group in a second molecule of compound **3.6**, forming a pseudo polymeric structure.

Neither reaction outcome was the expected heteroleptic europium amido complex, despite the assumption that the coordinating solvent would likely stabilise the desired product. This is surprising given that the strontium amide supported by the BDI^{Dipep} can be synthesised

by heating the free BDI^{Dipep} ligand with the strontium bis(HMDS) to 70 °C for 14 days in hexane. Therefore, an attempt was made to synthesise the heteroleptic Eu(II) alkyl precursor complex instead, reminiscent of the ytterbium(II) alkyl, **2.13**, discussed in Chapter Two.

The potassium salt of Lappert's alkyl, KCH(SiMe₃)₂, was cannula transferred to a stirring solution of **3.4** in Et₂O at –78 °C and left to warm up slowly to room temperature overnight (Scheme 3.3). The reaction was carried out at low temperatures to decrease the possibility of forming any Schlenk-type redistribution products or ligand rearrangement products, however, this was still observed. A single crystal X-ray diffraction experiment disclosed the product to be a dimeric europium(II) species, **3.7**, where one 3-pentyl chain of one Dipep *N*-substituent within each [(BDI^{Dipep})Eu] unit of the dimer has been deprotonated to generate an allyl functionality (Figure 3.6). This is confirmed by the shortening of the C14–C13 and C13–C12 bond lengths to 1.432 and 1.370 Å, respectively, in comparison to the C12–C15 and C15–C16 bond lengths of the second half of the 3-pentyl chain (1.502 and 1.533 Å, respectively).

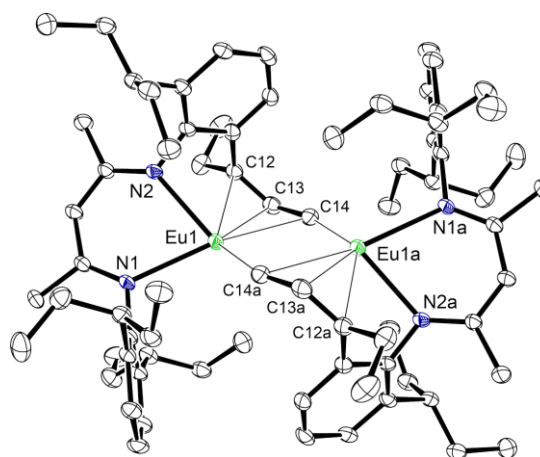


Figure 3.6. Ortep representation (30% probability ellipsoids) of compound **3.7**. Hydrogen atoms have been omitted for clarity. Selected bond lengths (Å) and angles (°): Eu1–N1 2.528(4), Eu1–N2 2.435(5), Eu1–C12 2.869(6), Eu1–C13 2.806(5), Eu1–C14 2.828(5), Eu1–C14a 2.683(7), C14–C13 1.433(9), C13–C12 1.371(8), C12–C15 1.502(8), C15–C16 1.533(1), N1–Eu1–N2 74.2(1), N1–Eu1–C14a 99.7(2), N2–Eu1–C12 63.3(2), N2–Eu1–C14 111.6(2).

The formation of an analogous Yb(II) allyl species was observed through preliminary studies of the solvated Yb(II) hydride supported by the same BDI^{Dipep} ligand mentioned in Chapter Two, however, low-quality crystallographic data obtained for **2.6** negates any further structural comparisons.

Initially, the yellow crystals of **3.7** were obtained from a saturated pentane solution, but the crystallographic data collected was insufficient for obtaining reliable bond distance and angle data, thus requiring recollection. An aliquot of the bulk sample was recrystallised from diethyl ether, but a new single crystal X-ray diffraction experiment on the resultant yellow blocks identified the Schlenk-like redistribution product, **3.8** (Figure 3.7).

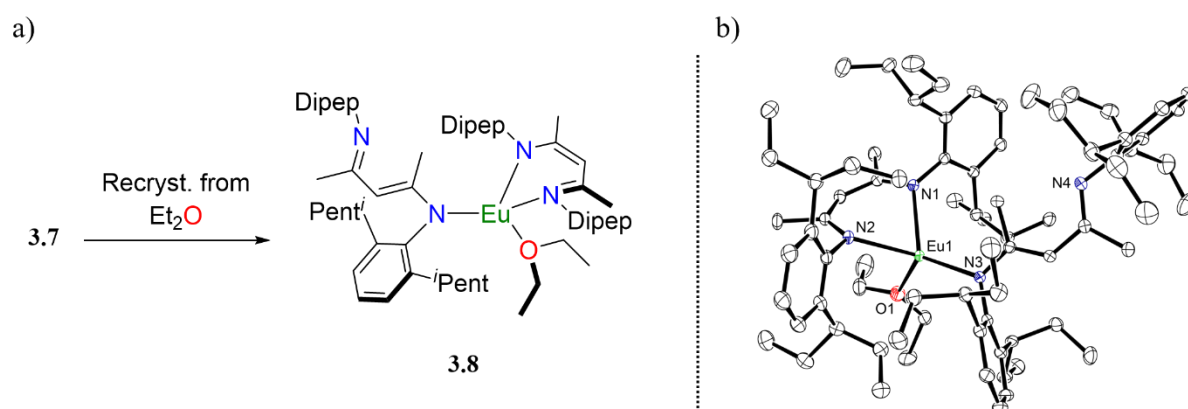


Figure 3.7. Left: Isolation of **3.8** after recrystallisation of compound **3.7**. Right: Ortep representations (30% probability ellipsoids) of compound **3.8**. Hydrogen atoms have been omitted for clarity. Selected bond lengths (Å) and angles (°): Eu1–N1 2.502(2), Eu1–N2 2.474(2), Eu1–N3 2.526(2), N3–C_{Dipep} 1.437(3), N3–C42 1.358(3), N4–C_{Dipep} 1.413(4), N4–C44 1.292(3), Eu1–O1 2.605(2), N1–Eu1–N2 81.14(6), N1–Eu1–N3 122.10(6), N1–Eu1–O1 96.71(6), N2–Eu1–N3 121.33(6).

The Eu(II) metal centre is *N,N*-binding to one BDI^{Dipep} ligand and κ^1 -bonding to one *N*-substituent of a second β -diketiminate ligand. The shorter N4–C₄₄ bond length (1.292(3) Å) within **3.8** is consistent with the N=C bond distance of typical imine substrates (1.27 – 1.31 Å)^{18, 19} and is therefore ascribed as an imine-like homoleptic species, like what was isolated for ytterbium bearing this same BDI^{Dipep} ancillary ligand (**2.3**). The Eu(II) ion has a larger ionic radius compared to Yb(II),^{2, 5} though seemingly not large enough that two BDI^{Dipep} frameworks

can saturate the coordination sphere of the Eu centre in a symmetrical *N,N*-binding mode. Instead, steric unsaturation in **3.8** is relieved through a fourth contact with the oxygen of a diethyl ether molecule.

Though **3.7** was not the desired mononuclear europium(II) alkyl, the subsequent reaction with a hydride source, 1,4-CHD, was attempted.²⁰ The reaction was carried out in C₆D₆ solvent in an NMR tube fitted with a J. Youngs tap. Despite the paramagnetic nature of the Eu(II) ion, the reaction progress was monitored by the decrease of the two singlet resonances representative of the 1,4-CHD reagent. After partial consumption of the signals at δ_{H} 5.59 ppm and δ_{H} 2.53 ppm, the yellow suspension was dried under vacuum and dissolved into Et₂O solvent, obtaining single crystals and allowing for an X-ray diffraction experiment (Figure 3.8).

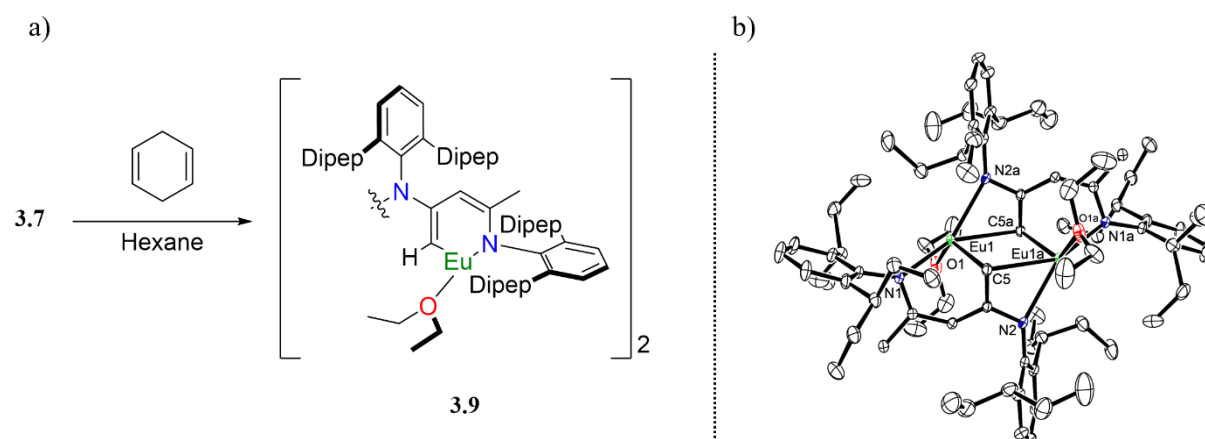


Figure 3.8. Left: Compound **3.9**, isolated from the attempted synthesis of a divalent europium hydride. Right: Ortep representation (30% probability ellipsoids) of compound **3.9**. Hydrogen atoms have been omitted for clarity. Poor crystal quality meant sufficient bond length and angle data could not be obtained.

Poor crystal quality meant reliable bond length and angle data could not be obtained; however, it was sufficient to determine the solid-state product (**3.9**) was not the desired europium(II) hydride but the result of ligand rearrangement, formed *via* deprotonation of a methyl group of the β -diketiminato backbone.

The previously reported BDI^{Dipep} framework has thus far proven to stabilise the europium ion in the 2+ oxidation state yet resulted in a series of decomposition and ligand rearrangement products, using either non-coordinating or coordinating solvent systems. This work demonstrates that complexes containing the Eu(II) ion display an increased sensitivity towards ligand environment and that the synthesis of a divalent europium hydride may not be a simple extension of Group 2 hydrides.^{1, 9, 10, 21}

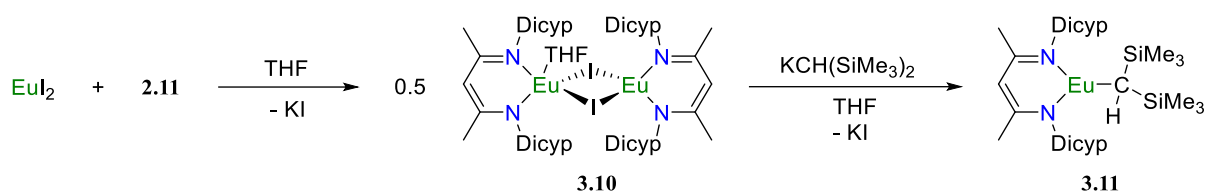
3.3 Synthesis of [(BDI^{Dicyp})EuH]₂

3.3.1 Synthesis *via* [(BDI^{Dicyp})EuI]₂

In Chapter Two, a new β -diketiminato ligand, BDI^{Dicyp} (**2.7**), was introduced.²² It was postulated that this BDI^{Dicyp} ancillary ligand would provide greater steric protection of the lanthanide metal centre, which was demonstrated by the isolation of a solvent-free, divalent ytterbium(II) hydride (**2.14**), despite conducting the entire synthetic method in THF solvent. Though the Eu(II) ion is larger in ionic radius than Yb(II),^{2, 5} it was plausible that this BDI^{Dicyp} framework could also allow for the isolation of a molecular, europium(II) hydride, though additional stabilisation from donor molecules may be required.

Given the success of isolating a heteroleptic Eu(II) iodide supported by the BDI^{Dipep} ligand system and the success of isolating a Yb(II) iodide complex bearing the BDI^{Dicyp} ligand, all attempts at synthesising a divalent europium hydride herein would follow a similar synthetic route. The formation of the heteroleptic europium iodide, **3.10**, was achieved *via* the addition of equimolar quantities of the potassium salt of the BDI^{Dicyp} ligand, **2.11**, to a slurry of europium diiodide in THF solvent (Scheme 3.4).

After 4 hours at room temperature, the reaction mixture appeared as a beige precipitate suspended in a yellow solution, and therefore, it was decided to work it up rather than leaving the reaction overnight.



Scheme 3.4. Synthesis overview to form the monoalkyl complex (**3.11**).

The volatiles were removed *in vacuo*, the crude product was extracted with toluene solvent and filtered through Celite. While crystallisation of a concentrated toluene solution at $-30\text{ }^\circ\text{C}$ could afford orange blocks suitable for an X-ray diffraction experiment, identifying the solvent-free, heteroleptic Eu(II) iodide, higher quality crystallographic data was obtained from yellow plates found within the mixture, found to be the mono-solvated system, **3.10** (Figure 3.9, a)).

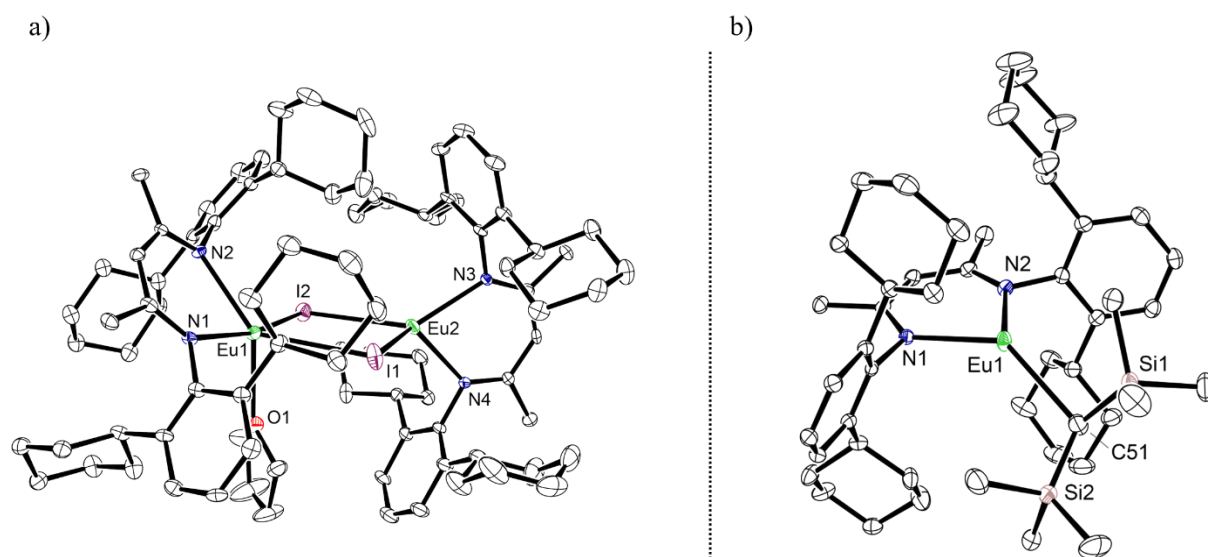


Figure 3.9. Ortep representations (30% probability ellipsoids) of compound **3.10** (left) and compound **3.11** (right).

Hydrogen atoms have been omitted for clarity. Selected bond lengths (\AA) and angles ($^\circ$): **3.10**: Eu1–I1 3.242(1), Eu1–I2 3.3375(6), Eu1–N1 2.509(6), Eu1–N2 2.528(4), Eu1–O1 2.545(6), Eu2–I1 3.1658(7), Eu2–I2 3.1391(9), Eu2–N3 2.432(5), Eu2–N4 2.433(5), I1–Eu1–I2 85.03(2), I1–Eu1–N1 133.0(1), I1–Eu1–N2 110.0(1), I1–Eu1–O1 86.5(1), N1–Eu1–N2 73.6(2), Eu1–I1–Eu2 93.16(2). **3.11**: Eu1–N1 2.482(2), Eu1–N2 2.469(2), Eu1–C51 2.644(4), Eu1...C52 3.036(3), N1–Eu1–N2 72.50(7), N1–Eu1–C51 135.05(9), N2–Eu1–C51 123.20(9).

In the solid-state, both Eu(II) ions within the dimer were found to κ^2 -*N,N*-chelate a BDI^{Dicyp} ancillary ligand, with Eu1–N1 and Eu1–N2 bond lengths (2.509(6) and 2.528(4) Å) that are slightly elongated compared to Eu2–N3 and Eu2–N4 bond lengths (2.432(5) and 2.433(5) Å) but are within the range of other Eu(II) complexes bearing β -diketiminate based ligands (2.407 – 2.603 Å).¹¹⁻¹⁴ Each metal centre is μ^2 -bridged by two iodide ligands, with the Eu1–I1 and Eu1–I2 bond lengths (3.242(1) and 3.23375(6) Å) also elongated in comparison to the Eu2–I1 and Eu2–I2 bond lengths (3.1658(7) and 3.1391(9) Å) but still similar to those found in **3.4** (Eu1–I2: 3.2078, Eu1–I2: 3.2367 Å). While one Eu(II) centre within the dimer is only four-coordinate, the second Eu(II) ion has accommodated a fifth contact to a THF molecule and is likely the cause of the subtle increases in bond lengths.

The subsequent salt metathesis reaction of **3.10** with the potassium salt of Lappert's alkyl, KCH(SiMe₃)₂, was also carried out in THF solvent and afforded the desired europium(II) monoalkyl complex, **3.11**, after 10 minutes at room temperature (Scheme 3.4).

The workup consists of hexane extractions, providing the purest monoalkyl, which was typically isolated as an orange crystalline solid at –30 °C, albeit in poor yields (ca. 30%). A single crystal X-ray diffraction experiment discloses the Eu(II) metal centre within **3.11** as low-coordinate; two contacts are made up by the N-atoms of the β -diketiminate ligand, with Eu1–N1 and Eu1–N2 bond lengths of 2.482(2) and 2.469(2) Å being similar to the Eu–N bond lengths observed in **3.10** (2.432(5) – 2.528(4) Å), and the third contact from the bis(trimethylsilyl)methyl ligand, completing the primary coordination sphere (Figure 3.9, b)). The Eu1–C51 bond length of 2.644(4) Å is closely related to the only other two Eu(II) complexes bearing a trimethylsilyl methyl-based ligand (2.605(6) – 2.65(1) Å).^{23, 24} Finally, steric unsaturation of the Eu(II) centre is relieved through an agostic interaction (Eu1...C52 3.036(3) Å) with a methyl group of the CH(SiMe₃)₂ ligand.

Compound **3.11** displays a low stability in the solution-state, as slow evaporation of pure hexane solutions containing **3.11** gave yellow blocks identified through crystallographic analysis as the Schlenk-type redistribution species, **3.12** (Figure 3.10). In the solid-state this species is reminiscent of **2.8**, however, lacks any solvent coordination to the Eu(II) centre, demonstrating the ability of the BDI^{Dicyp} to provide sufficient steric protection of the Eu(II) centre.

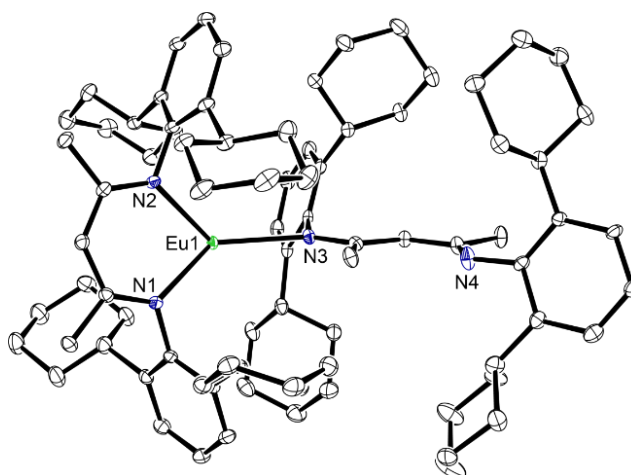


Figure 3.10. Ortep representations (30% probability ellipsoids) of compound **3.12**. Hydrogen atoms have been omitted for clarity. Selected bond lengths (Å) and angles (°): Eu1–N1 2.489(1), Eu1–N2 2.454(2), Eu1–N3 2.448(2), N3–C_{Dicyp} 1.425(3), N3–C52 1.354(3), N4–C_{Dicyp} 1.36(2), N4–C54 1.296(3), N1–Eu1–N2 73.33(6), N1–Eu1–N3 129.00(6), N2–Eu1–N3 125.71(6).

Given that **3.11** was consistently isolated in poor yields and displayed low stability in the solution-state, it was also beneficial to synthesise the heteroleptic amido precursor. The chemistry of the Ln(II) ions is dominated by electrostatic interactions,⁵ and as nitrogen is more electronegative in comparison to carbon (N: 3.04, C: 2.55)²⁵ it could be that the formation of the Ln–N bond would result in an overall more stable complex and thereby increase the yield of the respective product.

Repeating of this metathetical reaction between **3.10** and KHMDS resulted in the formation of the mononuclear europium(II) amide, **3.13**, in moderate yields (60%). Orange

single crystals were obtained from the slow evaporation of a saturated hexane/toluene solution at room temperature (Figure 3.11).

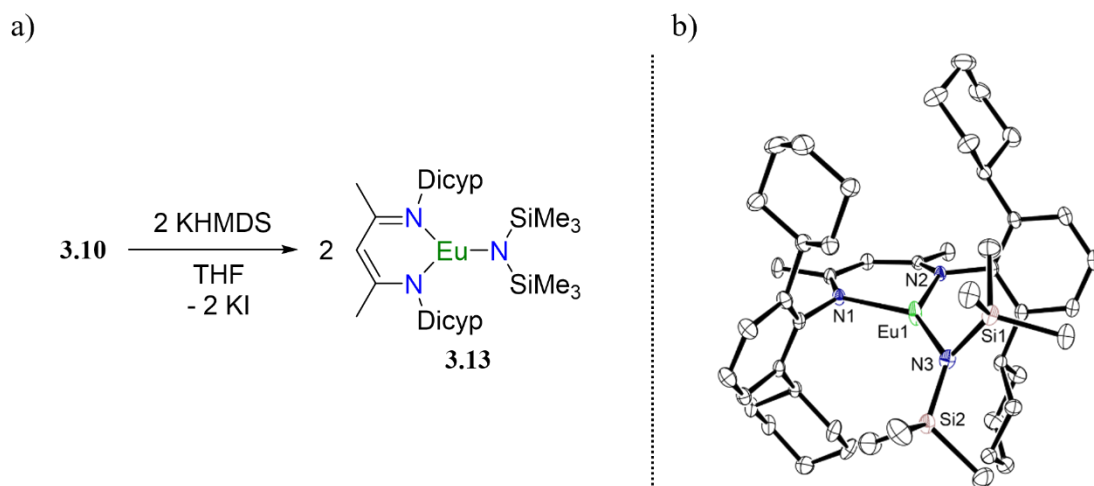
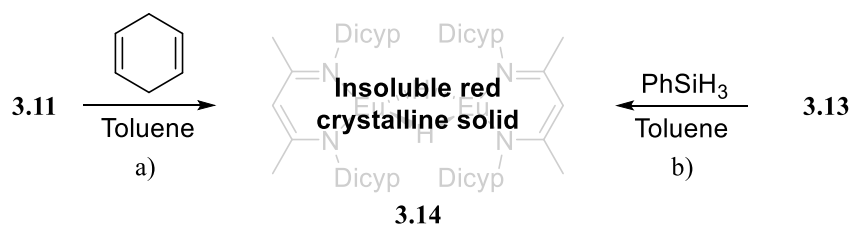


Figure 3.11. Left: Salt metathesis reaction to yield the heteroleptic Eu(II) amide (**3.13**). Right: Ortep representations (30% probability ellipsoids) of compound **3.13**. Hydrogen atoms have been omitted for clarity. Selected bond lengths (Å) and angles (°): Eu1–N1 2.477(2), Eu1–N2 2.495(2), Eu1–N3 2.453(2), N1–Eu1–N2 70.06(7), N1–Eu1–N3 143.64(8), N2–Eu1–N3 145.53(8).

In the solid-state, the Eu(II) centre within **3.13** is low-coordinate, with two contacts provided by bidentate *N,N*-bonding of the BDI^{Dicyc} ancillary ligand (Eu1–N1: 2.477(2), Eu1–N2: 2.495(2) Å) and a third contact from the bis(trimethylsilyl)amide ligand (Eu1–N3: 2.453(2) Å). The Eu1–N1 and Eu1–N2 bond lengths are consistent with the Eu(II) monoalkyl complex (**3.11**: 2.48(2) and 2.469(2) Å), and the Eu1–N3 bond length is consistent with other divalent Eu(II) complexes also containing the bis(trimethylsilyl)amide ligand (2.437 – 2.527 Å).^{4, 7}

The addition of a hydride source, 1,4-CHD or phenylsilane, to a stirring toluene solution of **3.11** (Scheme 3.5, a)) or **3.13** (Scheme 3.5, b)), respectively, resulted in the precipitation of a red, crystalline solid almost instantaneously (**3.14**).



Scheme 3.5. Attempted synthesis of a molecular Eu(II) hydride through a) the reaction of **3.11** with 1,4-CHD and b) the reaction of **3.13** with PhSiH₃.

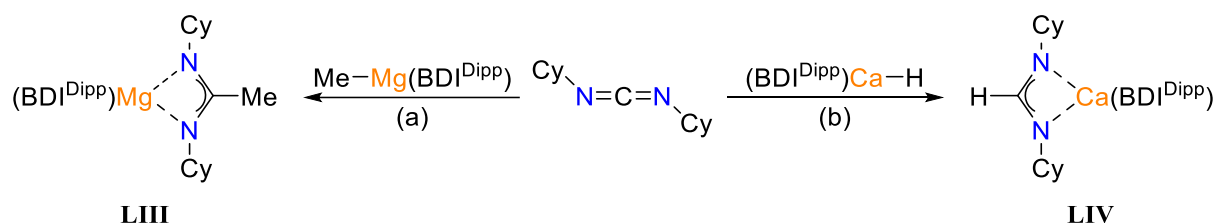
This clearly indicated some reaction had occurred, as the visual observation is in stark contrast to previous Eu(II) complexes, which are typically yellow-orange in colour and the products largely soluble in toluene solvent.

Attempts at structurally characterising this red crystalline solid by an X-ray diffraction experiment were made on an Agilent SuperNova diffractometer fitted with an EOS S2 detector; however, the red crystals were far too small and twinned for any sort of data collection on this machine. Attempts to recrystallise the red solid from THF failed, demonstrating a high insolubility of this compound in ethereal and aromatic solvents.

A layering technique was utilised to decrease the reaction time of forming the red solid. Pure samples of the monoalkyl precursor (**3.11**) or heteroleptic amido complex (**3.13**) were fully dissolved in toluene, a buffer toluene solution layered on top, followed by layering a toluene solution containing 1,4-CHD or phenylsilane, respectively. The sample was left unmoved at room temperature to slowly diffuse in hopes of forming larger, single crystals of **3.14**. Yet, attempts to gain solid-state data were still hindered by the sample being inherently twinned.

3.3.2 Preliminary Studies for Structural Confirmation of [(BDI^{Dicyp})EuH]₂

Preliminary studies were therefore conducted to structurally characterise the red solid (**3.14**) through reactivity. The reaction of carbodiimide derivatives with Group 2 hydride and alkyl complexes has been reported in the literature (Scheme 3.6).^{26, 27}



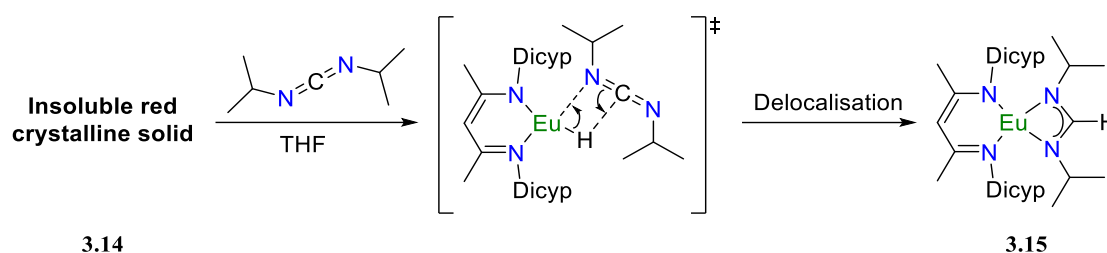
Scheme 3.6. Reaction of di-cyclohexylcarbodiimide with (a) a magnesium alkyl complex to give (**LIII**) and (b) a calcium hydride to give (**LIV**).

In example (Scheme 3.6, (a)), one of the N=C double bonds of the dicyclohexyl carbodiimide reagent inserts into the Mg–C bond of the heteroleptic Mg(II) alkyl complex. After delocalisation of the second N=C double bond, the respective alkyl-formamidinate derivative (**LIII**) is formed, in which the central amidinate carbon atom is now bonded to a methyl group.²⁷

In example (Scheme 3.6, (b)), the reaction of Hill's solvent-free calcium hydride, **XXXII**, with dicyclohexyl carbodiimide, affords the expected formamidinate compound, **LIV**. In this case, the central amidinate carbon atom is bonded to a hydrogen, originating from the insertion of a N=C double bond into the Ca–H bond of the starting compound.²⁶

If our red solid was indeed the desired europium(II) hydride as postulated, the reaction with a carbodiimide derivative would provide the heteroleptic Eu(II) formamidinate (**3.15**), as shown in Scheme 3.7. This would follow an analogous reaction mechanism as seen with the Group 2 starting materials: the N=C bond of diisopropyl carbodiimide (DIC) would first insert into the Eu–H bond of the hydride complex *via* a 4-membered transition state, and with

retention of the 2+ oxidation state of the Eu centre, delocalisation of the remaining C=N double bond would afford **3.15**.



Scheme 3.7. Proposed mechanism for the reaction between DIC and the postulated $[(\text{BDI}^{\text{Dicyp}})\text{EuH}]_2$ (**3.14**) to give the expected formamidinate (**3.15**).

An excess of DIC was added to a stirring suspension of the red solid in THF. After ca. 4 hours at room temperature, any residual red solid had reacted to give a clear, yellow solution. Volatiles were removed *in vacuo*, and the crude product dissolved into toluene and left to crystallise at $-30\text{ }^\circ\text{C}$, providing single yellow crystals of **3.15** suitable for an X-ray diffraction experiment (Figure 3.12).

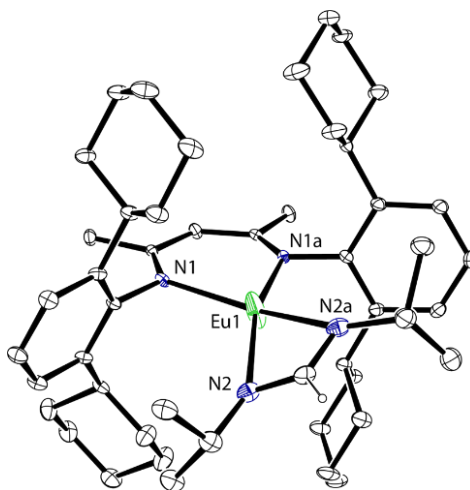


Figure 3.12. Ortep representations (30% probability ellipsoids) of compound **3.15**. Hydrogen atoms (except for the hydrogen of the formamidinate ligand) have been omitted for clarity. Selected bond lengths (\AA) and angles ($^\circ$): Eu1–N1 2.487(4), Eu1–N2 2.493(6), N2–C31 1.314(7), N2–C32 1.479(8), N1–Eu1–N2 119.16(2), N1–Eu1–N1a 71.22(2), N1–Eu1–N2a 162.91(1), N2–Eu1–N2a 54.9(3), Eu1–N2–C31 91.6(4), N2–C31–N2a 121.9(8).

In the solid-state, the coordination sphere of the Eu(II) centre is made up of four Eu–N contacts; two from the *N,N*-chelated β -diketiminato ligand (Eu1–N1: 2.487(4) Å) and two from the *N,N*-chelated formamidinate ligand (Eu1–N2: 2.493(6) Å). The N2–C31 and N2a–C31 bond length of 1.314(7) Å and the N2–C31–N2a bond angle of 121.9(8)° is consistent with the calcium formamidinate derivative, [(BDI^{Dipp})Ca(ⁱPrNC(H)NⁱPr)(ⁱPrNCNⁱPr)] (N–C bond lengths: 1.324(3) and 1.317(3) Å, N–C–N bond angle: 121.3(2)°).²⁶

The most important structural feature observed within this solid-state structure is the confirmation of the C–H bond of the central carbon atom of the formamidinate ligand, alluding to the red solid (**3.14**) being the desired molecular Eu(II) hydride complex.

3.4 Synthesis of [(BDI^{Dipp,Dicyp})EuH]₂

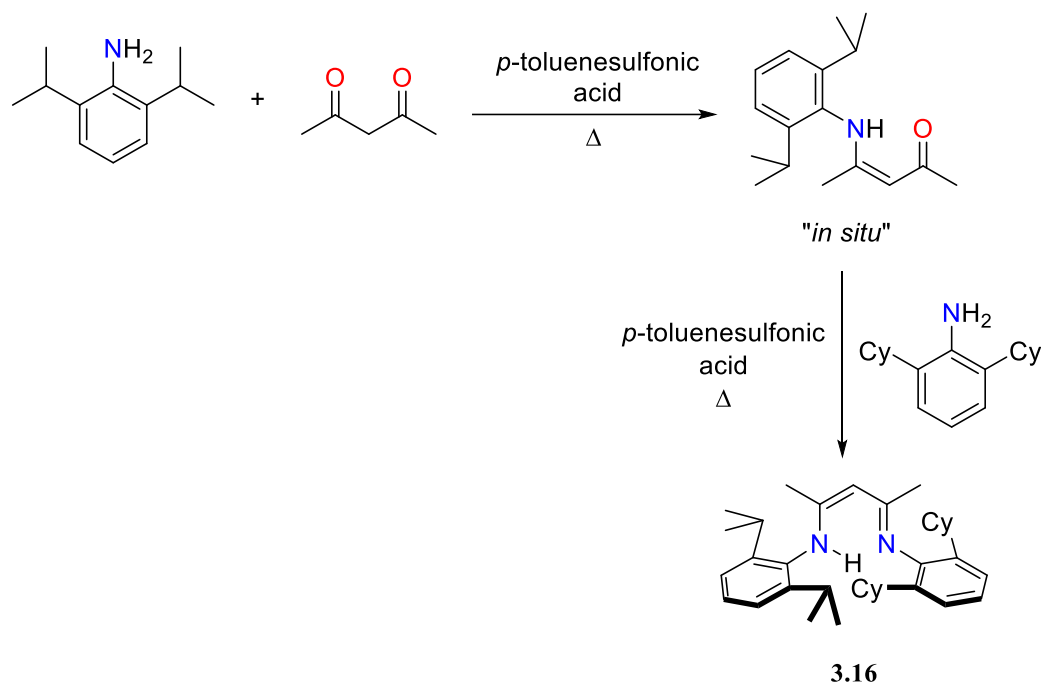
3.4.1 Synthesis of (BDI^{Dipp,Dicyp})H

Previous Sections in this Chapter have described the possible isolation of a divalent europium hydride supported by the BDI^{Dicyp} ancillary ligand (**3.14**). Given the poor solubility of **3.14** in aliphatic, aromatic, and ethereal solvents, the structure of this compound has thus far been confirmed primarily through reactivity studies. Therefore, it became beneficial to re-evaluate the design of our chosen β -diketiminato ligand framework.

This ligand system still needed to contain large, bulky *N*-substituents to kinetically stabilise the Eu(II) ion,⁵ but the solubility of these compounds in both aliphatic and aromatic solvents needed to be increased. To address this, an unsymmetrical derivative of the β -diketiminato ligand will be designed, in which the steric bulk will be sustained through one Dicyp *N*-substituent and the solubility aspect through the combination of this Dicyp group with a Dipp substituent.

The approach to synthesising the pro-ligand follows a two-step procedure, like other unsymmetrical BDI-based frameworks reported within the literature.²⁸⁻³¹ The first step

involves the addition of equimolar amounts of acetylacetone and Dipp aniline and catalytic amounts of *p*-toluenesulfonic acid in toluene to a round bottom flask fitted with a Dean-Stark condenser. Refluxing the mixture overnight results in a red-brown solution of the monosubstituted Dipp AcNac ($\text{AcNac} = [\text{H}_3\text{CC}(\text{O})\text{CHC}(\text{NDipp})\text{CH}_3]$), which can be subsequently used *in-situ* (Scheme 3.8).



Scheme 3.8. Synthesis of the unsymmetrical β -diketiminato ligand (**3.16**) *via* condensation reactions.

The second condensation step is akin to the first, with the addition of one equivalent of Dicyclopentadienyl amine and one equivalent of the acid catalyst to the round bottom flask containing Dipp AcNac. The round bottom flask was equipped with a Dean-Stark condenser, and the mixture was refluxed for an additional 16 hours before cooling to room temperature and quenching with triethylamine.

The mixture was transferred to a separating funnel, and the organic layer washed once with distilled water and twice with brine. The organic phase was dried over anhydrous MgSO_4 and the volatiles removed *in vacuo* to give a crude brown oil. This oil was largely insoluble in

aliphatic solvents, so much so that heating into large volumes of methanol was required, followed by stirring the solution overnight to afford **3.16** as an off-white powder (ca. 40%).

The structure of **3.16** was confirmed firstly through ^1H NMR spectroscopy. The spectrum indicated that two β -diketiminato ligand environments were present in a 2:1 ratio, by the appearance of two broad N–H resonances situated at δ_{H} 12.27 and 11.41 ppm and two possible BDI methine resonances situated at δ_{H} 4.88 and 4.83 ppm, respectively. To better distinguish between the two products, the crude solid was dissolved into a boiling ethanol/ethyl acetate solvent mix and the colourless solution was left to cool slowly to room temperature. After 24 hours, colourless blocks had grown and X-ray diffraction analysis identified these as the free-ligand $(\text{BDI}^{\text{Dicyclopentadienyl}})\text{H}$ (**2.7**).²²

The bulk solution was decanted and left to slowly evaporate, yielding a second crop of colourless crystals confirmed through crystallographic analysis as the unsymmetric ligand, **3.16** (Figure 3.13).

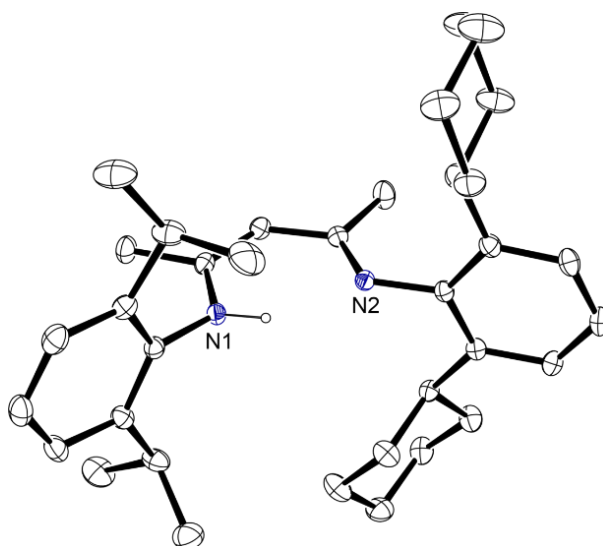


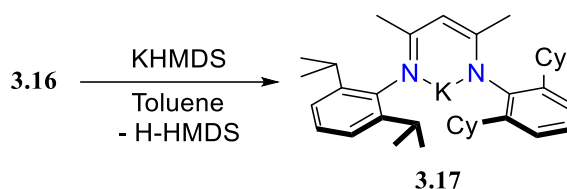
Figure 3.13. Ortep representations (30% probability ellipsoids) of compound **3.16**. Hydrogen atoms (except those on N1) have been omitted for clarity. Selected bond lengths (Å) and angles (°): N1–C24 1.435(2), N1–C2 1.355(2), N2–C6 1.426(2), N2–C4 1.298(2), C4–C3 1.438(3), C3–C2 1.364(3).

To check the purity of the second crystalline sample, the crystals were dried under vacuum, and an aliquot was dissolved in C₆D₆ solvent. An ¹H NMR experiment confirmed **3.16** as the sole organic product, apparent by only one N–H resonance at δ_{H} 12.27 ppm and one BDI methine resonance centred at δ_{H} 4.88 ppm.

Formation of this symmetrical ligand system alongside **3.16** suggests that either unreacted acetylacetone is present in solution prior to the addition of Dicyc aniline, or the reaction conditions could be favouring the backwards reaction as a competing pathway, thereby regenerating acetylacetone which could consequently react with two equivalents of Dicyc aniline to form **2.7**. For example, if the pH of the reaction mixture is too high, there will not be enough acid catalyst for protonation of the intermediate species thus inhibiting water elimination. However, if the reaction conditions are too acidic, the imine product can be hydrolysed back to regenerate the amine and acetyl starting materials.

To test the theory of unreacted starting materials, the unsymmetrical Dipp AcNac intermediate was isolated by precipitation of the crude red oil from hexane at –30 °C, then purified with further cold hexane washes (Scheme 3.8).^{29, 30} The resultant powder was then refluxed with Dicyc aniline and *p*-toluenesulfonic acid in a 1:1:1 molar ratio for 16 hours with a Dean-Stark condenser, followed by the same organic workup detailed earlier in this Section. Analysis of the reaction product by ¹H NMR spectroscopy indicated that both ligand systems had still been synthesised. Therefore, the reaction conditions need to be optimised to increase the isolated yields and purity of any β -diketiminate derivatives.

Compound **3.16** can then be deprotonated by a base, such as KHMDS, in toluene to generate the potassium salt of the ligand (**3.17**) as a beige precipitate (Scheme 3.9).

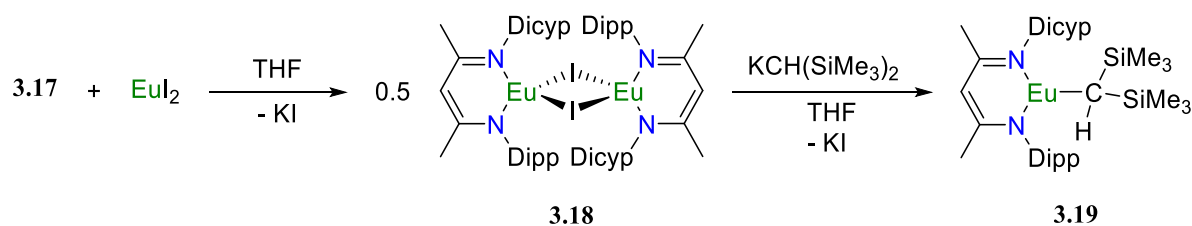


Scheme 3.9. Deprotonation of the free ligand, **3.16**, to give **3.17**.

After workup and drying the crude solid under vacuum, the product's structure was solely confirmed through ^1H NMR analysis by the disappearance of the broad low-field N–H signal, indicating no free ligand was present in the sample. Attempts were made to crystallise **3.17** from a dilute diethyl ether solution in a similar manner to **2.11**,²² albeit the resulting colourless crystals were too air sensitive for single crystal X-ray diffraction analysis.

3.4.2 Synthesis *via* $[(\text{BDI}^{\text{Dipp,Dicyp}})\text{EuI}]_2$

It was assumed that the procedure for synthesising the unsymmetrical Eu(II) hydride would follow an identical regime to that of the $\text{BDI}^{\text{Dicyp}}$ ancillary ligand. Therefore, **3.17** was added to a vial containing a slurry of EuI_2 in THF, and the mixture left to stir for 4 hours at room temperature to yield crude **3.18** as a dark yellow oil, after workup (Scheme 3.10).



Scheme 3.10. Synthesis overview to afford the monomeric Eu(II) alkyl (**3.19**).

This oil was re-dissolved into toluene and left to crystallise at room temperature for a few weeks. When this did not afford crystals, the concentrated toluene solution was left at -30°C for an extended period, which resulted in the product precipitating out as a fine yellow powder. Crystallisation attempts from saturated pentane solutions or THF solutions at room temperature or the freezer also failed to yield crystals. Thus, it was likely the reaction mix

contained some sort of contaminant, such as the symmetrical Eu(II) iodide (**3.10**), that was hindering the crystallisation process.

The addition of Lappert's alkyl precursor to a stirring THF solution of **3.18** showed a darkening of the yellow mixture to orange after 10 minutes at room temperature, hinting at the formation of **3.19** (Scheme 3.10). Removal of the volatiles and extraction into hexane gave a dark orange solution, from which orange blocks were obtained at room temperature. Crystallographic analysis on these single crystals disclosed the solid-state structure of **3.19** consists of a Eu(II) centre with two contacts to the unsymmetric β -diketiminato ligand and one to the carbon of the bis(trimethylsilyl)methane ligand (Figure 3.14).

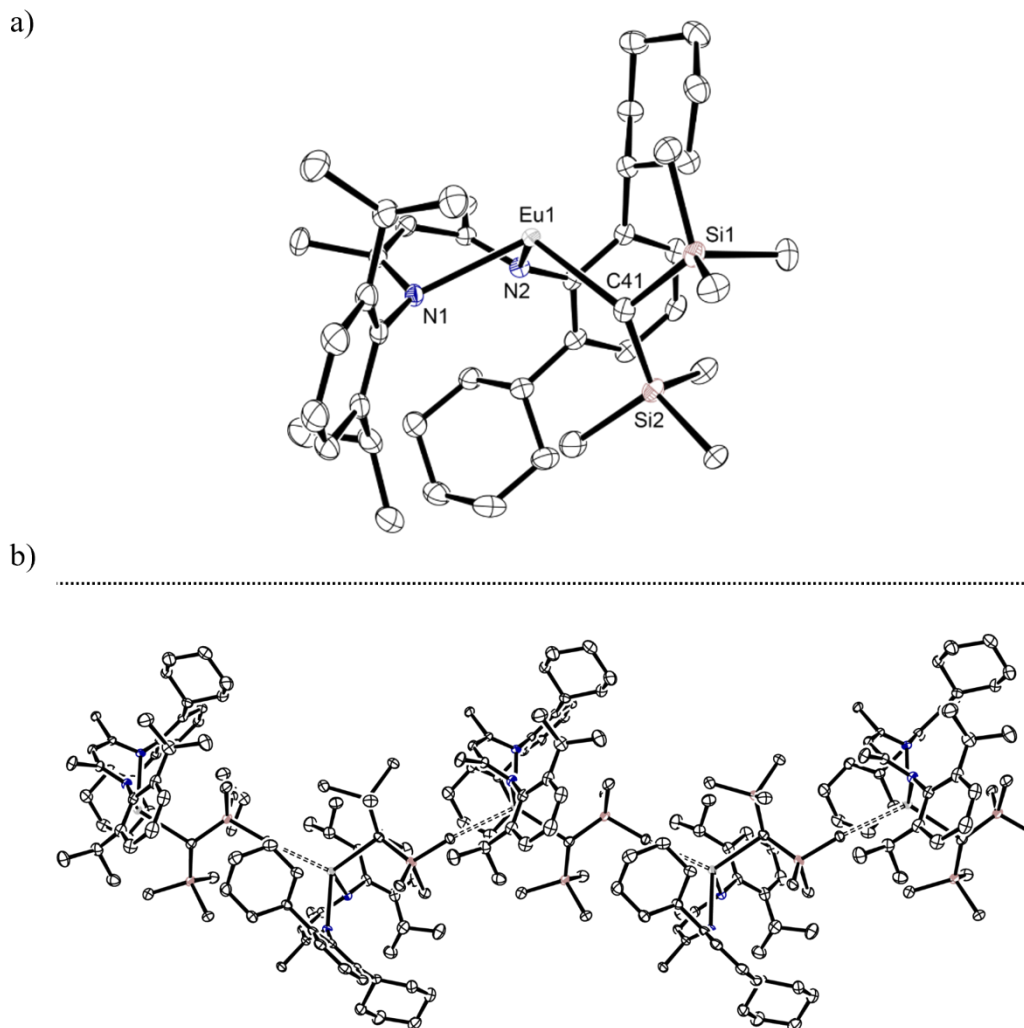
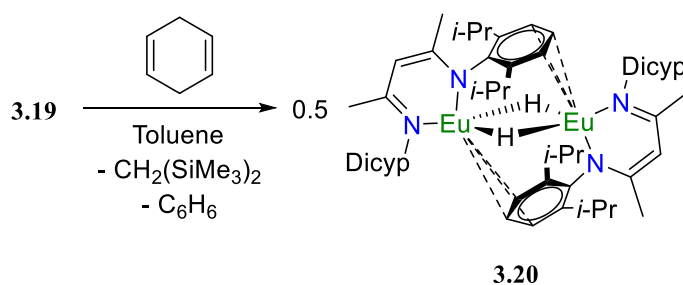


Figure 3.14. Ortep representations (30% probability ellipsoids) of the monomeric form of compound **3.19** (top) and pseudo polymer made up of five units of **3.19** (bottom). Hydrogen atoms have been omitted for clarity. Selected bond lengths (Å) and angles (°): Eu1–N1 2.453(2), Eu1–N2 2.442(2), Eu1–C41 2.599(3), N1–Eu1–N2 80.34(7), N1–Eu1–C41 110.38(7).

The Eu1–N1 and Eu1–N2 bond lengths (2.453(2) and 2.442(2) Å, respectively) are similar to the Eu1–N1 and Eu1–N2 bond lengths in the BDI^{Dicyp} Eu(II) alkyl (**3.11**) (2.482(2) and 2.469(2) Å) as well as in the amide complex (**3.13**) (2.477(2) and 2.495(2) Å). The Eu1–C41 bond length of 2.599(3) Å is slightly shorter than the Eu–C bond (2.644(4) Å) found in **3.11** but still within the range of the only other two Eu(II) complexes bearing a trimethylsilyl methyl-based ligand (2.605(6) – 2.65(1) Å).^{23, 24}

In the asymmetric unit, the Eu(II) centre displays a very distorted trigonal planar geometry, however, a fourth intermolecular contact is present between the Eu(II) centre and the methyl of the $\text{CH}(\text{SiMe}_3)_2$ functionality of a second $[(\text{BDI}^{\text{Dipp,Dicyp}})\text{EuCH}(\text{SiMe}_3)_2]$ monomer. This results in a pseudo polymeric structure and contrasts with what is observed for **3.11**.

Excited by the ease of synthesising **3.19**, we were eager to perform the sequential reaction with 1,4-CHD as the selected hydride source.²⁰ Despite the ideology that the swap to a Dipp *N*-substituent would increase the solubility of our hydride complex, to what extent was unknown. Therefore, a concentrated toluene solution of 1,4-CHD was layered atop a saturated toluene solution of the monoalkyl (**3.19**) and left to slowly diffuse at room temperature (Scheme 3.11).



Scheme 3.11. Synthesis of a divalent europium hydride (**3.20**).

Within 30 minutes, the reaction solution had darkened to a red colour, and small, red crystalline blocks of **3.20** began to deposit on the walls of the scintillation vial, demonstrating an average solubility in aromatic solvents. Despite the short growth period, these blocks proved large enough and single enough for a single crystal X-ray diffraction experiment (Figure 3.15).

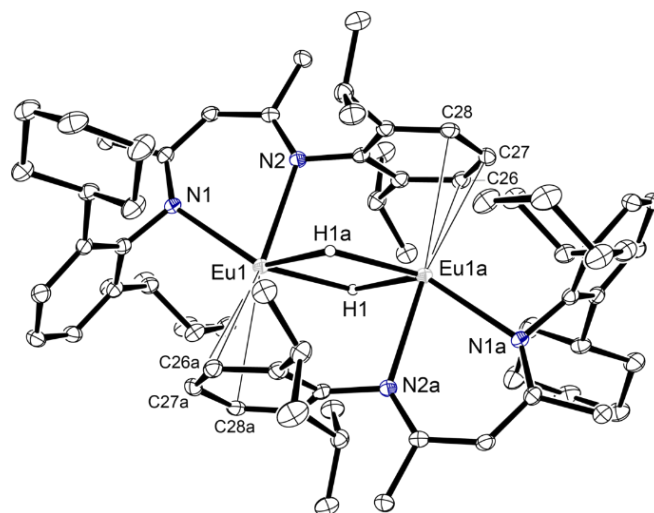


Figure 3.15. Ortep representations (30% probability ellipsoids) of compound **3.20**. Hydrogen atoms (except for the bridging H1 and H1a ligands) have been omitted for clarity. Selected bond lengths (Å) and angles (°): Eu1–N1 2.631(2), Eu1–N2 2.537(3), Eu1–C_{cent} 2.871(1), N1–Eu1–N2 70.30(8).

In the solid-state, **3.20** is a centrosymmetric dimer with two μ^2 -hydride ligands bridging the two Eu(II) centres. Each Eu(II) centre interacts in an η^3 -coordination mode with the phenyl ring of the smaller Dipp *N*-substituent of the second [(BDI^{Dipp,Dicyp})EuH] unit within the dimer. This geometry is like the solid-state structure of **XXV** and similar to Jones' strontium hydride supported by the bulky amidinate ligand,^{3, 9} both of which display metal-aryl interactions, however, contrasts **XLI** which does not possess this arene interaction.¹ To accommodate this arene interaction, the Eu1–N1 bond length (2.631(2) Å) has been elongated compared to the E1–N2 bond length (2.537(3) Å), though both values are still similar to other Eu(II) complexes bearing β -diketimate based ligands (2.407 – 2.603 Å).¹¹⁻¹⁴

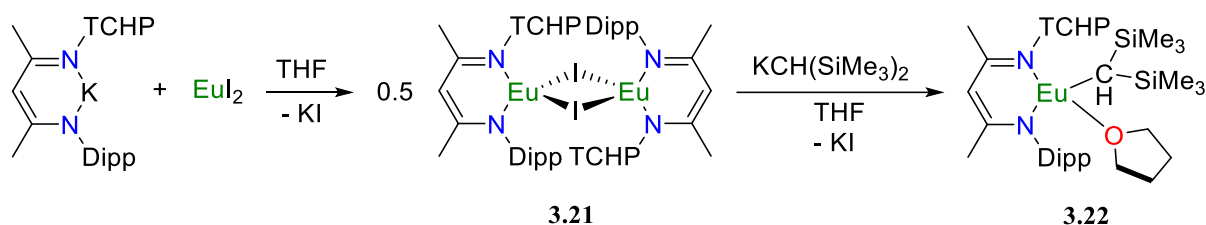
Once isolated, crystalline samples of **3.20** could be purified by washing with hexane, showing negligible solubility in aliphatic solvents but partial solubility in coordinating solvents, such as THF. This is in comparison to **3.14**, which is insoluble in both coordinating- and non-coordinating solvents.

3.5 Synthesis of $[(\text{BDI}^{\text{Dipp,TCHP}})\text{EuH}]_2$

3.5.1 Synthesis *via* $[(\text{BDI}^{\text{Dipp,TCHP}})\text{EuI}]_2$

The previous Section of this Chapter demonstrates that the unsymmetrical system, **3.17**, proved effective for the isolation and characterisation of one of the first examples of a molecular Eu(II) hydride complex (**3.20**). In 2021, Jones et al. reported on the characterisation of Group 1 complexes of the unsymmetrical β -diketiminate ancillary ligand containing one Dipp *N*-substituent and the bulky TCHP (TCHP = 2,4,6-tricyclohexylphenyl) *N*-substituent.²⁸ Therefore, given the success of **3.17**, this work was extended to the $\text{BDI}^{\text{Dipp,TCHP}}$ ancillary ligand; hence, the work presented herein is in collaboration with Prof. Cameron Jones and his research group at Monash University, Melbourne.

The potassium salt of the ligand, $(\text{BDI}^{\text{Dipp,TCHP}})\text{K}$, was added to a vial containing a slurry of EuI_2 in THF, and the mixture was left to stir for 4 hours at room temperature to give a yellow solution with beige precipitates (Scheme 3.12).



Scheme 3.12. Overview of the synthesis for the alkyl complex, **3.22**.

After removing the volatiles *in vacuo*, the crude product (**3.21**) was extracted with toluene solvent, filtered through Celite, concentrated then left to crystallise at room temperature, affording single, yellow crystals suitable for an X-ray diffraction experiment (Figure 3.16, a)).

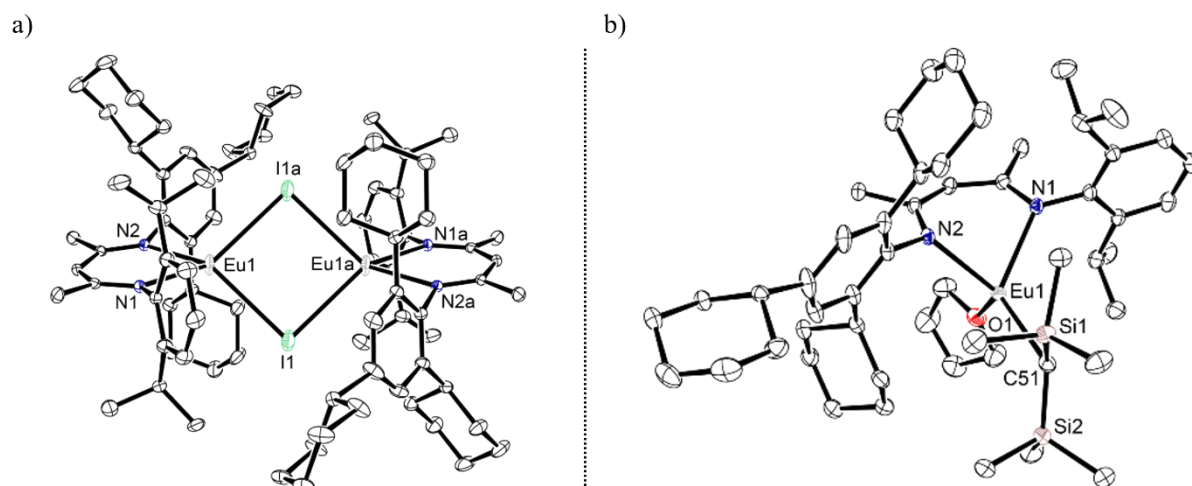


Figure 3.16. Ortep representations (30% probability ellipsoids) of compound **3.21** (left) and compound **3.22** (right).

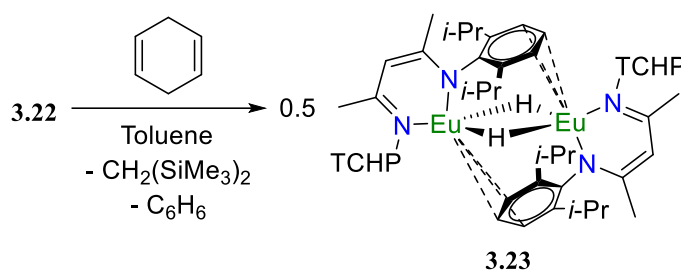
Hydrogen atoms have been omitted for clarity. Selected bond lengths (Å) and angles (°): **3.21**: Eu1–N1 2.477(2), Eu1–N2 2.429(3), Eu1–I1 3.2249(5), Eu1–I1 3.2233(4), N1–Eu1–N2 72.24(8), N1–Eu1–I1 110.66(6), N2–Eu1–I1 143.11(6), I1–Eu1–I1 88.39(1), Eu1–I1–Eu1 91.61(1). **3.22**: Eu1–N1 2.496(2), Eu1–N2 2.461(2), Eu1–C51 2.661(2), Eu1–O1 2.586(2), N1–Eu1–N2 79.58(5), N1–Eu1–C51 120.85(6), N1–Eu1–O1 99.28(6).

In the solid-state, the structure of **3.21** is dimeric with two low-coordinate Eu(II) metal centres. Each Eu(II) centre has two contacts to the N-atoms of the β -diketiminato ligand and are μ^2 -bridged by two iodide ligands. The Eu1–N1 and Eu1–N2 bond lengths (2.477(2) and 2.429(3) Å) and the Eu1–I1 and Eu1–I2 bond lengths (3.2249(5) and 3.2233(4) Å) align with Eu–N and Eu–I bond lengths of all crystallographically characterised heteroleptic Eu(II) iodides within this Chapter (2.459(5) – 2.528(4) Å and 3.2078 – 3.3375(6) Å, respectively).

The subsequent salt metathesis reaction between the potassium salt of Lappert's alkyl precursor and a THF solution of **3.21** generated the crude product (**3.22**) as an orange solid after workup (Scheme 3.12). Crystallisation of a saturated hexane/toluene solvent mix at room temperature yielded single crystals, allowing for structural elucidation *via* single crystal X-ray diffraction analysis (Figure 3.16, b)). The primary coordination sphere of **3.22** comprises of four contacts: two contacts are provided by the unsymmetric β -diketiminato ligand and one by the bis(trimethylsilyl)methane ligand, with the Eu1–N1 and Eu1–N2 bond lengths (2.496(2)

and 2.461(2) Å, respectively) and Eu1–C51 bond length of 2.661(2) Å are similar to the Eu1–N1 and Eu1–N2 bond lengths (2.43(2) – 2.482(2) Å) and Eu–C bond lengths (2.599(3) and 2.644(4) Å) of the other two heteroleptic Eu(II) complexes bearing the bis(trimethylsilyl)methane ligand reported in this Chapter (**3.11** and **3.19**, respectively). Unlike these two systems, **3.22** also has a fourth contact to a donor THF molecule (Eu1–O1 2.586(2) Å), alluding that the combination of the Dipp *N*-substituent and TCHP *N*-substituent may not provide ample protection of the Eu(II) centre alone, in comparison to the symmetrical BDI^{Dicyp} or unsymmetrical BDI^{Dipp,Dicyp} ligand frameworks.

The final step for synthesising a Eu(II) hydride complex was attempted by layering a saturated toluene solution containing 1,4-CHD atop an orange toluene solution of the solvated Eu(II) alkyl (**3.22**) and left to slowly diffuse at room temperature (Scheme 3.13).



Scheme 3.13. Synthesis of a divalent europium hydride complex (**3.23**).

Within 30 minutes, the reaction solution had turned dark red, and small, red crystalline blocks of **3.23** began to deposit on the walls of the scintillation vial, demonstrating average solubility in aromatic solvents. The solution was left to slowly evaporate overnight, generating large single blocks suitable for single crystal X-ray diffraction analysis (Figure 3.17).

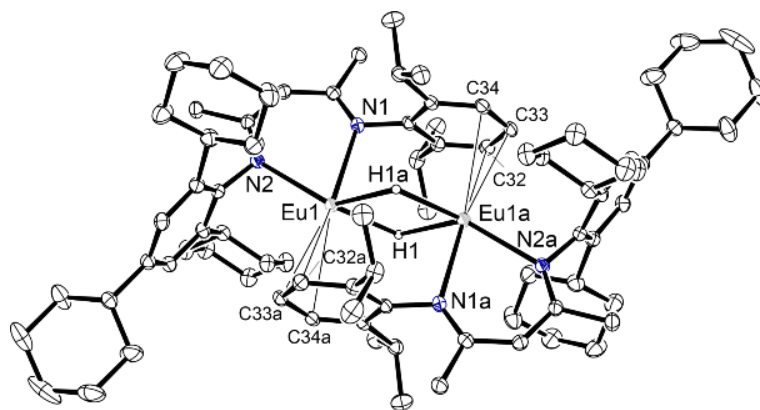


Figure 3.17. Ortep representations (30% probability ellipsoids) of compound **3.23**. Hydrogen atoms (except for the bridging H1 and H1a ligands) have been omitted for clarity. Selected bond lengths (Å) and angles (°): Eu1–N1 2.634(3), Eu1–N2 2.528(2), Eu1–C_{cent} 2.956(1), N1–Eu1–N2 69.61(8).

In the solid-state **3.23** is a centrosymmetric dimer with two μ^2 -hydride ligands bridging the two Eu(II) centres. Each Eu centre also interacts in an η^3 -coordination mode with the phenyl ring of the smaller Dipp *N*-substituent of the second [(BDI^{Dipp,TCHP})EuH] unit within the dimer, resulting in the elongation of the Eu1–N1 bond length (2.634(3) Å) compared to the Eu1–N2 bond length (2.528(2) Å). Despite the starting monoalkyl complex containing coordination from a donor solvent to the Eu(II) centre, the structural features of **3.23** are analogous to those of the unsymmetrical hydride species, **3.20** (Eu1–N1: 2.631(2), Eu1–N2: 2.537(3) Å) which contains similar *N*-substituents and the same arene interactions.

This hydride complex also demonstrates poor solubility in aliphatic solvents; therefore, the product is easily purified through hexane washes, followed by drying the solid under vacuum. Much like **3.20**, this compound is also sparingly soluble in the coordinating solvent, THF.

3.6 Structural Characterisation of $[(\text{BDI}^{\text{Dicy}})\text{EuH}]_2$

The syntheses of the three divalent europium hydrides presented in this Chapter have been reported chronologically but not with respect to the time it took to synthesise and characterise each hydride complex. For example, the initial isolation of the proposed Eu(II) hydride supported by the BDI^{Dicy} ligand framework (**3.14**) occurred within the first month of the second year of this PhD but was not characterised in the solid-state until the last month of the third year (*vide infra*). In contrast, the syntheses for the hydrides supported by the unsymmetrical derivatives of the β -diketiminato ligand (**3.20** and **3.23**) began within the last six months of this PhD: **3.20** and **3.23** were then structurally elucidated a month later. This timeline of events, therefore, sheds light on the reactivity Section below.

The structure of **3.14** has been elucidated in the solid-state by Macromolecular Crystallography (MX2) beamline at the Australian Synchrotron (ANSTO) (Figure 3.18).

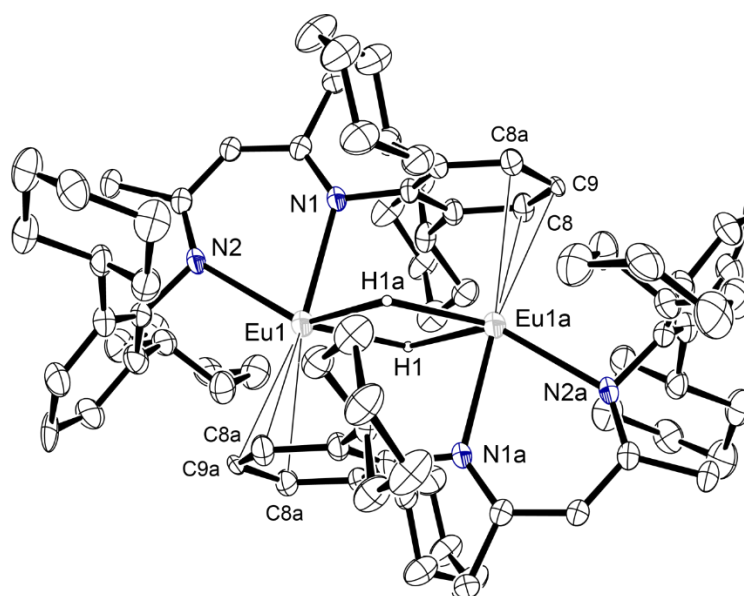


Figure 3.18. Ortep representations (20% probability ellipsoids) of compound **3.14**. Hydrogen atoms (except for the bridging H1 and H1a ligands) have been omitted for clarity. Selected bond lengths (Å) and angles (°): Eu1–N1 2.597(1), Eu1–N2 2.526(8), Eu1–C_{Cent} 2.804(6), N1–Eu1–N2 71.1(3).

Like the unsymmetrical analogues, **3.14** is a centrosymmetric dimer with two Eu(II) centres μ^2 -bridged by two hydride ligands. Each Eu(II) centre then η^3 -interacts with a phenyl group of one Dicyc *N*-substituent of the second [(BDI^{Dicyc})EuH] unit within the dimer. The Eu1–N1 bond length (2.597(10) Å) is slightly longer than the Eu1–N2 bond length (2.526(8) Å) and is consistent with the Eu–N bond lengths of the other two divalent europium hydrides (**3.20**: 2.61(2) and 2.537(3) Å, **3.23**: 2.634(3) and 2.528(2) Å). Despite the arene interaction of the Eu(II) centre with the larger Dicyc group in **3.14** compared to the interaction of the Eu(II) centres to the smaller Dipp substituent in **3.20** and **3.23**, the Eu–C_{cent} distance of 2.804(6) Å for **3.14** is slightly shorter than those for **3.20** and **3.23** (2.871(1) and 2.956(1) Å, respectively).

3.7 Preliminary Reactivity Studies of [(BDI^{Dicyc})EuH]₂, [(BDI^{Dipp,Dicyc})EuH]₂, and [(BDI^{Dipp,TCHP})EuH]₂

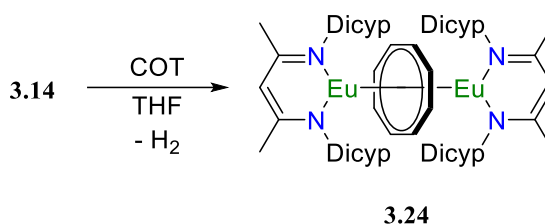
3.7.1 Two-Electron Aromatisation of COT

Chapter Three thus far has detailed the successful isolation of three new divalent europium hydride complexes bearing derivatives of the β -diketiminate ligand framework. Given how recent the isolation of **3.20** and **3.23**, this Section focuses on the single comparative study made between all three Eu(II) hydride complexes, in which the 2+ oxidation state will be maintained in the reaction products.

Ytterbium(II) hydrides have been found to facilitate the two-electron reduction of COT (–1.62 and –1.86 V vs SCE) within the literature, to give a dimeric Yb(II) sandwich complex containing the [COT]²⁻ dianion, proceeding *via* a series of consecutive polarised Yb–H/C=C insertion and σ -bond metathesis reactions and the extrusion of hydrogen gas.³² This mechanism is described in greater detail within Chapter Two, and the work also extended to the new ytterbium(II) hydride supported by the BDI^{Dicyc} ancillary ligand (**2.14**). Therefore, this

proved as a suitable test of the ability of our three new Eu(II) hydride systems to facilitate the same insertion and σ -bond metathesis chemistry as ytterbium(II).

The addition of the symmetrical system, **3.14**, to a colourless toluene solution containing COT resulted in no noticeable change after stirring for extended periods at room temperature, yet repeating the reaction in THF solvent gave the inverted Eu(II) sandwich complex (**3.24**) as a clear yellow solution after 24 hours at room temperature (Scheme 3.14).



Scheme 3.14. Two-electron aromatisation of COT by **3.14** to give an inverted sandwich complex (**3.24**).

The volatiles were removed *in vacuo* to give the crude product as an oily solid, which was then extracted into toluene, filtered, and crystallised at $-30\text{ }^{\circ}\text{C}$ to obtain yellow crystals suitable for single crystal X-ray diffraction analysis (Figure 3.19).

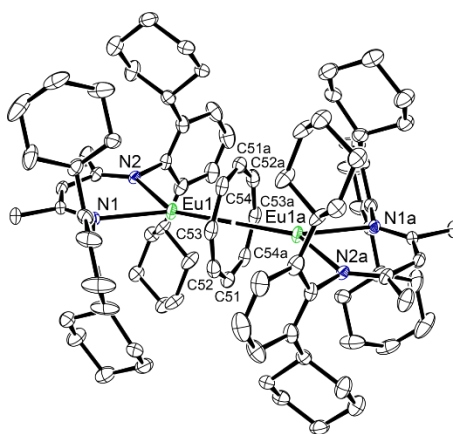
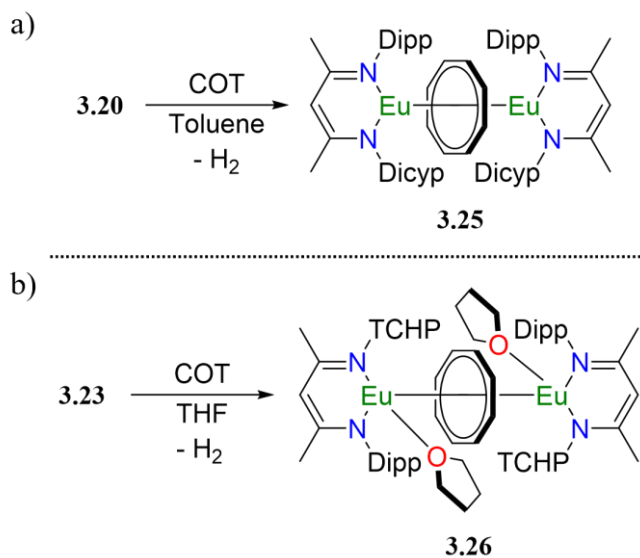


Figure 3.19. Ortep representation (30% probability ellipsoids) of compound **3.24**. Hydrogen atoms have been omitted for clarity. Selected bond lengths (\AA) and angles ($^{\circ}$): Eu1–N1 2.482(5), Eu1–N2 2.513(3), Eu1–C_{cent} 2.1383(4), N1–Eu1–N2 71.8(1), Eu1–C_{cent}–Eu1a 180.0(5).

The asymmetric unit of **3.24** comprises only half of the dimer, displaying an Eu(II) centre *N,N*-chelated to the BDI^{Dicyp} ligand and interacting with half of the [COT]²⁻ dianion. The Eu1–N1 and Eu1–N2 bond lengths (2.482(5) and 2.513(3) Å) are consistent with the Eu–N bond lengths of all Eu(II) complexes presented in this Chapter. The remainder of the complex is generated through an inversion centre coinciding with the centroid of the C₈-ring, giving the inverted sandwich complex in which two [(BDI^{Dicyp})Eu] units are bridged by the [COT]²⁻ dianion, in an η⁸-coordination mode. The Eu1–C_{cent} distance (2.1383(4) Å) and Eu1–C_{cent}–Eu1a angle of 180.0(5)° are like other Eu(II) inverted sandwich complexes containing the [COT]²⁻ dianion (2.129(5) – 2.505(4) Å and 163.92(3) – 177.54(2)°), however it should be noted that these compounds were synthesised through either salt metathesis reactions or a disproportionation reaction.^{33, 34}

The reactions of COT and the unsymmetrical hydrides, **3.20** and **3.23**, were also initially carried out in toluene as a further test of the improved solubility compared to the symmetrical Eu(II) hydride, **3.14**. With respect to **3.20**, the red solid suspended in a colourless toluene solution had become a clear yellow solution with a small amount of yellow precipitate within 24 hours, indicating the formation of the inverted Eu(II) sandwich complex, **3.25** (Scheme 3.15, a)).



Scheme 3.15. Two-electron aromatisation of COT by **3.20** (top) and by **3.23** (bottom) to afford the inverted sandwich complexes, **3.25** and **3.26**, respectively.

In comparison, the reaction of **3.23** and COT in toluene resulted in no change after multiple days at room temperature, whereas repeating the reaction in THF solvent afforded the inverted sandwich complex (**3.26**) within 10 minutes at room temperature (Scheme 3.15, b)). Slow evaporation of concentrated toluene solutions of both compounds obtained single yellow crystals, allowing for elucidation of the solid-state structures *via* crystallographic analysis (Figure 3.20, a) and b)).

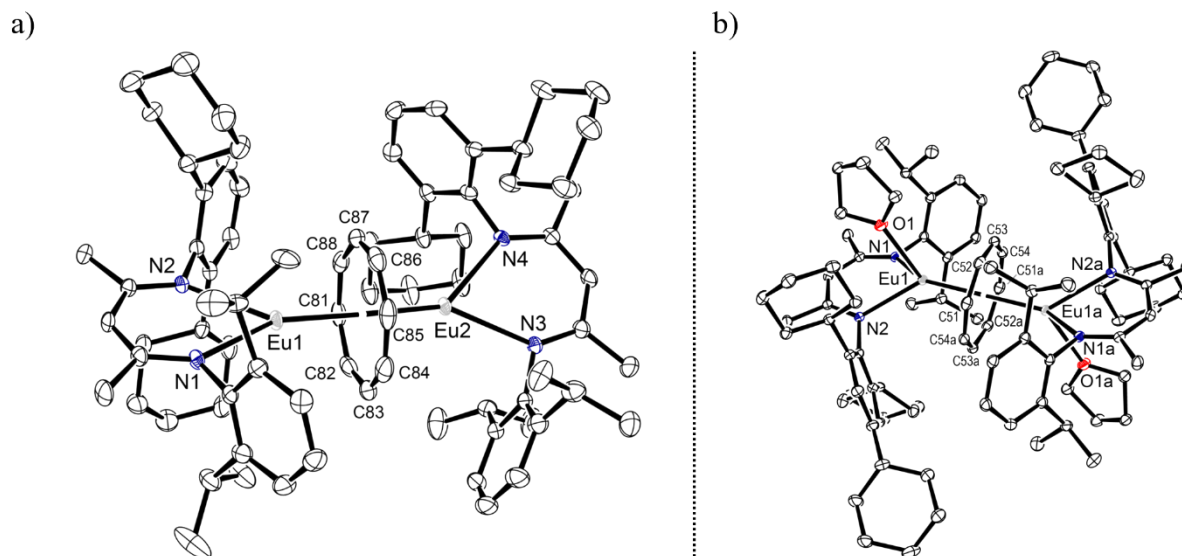


Figure 3.20. Ortep representations (30% probability ellipsoids) of compound **3.25** (left) and compound **3.26** (right).

Hydrogen atoms have been omitted for clarity. Selected bond lengths (Å) and angles (°): **3.25**: Eu1–N1 2.497(4), Eu1–N2 2.559(3), Eu2–N3 2.487(4), Eu2–N4 2.561(4), Eu1–C_{cent} 2.168(2), Eu2–C_{cent} 2.175(2), N1–Eu1–N2 69.4(1), Eu1–C_{cent}–Eu2 177.23(8). **3.26**: Eu1–N1 2.585(1), Eu1–N2 2.508(2), Eu1–O1 2.612(2), Eu1–C_{cent} 2.201(3), N1–Eu1–N2 73.48(6), N1–Eu1–O1 90.56(5), Eu1–C_{cent}–Eu1a 180.0(2).

Both **3.25** (Figure 3.20, a)) and **3.26** (Figure 3.20, b)) contain two Eu(II) metal centres bridged by a [COT]²⁻ dianion, with Eu–N bond lengths (2.487(4) – 2.585(1) Å) and Eu–C_{cent} distances and angles (2.168(2) and 2.201(3) Å, and 177.23(8) and 180.0(2)°, respectively) consistent with the BDI^{Dicyp} structure, **3.24**.

One structural difference of **3.26** is the additional steric stability provided by the coordination of a THF molecule to the Eu(II) centres (Eu1–O1 2.612(2) Å), a feature which was observed with the Eu(II) monoalkyl complex also bearing the BDI^{Dipp,TCHP} ligand system.

In the case of **3.25**, a structural difference is that the Dicyclopentadienyl (Dicyclopentadienyl) substituent of one [(BDI^{Dipp,Dicyp})Eu] unit is coincident with the second Dicyclopentadienyl substituent of the second [(BDI^{Dipp,Dicyp})Eu] unit within the dimer. As a result, the Eu1–N2 and Eu1–N4 bond lengths (2.559(3) and 2.561(4) Å) of the Dicyclopentadienyl substituents are elongated compared to the Eu1–N1 and Eu1–N3 bonds lengths (2.497(4) and 2.487(4) Å) of the Dipp groups. This contrasts all

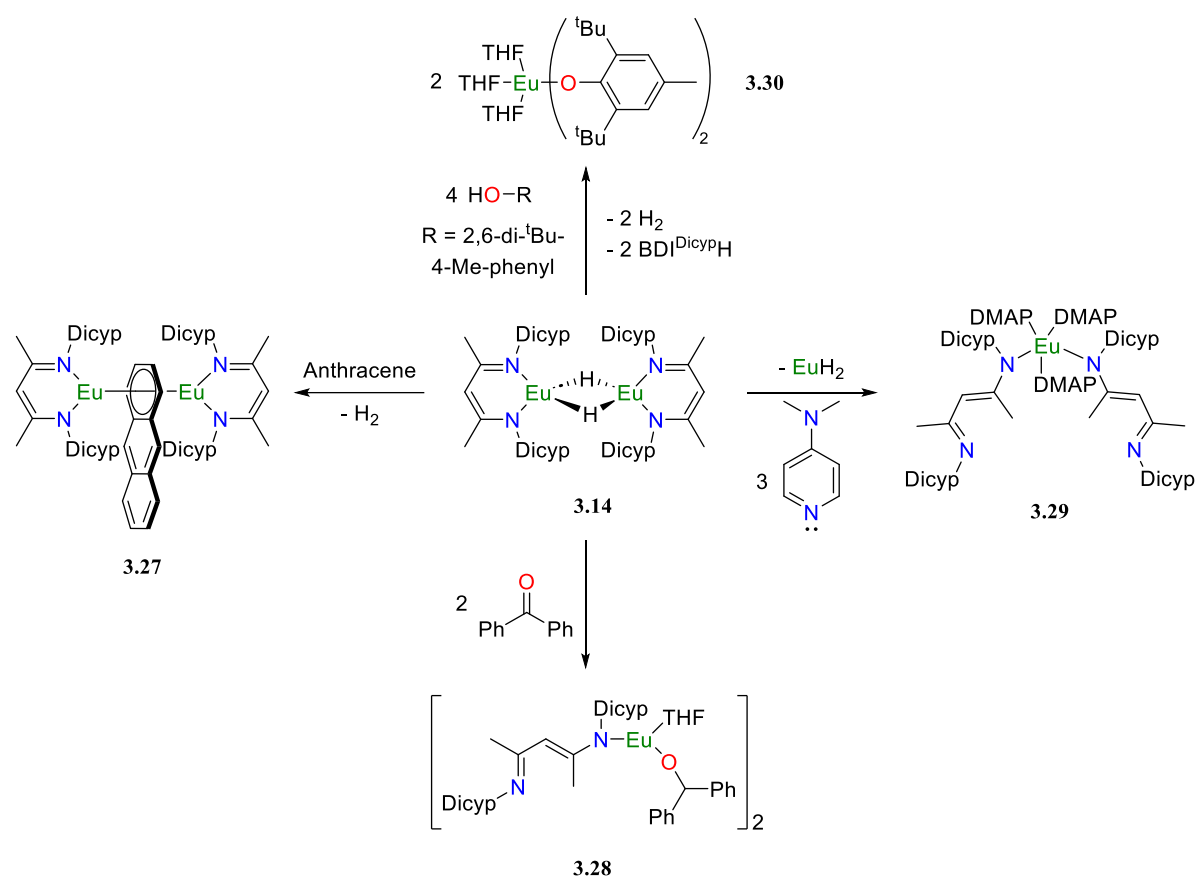
other Eu(II) complexes bearing either derivative of the unsymmetrical BDI ligand presented in this Chapter.

In previous studies, it was observed that the addition of an excess of COT to the ytterbium(II) hydride, **XXV**, resulted in the oxidation of the Yb(II) metal centre to Yb(III) to give the monomeric complex, **2.19**.³² An analogous Eu(III) complex was not observed when an excess of COT was added to any of the divalent europium hydrides and could reflect the higher stability of the Eu(II) ion (−0.35 V vs NHE) in comparison to the Yb(II) ion (−1.15 V vs NHE).⁵

3.7.2 Preliminary Reactivity of [(BDI^{Dicyp})EuH]₂

In Chapters One and Two, it has been established that the insertion chemistry and σ –bond metathesis reactivity of calcium hydrides is well documented within the literature,^{21, 26, 35–37} and as a result, comparative studies have been done with ytterbium(II) hydrides.^{3, 38–44} As there have been no reports on the synthesis of europium(II) hydrides and only a few strontium hydride examples, this comparative reactivity study has not yet been made.

This following Section focuses solely on the reactivity of the symmetrical BDI^{Dicyp} Eu(II) hydride complex and its reactivity with a range of saturated and unsaturated substrates, which we have been conducting over one year. Each substrate was selected to enable direct comparisons to both Group 2 hydrides and ytterbium(II) hydrides. Each transformation of **3.14** and the respective reaction product is summarised below in Scheme 3.16. These reactions will be segregated into subgroups for the purpose of discussion.



Scheme 3.16. Reactivity of **3.14** towards a range of saturated and unsaturated substrates.

Reactions with unsaturated polyaromatic substrates

The ability of the original ytterbium(II) hydride (**XXV**) to reduce the more challenging aromatic substrates, anthracene, and naphthalene (−1.98 and −2.60 V vs SCE, respectively),³² led us to extend this work to the more sterically bulky Yb(II) system, **2.14**, as discussed in Chapter Two. Earlier, it was then demonstrated that the analogous divalent europium hydride (**3.14**) could easily reduce COT (−1.62 and −1.86 V vs SCE) at room temperature to give the inverted sandwich complex **3.24**. As the $\text{Eu}^{3+}/\text{Eu}^{2+}$ reduction potential is less negative compared to ytterbium (−0.35 V and −1.15 V vs NHE, respectively),⁵ it implies greater stability of complexes containing the Eu(II) ion, and therefore it was beneficial to test whether **3.14** could also affect the two-electron reduction of the more challenging polyaromatic system, anthracene.

One equivalent of anthracene was added to a slurry of **3.14** in THF solvent, and the mixture was left to stir at room temperature. Within a few hours, the solution had become a green-blue colour, and after 24 hours, complete consumption of the Eu(II) hydride starting material was visually observed by the lack of any residual red solid. Single brown blocks of **3.27** were obtained from a saturated toluene solution at room temperature, allowing for structural confirmation by X-ray diffraction analysis (Figure 3.21).

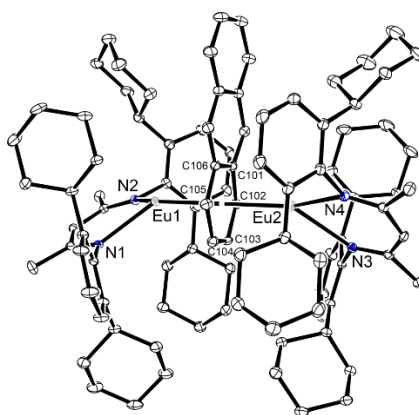


Figure 3.21. Ortep representations (30% probability ellipsoids) of compound **3.27**. Hydrogen atoms have been omitted for clarity. Selected bond lengths (Å) and angles (°): Eu1–N1 2.449(2), Eu1–N2 2.482(2), Eu1–C_{Cent} 2.453(1), Eu2–N3 2.483(3), Eu2–N4 2.452(2), Eu2–C_{Cent} 2.442(1), N1–Eu1–N2 71.74(8), N1–Eu1–C_{Cent} 137.84(8), Eu1–C_{Cent}–Eu2 176.49(6).

In the solid-state, the asymmetric unit comprises an entire molecule of the dimeric inverted sandwich complex, **3.27**. The coordination sphere of each Eu(II) metal centre is firstly made up by two contacts from the *N,N*-chelated β -diketiminate ligand, with Eu1–N1 and Eu1–N2 (2.449(2) and 2.482(2) Å) and Eu2–N3 and Eu2–N4 (2.483(3) and 2.452(2) Å) bond lengths sitting in the range of other Eu(II) complexes bearing the BDI^{Dicyp} ligand system (2.454(2) – 2.529(4) Å). Each Eu(II) centre then η^6 -interacts from opposing faces of the same terminal C₆-ring of the anthracene dianion (Eu1–C_{Cent}: 2.453(1) and 2.442(1) Å). To date, there are no crystallographically characterised examples of europium complexes containing the anthracene dianion ligand. There are three reports of lanthanide complexes containing this bridging [C₁₄H₁₀]²⁻ ligand to which the structural features of **3.27** are vastly different.^{32, 45, 46} In

the case of $[\text{Cp}^*_2\text{Ln}(\mu\text{-C}_{14}\text{H}_{10})\text{LnCp}^*_2]$ ($\text{Ln} = \text{La}, \text{Sm}$), the two $[\text{Cp}^*_2\text{Ln}]$ units are bonded in an η^3 -fashion to the central C_6 -ring of a nearly planar anthracene moiety, whereas in the BDI-based Yb(II) complex, **2.20**, each of the two $[(\text{BDI}^{\text{Dipp}})\text{Yb}]$ units η^4 -interact with one of the terminal C_6 -rings and from opposing faces of the anthracene dianion. The solid-state of **3.27** is analogous to the Yb(II) analogue discussed in Chapter Two, wherein the C–C bond lengths for the Eu-bound ring (average C–C: 1.431 Å) are also considerably longer than the C–C bond lengths of the uncoordinated ring (average C–C: 1.3983 Å) and is a result of less electron density located on the second terminal C_6 -ring of the anthracene dianion.⁴⁷ In **3.27**, the $[\text{C}_{14}\text{H}_{10}]^{2-}$ ligand was also no longer planar, exhibiting a slightly smaller C101–C102–C103–C104–C105–C106 to plane twist angle of 4.61(9)° (**2.23**: 5.81(7)°).

Insertion Reaction with Unsaturated C=O Bonds

Ytterbium(II) hydrides and calcium hydrides can undergo insertion reactions with ketones to yield the respective Yb(II) or calcium alkoxide products.^{35,38} Therefore, **3.14** was reacted with benzophenone in THF, giving a green-blue solution, where insertion of the C=O bond into the Eu–H σ -bond was observed, affording **3.28**. Analysis of the solid-state structure through an X-ray diffraction experiment confirmed the expected dimeric Eu(II) alkoxide product, in which two Eu(II) ions are bridged by two $[\text{Ph}_2\text{C}(\text{H})\text{O}]^-$ anions, much like the Yb(II) and calcium analogues (Figure 3.22).

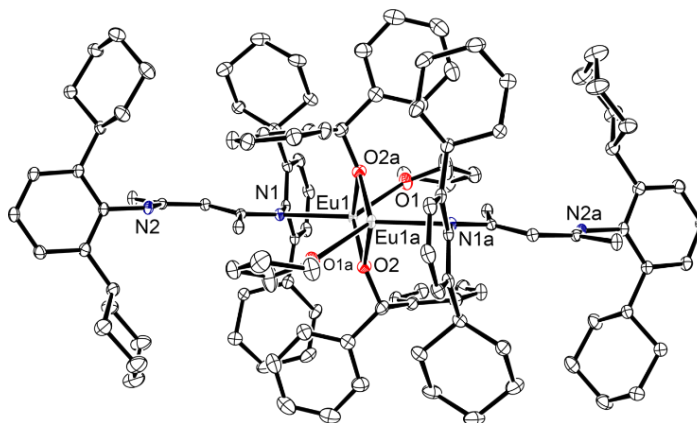


Figure 3.22. Ortep representations (30% probability ellipsoids) of compound **3.28**. Hydrogen atoms have been omitted for clarity. Selected bond lengths (Å) and angles (°): Eu1–N1 2.463(2), Eu1–O1 2.508(2), Eu1–O2 2.360(2), Eu1–O2a 2.404(2), N1–C_{Dicyp} 1.429(3), N2–C_{Dicyp} 1.410(3), N2–C4 1.300(3), O2–C67 1.409(4), N1–Eu1–O1 118.49(8), N1–Eu1–O2 112.52(7), N1–Eu1–O2a 107.80(7), O1–Eu1–O2 127.97(7), O1–Eu1–O2a 97.22(7), O2–Eu1–O2a 75.90(7), Eu1–O2–Eu1 104.10(8).

The C–O2 bond lengths within the alkoxide ligand are 1.409(4) Å and align with forming the C–O single bond. While the Eu1–O2 and Eu1–O2a bond lengths (2.360(2) and 2.404(2) Å, respectively) closely resemble those found in the only other reported Eu(II) aryloxide complexes (2.315(6) – 2.366(2) Å),^{48, 49} the small difference in values found in **3.28** shows the complex displays slight asymmetrical bridging of the alkoxide ligands. This could be due to the possible aryl-interaction of the Eu(II) centre to one of the phenyl rings of the [Ph₂C(H)O][–] units (the closest Eu...C contact is 3.135 Å).³⁵

Where the structure of **3.28** vastly differs from the ytterbium and calcium analogues is the bonding mode of the β-diketiminate ligand, now only κ¹–binding to the Eu(II) metal centre *via* a singular nitrogen of one Dicyp substituent, reminiscent of the ligand bonding found within the homoleptic species, where the Eu1–N1 bond length of 2.463(2) Å is consistent with the Eu–N bond length found within **3.12**.

The primary coordination sphere of the Eu(II) centres is completed by the solvation of a THF molecule, with Eu1–O1 bond lengths of 2.508(8) Å. It would be interesting to repeat this reaction in a non-coordinating solvent, such as toluene, to see whether an alternate reaction

product would be isolated. One possibility would be the formation of the same Eu(II) alkoxide product but containing the typical *N,N*-chelating BDI^{Dicyp} ligand environment, however, this outcome could be unfavoured given the steric bulk of the ligand system in combination with the bulky [Ph₂C(H)O]⁻ anion. However, given the poor solubility of the **3.14** in aromatic solvents, it is possible the reaction time with benzophenone could be lengthened, and therefore, increase the possibility of the formation of the homoleptic decomposition product, **3.12**.

Reaction with a Pyridinyl-Containing Substrate

A report by Chen et al. in 2021 detailed the ability of their ytterbium(II) hydride (**XXVIII**), supported by a β -diketiminato-based tetradentate ligand, to react with a range of substrates, including pyridine and (4-dimethylamino)pyridine (DMAP).⁴² In the case of DMAP, Chen observed the coordination of a DMAP molecule to the Yb(II) centre within **XXVIII**, which was followed by the addition of a Yb–H bond to the C=N bond of the ancillary ligand. A similar reactivity profile could be seen when reacting DMAP with **3.14**, with the strongly donating DMAP molecules coordinating to the Eu(II) centre through the lone pair on the nitrogen of the ring after breaking the Eu–arene interaction of the Dicyp *N*-substituent of the BDI^{Dicyp} ligand.

When two equivalents of DMAP were added to a stirring slurry of **3.14** in THF, the resultant mixture became a dark orange-brown solution after 24 hours at room temperature. The volatiles were removed under vacuum, and the crude product crystallised from toluene solvent, affording brown crystals suitable for analysis by an X-ray diffraction experiment (Figure 3.23).

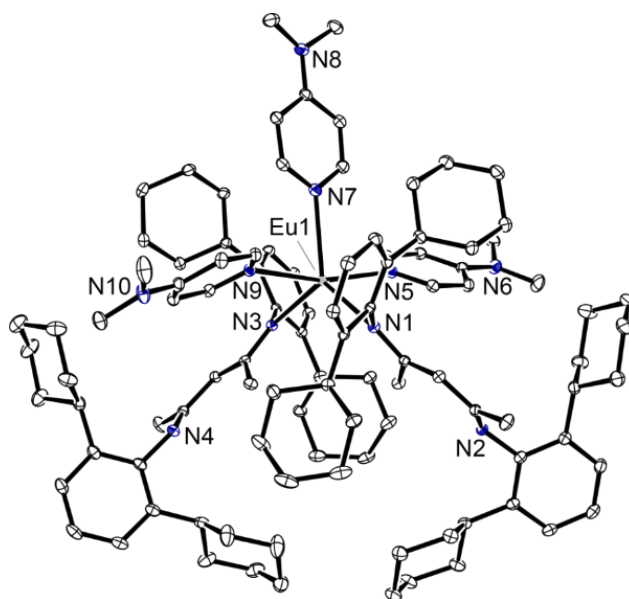


Figure 3.23. Ortep representations (30% probability ellipsoids) of compound **3.29**. Hydrogen atoms have been omitted for clarity. Selected bond lengths (Å) and angles (°): Eu1–N1 2.529(1), Eu1–N3 2.496(1), Eu1–N5 2.692(1), Eu1–N7 2.675(2), Eu1–N9 2.703(1), N1–C_{Dicyclopentadienyl} 1.424(2), N2–C4 1.299(2), N2–C_{Dicyclopentadienyl} 1.406(2), N1–Eu1–N3 115.99(4), N5–Eu1–N7 85.52(4), N7–Eu1–N9 82.11(4).

The solid-state structure of **3.29** was revealed to be a five-coordinate, homoleptic Eu(II) species. Two contacts to the Eu(II) centre were made up by κ^1 -binding of the BDI^{Dicyclopentadienyl} ancillary ligands, reminiscent of one of the ligand binding modes observed within the previously isolated decomposition product, **3.12**. The Eu1–N1 and Eu1–N3 bond lengths of 2.529(1) and 2.496(1) Å are slightly elongated compared to the analogous Eu1–N3 bond length within **3.12** (2.448(2) Å) but still like Eu–N bond lengths found in other Eu(II) complexes containing this BDI^{Dicyclopentadienyl} ligand framework (2.454(2) – 2.529(4) Å). This slight lengthening could be to accommodate the three strongly donating DMAP molecules to the Eu(II) metal centre (Eu–N: 2.692(1), 2.675(2) and 2.703(1) Å), completing the coordination sphere and giving the complex an overall geometry resembling trigonal bipyramidal.

σ -bond Metathesis Reactions

In Chapter One, it was demonstrated that the reaction between Takat's Yb(II) hydride (**XI**) and a terminal alcohol, HOMes (Mes = mesityl) could afford the monomeric Yb(II) aryloxide complex, **XII**, with the extrusion of hydrogen gas.³⁸ Here, the addition of the 2,6-di-*tert*-butyl-4-methylphenol substrate to a stirring slurry of **3.14** in THF resulted in bubbling and the formation of a clear yellow solution, hinting at the release of hydrogen as the by-product and the formation of a new europium-containing product, **3.30**. After workup, crystallisation of a saturated toluene solution yielded large, single blocks suitable for a single crystal X-ray diffraction experiment. The solid-state data revealed the product was not the expected heteroleptic Eu(II) aryloxide species but a previously reported homoleptic Eu(II) complex in which the metal centre is σ -bonded to two aryloxide ligands, with the remainder of the coordination sphere made up by three THF molecules.^{48, 49}

This structure has been synthesised through three main methods within the literature: two equivalents of the phenol reagent is reacted with either I₂-activated europium metal or complexes such as [Eu(C₅Me₅)₂] or [Eu(C₆F₅)₂] to form the product, **3.30**, concomitant with the formation of H₂, and C₅Me₅H or C₆F₅H, respectively. In this case, **3.20** was likely formed through extrusion of both H₂ and the free ligand, **2.7**, as the by-products.

3.7 Summary

In summary, this Chapter has demonstrated that synthesising the first examples of molecular, Eu(II) hydride complexes is not just a simple extension of Group Two chemistry, and that the stability of these Eu(II) complexes is largely correlated to the respective ligand environment. However, three new divalent Eu(II) hydride complexes bearing other derivatives of the β -diketiminato ancillary ligand were successfully isolated and characterised, representing the first examples of lanthanide(II) hydrides beyond Yb(II). This was followed by an introduction of how these three compounds react with respect to either saturated or unsaturated substrates, demonstrating the potential for Eu(II) hydrides in developing novel catalytic and stoichiometric chemical transformations. Though the preliminary results regarding the unsymmetrical Eu(II) hydrides have thus far been limited to the two-electron aromatisation of COT, further studies will be conducted in the future to better understand these new hydride systems.

3.8 References

1. B. Rösch, T. X. Gentner, H. Elsen, C. A. Fischer, J. Langer, M. Wiesinger and S. Harder, *Angew. Chem. Int. Ed.*, **2019**, 58 (16), 5396-5401.
2. R. Shannon, *Acta Cryst. A.*, **1976**, 32 (5), 751-767.
3. G. M. Richardson, I. Douair, S. A. Cameron, J. Bracegirdle, R. A. Keyzers, M. S. Hill, L. Maron and M. D. Anker, *Nat. Comm.*, **2021**, 12 (1), 1-7.
4. T. D. Tilley, R. A. Andersen and A. Zalkin, *Inorg. Chem.*, **1984**, 23 (15), 2271-2276.
5. W. J. Evans, *Inorg. Chem.*, **2007**, 46 (9), 3435-3449.
6. A. J. Pell, G. Pintacuda and C. P. Grey, *Prog. Nucl. Mag. Reason. Spectrosc.*, **2019**, 111, 1-271.
7. A. M. Bienfait, B. M. Wolf, K.W. Törnroos and R. Anwender, *Inorg. Chem.*, **2018**, 57 (9), 5204-5212.
8. E. Hevia, A. R. Kennedy, R. E. Mulvey and S. Weatherstone, *Angew. Chem. Int. Ed.*, **2004**, 43 (13), 1709-1712.
9. C. N. De Bruin-Dickason, T. Sutcliffe, C. Alvarez Lamsfus, G. B. Deacon, L. Maron and C. Jones, *Chem. Comm.*, **2018**, 54 (7), 786-789.
10. X. Shi, G. Qin, Y. Wang, L. Zhao, Z. Liu and J. Cheng, *Angew. Chem. Int. Ed.*, **2019**, 58 (13), 4356-4360.
11. R. Jiao, X. Shen, M. Xue, Y. Zhang, Y. Yao and Q. Shen, *Chem. Comm.*, **2010**, 46 (23), 4118-4120.
12. M. Xue, Y. Zheng, Y. Hong, Y. Yao, F. Xu, Y. Zhang and Q. Shen, *Dalton Trans.*, **2015**, 44 (46), 20075-20086.
13. M. Schmid, S. M. Guillaume and P. W. Roesky, *Organometallics*, **2014**, 33 (19), 5392-5401.
14. X. Shen, Y. Zhang, M. Xue and Q. Shen, *Dalton Trans.*, **2012**, 41 (13), 3668-3674.
15. S. Qayyum, A. Noor, G. Glatz and R. Kempe, *Z. Anorg. Allg. Chem.*, **2009**, 635 (15), 2455-2458.
16. A. A. Skatova, D. S. Yambulatov, I. L. Fedyushkin and E. V. Baranov, *Russ. J. Coord. Chem.*, **2018**, 44 (6), 400-409.
17. T. K. Panda, A. Zulys, M. T. Gamer and P. W. Roesky, *J. Organomet. Chem.*, **2005**, 690 (23), 5078-5089.
18. F. H. Allen, O. Kennard, D. G. Watson, L. Brammer, A. G. Orpen and R. Taylor, *J. Chem. Soc., Perkin Trans. 2.*, **1987**, (12), S1-S19.
19. C. Sandorfy, General and theoretical aspects. In Carbon–Nitrogen Double Bonds (1970), **1970**, 1-60.
20. H. Bauer, K. Thum, M. Alonso, C. Fischer and S. Harder, *Angew. Chem. Int. Ed.*, **2019**, 58 (13), 4248-4253.
21. B. Rösch, T. X. Gentner, J. Langer, C. Färber, J. Eyselein, L. Zhao, C. Ding, G. Frenking and S. Harder, *Science*, **2021**, 371 (6534), 1125-1128.
22. G. M. Richardson, T. Rajeshkumar, F. M. Burke, S. A. Cameron, B. Nicholls, J. Harvey, R. A. Keyzers, T. Butler, S. Granville, L. Liu, L. Maron and M. D. Anker, preprint out at *Nature Portfolio*, under revision (*Nat. Chem.*), **2023**.
23. C. Eaborn, P. B. Hitchcock, K. Izod, Z. R. Lu and J. D. Smith, *Organometallics*, **1996**, 15 (22), 4783-4790.
24. Z. Hou, Y. Zhang, M. Nishiura and Y. Wakatsuki, *Organometallics*, **2003**, 22 (1), 129-135.
25. A. L. Allred, *J. Inorg. Nucl. Chem.*, **1961**, 17 (3), 215-221.
26. J. Dyll, M. S. Hill, M. F. Mahon, L. The and A. S. S. Wilson, *Dalton Trans.*, **2019**, 48 (13), 4248-4254.

27. W. Ren, S. Zhang, Z. Xu and X. Ma, *Dalton Trans.*, **2019**, 48 (9), 3109-3115.
28. D. D. L. Jones, S. Watts and C. Jones, *Inorganics*, **2021**, 9 (9).
29. A. P. Dove, V. C. Gibson, E. L. Marshall, A. J. P. White and D. J. Williams, *Dalton Trans.*, **2004**, (4), 570-578.
30. E. A. Weerawardhana, A. Pena, M. Zeller and W. T. Lee, *Inorganica Chim. Acta.*, **2017**, 460, 29-34.
31. J. Li, M. Luo, X. Sheng, H. Hua, W. Yao, S. A. Pullarkat, L. Xu and M. Ma, *Org. Chem. Front.*, **2018**, 5 (24), 3538-3547.
32. G. M. Richardson, I. Douair, S. A. Cameron, L. Maron and M. D. Anker, *Chem. Eur. J.*, **2021**, 27 (52), 13144-13148.
33. W. J. Evans, J. L. Shreeve and J. W. Ziller, *Polyhedron*, **1995**, 14 (20), 2945-2951.
34. W. J. Evans, M. A. Johnston, M. A.; Greci and J. W. Ziller, *Organometallics*, **1999**, 18 (8), 1460-1464.
35. J. Spielmann and S. Harder, *Chem. Eur. J.*, **2007**, 13 (32), 8928-8938.
36. A. S. Wilson, M. S. Hill, M. F. Mahon, C. Dinoi and L. Maron, *Science*, **2017**, 358 (6367), 1168-1171.
37. S. Harder and J. Brettar, *Angew. Chem. Int. Ed.*, **2006**, 45 (21), 3474-3478.
38. G. M. Ferrence and J. Takats, *J. Organomet. Chem.*, **2002**, 647 (1-2), 84-93.
39. S. Harder, *Angew. Chem. Int. Ed.*, **2004**, 43 (20), 2714-2718.
40. C. Ruspici, J. Spielmann and S. Harder, *Inorg. Chem.*, **2007**, 46 (13), 5320-5326.
41. X. Shi, P. Deng, T. Rajeshkumar, L. Zhao, L. Maron and J. Cheng, *Chem. Comm.*, **2021**, 57 (78), 10047-10050.
42. Q. Wen, B. Feng, L. Xiang, X. Leng and Y. Chen, *Inorg. Chem.*, **2021**, 60 (18), 13913-13919.
43. I. V. Basalov, D. M. Lyubov, G. K. Fukin, A. S. Shavyrin and A. A. Trifonov, *Angew. Chem. Int. Ed.*, **2012**, 51 (14), 3444-3447.
44. I. V. Basalov, D. M. Lyubov, G. K. Fukin, A. V. Cherkasov and A. A. Trifonov, *Organometallics*, **2013**, 32 (5), 1507-1516.
45. K. H. Thiele, S. Bambirra, H. Schumann and H. Hemling, *J. Organomet. Chem.*, **1996**, 517 (1), 161-163.
46. W. J. Evans, S. L. Gonzales and J. W. Ziller, *J. Am. Chem. Soc.*, **1994**, 116 (6), 2600-2608.
47. J. Mai, B. Rösch, N. Patel, J. Langer and S. Harder, *Chem. Sci.*, **2023**, 14 (18), 4724-4734.
48. J. R. van den Hende, P. B. Hitchcock, S. A. Holmes, M. F. Lappert, W. P. Leung, T. C. W. Mak and S. Prashar, *J. Chem. Soc., Dalton Trans.*, **1995**, (9), 1427-1433.
49. G. B. Deacon, S. Hamidi, P. C. Junk, R. P. Kelly and J. Wang, *Eur. J. Inorg. Chem.*, **2014**, 2014 (3), 460-468.

Chapter Four

Four-Electron Reduction of Benzene by a Samarium(II) Alkyl

4.1 Introduction

To date, there are no reports on the isolation of a heteroleptic, divalent samarium hydrido complex. This can be ascribed to the larger ionic radius of the Sm(II) ion in comparison to Yb(II) and Eu(II) and the challenge of finding a suitable ligand to saturate the coordination sphere of the large Sm(II) centre. Additionally, the highly negative $\text{Sm}^{3+}/\text{Sm}^{2+}$ reduction potential (-1.55 V vs NHE) may have hindered previous attempts at isolating these Sm(II) hydride complexes.¹

Chapter One details the successful synthesis of two molecular barium(II) hydrides: one by utilising the tridentate tris(pyrazolyl)borate ligand (**XXXVIII**) and the second supported by an extremely bulky cyclopentadienyl ligand system (**XLb**) (Figure 4.1).^{2,3}

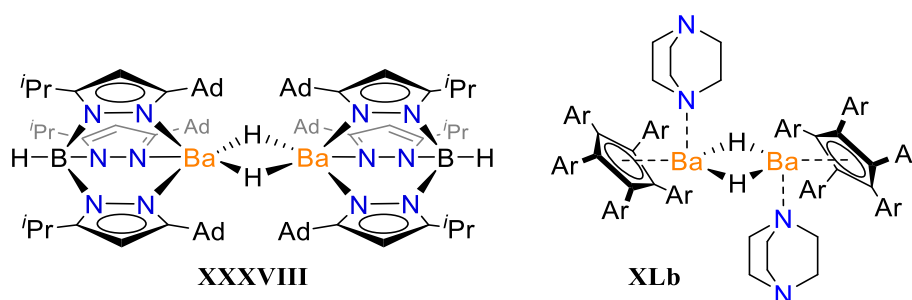


Figure 4.1. Two reported examples of molecular barium hydrides.

The barium ion has a far larger ionic radius in comparison to the Sm(II) ion (Ba^{2+} : 1.42 \AA , Sm^{2+} : 1.27 \AA),⁴ therefore, it seems plausible that, should we design a suitable ligand framework, we could synthesise and isolate a heteroleptic samarium(II) hydride.

In Chapter Three, utilising the β -diketiminato ligand framework in combination with the Dicyc *N*-substituent allowed for the isolation of a divalent europium hydride complex. The work presented herein, therefore, uses the same BDI^{Dicyc} ancillary ligand; however, early into our attempts at synthesising a molecular samarium(II) hydride, the chemistry was found to diverge from the work presented in Chapters Two and Three. Hence, this Chapter focuses on the reduction chemistry of a heteroleptic samarium(II) monoalkyl complex.⁵

4.1.1 Reduction of Benzene and its Derivatives by F-element Complexes

The benzene tetraanion, $[\text{C}_6\text{H}_6]^{4-}$, is a 10π -electron system and has been previously calculated to be stable and display aromaticity in accordance with Hückel's $(4n + 2)\pi$ -electron rule.⁶ It has also been calculated as having a planar conformation, with average C–C bond distances and angles of 1.507 Å and 120°, respectively. Despite this, there is only one example of a metal complex containing the parent benzene tetraanion, obtained by the four-electron reduction of benzene by a thorium(IV) chloride in the presence of KC_8 reducing agent.⁷ To date, there are no examples of the four-electron reduction of benzene without the need for a strong Group 1 reducing agent and can be attributed to the highly negative reduction potential of benzene (–3.42 V vs SCE).⁸

However, there are reports on the four-electron reduction of model systems, such as biphenyl (–2.80 V vs SCE).^{9–12} One example is the four-electron reduction of biphenyl by a Sm(III) halide in the presence of KC_8 , which afforded the samarium inverse sandwich complex, **XLIXa** (Figure 4.2).¹⁰

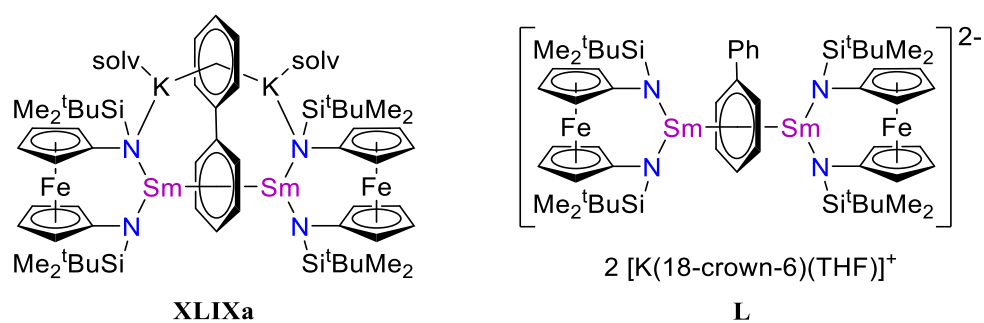


Figure 4.2. Inverse sandwich structures where the biphenyl tetraanion bridges two Sm(III) centres.

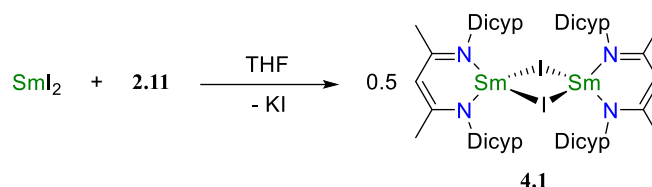
In this work, Diaconescu structurally characterised the samarium metal centres as being in the 3+ oxidation state and were $\mu\text{-}\eta^6\text{:}\eta^6$ -bridged by the biphenyl tetraanion.¹⁰ An analogous reduction of biphenyl was also made with a Yb(III) precursor and KC_8 , however, the oxidation state of the ytterbium metal centre in the resultant product was characterised as being Yb(II). Therefore, this was assigned as a reduced biphenyl dianion.

The following Section delves into the synthesis of a monomeric Sm(II) alkyl complex, where, over the course of our research, we found this species could also reduce benzene. Therefore, Section 4.1.1 served as a reminder of the previously reported reduction chemistry of benzene and the model system, biphenyl, which has also been detailed in Chapter One. This enables us to directly compare **XLIXa** and our own reduced benzene complex throughout the remainder of this Chapter.

4.2 Synthesis of $[(\text{BDI}^{\text{Dicyp}})\text{SmCH}(\text{SiMe}_3)_2]$

The ytterbium(II) and europium(II) monoalkyl precursors supported by the $\text{BDI}^{\text{Dicyp}}$ ligand were synthesised through the reaction of a heteroleptic Yb(II) and Eu(II) iodide with Lappert's alkyl, $\text{KCH}(\text{SiMe}_3)_3$, respectively. Each synthetic step was conducted in THF solvent, where even the large Eu(II) ion (Eu^{2+} : 1.25 Å)⁴ was found to be solvent-free. Therefore, this methodology was extended to the larger Sm(II) ion (Sm^{2+} : 1.27 Å),⁴ with the prediction of synthesising a low-coordinate, Sm(II) monoalkyl complex.

The heteroleptic samarium(II) iodide (**4.1**) could be synthesised after 4 hours at room temperature from the salt metathesis reaction between the homoleptic Sm(II) iodide and the potassium salt of the BDI^{Dicyp} ligand (**2.11**) in THF solvent (Scheme 4.1).⁵



Scheme 4.1. Synthesis of a heteroleptic Sm(II) iodide (**4.1**).

The divalent samarium ion has an f-configuration of [Xe]4f⁶ and can, therefore, have up to six unpaired electrons.¹ As a result, the Sm(II) nucleus is paramagnetic. However, unlike any complexes containing the paramagnetic Eu(II) ion, solution-state structural characterisation of most Sm(II) species herein could be obtained *via* multinuclear NMR techniques.¹³

Pure samples of **4.1** were dissolved in C₆D₆ in an NMR tube fitted with a J. Youngs tap, and full multinuclear NMR data was collected with increased line sweeps to account for the large chemical shift ranges that paramagnetic nuclei can display.¹³ These data indicated the presence of a single β-diketiminate environment in solution by a signal situated at δ_H -12.61 ppm in the ¹H NMR spectrum that we assigned as the methine proton, in a 1:6 ratio with a proton resonance at δ_H -2.54 ppm. Therefore, this was assigned as the methyl groups of the BDI^{Dicyp} ligand backbone, confirmed by the correlation in the ¹H-¹H COSY NMR spectrum.⁵ Typically, the ¹H NMR signals for the β-diketiminate methyl groups and methine proton within our BDI-based Yb(II) complexes sit within the range of ca. δ_H 4 – 5 ppm and δ_H 1.5 – 2 ppm, respectively,¹⁴⁻¹⁶ confirming the presence of the paramagnetic Sm(II) ion in solution.

For further confirmation, crystallisation of a dark army-green toluene solution containing **4.1** afforded dark crystals, allowing for structural elucidation *via* a single crystal X-ray diffraction experiment (Figure 4.3).

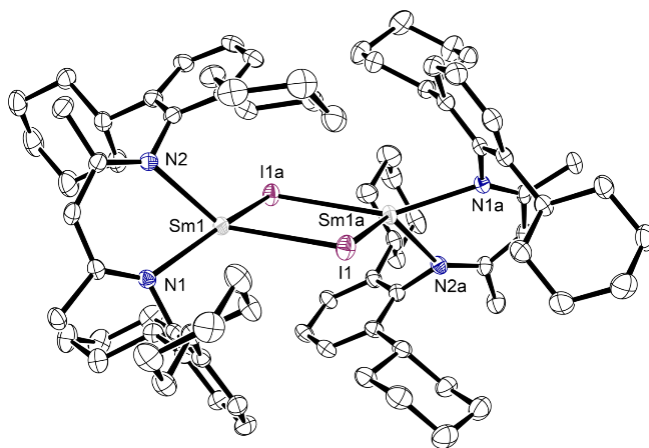
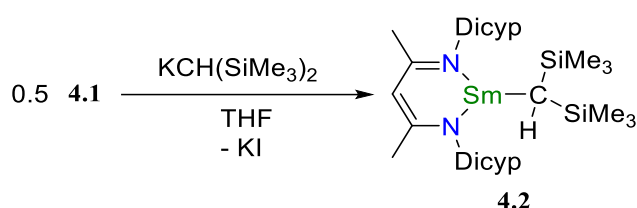


Figure 4.3. Ortep representation (30% probability ellipsoids) of compound **4.1**. Hydrogen atoms have been removed for clarity. Selected bond lengths (Å) and angles (°): Sm1–N1 2.475(4), Sm1–N2 2.440(4), Sm1–I1 3.2035(4), Sm1–I1a 3.2421(4), N1–Sm1–N2 70.0(1), N1–Sm1–I1 113.31(9), N2–Sm1–I1 129.59(1), I1–Sm1–I1a 88.99(1).

The solid-state structure of **4.1** is dimeric, with two Sm(II) centres containing bidentate *N,N*-bonding of the β -diketimate ligand and are μ^2 -bridged by two iodide ligands. Both Sm(II) centres are described as low-coordinate with no additional contacts from donor solvents; this is despite the larger ionic radius of the Sm(II) ion and conducting the reaction in THF solvent. The Sm1–N1 and Sm–N2 bond lengths are 2.475(4) and 2.440(4) Å and the Sm1–I1 and Sm1–I1a bond lengths are 3.2035(4) and 3.2421(4) Å, respectively. These Sm–N and Sm–I bond lengths within compound **4.1** are slightly shorter compared to the only other dimeric Sm(II) iodide complex bearing a derivative of the β -diketimate ligand (Sm–N: 2.521(4) and 2.564(4), Sm–I: 3.324(1) and 3.286(1) Å).¹⁷ The difference of the bond distances could be on account of the differences in coordination number, where this reported BDI-based Sm(II) iodide contains a Sm(II) centre that is five-coordinate, while the Sm(II) centres within **4.1** are only four-coordinate.^{5, 17}

The subsequent salt metathesis reaction between **4.1** and the potassium salt of Lappert's alkyl, $\text{KCH}(\text{SiMe}_3)_2$, was also carried out in THF solvent. After 20 minutes at room temperature, the green-brown solution had turned a true brown colour with beige precipitates. Removal of the THF solvent and extraction into hexane afforded the desired samarium(II) monoalkyl complex, **4.2** (Scheme 4.2). This contrasts the two previously reported Sm(II) alkyl complexes bearing the bis(trimethylsilyl)methane ligand, which were obtained at low temperatures ($-30\text{ }^\circ\text{C}$ or $-50\text{ }^\circ\text{C}$, respectively).^{17, 18}



Scheme 4.2. Synthesis of a monomeric Sm(II) alkyl complex (**4.2**).

The structure of **4.2** was first confirmed in the solution-state. Like the ^1H NMR spectrum of **4.1**, a singlet resonance at $\delta_{\text{H}} -12.63$ ppm was observed in the ^1H NMR spectrum of **4.2**, however, these data remained inconclusive on whether this could be confirmed as the methine proton of the β -diketiminato ligand or the C–H environment of the bis(trimethylsilyl)methyl ligand for this monoalkyl complex.⁵ This signal was in a 1:6 ratio with a peak at $\delta_{\text{H}} -1.77$ ppm, assigned as the methyl protons of the β -diketiminato ligand, respectively. Finally, the formation of **4.2** was confirmed through further 2D correlations of the BDI methyl groups and a singlet resonance integrated for 18H at $\delta_{\text{H}} -8.72$ ppm, corresponding to the methyl groups of the bis(trimethylsilyl)methyl ligand. Further structural confirmation was obtained in the solid-state through X-ray diffraction analysis (Figure 4.4).

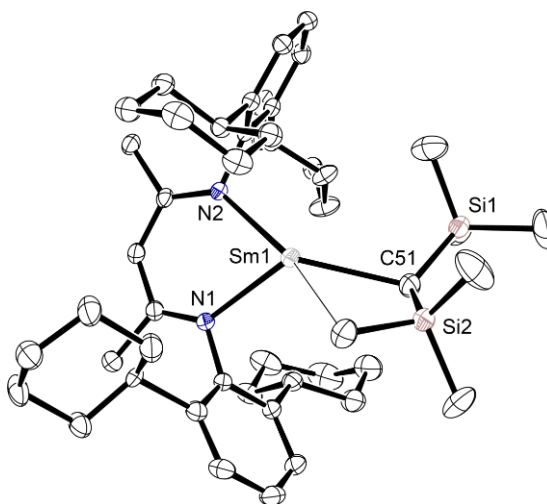


Figure 4.4. Ortep representation (30% probability ellipsoids) of compound **4.2**. Hydrogen atoms have been removed for clarity. Selected bond lengths (Å) and angles (°): Sm1–N1 2.481(2), Sm1–N2 2.484(2), Sm1–C51 2.646(4), Sm1–C57 3.044(4), N1–Sm1–N2 71.93(7), N1–Sm1–C51 125.3(1), N2–Sm1–C51 136.1(1).

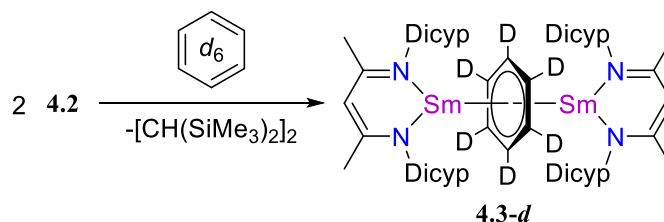
The Sm(II) metal centre within **4.2** is primarily three-coordinate, containing Sm–N contacts to both nitrogen atoms of the BDI^{Dicyl} ligand and a Sm–C final contact to the bis(trimethylsilyl)methyl ligand. The Sm1–N1 and Sm1–N2 bond lengths are 2.481(2) and 2.484(2) Å and are slightly shorter than the Sm–N bond lengths of other Sm(II) complexes supported by derivatives of the β-diketimate ancillary ligand (2.512(2) – 2.5790(16) Å).^{19–21} These other complexes contain Sm(II) centres that are either four- or five-coordinate, thus this decrease in bond length could be explained by the low coordination number of **4.2**.⁵ The Sm1–C51 bond length (2.646(4) Å) is comparable to other Sm(II) complexes bearing the bis(trimethylsilyl)methane ligand (2.652(9) – 2.707(5) Å).^{17, 18, 22} The Sm(II) centre also contains an intramolecular contact (Sm⋯C57 3.044(4) Å) to a methyl group of the bis(trimethylsilyl)methyl ligand, completing the coordination sphere.⁵ This solid-state structure of **4.2** is reminiscent of the geometry of the Yb(II) (**2.13**) and Eu(II) (**3.11**) monoalkyl complexes detailed in Chapters Two and Three, respectively.

4.3 Synthesis and Characterisation of a Benzene Tetraanion

The apparent ease of synthesising **4.2** and the ability to obtain pure, crystalline samples at room temperature meant it became beneficial to explore the relative stability of this complex in the solution-state.

We also recently reported the ability of a divalent ytterbium hydride (**XXV**) to react with ethene or propene to provide Yb(II) *n*-ethyl (**XXVIa**) or *n*-propyl (**XXVIb**) complexes, respectively.¹⁴ These ytterbium(II) alkyls could then facilitate the stoichiometric and catalytic alkylation of benzene, the chemistry of which is discussed in greater detail in Chapter One. Therefore, we sought to test the reactivity of **4.2** towards benzene and its derivatives.

A C₆D₆ solution of **4.2** was monitored by ¹H NMR spectroscopy, with no obvious change occurring after 2 days at room temperature. In contrast, heating the same reaction solution at 60 °C for 2 days resulted in complete consumption of the starting material, concurrent with the formation of a new samarium-containing product (**4.3-d**) (Scheme 4.3).⁵



Scheme 4.3. Synthesis of the inverted sandwich complex (**4.3-d**).

This was apparent by the loss of the signal at δ_{H} -12.63 ppm and the growth of a new methine resonance of the BDI^{Dicyl} ligand situated at δ_{H} 10.52 ppm in the ¹H NMR spectrum (Figure 4.5, (bottom)).

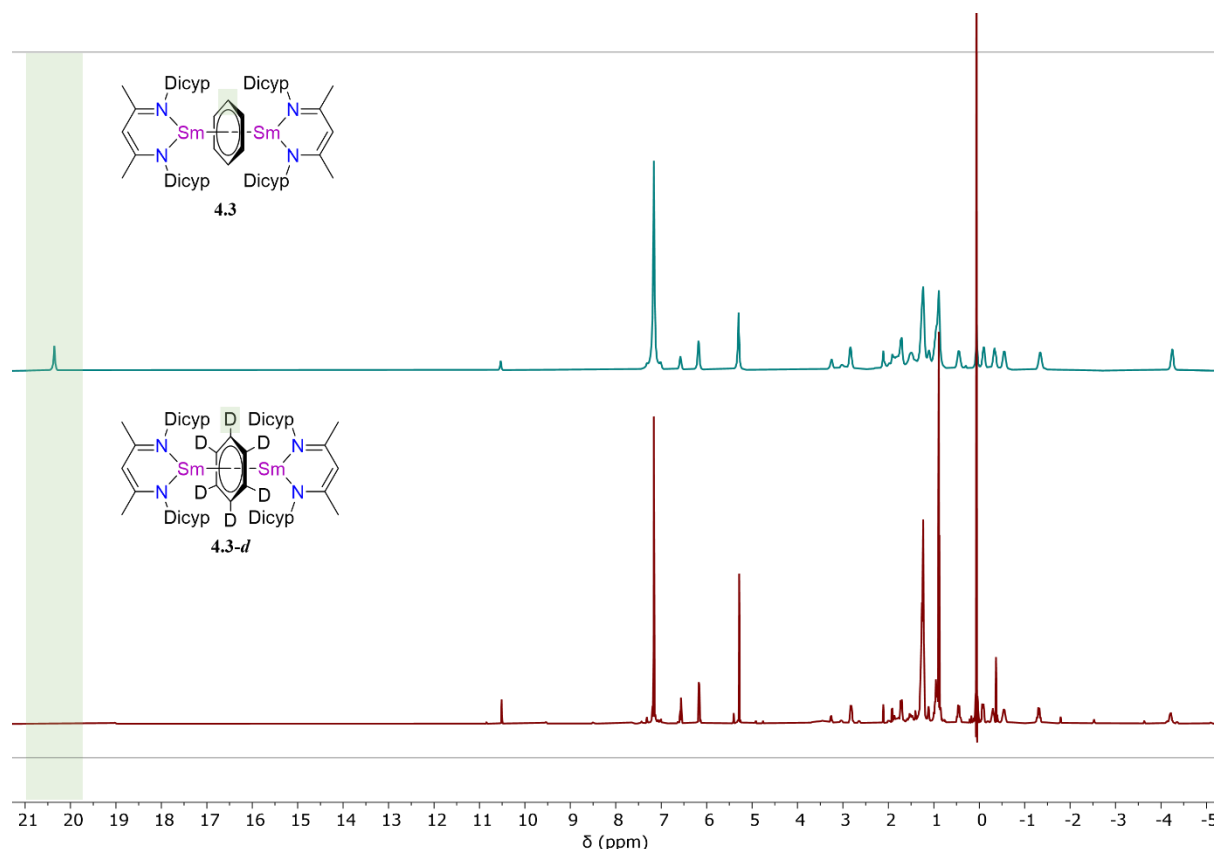


Figure 4.5. Stacked ¹H NMR spectrum (500 MHz, C₆D₆) of compound **4.3** (top) and the *in-situ* reaction of **4.2** and C₆D₆ solvent to give **4.3-d** (bottom).

Samples of **4.2** were then dissolved into proteo-benzene solvent in an NMR tube fitted with a J. Youngs tap, and the reaction was monitored *via* ¹H NMR spectroscopy, with the formation of the same samarium-containing product (**4.3**) occurring over 24 hours at 60 °C. However, a new low-field signal at δ_H 20.36 ppm was now present in a 3:1 ratio with the β-diketiminato methine signal at δ_H 10.52 ppm, suggesting the incorporation of a charged [C₆H₆]ⁿ⁻ moiety within the structure (Figure 4.5, (top)).⁵

The J. Youngs tap NMR tube containing benzene solutions of **4.3** was transferred inside the glovebox, the volatiles were removed *in vacuo*, and the crude product was recrystallised from toluene at room temperature, providing dark crystals of **4.3** suitable for a single crystal X-ray diffraction experiment (Figure 4.6).

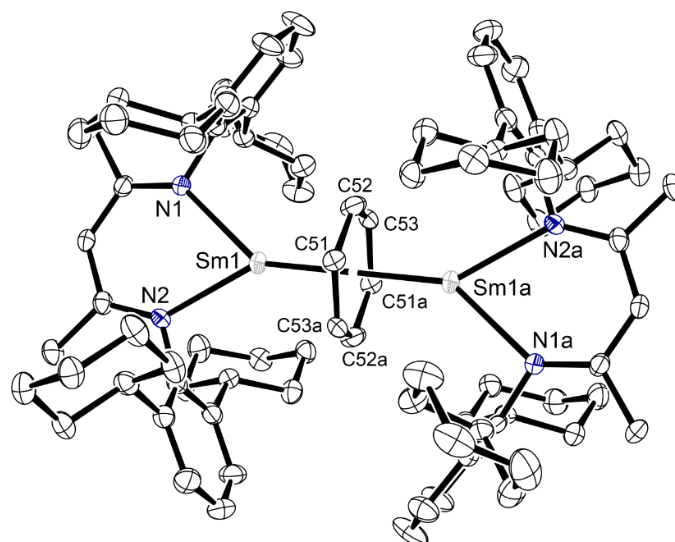


Figure 4.6. Ortep representation (30% probability ellipsoids) of compound **4.3**. Hydrogen atoms have been removed for clarity. Selected bond lengths (Å) and angles (°): Sm1–N1 2.431(7), Sm1–N2 2.426(4), Sm1–C_{cent} 2.0732(4), Sm1–Sm1a 4.1464(7), C51–C52 1.456(10), C52–C53 1.420(12), C53–C51a 1.464(10), N1–Sm1–N2 71.7(2), Sm1–C_{cent}–Sm2 180.0(3).

In the solid-state, **4.3** appears as a dimer, with a $[\text{C}_6\text{H}_6]^n$ unit bridging the two samarium metal centres. The Sm1–N1 and Sm1–N2 bond lengths are reported as 2.431(7) and 2.426(4) Å, respectively, and are slightly shorter than the reported Sm–N bond lengths within the Sm(II) monoalkyl precursor (**4.2**) also bearing the $\text{BDI}^{\text{Dicyp}}$ ancillary ligand (2.481(2) – 2.484(2) Å).⁵ They are also shorter than the Sm–N bond lengths for other previously reported β -diketiminato Sm(II) complexes (2.512(2) – 2.5790(16) Å)^{19–21} but sit within the range of Sm(III) complexes also supported by BDI-based ligands (2.290 – 2.503(3) Å).^{21, 23–25}

The decrease in ionic radius from the Sm(II) ion to the Sm(III) ion (1.27 to 1.132 Å, respectively)¹ mean that, generally, the metal-ligand bond distances will be shorter in complexes containing the trivalent samarium ion in comparison to those containing samarium in the 2+ oxidation state. However, the discrepancy in the bond distance range for Sm–N contacts in complexes containing either the Sm(II) or Sm(III) metal centre is attributed to the respective ligand environment and dependent on the coordination number.²⁶

The final contact to the samarium centres of **4.3** is the $\mu\text{-}\eta^6\text{:}\eta^6$ -bridging $[\text{C}_6\text{H}_6]^n$ -moiety.⁵ The Sm1–C_{Cent} and Sm1–Sm1a distances of 2.0732(4) Å and 4.1464(7) Å, respectively, are shorter than the Sm–C_{Cent} distance (2.196(7) Å) and Sm–Sm distance (4.336(1) Å) reported for the related samarium biphenyl complex, **XLIXa**.¹⁰ The C–C bond lengths within the $[\text{C}_6\text{H}_6]^n$ -unit of **4.3** range from 1.420(12) to 1.464(10) Å, aligning with the C–C bond lengths of the nearly planar samarium-bound ring in **XLIXa** (1.421(5) – 1.476(1) Å). While the C–C bond distances in these complexes are shorter than the predicted values for the benzene tetraanion,⁶ they are also within the range for C–C bond distances within complexes containing the benzene dianion (1.337(11) – 1.485 Å).^{10, 27-29} This results in some uncertainty regarding solid-state characterisation of the benzene ligand within **4.3**, however, the C–C bond distances are, on average, longer than the C–C bond distances found within complexes containing the benzene dianion, which typically display two shorter localised double bonds. On this basis, the overall structure features of **4.3** could suggest two Sm(III) ions that are bridged by a benzene tetraanion, $[\text{C}_6\text{H}_6]^{4-}$.

To confirm the presence of either the Sm(II) or Sm(III) ion within **4.3**, magnetic susceptibility measurements can be used to probe the ground state electronic configuration, where knowing the number of unpaired electrons can provide information on the oxidation state of the samarium centre.³⁰ This can be compared back to the literature, which reports that Sm(II) and Sm(III) ions display distinct magnetic susceptibilities (3.4 – 3.8 μ_B and 1.3 – 1.9 μ_B , respectively).^{10, 31-33}

The technique commonly used to measure the magnetic susceptibility of complexes in the solution-state is known as the Evans Method,^{30, 34} and can firstly be calculated by equation 4.1:

$$\chi_m = \frac{477\Delta f}{2fc}$$

Where χ_m = molar magnetic susceptibility (cm^3/mol), Δf = peak separation (Hz), f = NMR frequency (Hz) and c = concentration (mg/mL).

This molar magnetic susceptibility value can be input into equation 4.2 to give the values for the effective magnetic moment (μ_B):

$$\mu_{eff} = 2.827\sqrt{\chi_m T}$$

Where μ_{eff} is the effective magnetic moment (μ_B) and T is the temperature (K).

A weighed sample of compound **4.3** was dissolved into a known volume of $\text{C}_6\text{D}_6/\text{C}_6\text{H}_6$ solvent mixture inside an NMR tube containing a sealed capillary tube also containing a $\text{C}_6\text{D}_6/\text{C}_6\text{H}_6$ solvent mix and an ^1H NMR spectrum was recorded at room temperature (Figure 4.7).

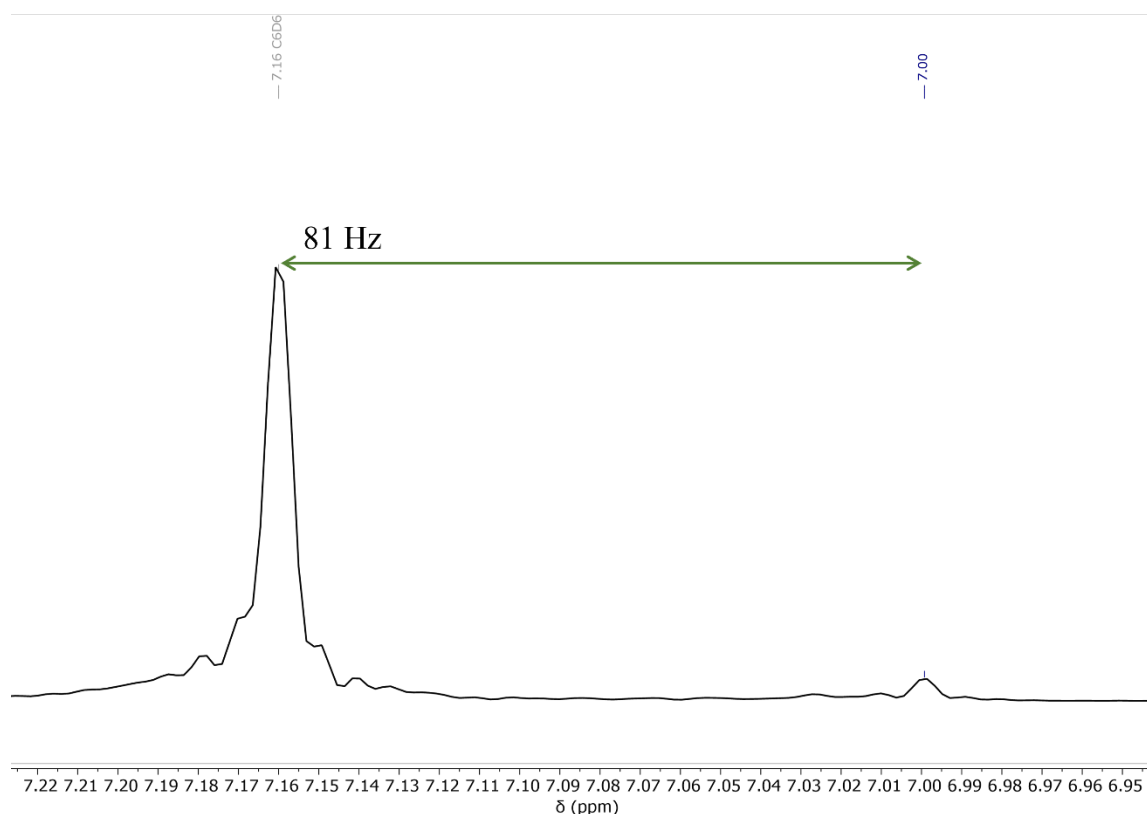


Figure 4.7. Close-up of the ^1H NMR spectrum (500 MHz, C_6D_6) of compound **4.3**, showing the solvent peaks used to calculate the Δf value for equation 4.1.

The difference in the chemical shift frequency of the C₆D₆/C₆H₆ solvent was calculated to be 81 Hz. Following equation 4.1 and equation 4.2, the effective magnetic moment for each Sm ion within **4.3** was calculated to be 1.82 μ_B .⁵ This value sits within the reported values for Sm(III) (1.3 – 1.9 μ_B)^{10, 31-33} and thus far supports the presence of two Sm(III) ions bridging a tetra-reduced [C₆H₆]⁴⁻ anion.

This was further corroborated in the solid-state by SQUID (superconducting quantum interference device) magnetometry, a technique used to measure extremely small magnetic fields.³⁵ Here, a weighed sample of **4.3** was sealed inside a diamagnetic glass tube and flame-sealed under an inert atmosphere. The sample was sent to the Robinson Research Institute (Victoria University of Wellington) where our collaborators, Simon Granville and Tane Butler, conducted SQUID measurements on **4.3**, and the resultant data was interpreted by Lujia Liu (Victoria University of Wellington).

A variable-temperature magnetic susceptibility measurement showed that **4.3** has a $\chi_m T$ value of 1.03 cm³ mol⁻¹ K at room temperature (293 K), which corresponds to an effective magnetic moment of $\mu_{\text{eff}} = 2.03 \mu_B$ for each samarium ion within **4.3** (Figure 4.8).⁵

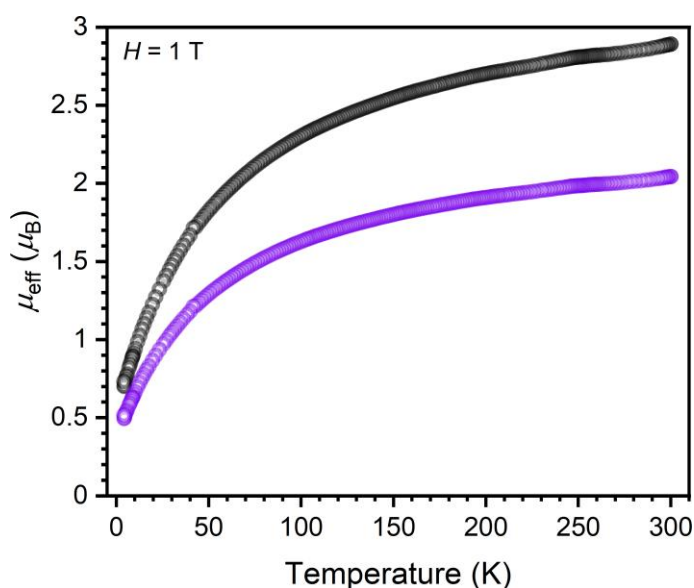


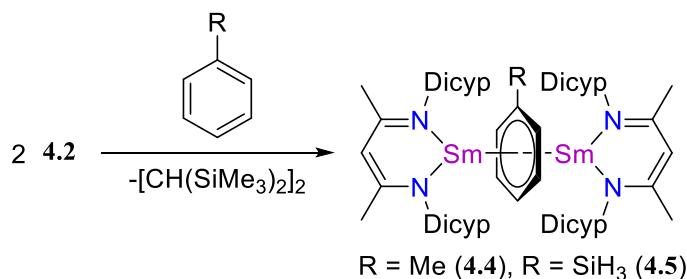
Figure 4.8. Variable-temperature effective magnetic moment plot for **4.3** (grey) and for each Sm(III) ion (purple).

This calculated value is slightly higher than the effective magnetic moment found for **4.3** in the solution-state, however, is still considerably lower than the magnetic susceptibility range found for the Sm(II) ion ($3.4 - 3.8 \mu_B$).¹⁰ This value of $\mu_{\text{eff}} = 2.03 \mu_B$ is also similar to the effective magnetic moment of **XLIXa** ($\mu_{\text{eff}} = 2.47 \mu_B$), suggesting the 3+ oxidation state of the samarium ions within **4.3**.^{5, 10}

Thus far, we have eluded to **4.3** as being an inverted sandwich complex containing a benzene tetraanion bridging two Sm(III) centres through single crystal X-ray diffraction analysis and magnetic susceptibility measurements.⁵ While not the first example of the four-electron reduction of benzene itself, this is the first example of the four-electron reduction of benzene without the need for an external Group 1 reducing agent.^{7, 36} Therefore, it became of interest to further test the reduction chemistry of this monomeric Sm(II) alkyl towards a range of aromatic substrates.

4.4 Synthesis of Tetraanionic Derivatives of Benzene

Reflecting the less negative reduction potential of toluene (-1.98 to -2.40 V vs SCE),³⁶ phenylsilane and *p*-xylene (-1.93 V vs SCE) in comparison to benzene,³⁷ the reduction chemistry was extended to these substituted arene substrates (Scheme 4.4).



Scheme 4.4. Synthesis of the inverted sandwich complexes **4.4** and **4.5**.

A toluene solution containing **4.2** was added to a J. Youngs tap NMR tube and monitored by ¹H NMR spectroscopy. An ¹H NMR spectrum disclosed no change had occurred

within 16 hours at room temperature; however, heating the reaction mixture to 60 °C overnight provided a new samarium-containing product (**4.4**), confirmed by the β -diketiminato methine resonance at δ_{H} 10.57 ppm in a 1:1.5 ratio with a signal at δ_{H} -10.85 ppm. This high-field peak showed clear ^1H - ^1H COSY correlations with three other low-field signals at δ_{H} 22.72, 19.59 and 16.70 ppm with proton integrations of 1H, 1H and 0.5H, respectively. Therefore, these four resonances were assigned as the hydrogen environments of an incorporated $[\text{C}_7\text{H}_8]^{n-}$ moiety.⁵

On the other hand, the addition of phenylsilane to a J. Youngs NMR tube containing a C_6D_6 solution of **4.2** resulted in complete consumption of **4.2** instantaneously, apparent by the disappearance of the two signals at δ_{H} -8.72 and -12.63 ppm, representative of the $\text{CH}(\text{SiMe}_3)_2$ ligand environment, in the ^1H NMR spectrum. This was concurrent with the presence of a new signal at δ_{H} 10.57 ppm in a 1:6 ratio with a peak at δ_{H} 5.26 ppm, which was assigned as the β -diketiminato methine and methyl groups of the backbone, respectively, of compound **4.5**. Notably, there are three low-field signals at δ_{H} 24.88, 17.29 and 13.08 ppm and a high-field resonance at δ_{H} -2.78 ppm in a 1:1:0.5:1.5 ratio, respectively, which were assigned as the protons of the incorporated $[\text{PhSiH}_3]^{n-}$ unit.⁵

Crystallisation of the two reaction mixtures allowed for structural confirmation of both **4.4** and **4.5** in the solid-state by X-ray diffraction experiments (Figure 4.9).

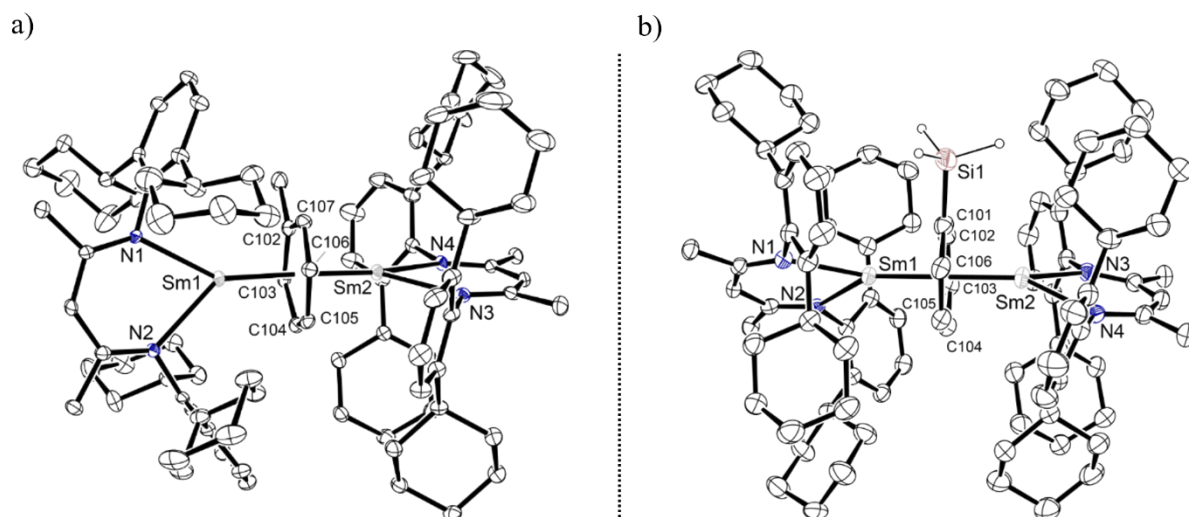


Figure 4.9. Ortep representation (30% probability ellipsoids) of compound **4.4** (left) and compound **4.5** (right). Hydrogen atoms (except those on Si1 for **4.5**) have been removed for clarity. Selected bond lengths (Å) and angles (°): **4.4**: Sm1–N1 2.433(4), Sm1–N2 2.477(3), Sm1–C_{cent} 2.091(2), Sm2–N3 2.485(4), Sm2–N4 2.410(4), Sm2–C_{cent} 2.082(2), Sm1–Sm2 4.1715(5), C102–C103 1.442(5), C103–C104 1.470(7), C104–C105 1.446(7), C105–C106 1.449(5), C106–C107 1.481(7), C107–C102 1.449(7), N1–Sm1–N2 71.1(8), Sm1–C_{cent}–Sm2 176.68(12). **4.5**: Sm1–N1 4.412(4), Sm1–N2 2.483(4), Sm2–N3 2.462(4), Sm2–N4 2.414(4), Sm1–C_{cent} 2.084(2), Sm2–C_{cent} 2.075(2), Sm1–Sm2 4.1586(8), C101–C102 1.472(9), C102–C103 1.455(9), C103–C104 1.443(8), C104–C105 1.465(9), C105–C106 1.445(9), C106–C101 1.470(8), C101–Si1 1.832(7), N1–Sm1–N2 73.13(13), N3–Sm2–N4 75.01(15), Sm1–C_{cent}–Sm2 179.24(14),

Compound **4.4** (Figure 4.9, a)) was disclosed as a dimer in the solid-state, with a bridging $[\text{C}_7\text{H}_8]^{n-}$ ligand between two samarium centres. The Sm1–C_{Cent} and Sm2–C_{Cent} distances of 2.091(2) and 2.082(2) Å and the Sm1–Sm2 bond distance (4.1715(5) Å) are comparable to the Sm–C_{Cent} and Sm–Sm bond distances found in **4.3** (2.0732(4) and 4.1464(7) Å, respectively).⁵ The Sm1–N1 and Sm2–N4 bond distances are 2.410(4) and 2.433(4) Å and are similar to the Sm–N bond lengths for **4.3** (2.426(4) and 2.431(7) Å), while the Sm1–N2 and Sm2–N3 bond lengths are slightly elongated (2.477(3) and 2.485(4) Å) and are more comparable to the Sm–N bond lengths in **4.2** (2.481(2) and 2.484(2) Å). The C–C bond distances of the phenyl ring within the $[\text{C}_7\text{H}_8]^{n-}$ moiety range from 1.442(5) to 1.481(7) Å and are, on average, marginally longer than the C–C bond lengths of the tetraanionic ring in **4.3**

(1.420(12) – 1.464(10) Å) but still comparable to those in the samarium-bound ring of the biphenyl complex, **XLIXa** (1.421(5) – 1.476(1) Å).^{5, 10}

Compound **4.5** (Figure 4.9, b)) also displayed similar structural features to **4.3** and **4.4** in the solid-state, with two Sm ions $\mu\text{-}\eta^6\text{:}\eta^6\text{-}$ bridged by a $[\text{PhSiH}_3]^{n-}$ ligand. The Sm1–N1 (2.412(4) Å) and Sm2–N4 (2.414(4) Å) bond lengths within **4.5** are shorter than the Sm–N bond lengths reported for **4.3**, however, the Sm1–N2 (2.483(4) Å) and Sm2–N3 (2.462(4) Å) bond lengths are slightly elongated by comparison. The Sm1–C_{Cent} and Sm2–C_{Cent} distances of 2.084(2) and 2.075(2) Å, respectively, and the Sm1–Sm2 bond distance (4.1586(8) Å) are also comparable to those found within **4.3** (2.0732(4) and 4.1464(7) Å, respectively).⁵ Finally, the C–C bond distances of the phenyl ring within the $[\text{PhSiH}_3]^{n-}$ moiety (1.443(8) – 1.472(9) Å) are similar to both those of the $[\text{C}_6\text{H}_6]^{4-}$ tetraanion in **4.3** (1.420(12) – 1.464(10) Å) and the biphenyl complex, **XLIXa** (1.421(5) – 1.476(1) Å).^{5, 10}

Overall, the gross structural features of both **4.4** and **4.5** align with the solid-state data of **4.3** and the model tetra-reduced biphenyl system, **XLIXa**. Therefore, we assign **4.4** and **4.5** as two Sm(III) centres bridged by either a $[\text{C}_7\text{H}_8]^{4-}$ or $[\text{PhSiH}_3]^{4-}$ tetraanionic ligand, respectively.⁵

Lastly, we probed the ground state electronic structures of both dimeric complexes by calculating their magnetic susceptibilities in the solution-state by the Evans method.^{30, 34} According to equations 4.1 and 4.2, compound **4.4** was calculated as having a magnetic susceptibility of 1.94 μ_B and compound **4.5**, 1.78 μ_B .⁵ Both values lie within the reported range for the Sm(III) ion (1.3–1.9 μ_B) and confirm the 3+ oxidation state of the samarium ions and the tetra-reduced toluene or phenylsilane ligand, respectively.^{10, 31-33} It should be noted that solid-state SQUID magnetometry has not yet been conducted for compound **4.4** or compound **4.5**.

This work was also extended to *p*-xylene, where **4.2** was dissolved into *p*-xylene solvent and left to react over 48 hours at room temperature. However, instead of isolating the expected sandwich complex, in which a reduced xylene anion bridges two [(BDI^{Dicyp})Sm] units, a single crystal X-ray diffraction experiment identified the reaction product as the Schlenk-type redistribution complex, **4.6** (Figure 4.10).

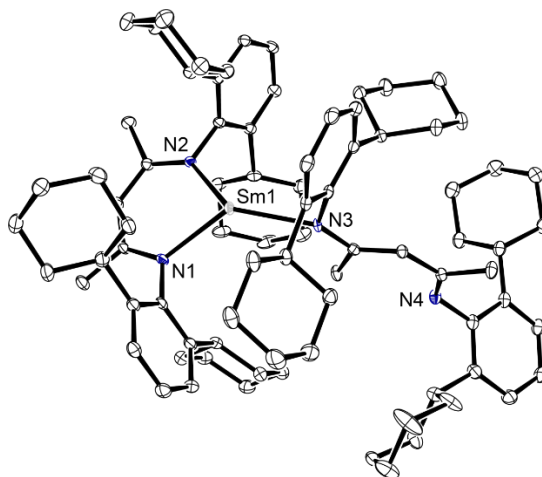


Figure 4.10. Ortep representation (30% probability ellipsoids) of compound **4.6**. Hydrogen atoms have been removed for clarity. Selected bond lengths (Å) and angles (°): Sm1–N1 2.497(2), Sm1–N2 2.463(2), Sm1–N3 2.445(2), N3–C_{Dicyp} 1.422(3), N3–C52 1.359(4), N4–C_{Dicyp} 1.409(4), N4–C54 1.300(3), N1–Sm1–N2 73.08(7), N1–Sm1–N3 130.32(7), N2–Sm1–N3 126.21(7).

In the solid-state, the Sm(II) centre of **4.6** is three-coordinate: two Sm–N contacts are provided by one β -diketiminato (2.497(2) and 2.463(2) Å) in an *N,N*-coordination mode and a third Sm–N contact is provided by a second BDI^{Dicyp} ligand κ^1 -bonding through a single *N*-substituent of the β -diketiminato framework (2.445(2) Å). The Sm–N bond lengths sit within the range of all other Sm(II) complexes supported by the BDI^{Dicyp} ancillary ligand presented in this Chapter (2.440(3) – 2.484(2) Å).⁵

The N4–C54 bond length of 1.300(3) Å is shorter than the other N–C bond lengths within the κ^1 -bonded β -diketiminato ligand, sitting in the range of N=C double bonds and

therefore results in an imine-like structure.^{38, 39} This is reminiscent of the homoleptic Eu(II) complex (**3.12**) in Chapter Three, which displays analogous structural features to **4.6**.

4.5 Two-Electron Aromatisation of COT

Isolation and characterisation of the benzene tetraanion alludes to the two-electron reduction by each samarium centre within **4.3**. This results in an overall four-electron reduction of benzene and contradicts the well-reported reduction chemistry of samarium(II), which typically undergoes one-electron reduction processes at a single Sm(II) centre.^{40, 41} An example is presented in Chapter One, where two Sm(II) metal centres were observed to undergo a single-electron transfer to anthracene, performing an overall two-electron reduction of anthracene to give two Sm(III) ions bridged by the $[C_{14}H_{10}]^{2-}$ dianion (**IV**).⁴²

The reduction potential of the Sm^{3+}/Sm^{2+} couple is -1.55 V and is not capable of reducing benzene (-3.42 V).^{1, 8} Therefore, it is proposed that this four-electron reduction mechanism could be occurring through a transient Sm(I) intermediate, thus possibly involving a Sm(I)/Sm(III) redox couple.⁵

Similar transient species have been proposed before in the literature. For example, Lappert reported on the activation of the C–O bonds in dimethyl ether (DME) by tris(cyclopentadienyl)lanthanide(III) complexes and a Group 1 metal reducing agent.⁴³ He proposed that this reaction was proceeding through an initial single-electron transfer to give $Cp_2Ln(II)$ as a transient intermediate prior to the formation of the bis(cyclopentadienyl)lanthanide(III) methoxide products.

In previous Chapters, we have demonstrated that ytterbium(II) and europium(II) hydrides can affect the two-electron aromatisation of COT to the $[COT]^{2-}$ dianion.¹⁵ Therefore, the reduction of COT by **4.2** served as a suitable test for this Sm(I)/Sm(III) redox couple as it

would demonstrate the ability of a single samarium(II) centre to carry out a two-electron reduction process.⁵

A colourless hexane solution of COT was added to one equivalent of **4.2** in hexane in a scintillation vial inside the glovebox. Within 1 hour, the dark brown solution was clear yellow with a yellow precipitate. The volatiles were removed *in vacuo*, and the crude product was recrystallised from toluene, providing yellow-brown crystals of **4.7** suitable for crystallographic analysis (Figure 4.11).

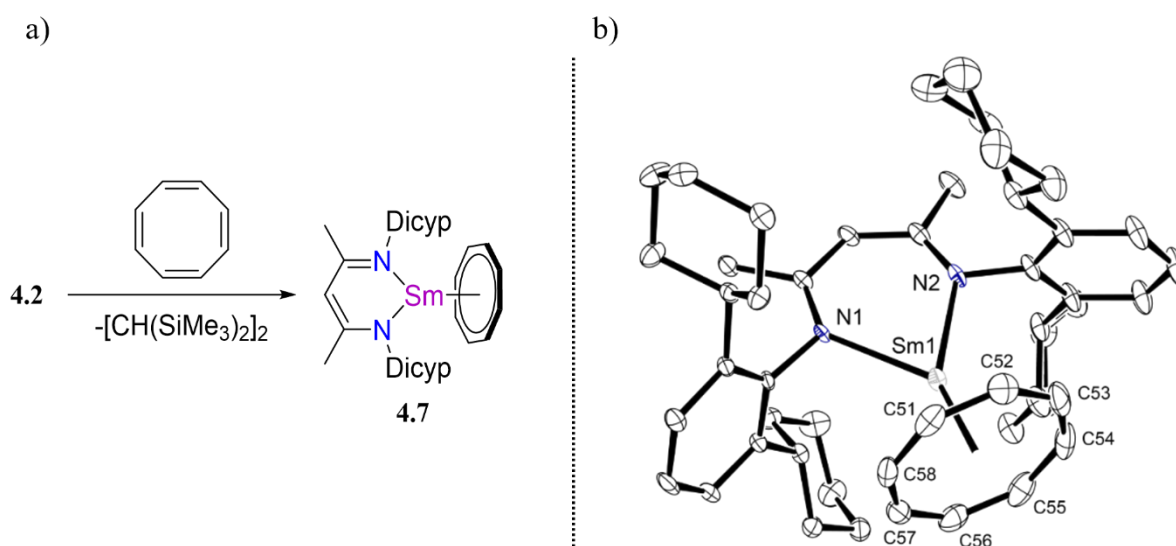


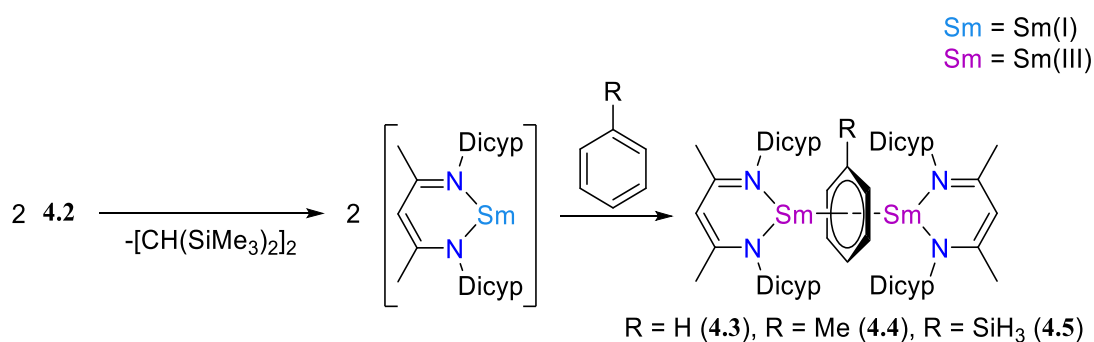
Figure 4.11. Left: Two-electron aromatisation of COT by compound **4.2**. Right: Ortep representation (30% probability ellipsoids) of compound **4.7**. Hydrogen atoms have been removed for clarity. Selected bond lengths (Å) and angles (°):

Sm1–N1 2.465(2), Sm1–N2 2.413(3), Sm1–C_{Cent} 1.9043(13), N1–Sm1–N2 72.27(8).

The solid-state data of **4.7** disclosed a mononuclear constitution, where the coordination sphere of the samarium metal centre is made up of three contacts: two contacts are provided by the N-atoms of the β -diketiminate ligand (Sm1–N1: 2.465(2), Sm1–N2: 2.413(3) Å) and the final contact is the η^8 -coordination of the $[\text{COT}]^{2-}$ dianion (Sm1–C_{Cent}: 1.9043(13) Å). The Sm–N bond lengths are slightly shorter than the Sm–N bond lengths within the Sm(II) monoalkyl precursor (**4.2**: 2.481(2) and 2.484(2) Å), consistent with the oxidation of the Sm(II) ion to Sm(III). The Sm1–C_{Cent} distance is considerably shorter than the Sm–C_{Cent} distances

found within all three dimeric Sm(III) arene complexes reported within this Chapter (2.0732(4) – 2.091(2) Å) but comparable to the related Sm(III) complex, [(Cp*)Sm(COT)], which reports a Sm–C_{COT} centroid distance of 1.838 Å.⁴⁴

The isolation of **4.7** demonstrates the ability of the single samarium centre within **4.2** to perform the two-electron aromatisation of COT.⁵ Should this reactivity occur through a transient Sm(I) intermediate, this reduction process would involve the homolytic cleavage of the Sm–C bond within **4.2** to give [(BDI^{Dicyp})Sm] and the organic radical species, [•]CH(SiMe₃)₂, which can subsequently spin pair and dimerise to give [CH(SiMe₃)₂]₂ (Scheme 4.5).^{45, 46}



Scheme 4.5. Overview to form the Sm(III) inverse sandwich complexes *via* the proposed transient Sm(I) intermediate.

Therefore, the reaction of **4.2** and COT was repeated in C₆D₆ in an NMR tube fitted with a J. Youngs tap and monitored by ¹H NMR spectroscopy in hopes of observing the formation of the [CH(SiMe₃)₂]₂ by-product in the solution-state.⁵

Within 5 minutes at room temperature, the solution was a clear yellow colour and the subsequent ¹H NMR spectrum of the crude reaction mixture indicated that there was no unreacted **4.2** left in solution with clean conversion to the new samarium-containing compound (**4.7**). The peak centred at δ_H 7.70 ppm was identified as the methine resonance of the β-diketiminato ligand of **4.7** and was in a 1:8 ratio with a broad signal at δ_H 8.11 ppm, assigned as the proton environment of COT. This is consistent with the solid-state data and the formation of the monomeric Sm(III) centre and a [C₈H₈]²⁻ dianion (Figure 4.12).⁵

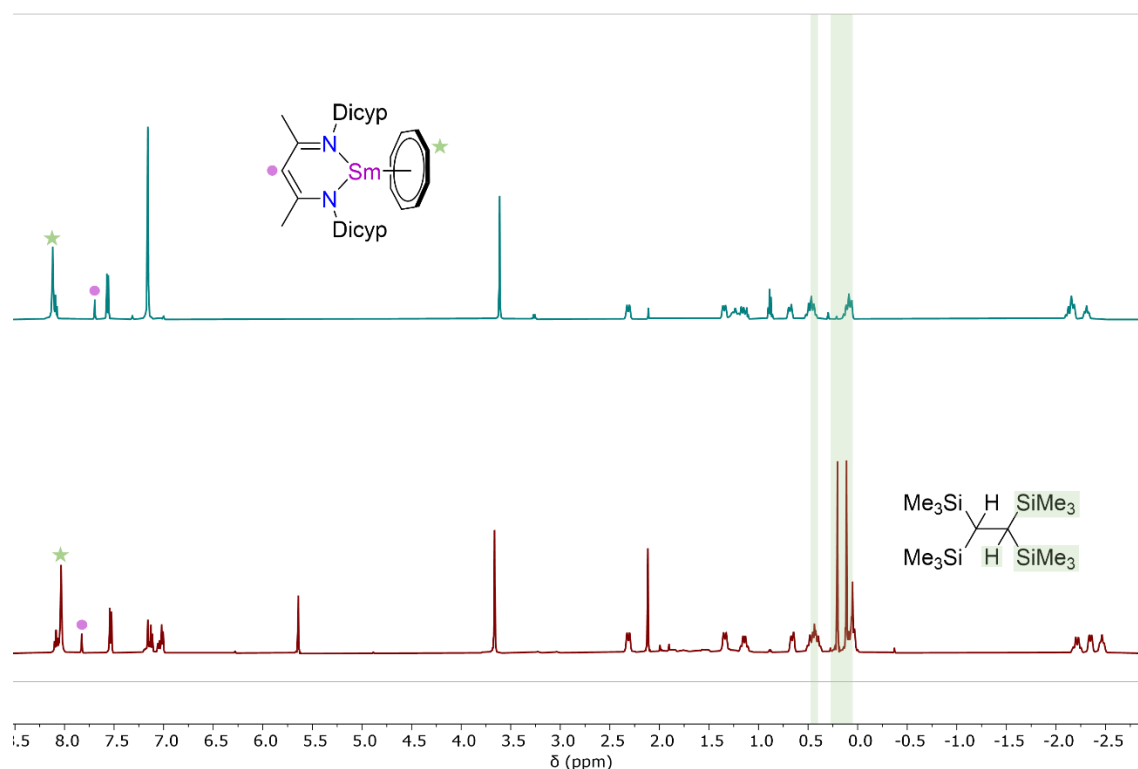


Figure 4.12. Stacked ^1H NMR spectrum (500 MHz, C_6D_6) of isolated **4.7** (top) and of the *in-situ* reaction of **4.2** and COT to give compound **4.7** in a 2:1 ratio with the organic by-product, $[\text{CH}(\text{SiMe}_3)_2]_2$ (bottom).

The important feature of the ^1H NMR spectrum is the presence of two singlet resonances situated at δ_{H} 0.20 and 0.11 ppm, integrating for 9H each (Figure 4.12, (bottom)). These are assigned as the methyl groups of the dimerised $[\text{CH}(\text{SiMe}_3)_2]_2$ organic by-product, respectively, with chemical shifts aligning with those reported in the literature.^{45, 46} The volatiles for the crude reaction solution of **4.7** could then be vacuum transferred *via* trap-to-trap distillation, and the resultant colourless solution was analysed by GC–MS. The GC–MS chromatogram showed a peak for organic by-product at a retention time of 14.78 minutes, identified through the mass spectrometry trace for $[\text{CH}(\text{SiMe}_3)_2]_2$, which has been published within the literature.⁴⁵ These data further confirm that the two-electron reduction is occurring at a single samarium centre.

Overall, this Section proposes that this reduction chemistry could occur through a transient Sm(I) intermediate.⁵ This reaction mechanism has thus far been confirmed in the

solution-state with respect to the ability of **4.2** to carry out the two-electron aromatisation of COT. However, corroboration of this proposed reaction mechanism for the four-electron reduction of benzene through computation calculations was required.

4.6 Computational Studies

Density Functional Theory (DFT) studies (B3PW91) on the reaction between **4.2** and benzene were calculated by international collaborators Prof. Laurent Maron and Thayalan Rajeshkumar at Université de Toulouse, to provide insights on the reaction mechanism for the formation of **4.3** (Figure 4.13).⁵

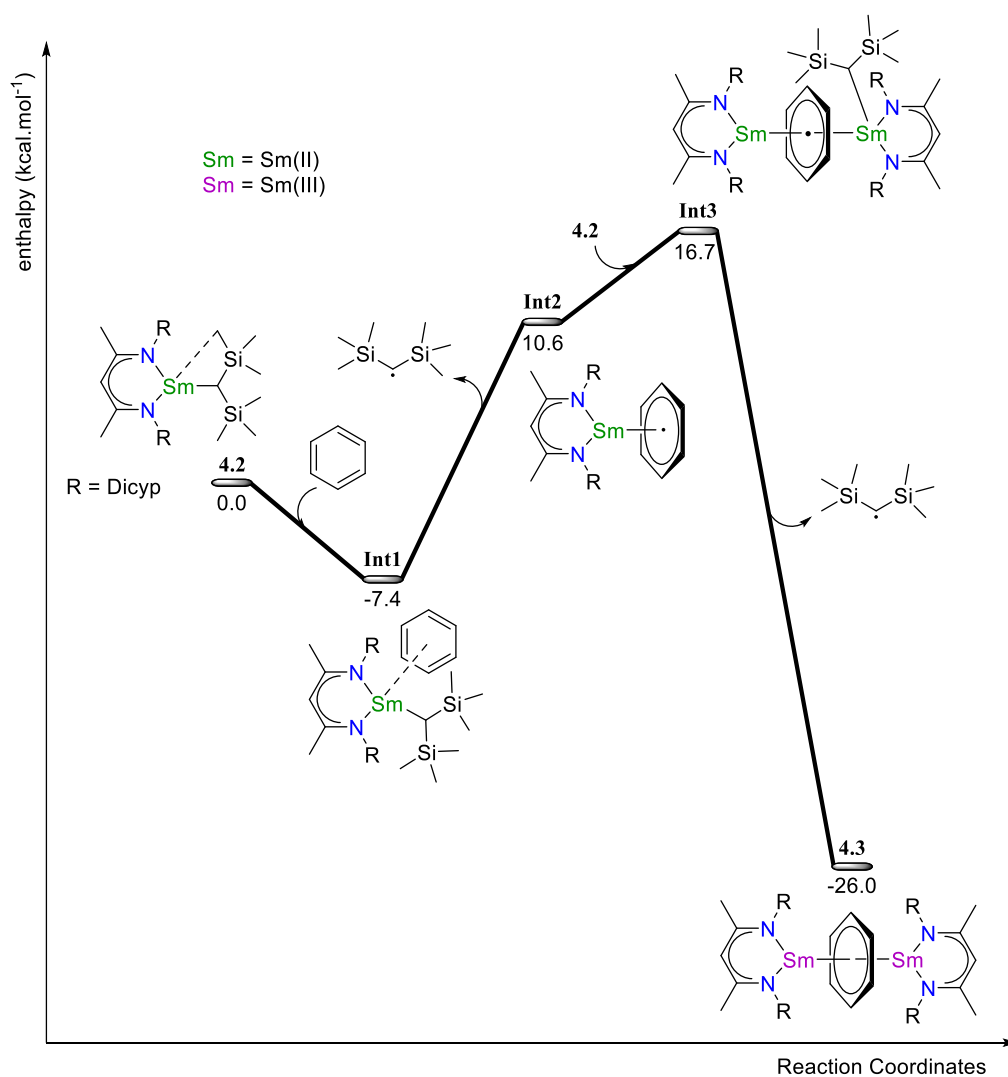


Figure 4.13. Computed enthalpy pathway for the reaction of the monomeric alkyl (**4.2**) with benzene to give **4.3**.

It was calculated that a benzene molecule first coordinates to the Sm(II) centre within **4.2** and is exothermically favourable ($-7.4 \text{ kcal.mol}^{-1}$). This gives **Int1**, where the samarium-arene interaction was computed to be strong as a result of dispersion effects and where the LUMO (Lowest Unoccupied Molecular Orbital) displays a δ -type bonding interaction between the Sm(II) ion and the benzene ring. The second step is the homolytic cleavage of the Sm-C bond, concomitant with the release of the organic radical $\cdot\text{CH}(\text{SiMe}_3)_2$. This step can be perceived as the initial formation of the transient Sm(I) complex, prior to the single-electron transfer to afford **Int2** (18 kcal.mol^{-1}), where the benzene has been singly reduced, and the samarium centre is in the 2+ oxidation state. The SOMO (Singly Occupied Molecular Orbital) for **Int2** shows a δ -bond and the unpaired spin density plot displays some spin density on the benzene ring. There were 7 unpaired electrons found within **Int2**, with 6 that were purely 4f-electrons and the highest SOMO is a δ -bond. The Conical Molecular Orbital (CMO) analysis of the Natural Bonding Orbital (NBO) was calculated and shows the SOMO implies 23% of a 3-centre Sm-C-C bond, implying the interaction is not solely coming from the ligand and that **Int2** has some Sm(I) character. The formation of **Int3** occurs through the binding of a second molecule of **4.2** to the benzene ring within **Int2**, where the benzene is still singly reduced and both Sm centres are in the +2 oxidation state. Homolytic cleavage of the Sm-C bond within **Int3** and extrusion of the organic radical ($-26 \text{ kcal.mol}^{-1}$) gives the inverted sandwich complex, **4.3**, in which the tetra-reduced benzene $\mu-\eta^6:\eta^6$ -bridges two Sm(III) centres. This last step could be explained as occurring through a second transient Sm(I) centre, followed by the single-electron transfer to give an inverted sandwich intermediate containing two Sm(II) centres and a doubly reduced benzene, prior to a final single-electron transfer from each Sm centre to give **4.3**.

Finally, to probe the oxidation states of **4.2** and **4.3** computationally, the structures of **4.2** and **4.3** were optimised (B3PW91) with either Sm(II) or Sm(III) ions in each of the two complexes.⁴⁷

Table 4.1. Comparison of selected experimental and calculated values of the optimised structures for complex **4.2** and **4.3**. Note that for **4.2**, the calculated values presented below are for the optimised structure in the +2 oxidation state (green), whilst for **4.3** the values listed are for the +3 oxidation state (purple).

| Complex | Bond length/angles | Experimental | Calculated |
|------------|---------------------------------------|--------------|------------|
| 4.2 | Sm–N (average) (Å) | 2.48 | 2.47 |
| | Sm–C (Å) | 2.64 | 2.56 |
| 4.3 | Sm–N (average) (Å) | 2.43 | 2.45 |
| | Sm–C _{Benzene} (average) (Å) | 2.53 | 2.56 |
| | Sm–C _{Centroid} (Å) | 2.07 | 2.10 |
| | Sm–N–C (°) | 137 | 137 |
| | N–C–C (°) | 122 | 123 |
| | Sm–N–C _{IpsO} (°) | 101 | 99 |

In the case of the samarium monoalkyl, **4.2**, only the computationally optimised structure with the Sm(II) ions yielded results consistent with the solid-state X-ray data, corroborating the +2 oxidation state. For the inverted sandwich complex, **4.3**, only the computationally optimised structure with the Sm(III) ions afforded results consistent with the solid-state X-ray data, providing further evidence for the isolation of a benzene tetraanion.⁵

4.7 Preliminary Reactivity Studies

The previous Sections of this Chapter have outlined the synthesis of a heteroleptic Sm(II) monoalkyl complex (**4.2**) and the subsequent four-electron reduction of benzene to give a

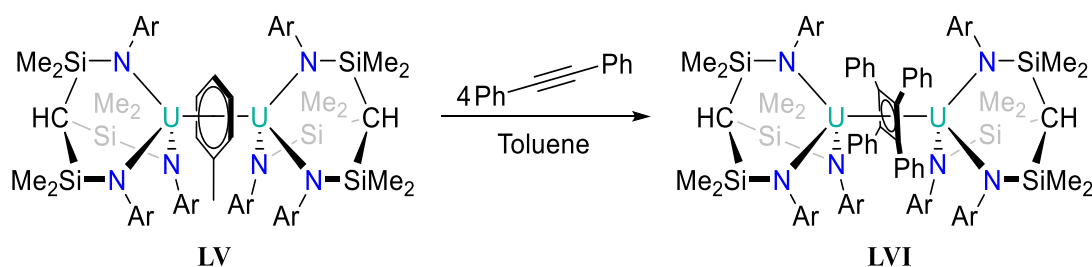
benzene tetraanion, **4.3**.⁵ This next Section is split into two parts: first it will discuss preliminary reactivity results of the benzene tetraanion (**4.3**) followed by reactivity studies of the Sm(II) alkyl complex (**4.2**), with the overarching goal of further understanding the reductive nature of both species.

4.7.1 Exploring the Reduction Chemistry of a Benzene Tetraanion

Reductive Cyclisation of Diphenylacetylene

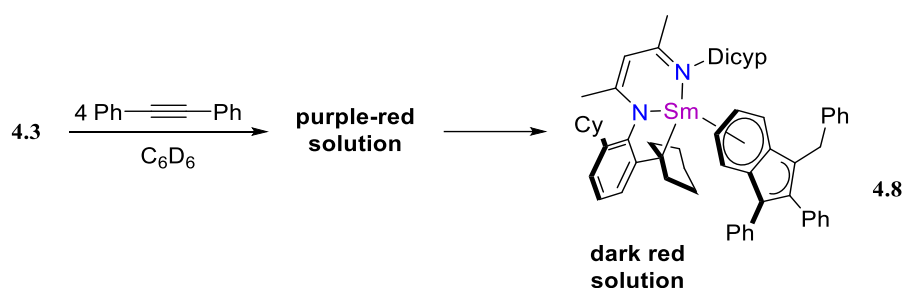
It is common for lanthanide complexes to contain aromatic hydrocarbon ligands, an example being the installation of COT to lanthanide complexes,^{15, 48, 49} which is becoming more prevalent within the literature: this Thesis discloses a total of five new examples of Ln(II) (Ln = Yb, Eu) inverse sandwich complexes containing the [COT]²⁻ dianion (**2.18**, **2.22** and **3.24**, **3.25**, **3.26**, respectively), and two examples of Ln(III) (Ln = Yb, Sm) species containing the [COT]²⁻ ligand.^{5, 15} In comparison, there are no examples of a lanthanide cyclobutadienyl derivative.

In 2011, Liddle reported the isolation of a uranium inverse sandwich complex (**LV**) containing two U(V) centres bridged by the toluene tetraanion, which was found to be a highly reducing species (Scheme 4.6).⁵⁰ This was succeeded by a report in 2012, where Liddle demonstrates the ability of **LV** to react with four equivalents of diphenylacetylene to give the formal [2+2] cycloaddition product, **LVI**, which two U(V) centres are bridged by a cyclobutadienyl ring.⁵¹



Scheme 4.6. [2+2] cycloaddition of diphenylacetylene to give **LVI**.

Given the structural and electronic similarities between **4.3** and **LV**, we sought to test the reductive abilities of our tetraanionic benzene system towards the same substrate, diphenylacetylene. The addition of four equivalents of diphenylacetylene to a brown C_6D_6 solution containing **4.3** resulted in an almost immediate colour change to a purple-red solution. Attempts to gain an initial 1H NMR spectrum of the crude reaction mixture proved inconclusive due to the paramagnetic nature of the samarium ion present in solution.¹³ The J. Youngs tap NMR tube was left overnight at room temperature, affording a dark red solution of **4.8** (Scheme 4.7).



Scheme 4.7. Reaction of **4.3** and diphenylacetylene to give **4.8**.

The solvent was removed under vacuum and the red residue was dissolved in the minimal amount of toluene, with dark crystals of **4.8** suitable for a single crystal X-ray diffraction experiment obtained at room temperature (Figure 4.14).

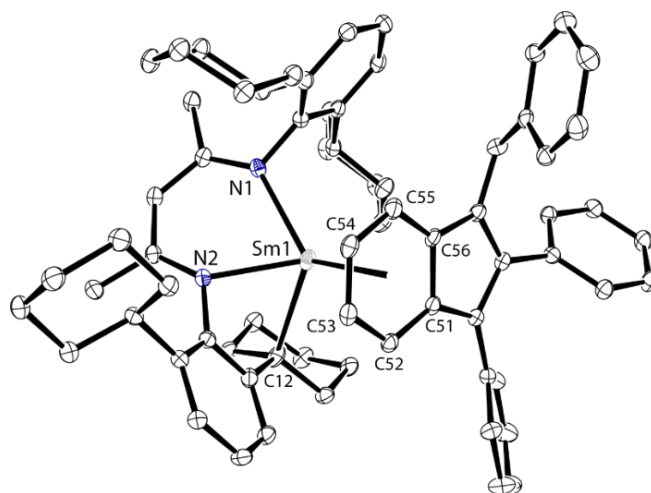


Figure 4.14. Ortep representation (30% probability ellipsoids) of compound **4.8**. Hydrogen atoms have been removed for clarity. Selected bond lengths (Å) and angles (°): Sm1–N1 2.371(3), Sm1–N2 2.319(4), Sm1–C12 2.59(1), Sm1–C_{cent} 2.5051(16), N1–Sm1–N2 73.5(1), N1–Sm1–C12 119.2(2), N2–Sm1–C12 69.0(2).

The solid-state structure was not the expected cyclobutadienyl ring bridging two Sm(III) centres but a new mononuclear complex containing a 1-benzyl-2,3-di-phenylindene dianionic ligand. The Sm(III) centre within **4.8** is bound to the nitrogen atoms of the β -diketiminato ligand in a bidentate *N,N*-coordination mode and η^6 -interacts with the phenyl ring of the indene functionality. The Sm1–N1 and Sm1–N2 bond lengths are 2.371(3) and 2.319(4) Å and are considerably shorter than the Sm–N bond lengths of all samarium complexes supported by the BDI^{Dicyp} ancillary ligand (2.410(4) – 2.524(2) Å) and is a result of the final contact of the Sm(III) centre to the deprotonated C12 carbon (Sm1–C12 2.59(1) Å) of a cyclohexyl ring of one of the Dicyp *N*-substituents. Nevertheless, these short Sm–N bond distances also confirm the trivalent oxidation state of the samarium metal centre. The Sm1–C_{Cent} distance is 2.5051(16) Å and is considerably longer compared to the Sm–C_{Cent} distances found in **4.7** (1.9043(13) Å) and can be attributed to the steric bulk of the indene group substituted with the two phenyl groups and the flexible benzyl group.²⁶

When conducting the reaction of the tetraanionic toluene complex (**LV**) with diphenylacetylene in a J. Youngs tap NMR tube, Liddle identified an intermediate species

within the crude ^1H NMR spectrum.⁵¹ Though not confirmed, it was speculated that this intermediate was a coupled but not ring-closed butadiene dianion reminiscent of previously reported uranium complexes obtained from U(III) mediated C–C coupling of alkyne substrates.⁵² In 1993, a report by Krüger details the rearrangement of tetra-phenyl butadiene in a nickel complex, predicted to occur through hydrogen migration and subsequent C–C bond formation, whereby the resulting product contained the same indenyl moiety as **4.8**.⁵³

The formation of **4.8** could be occurring in a similar manner with C–C coupling of two diphenylacetylene substrates and rather than undergoing a reductive [2+2] cycloaddition like in the formation of **LVI**,⁵¹ the proposed butadienyl intermediate has a ring closed to give **4.8**. This seems more favourable than ring-closing to generate the highly strained 4-membered cyclobutadienyl ring.⁵⁴

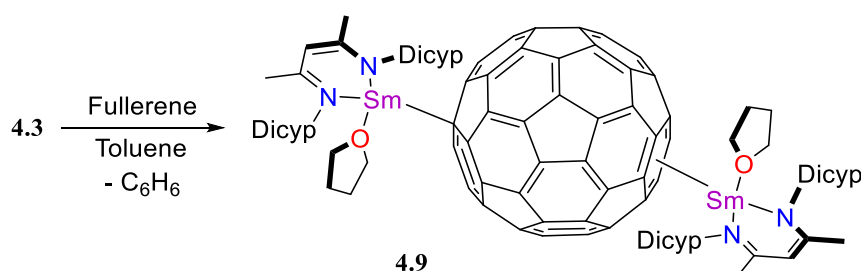
It became beneficial to try and isolate the purple-red coloured intermediate to further understand the formation of **4.8**. The reaction was repeated in a scintillation vial using the minimum amount of toluene required to dissolve both starting materials. After the rapid colour change to a purple-red solution, the vial was left at $-30\text{ }^\circ\text{C}$ to try and hinder the formation of the isolated species, **4.8**. After a few weeks, the solution was carefully concentrated under vacuum, the minimum volume of pentane solvent was added, and the vial was placed back in the freezer. After ca. 2 months, it was assumed that conversion to **4.8** had not yet occurred, as the solution remained purple-red in colour. However, single crystals suitable for an X-ray diffraction experiment could not be obtained; thus, following up on this reactivity is beyond the scope of this Thesis.

Reduction of Fullerene

Fullerene is an allotrope of carbon consisting of a C_{60} cage-like fused ring structure. It displays a range of electronic and physical properties, such that this compound is widely used in physical

sciences.⁵⁵ Relevant to this Thesis is the reduction of this C₆₀ structure by a series of highly reducing Mg(I) complexes to afford a range of soluble fulleride complexes.⁵⁶ In this work, the *N*-substituent of the β-diketiminato is altered to provide varying degrees of steric protection to the Mg(I) centre, which in turn affected the stoichiometry of the fulleride complexes: fullerene could be reduced to either the C₆₀²⁻ dianion, C₆₀⁴⁻ tetraanion and C₆₀⁶⁻ hexaanion, respectively.

Therefore, to test the reducing abilities of the benzene complex **4.3**, as well as the relative steric bulk of the BDI^{Dicyp} ancillary ligand, compound **4.3** was added to a scintillation vial containing a purple toluene solution of fullerene and stirred at room temperature. Within 1 hour, the reaction mixture had changed to a true brown colour accompanied by a dark precipitate, however, this was left overnight to ensure full conversion to the fulleride complex (**4.9**) through extrusion of benzene (Scheme 4.8).



Scheme 4.8. Reduction of fullerene to give compound **4.9**.

The mixture was left to settle, then the solution was filtered and left to crystallise at room temperature. The vial walls were dotted with small, dark crystals within a few hours. While these crystals were adequate to run a single crystal X-ray diffraction experiment, the data obtained was insufficient, thus only allowing structural connectivity of the product in the solid-state (Figure 4.15).

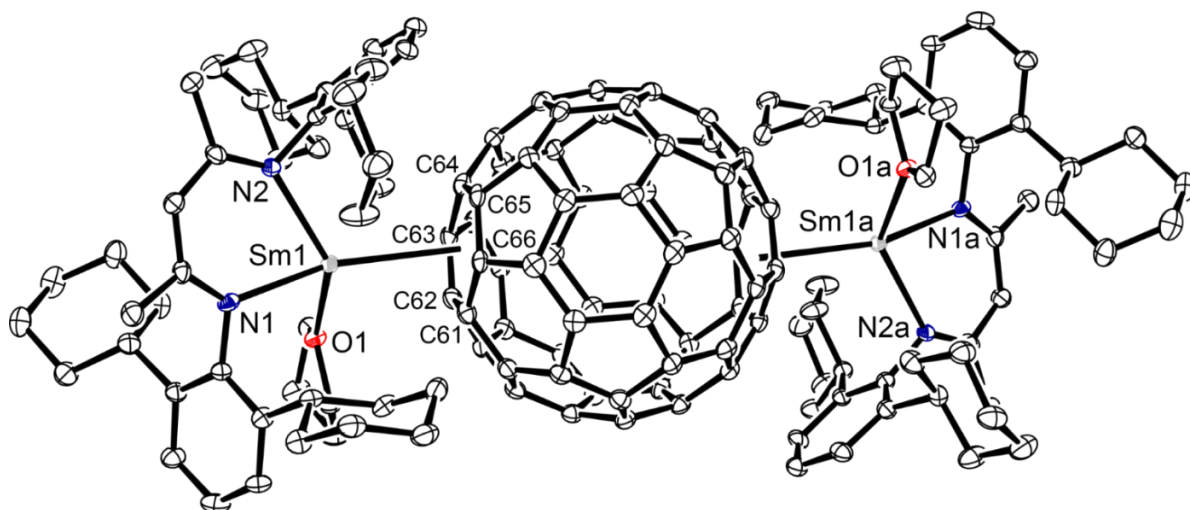


Figure 4.15. Ortep representation (30% ellipsoid probability) of compound **4.9**. Hydrogen atoms have been removed for clarity. Poor crystal quality meant accurate bond length and bond angle data could not be obtained.

Consistent with the stoichiometry of the reaction starting materials, the structural features of **4.9** indicated the formation of the fulleride $[C_{60}]^{n-}$ anion that is η^6 -bound to two $[(BDI^{DicyP})Sm]$ units. No THF solvent was present within the reaction mixture, yet the samarium centres are coordinated by THF molecules, meaning that during the reaction or crystallisation process, solvent ligation occurred from THF vapours residing within the atmosphere of the glovebox.

Comparing back to the reported Mg(II) fulleride complexes, **4.9** appears as two Sm(II) ions coordinated to a doubly reduced $[C_{60}]^{2-}$ dianion.⁵⁶ However, given the assignment of two Sm(III) centres within **4.3**, and the high stability of samarium in the 3+ oxidation state,^{1, 57} this complex likely consists of a bridging $[C_{60}]^{4-}$ tetraanion moiety.

With respect to the Mg(I) reduction of fullerene, one example of a related $[C_{60}]^{4-}$ tetraanion is bound to four $[(BDI^{Dipp})Mg]^+$ units to achieve the overall charge balance of the complex.⁵⁶ However, the steric bulk of the Dipp *N*-substituent is less than that of the DicyP substituent. This can be demonstrated by the reported Sm(II) homoleptic complex, $[(BDI^{Dipp})_2Sm]$, where both BDI^{Dipp} ligands coordinate to the Sm(II) centre in a bidentate *N,N*-

coordination mode.¹⁹ In comparison, in the related homoleptic species, **4.6**, only one BDI^{Dicyp} ligand *N,N*-binds to the Sm(II) centre with the second κ^1 -binding through a single N-atom of the second BDI^{Dicyp} ligand, favouring a lower coordination number to minimise steric repulsion. Therefore, the larger steric size of the BDI^{Dicyp} ancillary ligand is consistent with the coordination of only two Sm(III) centres and a [C₆₀]⁴⁻ tetraanion in **4.9**.

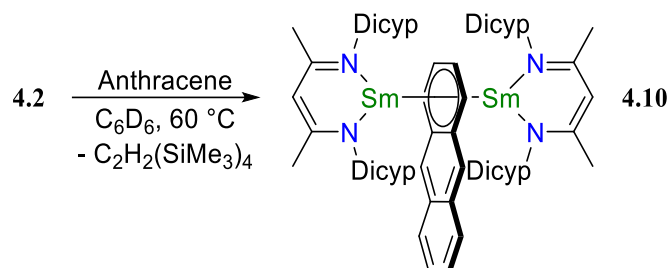
To test whether the C₆₀ molecule could accommodate the coordination of more [(BDI^{Dicyp})Sm] units and thus further reduce fullerene, two molar equivalents of **4.3** was reacted with fullerene in toluene. Despite the molar ratio of the starting materials, an X-ray diffraction experiment disclosed the same reaction product, **4.9**, where poor crystal quality once again meant full crystallographic analysis could not be obtained. Due to the insolubility of **4.9** in aliphatic solvents and the poor solubility in aromatic solvents, structural characterisation of **4.9** was not obtained in the solution-state.

4.7.2 Exploring the Reduction Chemistry of [(BDI^{Dicyp})SmCH(SiMe₃)₂]

Two-Electron Reduction of Polycyclic Hydrocarbons

Earlier in this Chapter, it was demonstrated that the heteroleptic Sm(II) monoalkyl complex, **4.2**, could facilitate the two-electron reduction of COT at a single samarium centre to give the Sm(III) complex, **4.7**.⁵ Therefore, it became of interest to continually test the reductive abilities of **4.2**, and extend this reactivity to the more challenging polyaromatic substrates, anthracene and naphthalene (−1.83 and −2.60 V vs SCE, respectively).¹²

One equivalent of anthracene was added to a brown C₆D₆ solution of **4.2** and the reaction progress was monitored by ¹H NMR spectroscopy (Scheme 4.9).



Scheme 4.9. Reduction of anthracene by compound **4.2**.

Over the course 48 hours at 60 °C, the reaction solution had become a blue-black colour, and an ^1H NMR spectrum confirmed the consumption of **4.2** by the disappearance of the resonances at δ_{H} –12.62 and –8.73 ppm, representative of the two hydrogen environments of the $\text{CH}(\text{SiMe}_3)_2$ ligand.

The J. Youngs tap NMR tube was transferred into the glovebox, the volatiles removed under vacuum, and the crude product recrystallised from toluene solvent, allowing for structural elucidation in the solid-state through a single crystal X-ray diffraction experiment (Figure 4.16).

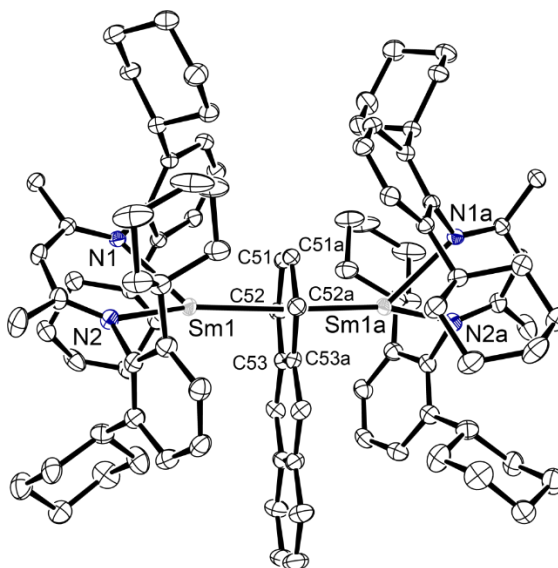


Figure 4.16. Ortep representation (30% probability ellipsoids) of compound **4.10**. Hydrogen atoms have been removed for clarity. Selected bond lengths (Å) and angles (°): Sm1–N1 2.485(2), Sm1–N2 2.454(2), Sm1–C_{Cent} 2.4429(3), N1–Sm1–N2 70.11(6), Sm1–C_{Cent}–Sm1a 177.02(6).

The asymmetric unit of **4.10** comprises only half the dimer, displaying a samarium centre that is *N,N*-chelated to the N-atoms of the β -diketimate ligand and interacting with half of the anthracene moiety. The remainder of the complex is generated through a mirror plane through the C51–C57 plane of the anthracene rings to give the inverted sandwich complex, **4.10**, where two [(BDI^{Dicyp})Sm] units are η^6 -interacting with the same terminal C₆-ring from opposing faces of the [C₁₄H₁₀] ligand (plane twist angle: 2.87(10)°). The C–C bond lengths for the Sm-bound C₆-ring average 1.437 Å, which are considerably longer than the C–C bond lengths of the uncoordinated ring (average C–C: 1.396 Å), resulting from the lesser electron density located on the second terminal ring of the anthracene dianion.⁵⁸

The Sm1–N1 and Sm1–N2 bonds are 2.485(2) and 2.454(2) Å, respectively and align with the Sm–N bond lengths in the iodide (**4.1**: 2.440(4) and 2.475(4) Å) and monoalkyl complex (**4.2**: 2.481(2) and 2.484(2) Å) but are slightly longer than the Sm–N bond lengths found in **4.3** (2.431(7) and 2.426(4) Å). The Sm1–C_{Cent} distance of 2.4429(2) Å is also considerably longer than the Sm–C_{Cent} distance (2.0732(4) Å) in **4.3**.⁵

There is one example of a samarium(III) complex containing the anthracene dianion, which displays very different structural features to **4.10** in the solid-state.⁴² [Cp*₂Sm(μ -C₁₄H₁₀)SmCp*₂] (**IV**) is comprised of two [Cp*₂Sm] units that are η^3 -bound to the carbons of the central C₆-ring of a nearly planar anthracene dianion. Both samarium centres are in the 3+ oxidation state and display a longer Sm–C_{Cent} distance of 2.721(22) Å compared to that within **4.10**, however, this can be ascribed to the difference in coordination modes of the Sm centres to the [C₁₄H₁₀]²⁻ dianion as well as the differing ligand environments. Overall, the structural features of **4.10** align with an [C₁₄H₁₀]²⁻ ligand bridging two Sm(II) centres, consistent with a one-electron reduction of anthracene by two molecules of **4.2**, giving an overall two-electron reduction to the [C₁₄H₁₀]²⁻ dianion. The structure of compound **4.10** is also comparable to the reduced anthracene complexes **2.23** and **3.27**, discussed in Chapters Two and Three,

respectively. Both are dimers with two Ln(II) centres (Ln = Yb: **2.23**, Ln = Eu: **3.27**) binding in an η^6 -fashion to the same terminal rings of the $[\text{C}_{14}\text{H}_{10}]^{2-}$ ligand. However, these were formed through the two-electron reduction of anthracene by dimeric lanthanide(II) hydride species, and therefore, negates further comments.

The reaction of **4.2** with one equivalent of naphthalene was conducted in hexane inside an NMR tube fitted with a J. Youngs tap. The reaction mixture was heated to 60 °C over 1 week, and the solution had become more blue-black in colour. A subsequent ^1H NMR experiment inferred the possibility of a multiple species present, including a new samarium-containing product, unreacted **4.2** and unreacted naphthalene.

It was decided to work up the crude reaction mixture, and the mixture was transferred to a scintillation vial inside the glovebox and left to crystallise at room temperature, providing dark single blocks of **4.11** suitable for an X-ray diffraction experiment (Figure 4.17).

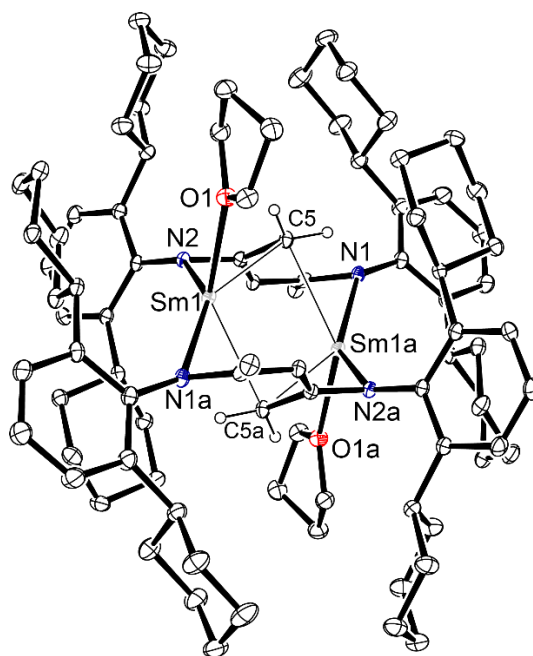


Figure 4.17. Ortep representation (30% probability ellipsoids) of compound **4.11**. Hydrogen atoms (except those of C5) have been removed for clarity. Selected bond lengths (Å) and angles (°): Sm1–N2 2.522(2), Sm1–N1a 2.578(2), Sm1–C5 2.760(3), Sm1–C5a 2.831(3), Sm1–O1 2.599(2), N2–Sm1–C5 52.21(7), N2–Sm1–C5a 101.56(7), N2–Sm1–N1a 146.57(7), N2–Sm1–O1 107.28(7).

The solid-state data disclosed that **4.11** was not the expected reduced naphthalene dianion complex but a product of ligand rearrangement. In the asymmetric unit **4.11** is a monomer with the primary coordination sphere made up of two contacts: the first is from the BDI^{Dicyp} ligand, which is κ^1 -bound through one N-atom of a Dicyp substituent and the second is to the oxygen of a donor THF molecule (2.599(2) Å). The Sm1–N2 bond length of 2.522(2) Å is slightly elongated but still comparable to other Sm(II) complexes supported by the BDI^{Dicyp} ligand presented in this Chapter (2.440(4) – 2.497 Å). A third contact arises from deprotonation and subsequent interaction of the C5 methyl of the β -diketiminato ligand backbone to the Sm(II) metal centre (2.760(3) Å).

Overall, **4.11** is a dimer, with the Sm(II) centre κ^2 -chelating the nitrogen of a Dicyp substituent (Sm1–N1a: 2.578(2) Å) as well as the deprotonated methyl group of the ligand backbone (2.831(3) Å) of the second [(BDI^{Dicyp})Sm] unit. Compound **4.11** demonstrates structural features reminiscent of a Eu(II) ligand deprotonation product (**3.9**) mentioned in Chapter Three, however, poor quality crystal data on **3.9** negates any further comparisons.

4.8 Summary

This Chapter demonstrates the BDI^{Dicyp} ancillary ligand's suitability for the synthesis and isolation of a low-coordinate, samarium(II) monoalkyl complex (**4.2**) at room temperature.⁵ This Sm(II) species could activate both proteo- and deuterio-benzene solvent, to afford an inverse sandwich complex where two samarium ions are bridged by a [C₆H₆]ⁿ⁻ moiety. Through X-ray diffraction experiments, magnetic susceptibility measurements, reactivity studies and computational techniques, we have characterised this inverse sandwich complex as being two Sm(III) ions bridged by a [C₆H₆]⁴⁻ unit. This demonstrates that **4.2** is a sufficiently potent reducing agent and can affect the four-electron reduction of benzene to the tetraanion without the need for a strong Group 1 reducing agent, which we have proposed is going through a transient Sm(I) intermediate. This chemistry has also been extended to benzene derivatives,

such as toluene and PhSiH_3 , to give inverted sandwich complexes containing the toluene or PhSiH_3 tetraanions, respectively. Finally, this Chapter further explores the reduction chemistry of **4.2** towards the polyaromatic hydrocarbon, anthracene and the reduction chemistry of the benzene tetraanion towards diphenylacetylene and fullerene.

4.9 Conclusions

In conclusion, this Thesis has described the utility of the β -diketiminato ligand framework for isolating a series of divalent lanthanide hydrides. Chapter Two first introduced the synthesis of THF-solvated Yb(II) hydride (**2.5**) supported by the previously reported $\text{BDI}^{\text{Dipep}}$ ancillary ligand. This was followed by the synthesis of a novel β -diketiminato ligand containing bulky dicyclohexylphenyl substituents, $\text{BDI}^{\text{Dicyp}}$, which in turn resulted in the isolation of a new solvent-free Yb(II) hydride (**2.14**). The structure and reactivity of these two species were then compared to our original BDI^{Dipp} Yb(II) hydride (**XXV**). The smallest system, **XXV**, has been reported to affect the catalytic alkylation of benzene, whereas **2.5** underwent ligand activation instead. **XXV** could also facilitate the two-electron aromatisation of COT, anthracene, and naphthalene but was also found to undergo oxidation to give a Yb(III) COT species. In comparison, **2.14** could reduce COT and anthracene, albeit poorly, because of its negligible solubility in all solvents. All three systems could functionalise white phosphorus, with **2.5** and **2.14** affording similar P_4 structures to varying degrees of success, while **XXV** gave a trinuclear complex containing the P_7 Zintl ion cage, much like its calcium hydride analogue.

Chapter Three demonstrates that the synthesis of a molecular Eu(II) hydride is not a simple extension of Group 2 chemistry, where utilisation of the previously reported $\text{BDI}^{\text{Dipep}}$ ligand system afforded a plethora of Schlenk-type redistribution or ligand rearrangement products. Instead, the use of the $\text{BDI}^{\text{Dicyp}}$ ligand introduced in Chapter One was extended toward Eu(II), where we isolated an insoluble red solid postulated to be a Eu(II) hydride. Over a year, this was proven through a range of reactivity studies, including the formation of a Eu(II)

formamidinate complex. This red solid was later structurally characterised and confirmed as the first example of a divalent Eu(II) hydride. Lastly, this Chapter employed unsymmetrical derivatives of the β -diketiminato ligand; one was previously reported within the literature and one novel, providing the second and third examples of Eu(II) hydrides complexes. These unsymmetrical systems displayed an increase in solubility compared to the symmetrical BDI^{Dicyp} Eu(II) hydride. All three systems were proven to affect the two-electron aromatisation of COT to solely produce the respective inverted Eu(II) sandwich complexes, demonstrating the high stability of the europium ion in the 2+ oxidation state.

Chapter Four described the success of the same BDI^{Dicyp} ancillary ligand for the isolation of a low-coordinate, samarium(II) monoalkyl complex. This species was found to reduce benzene and its derivatives to give the respective inverted sandwich complexes containing two Sm(III) ions bridged by a tetraanionic arene. This was confirmed by X-ray crystallography and magnetic susceptibility calculations in the solution- and solid-state. It was proposed that this reaction mechanism proceeded *via* a transient Sm(I) intermediate. This mechanism has been supported by the ability of this same samarium(II) monoalkyl to affect the two-electron reduction of COT at a single samarium centre, which has also been corroborated through DTF calculations. This Chapter began to explore further the reduction chemistry of the Sm(II) alkyl, where the reaction with anthracene afforded the inverse Sm(II) sandwich complex much like the Yb(II) and Eu(II) analogues, demonstrating this Sm(II) alkyl to also act as a one-electron reducing agent. Finally, this Chapter details the ability of the benzene tetraanion complex to reduce unsaturated substrates such as fullerene and diphenylacetylene.

4.10 References

1. W. J. Evans, *Inorg. Chem.*, **2007**, 46 (9), 3435-3449.
2. X. Shi, C. Hou, C. Zhou, Y. Song and J. Cheng, *Angew. Chem. Int. Ed.*, **2017**, 56 (52), 16650-16653.
3. X. Shi, G. Qin, Y. Wang, L. Zhao, Z. Liu and J. Cheng, *Angew. Chem. Int. Ed.*, **2019**, 58 (13), 4356-4360.
4. R. Shannon, *Acta Cryst. A.*, **1976**, 32 (5), 751-767.
5. G. M. Richardson, T. Rajeshkumar, F. M. Burke, S. A. Cameron, B. Nicholls, J. Harvey, R. A. Keyzers, T. Butler, S. Granville, L. Liu, L. Maron and M. D. Anker, preprint out at *Nature Portfolio*, under revision (*Nat. Chem.*), **2023**.
6. J. Li, C. W. Liu and J. X. Lu, *J. Mol. Struct.*, **1993**, 280 (2), 223-231.
7. C. Yu, J. Liang, C. Deng, G. Lefèvre, T. Cantat, P. L. Diaconescu and W. Huang, *J. Am. Chem. Soc.*, **2020**, 142 (51), 21292-21297.
8. J. Mortensen and J. Heinze, *Angew. Chem. Int. Ed.*, **1984**, 23 (1), 84-85.
9. W. Huang, J. J. Le Roy, S. I. Khan, L. Ungur, M. Murugesu and P. L. Diaconescu, *Inorg. Chem.*, **2015**, 54 (5), 2374-2382.
10. Y. Xiao, X. K. Zhao, T. Wu, J. T. Miller, H. S. Hu, J. Li, W. Huang and P. L. Diaconescu, *Chem. Sci.*, **2021**, 12 (1), 227-238.
11. W. Huang, F. Dulong, T. Wu, S. I. Khan, J. T. Miller, T. Cantat and P. L. Diaconescu, *Nat. Comm.*, **2013**, 4 (1), 1448.
12. S. Bank and D. A. Juckett, *J. Am. Chem. Soc.*, **1976**, 98 (24), 7742-7746.
13. A. J. Pell, G. Pintacuda and C. P. Grey, *Prog. Nucl. Mag. Reason. Spectrosc.*, **2019**, 111, 1-271.
14. G. M. Richardson, I. Douair, S. A. Cameron, J. Bracegirdle, R. A. Keyzers, M. S. Hill, L. Maron and M. D. Anker, *Nat. Comm.*, **2021**, 12 (1), 1-7.
15. G. M. Richardson, I. Douair, S. A. Cameron, L. Maron and M. D. Anker, *Chem. Eur. J.*, **2021**, 27 (52), 13144-13148.
16. G. M. Richardson, J. Howarth, M. J. Evans, A. J. Edwards, S. A. Cameron and M. D. Anker, *J. Coord. Chem.*, **2022**, 75 (11-14), 1954-1966.
17. X. Liu, Q. Wen, L. Xiang, X. Leng and Y. Chen, *Chem. Eur. J.*, **2020**, 26 (24), 5494-5499.
18. X. W. Zhang, G. H. Maunder, S. Gießmann, R. MacDonald, M. J. Ferguson, A. H. Bond, R. D. Rogers, A. Sella and J. Takats, *Dalton Trans.*, **2011**, 40 (1), 195-210.
19. M. Xue, Y. Zheng, Y. Hong, Y. Yao, F. Xu, Y. Zhang and Q. Shen, *Dalton Trans.*, **2015**, 44 (46), 20075-20086.
20. O. A. Mironova, T. S. Sukhikh, S. N. Konchenko and N. A. Pushkarevsky, *Russ. J. Coord. Chem.*, **2020**, 46 (4), 241-250.
21. M. Schmid, S. M. Guillaume and P. W. Roesky, *Organometallics*, **2014**, 33 (19), 5392-5401.
22. Z. Hou, Y. Zhang, O. Tardif and Y. Wakatsuki, *J. Am. Chem. Soc.*, **2001**, 123 (37), 9216-9217.
23. O. A. Mironova, T. S. Sukhikh, S. N. Konchenko and N. A. Pushkarevsky, *Polyhedron*, **2019**, 159, 337-344.
24. M. Xue, R. Jiao, Y. Zhang, Y. Yao and Q. Shen, *Eur. J. Inorg. Chem.*, **2009** (27), 4110-4118.
25. Y. M. Yao, Y. J. Luo, R. Jiao, Q. Shen, K. B. Yu and L. H. Weng, *Polyhedron*, **2003**, 22 (3), 441-446.

26. O. V. Kuznetsova, A. N. Egorochkin, N. M. Khamaletdinova and L. G. Domratcheva-Lvova, *J. Organomet. Chem.*, **2013**, 745-746, 34-41.
27. M. C. Cassani, Y. K. Gun'ko, P. B. Hitchcock and M. F. Lappert, *Chem. Comm.*, **1996**, (16), 1987-1988.
28. B. Rösch, T. X. Gentner, J. Langer, C. Färber, J. Eyselein, L. Zhao, C. Ding, G. Frenking and S. Harder, *Science*, **2021**, 371 (6534), 1125-1128.
29. J. Mai, B. Rösch, J. Langer, S. Grams, M. Morasch and S. Harder, *Eur. J. Inorg. Chem.*, **2023**, 26 (31), e202300421.
30. C. G. Lin, M. Hutin, C. Busche, N. L. Bell, D. L. Long and L. Cronin, *Dalton Trans.*, **2021**, 50 (7), 2350-2353.
31. W. J. Evans, J. W. Grate, I. Bloom, W. E. Hunter and J. L. Atwood, *J. Am. Chem. Soc.*, **1985**, 107 (2), 405-409.
32. W. J. Evans, J. W. Grate and R. J. Doedens, *J. Am. Chem. Soc.*, **1985**, 107 (6), 1671-1679.
33. W. J. Evans and T. A. Ulibarri, *J. Am. Chem. Soc.*, **1987**, 109 (14), 4292-4297.
34. D. F. Evans, *J. Chem. Soc.*, **1959**, (0), 2003-2005.
35. S. Mugiraneza and A. M. Hallas, *Comm. Phys.*, **2022**, 5 (1), 95.
36. P. B. Merkel, P. Luo, J. P. Dinnocenzo and S. Farid, *J. Org. Chem.*, **2009**, 74 (15), 5163-5173.
37. Y. Yamada, K. Maeda, K. Ohkubo, K. D. Karlin and S. Fukuzumi, *Phys. Chem.*, **2012**, 14 (27), 9654-9.
38. C. Sandorfy, General and theoretical aspects. In Carbon–Nitrogen Double Bonds (1970), **1970**; pp 1-60.
39. F. H. Allen, O. Kennard, D. G. Watson, L. Brammer, A. G. Orpen and R. Taylor, *J. Chem. Soc., Perkin Trans.*, **1987**, (12), S1-S19.
40. W. J. Evans, *Coord. Chem. Rev.*, **2000**, 206-207, 263-283.
41. J. C. Wedal and W. J. Evans, *J. Am. Chem. Soc.*, **2021**, 143 (44), 18354-18367.
42. W. J. Evans, S. L. Gonzales and J. W. Ziller, *J. Am. Chem. Soc.*, **1994**, 116 (6), 2600-2608.
43. Y. K. Gun'ko, P. B. Hitchcock and M. F. Lappert, *J. Organomet. Chem.*, **1995**, 499 (1), 213-219.
44. W. J. Evans, M. A. Johnston, R. D. Clark, and J. W. Ziller, *J. Chem. Soc., Dalton Trans.*, **2000**, (10), 1609-1612.
45. C. A. Laskowski, D. J. Bungum, S. M. Baldwin, S. A. Del Ciello, V. M. Iluc and G. L. Hillhouse, *J. Am. Chem. Soc.*, **2013**, 135 (49), 18272-18275.
46. S. Brownstein, J. Dunogues, D. Lindsay and K. U. Ingold, *J. Am. Chem. Soc.*, **1977**, 99 (7), 2073-2078.
47. L. Maron and O. Eisenstein, *J. Phys. Chem. A.*, **2000**, 104 (30), 7140-7143.
48. M. N. Bochkarev, *Chem. Rev.*, **2002**, 102 (6), 2089-2118.
49. F. M. Sroor, *J. Organomet. Chem.*, **2021**, 948, 121878.
50. D. Patel, F. Moro, J. McMaster, W. Lewis, A. J. Blake and S. T. Liddle, *Angew. Chem. Int. Ed.*, **2011**, 50 (44), 10388-10392.
51. D. Patel, J. McMaster, W. Lewis, A. J. Blake and S. T. Liddle, *Nat. Comm.*, **2013**, 4 (1), 2323.
52. B. Kosog, C. E. Kefalidis, F. W. Heinemann, L. Maron and K. Meyer, *J. Am. Chem. Soc.*, **2012**, 134 (30), 12792-12797.
53. U. Denninger, J. J. Schneider, G. Wilke, R. Goddard, R. Krömer and C. Krüger, *J. Organomet. Chem.*, **1993**, 459 (1), 349-357.
54. J. I. C. Wu, Y. Mo, F. A. Evangelista, and P. von Ragué Schleyer, *Chem. Comm.*, **2012**, 48 (67), 8437-8439.

55. B. C. Yadav and R. Kumar, *Int. J. Nanotechnol. Appl.*, **2008**, 2 (1), 15-24.
56. S. R. Lawrence, C. A. Ohlin, D. B. Cordes, A. M. Z. Slawin and A. Stasch, *Chem. Sci.*, **2019**, 10 (46), 10755-10764.
57. P. F. Lang and B. C. Smith, *J. Chem. Ed.*, **2010**, 87 (8), 875-881.
58. J. Mai, B. Rösch, N. Patel, J. Langer and S. Harder, *Chem. Sci.*, **2023**, 14 (18), 4724-4734.